

UNIVERSITAT JAUME I

Departament d'Enginyeria de Sistemes Industrials i Disseny



**Development of hybrid coatings for
osseointegration improvement of metal
dental implants**

Memoria presentada por:

Sara Maria da Silva Barros

Para optar al grado de doctor

Dirigida por:

Dr. Julio José Suay Antón

Dr. Raúl Izquierdo Escrig

Castellón de la Plana, julio de 2016

Aos meus pais

AGRADECIMIENTOS

Empiezo por agradecer a la institución Universitat Jaume I por acogerme durante cinco años, especialmente agradecer al departamento d'Enginyeria de Sistemes Industrials i Disseny. A Isabel Badal, a Javier Vicente, a Roberto Sanchis y a Carlos Vila, gracias por poder contar con vuestra ayuda en todo momento para los trámites y desarrollo de este trabajo.

A mis directores, Julio Suay y Raúl Izquierdo, les agradezco su confianza, apoyo y dedicación. De forma especial a Julio por hacerme sentir en todo momento que no estaba sola en este viaje. Gracias por todo lo que me habéis enseñado y por vuestra paciencia en mi proceso de “crecimiento” profesional y personal.

Me gustaría agradecer también a Isabel Goñi y Marilo Gurruchaga su ayuda e interés demostrado en el desarrollo de este trabajo. Gracias también por vuestra paciencia y apoyo desde la Universidad del País Vasco. No puedo olvidarme de Beatriz, María y Marije por su esfuerzo y ayuda, gracias.

Agradezco también a Luis Cabedo, Jose Gámez y José Javier Gracenea su ayuda y conocimientos transmitidos siempre que os he necesitado.

A José Ortega y Raquel Oliver les agradezco su apoyo en todo momento, confianza, paciencia y los buenos ratos que pasamos en los laboratorios. Gracias por vuestros consejos, por escucharnos y atendernos.

Quiero mencionar también mi agradecimiento a José Javier Gómez y José Miguel Pedra del Servei d'instrumentació Científica de la UJI por su interés y ayuda.

A José Luis Gómez, Laura Teruel y los compañeros del Centro de Biomateriales e Ingeniería Tisular de la Universidad Politécnica de Valencia, gracias por hacerme sentir cómo una persona más de vuestro equipo.

A María José Gimeno y Sandra Chamorro por permitirme acceder a las instalaciones de MEDCO y ayudarme siempre que os buscaba. Os agradezco además vuestra amistad y conversaciones sobre “la tesis”.

Debo referir mi agradecimiento especial a Miriam Hernández, por introducirme en “el sol-gel” y en el mundo de la investigación. Gracias por la gran lección de humildad que me has dado.

Agradezco a mis compañeras y amigas Montse, Irene y Ane todo el apoyo, amistad y enseñanzas desde los inicios del grupo PIMA. Gracias Irene por transmitirme tus conocimientos y escucharme en mis “malos momentos”. Gracias Montse por tu predisposición siempre por ayudarme y por tus consejos. Gracias Ane por tu ayuda.

A Estefanía le agradezco su compañía y ayuda en esos momentos en que su tiempo valía más que el oro, gracias.

A Fran, le agradezco su amistad y su apoyo incondicional. Ha sido una maravilla trabajar contigo!

A Javi y a Jennifer, unos compañeros siempre dispuestos a ayudar.

A todos vosotros, mis compañeros y amigos, gracias por enseñarme el verdadero significado de la palabra “compañerismo” y por tornar más ameno este duro viaje

Por fin, me gustaría agradecer a todas aquellas personas sin las cuales no hubiese sido posible concluir este trabajo.

Gracias Pili, Ainara, José y Rosa por “estar ahí” siempre que os he necesitado.

Gracias Gustavo por tu ayuda, por animarme, por tu confianza en mí y por mimarme en esos días en que uno se siente pequeño.

Obrigada Sofia por ser um bebé tão bom.

Obrigado mãe e pai por me ensinar sempre que na vida há muitas coisas que são difíceis mas que não são impossíveis.

A todos vosotros muchas gracias!

RESUMEN

Se ha comprobado que los implantes dentales de titanio presentan características como biocompatibilidad y osteointegración. No obstante, carecen de propiedades osteoinductoras y son biológicamente inactivos a escala molecular. Actualmente, la estrategia habitual que emplean los fabricantes consiste en modificar la superficie de los implantes dentales de titanio mediante tratamientos mecánicos y químicos para conseguir éxito del implante en los pacientes aptos para recibir el tratamiento. Ahora bien, estas acciones no resultan plenamente efectivas en los casos particulares en que la calidad y/o cantidad de hueso receptor del implante es pobre.

La presente tesis doctoral se centra en plantear una nueva estrategia con la que conferir propiedades bioactivas a la superficie de los implantes de titanio, tratando así de conseguir una mejora en el éxito de dichos implantes.

Esta estrategia consiste en desarrollar recubrimientos superficiales bioabsorbibles híbridos de base silicio, sintetizados vía sol-gel. Adicionalmente, estos recubrimientos deben constituir una matriz de soporte o andamiaje que permita la adhesión celular e, igualmente, actúe como vehículo de transporte y liberación de biomoléculas con capacidad para actuar en momentos específicos del proceso de regeneración ósea.

Para alcanzar los objetivos que se han propuesto, se han formulado recubrimientos a partir de tres precursores de silicio: trimetoximetilsilano (MTMOS), 3-glicidiloxipropiltrimetoxisilano (GPTMS) y tetraetoxisilano (TEOS). Los contenidos en TEOS y GPTMS se han variado en las formulaciones para controlar la velocidad de degradación de los recubrimientos y para lograr una presencia suficiente de agente ligante que asegure la retención de biomoléculas, respectivamente. Además, en el último caso, se pretende que las buenas propiedades que se ha visto

presenta el recubrimiento sol-gel de base silicio que se ha considerado como referencia (50%MTMOS:50%GPTMS) no se vean afectadas.

Se ha realizado una detallada caracterización de los nuevos recubrimientos formulados, especialmente en lo que a sus propiedades físicas, químicas y biológicas se refiere. Con la caracterización físico-química se ha analizado tanto las propiedades estructurales como superficiales de estas matrices, así como su velocidad de degradación o el efecto barrera que ofrece el recubrimiento frente a la corrosión del implante metálico. Por otra parte, los ensayos biológicos han servido para evaluar la biocompatibilidad de los recubrimientos y, así, poder escoger un prototipo final con el que estudiar su respuesta frente a la interacción con tejidos vivos.

Los resultados obtenidos muestran que todos los recubrimientos se encuentran bien adheridos a la superficie metálica. La incorporación de TEOS a la doble composición del material de referencia (50%MTMOS:50%GPTMS) ha incrementado la rugosidad superficial, la mojabilidad y la degradación de los recubrimientos. La fracción orgánica proporcionada por la base silánica GPTMS se ha podido ajustar para conseguir la correcta funcionalización de los recubrimientos con una biomolécula como la gelatina sin desmejorar las propiedades positivas detectadas para los materiales no funcionalizados.

El prototipo final ha demostrado ser claramente biocompatible con los tejidos vivos, mejorando las prestaciones del material de referencia (50%MTMOS:50%GPTMS) pero sin que se vean mermadas las propiedades osteoconductoras de los implantes dentales de titanio comerciales.

RESUM

Els implants dentals són reconeguts com a biocompatibles i osteointegradors, no obstant això, manquen de propietats osteoindutores i són biològicament inactius (material inert). Actualment, l'estratègia emprada pels fabricants per tal de modificar la superfície dels implants consisteix en realitzar tractaments mixtes mecànics i químics que garanteixen l'èxit de l'implant en cas de selecció de pacients, però no és efectiva en aquells casos de menor qualitat i quantitat d'os receptor de l'implant.

Aquesta tesi doctoral es centra en formular una nova estratègia per a conferir a la superfície metàl·lica dels implants funcions bioactives i un paper més actiu en el procés d'osteointegració.

L'estratègia consisteix en desenvolupar recobriments híbrids de base silici, sintetitzats via sol-gel que han de ser, a més a més, biodegradables. Addicionalment, els recobriments han de servir com a matriu de suport per a l'adhesió cel·lular i actuar com a vehicle de transport i alliberació de biomolècules amb capacitat d'actuar en moments específics del procés de regeneració de l'os.

Per a assolir els objectius proposats en aquest treball, es formulen diversos recobriments a partir de tres precursors de silici: MTMOS: GPTMS: TEOS. El contingut en TEOS s'ha modificat amb el propòsit de controlar la degradació dels recobriments. Per altra banda, el contingut en GPTMS es canvia per a aconseguir una quantitat suficient d'agent lligant que assegure la retenció de biomolècules sense afectar les bones propietats aconseguides prèviament amb el recobriment sol-gel de referència (50MTMOS:50GPTMS).

Així mateix, s'ha dut a terme una caracterització completa dels nous recobriments, en concret s'han estudiat les seues propietats

fisicoquímiques i s'ha completat la caracterització amb l'avaluació de la resposta cel·lular i de teixits vius als recobriments.

La caracterització fisicoquímica s'ha dissenyat per a conèixer les propietats estructurals de la matriu siloxànica i propietats superficials dels recobriments, a més a més d'estudiar els perfils de degradació hidrolítica i propietats barrera anticorrosives. La caracterització biològica s'ha planificat per a comprovar la biocompatibilitat dels nous recobriments i seleccionar un prototip final per a l'estudi *in vivo*.

Els resultats indiquen que els recobriments es troben ben adherits a la superfície metàl·lica. La incorporació del TEOS a la doble composició 50MTMOS:50GPTMS (material de referència) ha conduït a un augment de la rugositat superficial, la mullabilitat i la degradació dels recobriments sol-gel. El contingut en GPTMS és adequat per a aconseguir la correcta funcionalització dels recobriments amb gelatina (biomolècula) sense interferir en les propietats correctes i verificades per al material de referència.

El prototip final que s'ha desenvolupat en aquest treball de tesi ha demostrat ser biocompatible amb els teixits vius i millora la prestació del 50MTMOS:50GPTMS sense afectar de cap manera les propietats osteoconductores de les superfícies de titani dels implants dentals comercials.

ABSTRACT

Titanium dental implants have proved biocompatibility, as well as osseointegrative properties; nevertheless, they lack of osteoinductive properties and they are also biologically inactive at the molecular level. Nowadays, the usual strategy used by the majority of manufacturers consists of modifying titanium dental implants' surfaces by mechanical-chemical treatments in order to ensure a successful implantation in selected patients but this is not fully effective in the special situations of poor bone quality and/or quantity.

This work focuses on a new strategy to endow bioactivity to titanium implants' surfaces, thus improving these implants' success.

This strategy consists of developing synthetic, hybrid and biologically absorbable silica-based external coatings by means of sol-gel technology. Additionally, these coatings might act as a scaffold for cellular adhesion and as a vehicle capable of retaining and releasing biomolecules with specific roles on bone regeneration processes.

In order to achieve this purpose, triple silane coatings based on the precursors tetraethoxysilane (TEOS), trimethoxymethylsilane (MTMOS) and 3-glycidyloxypropyltrimethoxysilane (GPTMS) have been synthesized. TEOS and GPTMS contents were varied in the formulations to control the degradation rate of the coating and to achieve a satisfactory amount of the coupling agent for bioactive molecules, respectively. In the latter case, it was expected not to diminish the interesting characteristics of the silica-based sol-gel coating considered as reference material (50%MTMOS:50%GPTMS).

The different obtained coatings were thoroughly characterized, specifically focusing on their physical and chemical properties as well as on their biological performance. The physical-chemical characterization was

designed to investigate the structural and surface properties of the matrices, apart from studying their degradation rate and barrier effectiveness of the coatings against metal implants corrosion. On the other hand, the biological tests were planned to ascertain the biocompatibility of the coatings and select a final prototype to study its interaction with living tissues.

Results show that all the synthesized coatings were well adhered to the metal surface. The incorporation of TEOS to the double reference material (50%MTMOS:50%GPTMS) increases surface roughness, wettability and degradation of the coating. The organic content, provided by the GPTMS silane could be adjusted to achieve successful functionalization of the coatings with a biomolecule as gelatin without worsening the interesting characteristics of the non-functionalized coatings.

The final prototype shows clear biocompatibility with living tissues, thus improving the biological performance of the reference material (50%MTMOS:50%GPTMS), without affecting the osteoconductive properties of the commercial titanium dental implants.

TABLE OF CONTENTS

CHAPTER 1.	INTRODUCTION	1
CHAPTER 2.	OBJECTIVES	67
	OBJETIVOS	80
CHAPTER 3.	MATERIALS AND METHODS	95
CHAPTER 4.	RESULTS	133
CHAPTER 5.	CONCLUSIONS	286
	CONCLUSIONES	289

CHAPTER 1. INTRODUCTION

MOTIVATION

According to World Health Statistics 2014 report published by World Health Organization, globally life expectancy has increased by six years since 1990. The progressive rise of life expectancy and the interest in healing traumas caused by accidents and diseases (congenital or degenerative) encourage investigation of new materials capable of replace tissue lost and recover the biomechanical function of injured biosystems with a positive impact in the quality of patients live and social benefits¹.

It is possible to find in bibliography that about 2.2 million bone graft surgeries related to bone defects repair in orthopedics, neurosurgery and oral-maxillofacial are performed each year with estimated costs of 2 billion euros^{2,3}.

From a clinical point of view, new methods and materials used for bone regeneration that reduces surgical trauma for the patient and associated costs are important factors on surgical management and biomedical research.

Bone tissue engineering and precisely tissue engineered implant surfaces may be another tactic of permanently stabilize implants by coating the devices with cells or tissue before implantation⁴.

Bone substitute synthetic materials can be developed as a simple medium of fill in the tissue gap or as a carefully designed material that also assists the regenerative process and formation of new bone.

The “perfect” synthetic bone graft should be biocompatible, biologically absorbable, with a structure similar to bone and guide patient’s bone tissue towards a bioregenerative process for an entirely bone replacement^{5,6,7}.

It is crucial for the clinical success of new bone substitutes materials the accomplishment of special biomimetic requirements as osteoconduction, osTeoinduction, favorable porosity, stability under stress, plasticity,

INTRODUCTION

sterility and long-term integration, besides the upper cited biocompatibility and absorbability in the physiological medium. Moreover, other desired features of synthetic materials are related with functional assignments as space maintenance for bone regeneration, pre-setting of the desired anatomical form, acceleration of bone remodeling, osteoconductive structural guidance for the tissue regeneration, carrier support for antibiotics or growth factors or approaches by gene therapy and scaffold for tissue engineering.

Metals and their alloys have played a important role as structural biomaterials in reconstructive surgery, specially orthopedics, with more recent uses in non-osseous tissues.⁸ Many years of study of the interaction between metal implants (as bone substitute materials) and tissues show that the implant material provide an acceptable degree of biocompatibility and that is the nature and design of its surface that most affect the host response.⁹

Titanium is the most prevalent metallic material for use in orthopedics and dental implants because of its mechanical properties and osteoconductivity. That is to say, its successful osteointegration arises from standardize topography and chemistry that causes an exceptional resistance to corrosion making it suitable for biomedical applications.^{10,11} At the present time, dental implantology aim to develop surfaces with osseoinductive capacity to enhance the actual clinical success of titanium dental implants (only osteoconductive). This progress could be the response to the actual difficult clinical situations with poor bone quality and quantity. This new therapeutic strategy includes the development of biocompatible and biodegradable matrices with the ability to release bone stimulating biomolecules and drugs.

INTRODUCTION

BIOMATERIALS

The demand for suitable biomaterials arises from the actual older population with higher expectations related with their quality of life. Nevertheless, the essential nature of a biomaterial has changed since the first generation of biomaterials in the decades of 1960's and 1970's. The first biomaterials used on a human body seek for replace damaged tissue with a minimal toxic response and provide structural support. So the desired properties of the early biomaterials were an appropriated combination of physical and chemical characteristics compatible with the injured tissue and biological "inertness". The prostheses firstly used were metallic, some of them made with carbon and vanadium, latter some evident corrosion damage was identified what encourage the use of passive metallic alloys like stainless steel and Co-Cr, NiTi shape memory alloys come into view on the 60's due to their special mechanical properties nevertheless some allergenic effects of Ni bring to an end their use^{12,6,13}. The evolution of first generation metallic biomaterials materialize some improved alloys used nowadays like austenitic stainless steel with high Cr content and partial substitution of Ni by Mn, also Ti and Ti6Al4V devices were found to become tightly integrated into bone with a long-term behavior and few failure incidences¹⁴. Polymers like nylons and polyesters were used as biomaterials, even so other synthetic materials not so degradable as polytetrafluorethylene (PTFE), polymethylmetacrylate (PMMA), polyethylene (PE) and silicones¹². Afterward, on the 1980's and 1990's, a second generation of biomaterials was achieved with a more specific goal looking for bioactive components that encourage specific biologic responses of the physiologic environment. Bioactive materials like titanium and bioceramics were clinically used on orthopedic, dental and cardiovascular interventions. It was found that implants with porous structures stimulate tissue ingrowth,

INTRODUCTION

this behavior was detected with bioactive glasses experiments where the reactions induced on living tissue entail a sequence of biologic steps that leads to a strong mechanical bonding between the bones and implant surface. In a first stage a rapid ion exchange of Na^+ with H^+ and H_3O^+ occurs on the surface of bioglasses followed by the polycondensation of silanols what leads to a silica high surface area that provides an ideal environment for heterogeneous nucleation and crystallization of biologically reactive hydroxycarbonate apatite (HCA) layer similar to the bone inorganic mineral part. The HCA deposited on the biomaterial surface provide an agreeable environment for some biological reactions as osteoblasts (cells that produce bone) colonization followed by proliferation and differentiation to form new bone attached to the implant⁶. As a result from osteoblasts activity, the surrounding bone can contact directly with the surface apatite without formation of fibrous tissue¹⁵. With this achievement synthetic hydroxyapatite $\text{Ca}_{10}(\text{PO}_4)_6(\text{OH})_2$ (HA) ceramics started to be applied as porous implants, powders and coatings on metallic devices to induce biological reactions and bioactive fixation, however, it has low solubility rate due to intrinsic chemical stability and may remain integrated into the regenerated bone tissue. Besides, other ceramic materials generally identified as calcium phosphates (CaP's) are reabsorbed and demonstrate good bioactive properties as well^{14,16,17}. Clinically, HA and tricalcium phosphate $\text{Ca}_3(\text{PO}_4)_2$ (TCP) are some of the usual bioactive ceramics used as bone substitute materials (fillers)^{12,17}. Aside from the osteoconductive properties attained on second generation materials also biologically absorbable products with controlled chemical breakdown and resorption were studied and produced, a clear example are the biodegradable polymers composed of polylactic (PLA) and polyglycolic (PGA) acids and polydioxanone (PDS) used as sutures or as biologically absorbable bone fixation devices. Many of the biomaterials developed on this second generation still constitute commercial products used clinically nowadays, specifically in orthopedics and dentistry^{12,14}. The clear advances reached on the first and second generation materials resulted insufficient as the physical and chemical properties of permanent

prosthesis resulted damaged after 10-20 years of implantation in many patients, requiring additional replacing surgery⁶. The purpose of achieving biomaterials capable of substitute in a long-term damaged tissue was replaced by the need to overcome new biological strategies that focus on repair and regenerate tissues structures and functions^{12,6}.

In the 2000s years many advances in molecular biology and proteomics took place in order to start and understand a new concept of biomaterial able to stimulate specific cellular reactions at molecular level^{6,12}. The strategies used to produce the third generation biomaterials are basically the development of biomimetic and absorbable matrices as a structure for progenitor cells seeding or the use of powders and micro/nano particles to stimulate *in situ* tissue regeneration as the controlled release of specific products like growth factors (protein signaling molecules with the ability to enhance intercellular communication) that participate on the self-assembling of growing cells.

The upper cited three generations should not be understood as a chronological sequence but a conceptual evolution since each period represents the achievement of particular properties and requirements (Figure 1.1), what is more, nowadays studies and research still fall upon biomaterials that according to their properties could be recognized as first and second generation.

INTRODUCTION

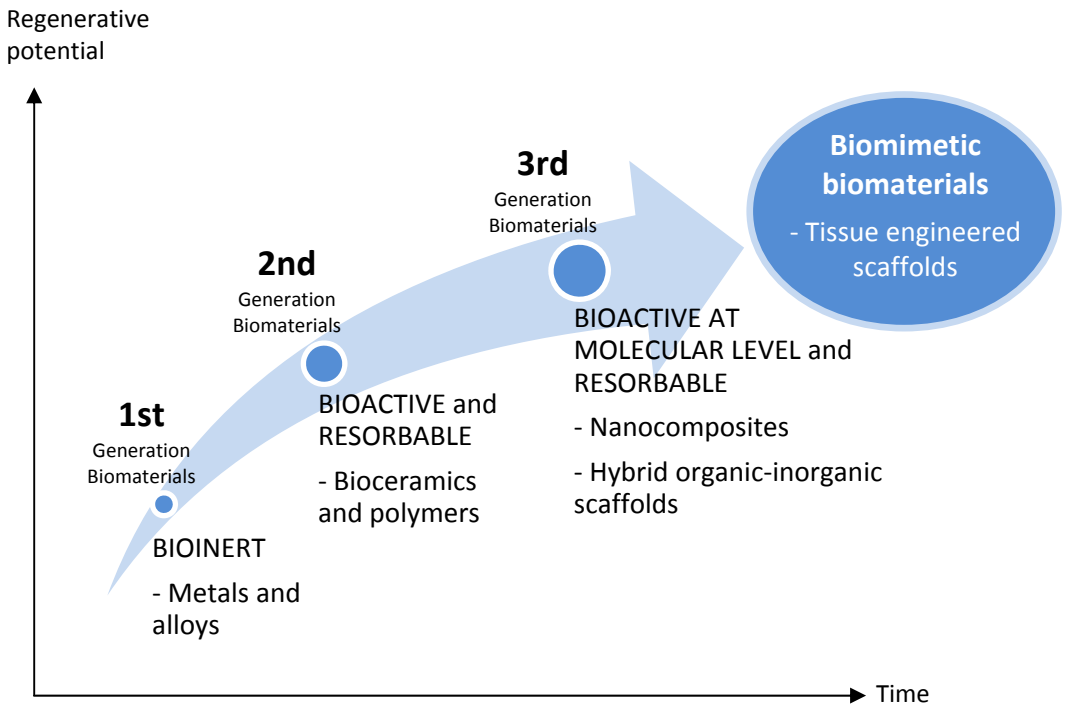


Figure 1.1 – Schematic evolution of biomaterials.

The *metals* show up as an important group of synthetic materials used as bone replacement biomaterials. For many decades, permanent hip, knee, spinal and dental implants of stainless steel (SUS316L), cobalt-chromium (Co-Cr) alloys and titanium and its alloys have been applied and nowadays still constitute the main permanent implants used on clinic treatments^{18,12}. Even though widespread applications of metal implants remain in our time some limitations related with these materials have been detected as corrosion products that can lead to toxic reactions and hypersensitivity. The well-known suitable mechanical properties of metals, as high tensile strength and fatigue resistance makes it appropriate for load-bearing applications, however, the key factor that establish the material that best fits in a particular injury is Young's modulus, in this way titanium and its alloys come closest to elastic modulus of natural bone as their use can reduce the extent of stress-shielding, inhibiting the extension of bone resorption detected in other alloys as stainless steel and Co-Cr

alloys. In the main, metal is classified as a bioinert material, thus many research developed nowadays fall upon the activation of the surface of metal implants through chemical or physical treatments. Recent advances on magnesium based metal implants may open a new concept of soluble metallic materials^{12,19}.

To better understand the interest on metals as bone replacement biomaterials it is important to clarify the real meaning of the term "Biomaterial". There are several definitions for *Biomaterial*, from a medical point of view a biomaterial is a natural or synthetic material that is projected for introduction into living tissue as a part of a medical device or implant, besides, from a healthcare perception can be defined as a material that possess specific properties that make it suitable to come in direct contact with living tissue without any elicit adverse immune rejection reaction^{20,21}. One of the most generalized descriptions of biomaterial is the one referred by the American National Institute of Health that define biomaterial as "any substance or combination of substances, other than drugs, with synthetic or natural origin, that can be used for any period of time, which augments or replaces partially or totally any tissue, organ or function of the body in order to maintain or improve the quality of life of the individual". Recent advances on the bioengineering field have changed the classic idea of biomaterial and made them more versatile and increased their utility somehow due to their current use in drug-delivery systems, as biosensors or devices operating outside the body but connected with it²⁰. To define in a better way such a widespread of units, in this work, the term biomaterial will be considered from a health care perspective and must have an interface with tissues or tissue component¹³.

INTRODUCTION

CONCEPTS ABOUT THE BIOLOGIC PROCESS OF BONE REGENERATION

Bone is a complex and highly organized mineralized tissue and there are two types of mature bone, *cancellous* and *cortical*.

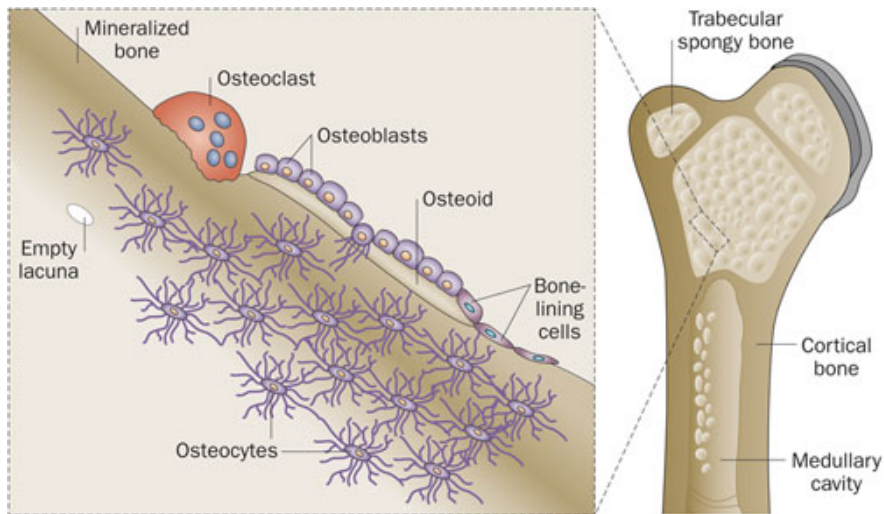


Figure 1.2 - Microstructure (left) of bone with a schematic representation of the remodeling process of trabecular bone surface. Macrostructure of bone (right)²².

Cortical bone or *compact bone* is a mineralized connective tissue (Figure 1.2). It is a complex and highly organized matrix of collagen combined with crystalline mineral and has a porosity of 5-10% approximately. Osteoblasts, cells that are differentiated from mesenchymal stem cells available on bone marrow, produce a disordered matrix of collagen Type 1 that subsequently mineralize with hydroxyapatite (HA) crystals to form woven bone (unorganized bone primary structure). On the other hand, osteoclasts, specialized cells derived from macrophages, resorb areas of woven bone which permits it to be remodeled into a highly organized structure of parallel fibers in well-defined directions.

Compact bone forms a shell around *cancellous* or *trabecular bone*, the internal cancellous bone is a porous framework with about 50-95%

porosity. The pores are interconnected and filled with bone marrow rich in stem-cells necessary for new connective tissue growth and production of blood cells²³.

The both types of bone are formed by two different tissues, *woven* and *lamellar bone*. In a first embryo stage the skeleton consist of woven bone which is later replaced by lamellar bone. Typically, an adult does not have woven bone in the skeleton, nevertheless, it reemerges during healing process after fracture; this internal bone remodeling process occurs throughout our lifetime as it is a fundamental process for the evolution of the bone microstructure and consequent adaptation of structural properties and micro-damage repair. Woven bone formed during the remodeling process is necessary for the stabilization of the fractured tissue and implant; it acts as a filling material of the grooves of the implant threads⁹.

Bone remodeling only occurs on endocortical surface, trabecular surfaces of cancellous bone or Harvesian systems of cortical bone²⁴. Trabecular surfaces can be found at the end of the medullary cavities of hollow long bones throughout the skeleton (Figure 1.2 and Figure 1.3).

INTRODUCTION

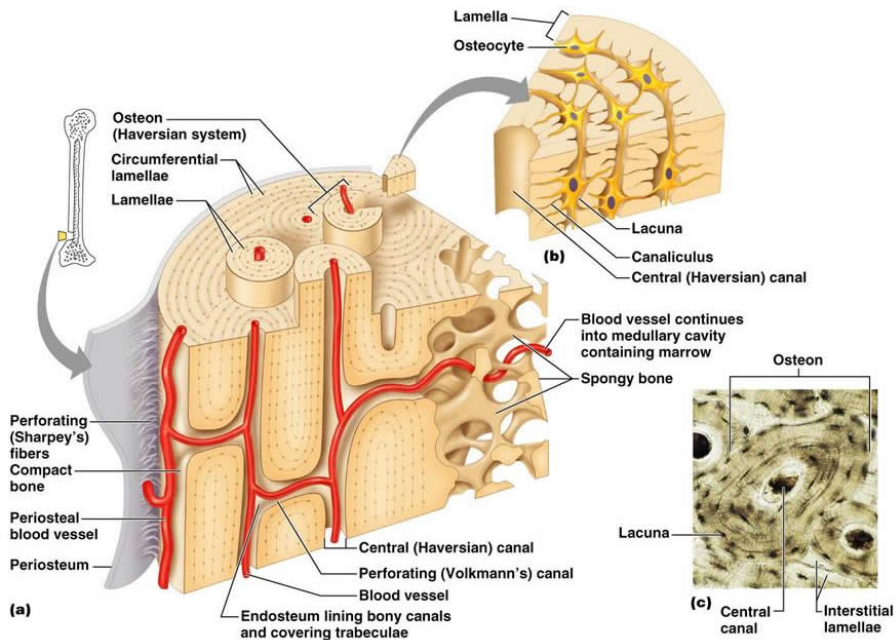


Figure 1.3 - Microscopical structure of cortical bone. (a) 3D sketch of cortical bone, (b) cut of a Haversian system, (c) photomicrograph of a Haversian system.^{24,25}

From a regenerative medicine point of view, the process of bone repair after the injury starts with the bleeding process from contiguous structures and a haematoma is formed²³. A cascade of events follow to continue the physiologic mechanism, inflammation, angiogenesis and granulation tissue formation, fibrous tissue formation, fibrocartilage, hyaline cartilage (soft callus), cartilage mineralization, woven bone (hard callus) and finally remodeling that can take several months to be accomplished^{23,26}.

In a first stage of the establishment of bone-biomaterial contact, micromotion disrupt the newly forming tissue leading to the formation of a fibrous capsule that can have different thickness and appearance depending on the implant surface, biological environment and other elements²⁷.

Although biological safety and some material properties remain vital for the success of an implant, the host response and associated effects upon

biomaterial form and function is determinant for an operative remodeling process (Figure 1.4).

The material reaction when it is exposed to a physiologic medium after implantation is also relevant for a successful bone regenerative process. The first mechanism that takes place after inserting a biomaterial is protein adsorption that comes from blood and tissue fluids of injury adjacent sites and in a second stage from the cellular activity that takes place at the periprosthetic region. In the particular case of metallic implants, several studies demonstrate that surface stabilization is not always achieved and also the presence of some elements as Ca, P and S can affect the chemical composition of protective oxide films of metallic prosthesis^{27,28}. *In vitro* studies reveal that metal ions released from the electrochemical corrosion, even detected at sublethal doses, can affect the osteoblasts and osteoclasts differentiation^{27,29,28}. Metal implants can degrade through corrosion and wear process, nevertheless, synthetic hardware as polyethylene degrades only through wear process²⁸. Moreover, dissolution products from bioactive silicate glasses have been detected as elements that stimulate osteogenesis (formation and development of bone tissue) and angiogenesis (the process by which the organism establishes new blood vessels from pre-existing ones) activating several genes associated with bone formation and vascularization^{30,31}. Even though the behavior and stability of the biomaterial in the host is important, the biologic mechanism denominated as “host response” remains the object of several actual studies as a fundamental knowledge to approach biomimetic implants with very specific biologic action.

INTRODUCTION

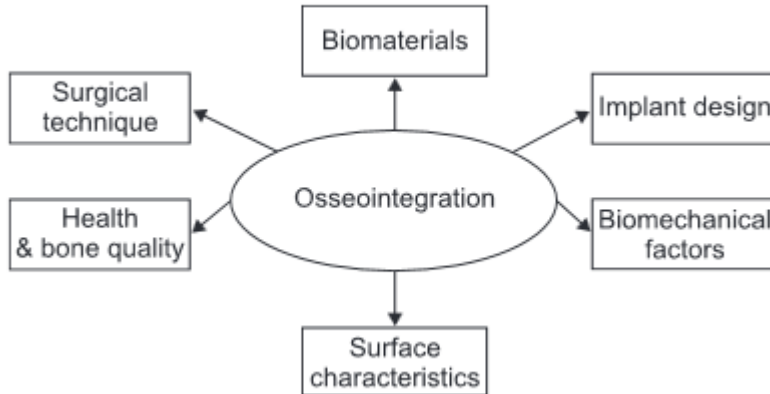


Figure 1.4 – Elements that affect implants osseointegration process.³²

The classical explanation of host response to injury was described as a sequence of steps starting with the injury, then protein adsorption, severe inflammation, chronic inflammation, foreign body reaction, granulation tissue formation and finally encapsulation^{21,33}. This description is associated with the biomaterials that seek “inertness” and a direct host response of fibrous connective tissue encapsulation. Recent concepts describe the satisfactory host response as an intimate adjunction of bone to biomaterial without encapsulation denominated as *osseointegration*. For the achievement of this target several biologic mechanisms must take place, breaches between bone and implant must be filled and bone damage must be repaired.

Basically, a fracture bone healing has three stages^{34,35,26,9}.

Reactive phase or inflammatory phase

Bleeding from the bone and adjacent tissues results in haematoma formation and a clot of insoluble fibrin is created. The clot arrangement is a structure that stimulates the influx of migrating cells (neutrophils, lymphocytes, monocytes, macrophages, mast cells, platelets) that release cytokines (polypeptides that play an important role in the immunological response, inflammation process and hematopoiesis), these cytokines otherwise attract stem cells to the injury site.

This environment motivates a capillary permeability increase, chemotaxis and small vessel dilatation. Due to the interfragmentary motion granulation tissue is formed to reduce strain through the fracture site. Osteoclasts start to resorb the dead bone and phagocytes also eliminate other necrotic tissue.

Osteoclasts are giant nucleated cells that attach to bone with integrins (heterodimeric adhesion receptors that mediate cell-matrix and cell-cell interactions³⁶) and secrete hydrogen ions and enzymes to dissolve the bone mineral and disarrange the matrix. The decomposition process of osteoid matrix by osteoclasts and supported by macrophages allows the release of *growth factors* (polypeptides that act as modulators of several cellular functions as growth, differentiation and proliferation) contained within the matrix.

Reparative phase

Cartilaginous callous is formed and sustain the fracture, then collagen type II is produced in the fracture healing followed by collagen type I expression as new bone. Once this cartilaginous bone mineralizes, woven bone is generated by the action of chondrocytes (mature cartilage cells) and osteoblasts. The chondrocytes become hypertrophic, calcify and die, allowing an angiogenesis process to take place, on the other hand, over this collagen framework left by the chondrocytes the osteoblasts establish woven bone.

Osteoblasts are mononucleated cells responsible for regulation of osteoclasts and deposition of bone matrix.

Bone morphogenetic proteins (BMP's) are important on the regulating process of osteoblastogenesis and stimulation of bone matrix formation by mean of their regulatory action on growth, differentiation and apoptosis of several cell types. Their regulatory effect depends on the cellular target, its differentiation stage, the local concentration of ligand and interaction with other proximate factors. The extracellular matrix is the main source of BMP's and their creators are osteoprogenitors, mesenchymal cells, osteoblasts and chondrocytes. Within BMP's family, there are several

INTRODUCTION

proteins that are structurally and functionally similar; nevertheless, each one plays a different role and have individual temporal expression pattern during the fracture repair process³⁷.

Remodeling phase

In order to restore the biomechanical properties of injured bone, the initially formed woven bone is remodeled into lamellar bone through stimulation of osteoclast activity by RANK (signaling receptor) ligand secretion from osteoblasts in the repair callus. RANKL is the ligand and activator of RANK, which is an osteoclast surface receptor and otherwise tips the activation of some nuclear factors and macrophage colony stimulating factors that stimulates the differentiation and activation of osteoclasts.

The remodeling process is a balance between hard callus resorption by osteoclasts and lamellar bone deposition by osteoblasts regulated by osteocytes and several signaling pathways and molecules. Osteoclasts, osteoblasts and RANK altogether represent the mediators of remodeling, nevertheless many other signaling molecules and messenger molecules play an important role on the biologic mechanism^{9,37}.

An extensive explanation of the biologic steps, molecular activity and effects of the biologic mechanisms that entails an implant osseointegrative process is described in a previous work of Tejero and co-workers⁹.

DENTAL IMPLANTS

Endosseous dental implants are a common clinical practice and have been used on dental, oral and maxillofacial surgery for more than thirty years³⁸. In a previous work³⁹, dental implants were defined as “Alloplastic materials embedded in the maxilla and/or mandible for the management of tooth loss and to aid replace lost orofacial structures as a result of trauma, neoplasia and congenital defects”.

Two concepts must be clear to better understand the clinical practice of endosseous dental implants, the terms *Osseointegration* and *Biocompatibility*.

Osseointegration was previously described as the satisfactory host response with an intimate adjunction of bone to biomaterial without encapsulation.

Ratner described in 2011⁴⁰ that *Biocompatibility* is the ability of a material to locally trigger and guide the healing process (in absence of fibrotic tissue), reconstruction and tissue integration. What is more, he separate the concept biocompatibility associated with materials that seek to integrate on the host tissue by a regenerative process from the concept *biotolerability*, related with permanent medical implants that aspire to be present in the host body for long periods of time with minimal degree of inflammatory reaction^{40,21,41}.

The successful use of dental implants on management of tooth loss is due to their early osseointegration and many clinical studies reveal that the failure of osseointegrated implants is usually related with bone weakening or loss at the periimplant region and not with a mechanical failure of the artificial structure⁴².

The first accepted material by clinical experts used on dental implants that accomplish an appropriate osseointegration was commercially pure titanium³⁸. At the present time, other materials as tantalum, niobium, gold, titanium alloys, chrome alloys and ceramic materials are used and also attain positive and stable results.

INTRODUCTION

Table 1.1 – Mechanical properties of metallic materials and cortical bone^{8,43}.

Metallic Materials	Young's modulus (Gpa)	Ultimate tensile strength (Mpa)	Fracture toughness (MPa m)
CoCrMo alloys	240	900–1540	around 100
316L stainless steel	200	540–1000	around 100
Ti alloys	105–125	900	around 80
Mg alloys	40–45	100–250	15–40
NiTi alloy	30–50	1355	30–60
Cortical bone	10–30	130–150	2–12

There are some crucial factors for the success of a dental implant as *biocompatibility*, design, surface properties, patient health and surgical/prosthetic practice. Regarding the hardware design, a thread form and turned surface are accepted as the most proper forms for a favorable osseointegration outcome.³⁸

The main dental implants used for tooth replacement are endosseous prosthesis produced as a single unit, with screw or cylinder shape, placed within a drilled space inside dentoalveolar bone (Figure 1.5).³⁹

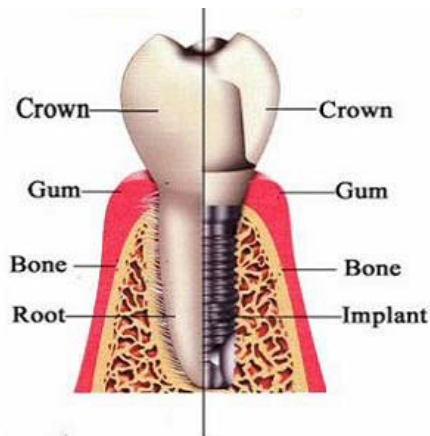


Figure 1.5 - Structure of tooth situation (left) and structure of dental implant (right).

Titanium and alloys are the most used materials for orthopedic and dental implants because its mechanical properties are very similar to those of bone (Table 1.1 and Table 1.2) and its proven osteoconductivity^{47,48,50–8}. The chemical composition of titanium implants can differ according to their

bulk composition and surface treatments, usually the materials used are commercially pure titanium (cpTi) that have purity ASTM degrees classified from 1-4 according to oxygen, carbon and iron content and grade 5 titanium alloy - Ti6Al4V^{10,46}.

Most of the commercially available dental implants are made of cpTi grade 4 because is the stronger of the four pure grades. Also Ti6Al4V is extensively used because of the greater yield strength and superior fatigue properties in comparison to cpTi grades^{10,46}.

Table 1.2 - Smooth (unnotched) fatigue strength of orthopaedic implant alloys.⁸

Alloy	Test condition ^a	Fatigue limit at 10 ⁷ cycles/Mpa	Fatigue limit/yield strength
α microstructure cp Ti (grade 1) cp Ti (grade 2) cp Ti (grade 3 and 4)	RBF (R= -1,100Hz) RBF (R=-1,100Hz) RBF (R=-1,100Hz)	88 215 430	0,5 0,8 0,6
α - β microstructure Ti-6Al-4V Ti-6Al-7Nb Ti-5Al-2,5Fe Ti-15Mo-5Zr-3Al	Axial (R= -1,292Hz) Axial (R= -1,292Hz) RBF (R= -1,60Hz) RBF (R= -1) RBF (R= -1) RBF (R= -1,100Hz)	500 330 610 500-600 580 560-640	0,6 0,4 0,7 0,7 0,8 0,5
β microstructure Ti-13Nb-13Zr Ti-12Mo-6Zr-2Fe (TMZF) Ti-15Mo-3Nb-0,3O (21SRx) TNZT TNZT-0,4O	RBF (R= 0,1,60Hz) RBF (R= -1,67Hz) RBF (R= -1,60Hz) RBF (R= -1,60Hz) RBF (R= -1,60Hz)	500 525 490 265 450	0,6 0,5 0,5 0,5 0,5
Stainless steels and Co-alloys 316L CoCrMo (cast) CoCrMo (wrought)	Axial (R= -1,120Hz) Axial (R= -1,100Hz) Axial (R= -1,20-100Hz)	300 200-300 400-500	0,5 0,5-0,6 0,5-0,6

^a RBF - rotating bending fatigue

The surface properties of an implant are a key factor for a good interaction with the biological environment and there are four surface properties that play a crucial role on bone formation, which are composition, surface energy, topography and roughness^{45,47}.

INTRODUCTION

Titanium is a naturally reactive metal, in contact with air and/or aqueous medium forms spontaneously a dense oxide film (TiO_2) at the surface, which can be reformed at body temperatures and in contact with physiological fluids leading to an excellent corrosion resistance. This TiO_2 passive layer is the real contact surface with the physiological environment and it is thought that is the real accountable for the “biocompatibility” granted to titanium dental implants⁸. In other studies is mentioned that the surface roughness of bone is approximately 32 nm which value is contained on the nano-size range 1-100nm (10^{-9} m), what is more, it is mentioned that appropriate bone responses occur at nanostructured surfaces tested in-vitro and in-vivo^{44,48}. The amorphous or nanocrystalline titanium oxide films usually present a thick range of 3-7 nm and can exist on different crystallographic forms and stoichiometry (Table 1.3 and Table 1.4). TiO_2 forms rutile, anatase and brookite are the most common crystallographic structures; nevertheless, rutile and anatase are the most studied forms by surface science⁴⁹. The treatment performed on the titanium surface is one of the most critical factors that determine the structure of the oxide layer⁵⁰.

On the border of TiO_2 surface there are hydroxide ions (OH^-) attached to metal and hydro-complexes of multivalent cations with amphoteric properties. In an aqueous medium with neutral pH the titanium surface show a slight negative charge caused by deprotonation of acidic hydroxides, even though alkaline hydroxides and a part of unreacted acidic hydroxides remain on the surface in a neutral state⁵¹.

On the other hand, it was stated that the TiO_2/Ti interface has an O/Ti concentration ratio that became smaller from the surface oxide film to the bulk, this high affinity of titanium to oxygen is beneficial for the regenerating process of the protective oxide layer (Figure 1.7)^{51,52}. The bioactive properties of titania (TiO_2) are so marked that many studies were made to use this material as a biologic additive to enhance biomaterials performance^{53,54,5,44,55,23,56}.

Table 1.3 – Oxide forms on titanium and alloys⁵².

Material	TiO ₂	Al ₂ O ₃	Nb ₂ O ₅	MoO ₃ /MoO ₂	ZrO ₂
CP Ti	Yes	Yes	No	No	No
Ti-6Al-4V	Yes	Yes	No	No	No
Ti-5Al-2,5Fe	Yes	Yes	No	No	No
Ti-6Al-7Nb	Yes	Yes	Yes	No	No
Ti-15Mo-5Zr-3Al	Yes	No	No	Yes	Yes

Table 1.4 – Properties of titanium oxides⁵².

Name	Formula	Ti-O Bond length (Å)	Density (g/cm ³)	Color
Anatase	TiO ₂	1,91	3,90	White
Brookite	TiO ₂	1,84 – 2,03	4,13	x
Rutile	TiO ₂	1,988	4,27	x
Ti Sesquioxide	Ti ₂ O ₃	x	4,486	Purple-Violet
Ti Oxide	TiO	x	4,888	Gold/Bronze

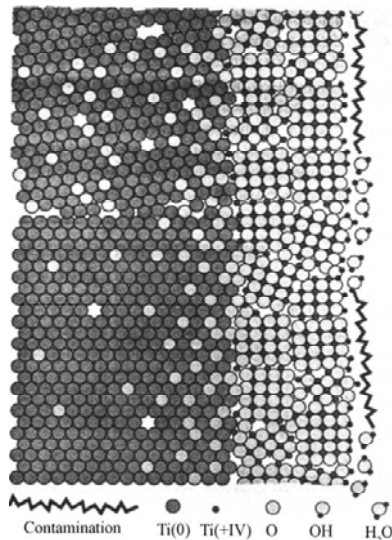


Figure 1.7 – Schematic view of the protective oxide layer on pure titanium⁵¹.

INTRODUCTION

NEW STRATEGIES FOR IMPROVEMENT OF BIOMATERIALS PERFORMANCE

Despite the fact that titanium and alloys have a very high resistance against corrosion in comparison with other metal biomaterials as stainless steels and cobalt-based alloys, the low wear resistance and the possibility of vanadium and aluminum release from Ti6Al4V alloy may lead to aseptic loosening during long term implantation^{8,57}. It was mentioned on bibliography that the oxide layer of titanium alloys can be broke by externally applied stresses and until the restore process is completed some material loss can arise⁸.

Commercial pure titanium (cp Ti) is still chosen for dental applications where corrosion resistance is most appreciated other than mechanical properties, nevertheless, nowadays the improvement of biomaterials performance is sustained on innovative strategies with a direct and specific biological action on cells behavior, with the ability to modulate the release of bioactive molecules and drugs and with the ability to conduct the host response.

With the access to incoming analysis techniques and the knowledge of more specific biological mechanisms that play a major role on the bone regenerative process and of implantology science many surface modification methods arise and are study subject of many researchers.

Taking into account a previous work developed by Arzt⁵⁸ about the structured contact elements that mediate the adhesion mechanism to surfaces of some insects and the strategy of mimicking those mechanism on a micro and nano scale to produce bio-inspired attachment structures leads to an interesting classification of implants design principles⁹:

Hierarchy systems – several natural structures have a complex organization of successive layers that combine organic and inorganic portions leading to new balanced properties different from the original ones. In bone, cells and sheets of mineralized collagen are the precursors of several microstructures.

Chemistry and water affinity – many materials have the ability to interact with aqueous environment, regulating some of their properties or simply generating the perfect environment for other events to take place. The water affinity of implants surface is extremely relevant as one of the first events on healing process is protein adsorption on surface.

Multifunctionality – in nature, many structures readapt themselves to play different roles and perform more than one single function. Non-linear properties modifications lead to multifunctional materials with interesting properties, bone for instance, is a flexible structure that can resist heavy loads. Bone tissues and biomolecules play different roles in many events of bone remodeling process, sometimes activated by environmental conditions or by other surrounding elements can change and adapt their conformation according to biologic requirements.

Environment bias – This concept associated with the before mentioned multifunctionality of natural systems represent a perfect coordinated natural mechanism between environmental circumstances and elements with interpretation capacity. In the specific bone case, it was stated that mechanosensitive cells “read” the environmental messages/demands and activate or reorganize many mechanisms and biologic elements.

Self-renewal – For implantology, it stills remain a big challenge to calk the natural mechanism of self-repairing seen in many natural systems, as the bone tissue.

Limited lifetime and biocompatible synthesis conditions – biologic elements are synthesized at ambient conditions and usually are biodegradable. For instance, the display of biodegradability of the extracellular matrix units is the precursor of an important research line on biomaterials as it works as a vehicle to other biologic processes like liberation of cell-signalling molecules or preparation of supportive structures to more complex demands.

These principles sustain the biomimetic properties required nowadays for new biomaterials and pursuit for many actual research works.

INTRODUCTION

TITANIUM DENTAL IMPLANTS SURFACE MODIFICATION

The aim of all modification techniques applied to titanium surfaces is the improvement of bone-cells interaction with a final clinical purpose of a good bone-implant contact and reduction of the implant integration time.

Titanium surfaces are relatively inert due to the passive oxide layer (TiO_2) naturally formed in contact with air or aqueous medium, as a result, the binding process with bone becomes a hard and long term process⁵⁹.

There are three focal types of titanium surface modification, morphological, physicochemical and biochemical⁵⁹ (Figure 1.8).

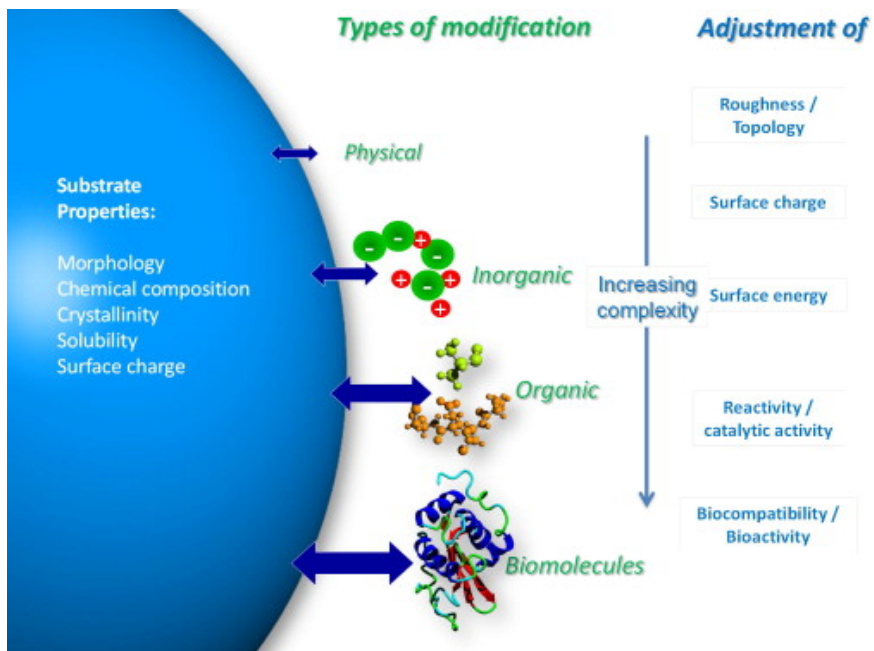


Figure 1.8 – Implants surface properties, types of treatments and resultant properties affected⁵⁶.

Many researchers advocate the direct and positive results that surface roughness have on the osseointegration rate of titanium dental implants^{10,44,45,9,48,59}. Rough machined surfaces stimulate bone anchoring and biomechanical stability, otherwise than bone cell attachment.

Surface roughness can be classified into three levels taking into account the range, macro: $>10\ \mu\text{m}$, micro: $1\text{--}10\ \mu\text{m}$, and nano: $1\text{--}100\ \text{nm}$ (Figure 1.9)¹⁰.

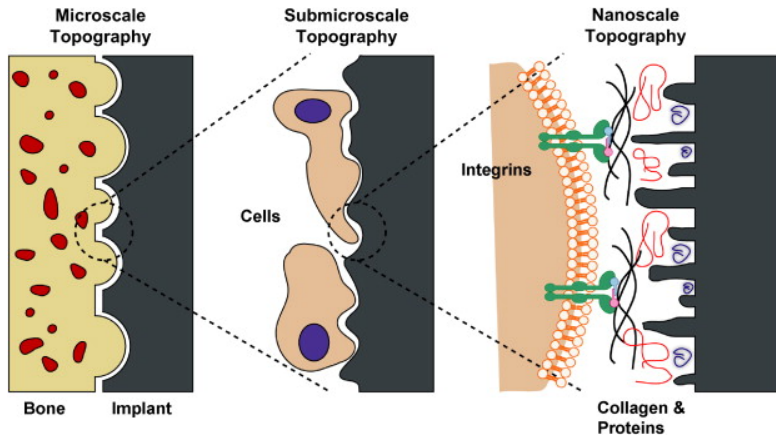


Figure 1.9 – Range size of titanium dental implants modification⁶⁰.

Modifications on physical and chemical properties of implants surface, for instance chemical composition, surface energy and hydrophilicity search for an appropriate environment to biomolecular adsorption and consequent cell adhesion.

On early studies, the qualification of implant surfaces properties was divided into three categories: mechanical properties, topographic properties and physicochemical properties and it was referred that they are not independent of each other, they are related and a change on any of those properties affects the other(s)^{61,44}.

Titanium surface modification techniques are listed on Table 1.5.

INTRODUCTION

Table 1.5 – Titanium dental implants surface modification: types, methods and techniques^{59,9,62}.

Type of surface modification	Method	Techniques
Morphological and physicochemical	Mechanical	Plasma spraying ^a
		Particle blasting ^a
	Chemical	Acid etching ^a
		Anodization ^a
		Peroxidation
	Others	Lithography
Biochemical	External coatings	Osteoinductive biomolecular cues (cell adhesive proteins and growth factors like BMP's)
		Microscale and nanoscale coatings of hydroxyapatite (HA) - calcium phosphate – alumina with bioactive molecular cues, osteoinductive growth factors and antibacterial drugs
		Organic nanoscale SAMs (Self Assembled Monolayers)
		Bioactive/biodegradable hydrogels
		Antibacterial agents or antibacterial drug delivery directly from titanium surface

^a – range of micro surface topography

Morphological and Physicochemical modifications:

Several morphological methods have been developed to provide rough surfaces with a direct and/or indirect impact on cell adhesion mechanisms promoting a better bone-implant contact and consequently a good mechanical junction between implant and surrounding tissues^{10,44,11}.

Titanium plasma spraying (TPS) is a technique sustained on powders of titanium injected hooked on a plasma torch at high temperatures. In those conditions, titanium melts in the plasma jet and adheres to the surface forming a coating with 30 - 50 μm and a roughness about 7 μm ^{10,63}. A previous *in vivo* study about the influence of different surface treatments

of titanium implants on bone integration when implanted on metaphyses of tibia and femur of miniature pigs show that 30-40% of bone-implant contact was measured for sandblasted implants and plasma sprayed implants⁶⁴.

Nevertheless, other methods listed subsequently for morphological surface modification show better results^{64,65,10}.

Particle blasting, also called Sandblasting (SB) is basically the projection of abrasive particles as Al_2O_3 , TiO_2 , SiO_2 , β -TCP (tricalcium phosphate) and HA (hydroxyapatite) through a nozzle at high velocity dragged by compressed air. The surface roughness will be totally dependent on the size of the particles and for dental implants the typical seek range is 0,6 – 3 μm ^{10,9}. The blasting particles must be chemically stable with proved biocompatibility so the impact with the metallic implant surface leaves craters of plastic deformation on the contact sites. Alumina (Al_2O_3) particles are difficult to eliminate from the turned surface so remains the drawback of some ceramic particles release and possible disturbance of the osseointegration process. Calcium phosphates are special blasting materials due to their chemical stability, osteoconductive properties and bioresorbability.

Several *in vivo* experiments prove that roughening titanium dental implants by blasting methods with any of the upper cited particles improve bone-implant mechanical fixation but does not have a clear role on biological events of bone regenerative process^{64,66,67,10,9}.

Acid etching methods to induce micro roughness are performed by immersion of titanium implants on strong acids dissolutions at elevated temperatures (above 100°C) for a specific period of time. Usually, acid etching is implemented as a post-cleaning step after blasting treatments to dissolve substrate grains and refine surface roughness, respecting as far as possible the native state of blasting surface.

Some previous biological studies refer that blasted surfaces treatments combined with acid etching finishing treatments reduce the

INTRODUCTION

osseointegration time of titanium dental implants improving the host recovery^{10,44,11,45}. HCl and H₂SO₄ dual acid etched surfaces yield the attachment of fibrin scaffold and osteogenic cells adhesion displaying osteoconductive properties due to the specific topography obtained with these treatments and probably also due to some changed surface chemical properties as wettability^{10,68,69}. On the other hand, studies related to titanium dental implants treated with HF show promising results caused by improvements on bone-implant contact and osteoblastic differentiation. The new physicochemical surface properties achieved (some specific examples are soluble TiF₄ species, wettability, among others) demonstrate *in vitro* and *in vivo* enhancements on osteoblastic differentiation and on interfacial bone formation. Nevertheless it was not clear the exact surface property affected by fluoride ion modification that cause positive consequences on biologic mechanisms of bone regeneration⁷⁰. Although the acid-etching treatments show promising results on topographic modification and perhaps on surface bioactivity, chemical treatments might affect titanium biomechanical properties.

Anodization is a complex method to achieve modifications on the titanium oxide layer, changing its microstructure and crystallinity. The technique is supported by an anodic voltage applied on the implant surface submerged in an ionic solution (usually H₂SO₄, H₃PO₄, CH₃COOH, HNO₃, HF) above the electrical breakdown of the metallic oxide layer, this polarization leads to a thicker TiO₂ (more than 1000nm) layer with micro sized roughness^{10,9}. The characteristics of the final oxide layer will be defined specially by applied voltage, electrolyte composition, temperature, time of exposure and initial surface situation. The resulting anodized implants surfaces cause changes on the biomechanical performance of the prosthesis, as stated on previous studies where higher grades of clinical success were detected in comparison to turned surfaces with similar shapes^{10,71}. The proposed mechanisms by which these anodized treated surfaces improve biomechanical performance of implants were mechanical interlocking through bone ingrowth on pores and biochemical linking^{72,10}.

Another chemical treatment is peroxidation with H_2O_2 , this method is usually applied before the acid treatment⁴⁴. Some studies state that the gel layer formed on a titanium surface after H_2O_2 /HCl treatment (more than 0,2 μm) treated with a specific heat treatment leads to a nanostructure topography that show *in vitro* apatite deposition and bioactivity⁸³. Other studies related with the adsorption of peptides on implants surfaces treated by peroxidation show an increase on the amount of adsorbed RGD peptides and on mineralization⁷⁴.

Other process used to achieve nanotopography on metallic implants is lithography; it is an optical method that usually entails much previous work prior to clinical implementation. Using laser irradiation micropatterning can be achieved with a non-contact method and without contamination, nevertheless some limitations related with debris formation, mechanical deformation and physical/chemical modification of titanium dioxide film properties represent an handicap for the use of this technique^{75,76}.

The usual surface roughness attained with the application of some upper cited morphological and physico-chemical surface modification methods are listed on Table 1.6.

Table 1.6 - Surface properties of turned titanium dental implants.¹⁰

Type of implant	Surface roughness (μm)	Contact angle ($^\circ$)
cpTi (machined and polished)	Ra = 0,22 \pm 0,01	55,4 \pm 4,1
Ti6Al4V (machined and polished)	Ra = 0,23 \pm 0,01	56,3 \pm 2,7
TPS (titanium plasma spraying)	Ra = 7,01 \pm 2,09	n.d.
SLA (blasting + acid etching)	Sa = 1,15 \pm 0,05	138,3 \pm 4,2
Modified SLA	Sa = 1,16 \pm 0,04	0
Plasma-sprayed HA coating	Ra = 1,06 \pm 0,21	57,4 \pm 3,2
Biomimetic CaP coating	Ra = 1,83 \pm 0,64	13,4 \pm 0,17

INTRODUCTION

Biochemical modifications:

The biochemical modification main objective is to promote biofunctionalization of metallic implants surfaces through a platform of bioactive proteins, enzymes and peptides that encourage specific cell responses.

The use of growth factor's as a biomimetic approach represents an interesting manner of improving peri-implants establishment. Cytokines and chemokines (growth factors) play a crucial role on the regenerative process, maintenance and development of tissues because they run the mechanisms that inform the destiny of many cells and their interactions. Although many studies report *in-vitro* and *in-vivo* experiments with growth factor's BMP's, VEGF, bFGF, IGF, TGF- β , GDF, PDGF-BB, among others, not all of them achieved positive results^{9,77,44,20,62,78,17}. The manner by which they are incorporated and presented/delivered on the action site affects significantly their performance and effects on biological activity. This strategy is very susceptible to dose variations and to the short-range activity of growth factors in soluble form, consequently a perfect spatio-temporal adjustment must be achieved for a correct use of this technology⁹.

Although the two first biochemical strategies (Osteoinductive biomolecular cues and Microscale and nanoscale coatings) presented on Table 1.5 about the biochemical modification techniques are presented as separated strategies they could be inserted in a single group as sometimes are applied at the same time and could be categorized as multifunction bioactive coatings.

The osteoinductive biomolecular cues method is based on the attachment of certain biomolecules to the titanium surface through adsorption or covalent bonding. Usually adsorption is supported by weak Van der Waals forces or electrostatic interactions.

As cited previously in this work, integrins (heterodimeric proteins) sited on the membrane of specific cells recognize defined aminoacid sequences present on the peptide chains of subunits of extracellular matrix (as collagen, fibrin or non-collagenous proteins) and link the extracellular matrix (ECM) with the actin skeleton of cells (the organizational flexibility of actin skeleton control and easily change cell shape⁷⁹). The association of integrins at specific points of cells consolidate the attachment of ECM with actin skeleton otherwise than establish the signals to trigger important processes on bone remodeling as migration and differentiation. So, the strategy of producing biochemical surface modification of titanium dental implants by means of bioactivation of the metallic inactive surface with ECM components, specially structural fibrous proteins and cell adhesive proteins also denominated “biopolymers” (some examples are fibrin, collagen, and non-collagenous proteins), represents an interesting biomimetic tactic^{9,80,81}. Some *in-vitro* studies test out this approach as it was found that adsorbed ECM proteins (fibronectin and vitronectin) on titanium surface improve osteoblastic performance increasing adhesion, proliferation and differentiation compared to non-treated titanium surfaces^{82,59}. In addition, experiments with collagen adsorbed on Ti6Al4V surfaces refer improvements on mineralization ratio of rat osteoblasts and collagen synthesis^{83,84,59}. One advantage of this fixing process is that the involved fragile forces are unlikely to alter the conformation state and functionality of adsorbed biomolecules, nevertheless it is problematic the control of release kinetics, molecular orientation and easy wash out. Some experts studied the physical entrapment of collagen and cell adhesive aptamers (highly specific cell binding nucleic acids) by partial incorporation on the oxide layer thickened by anodization^{82,85}. This new process is an interesting proposal to ensure a stronger fixation of biomolecules and lengthy activity.

From now on the presented techniques on Table 1.5 as biochemical surface modifications pursue a stable and controllable manner of fixing biomolecules using external added elements by means of different technologies, micro-nano coatings, SAM's or hydrogels to link the inactive

INTRODUCTION

metallic surface with specific biologic elements. Generally, the nature of the biomolecules used to functionalize the metallic surface determines the type of technology adopted.

Silanization is a process that uses a silane molecule as a union element between a metallic substrate and biomolecules. Silane hydrolysable groups (-O-R) react with hydroxyl groups (-OH) of TiO₂ surface establishing covalent bondings with the metallic surface, otherwise, usually the organofunctional termination(s) (unreactive chains) of silanes are susceptible of reacting with peptide motifs and other osteoinductive growth factors immobilizing this way biomolecules on titanium surfaces (Figure 1.10).

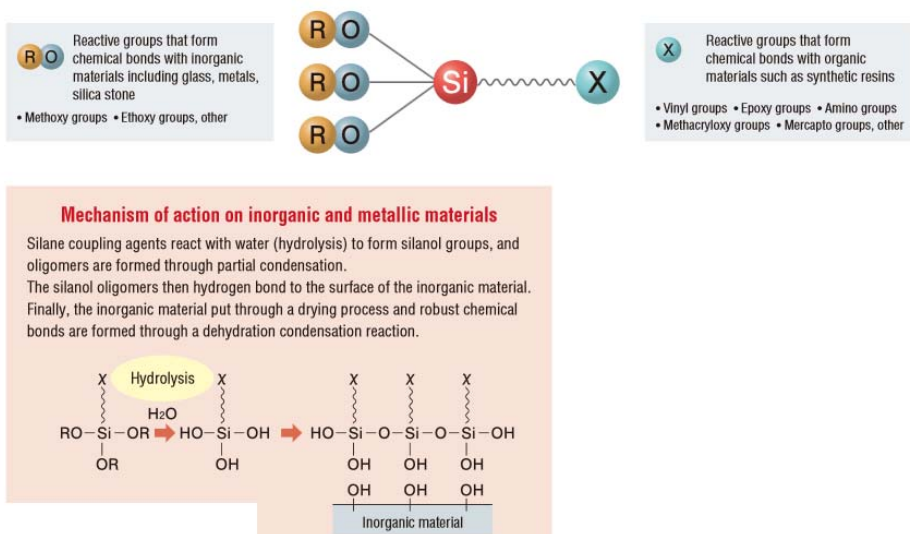


Figure 1.10 – Silanes molecular structure and mechanism of union with a metallic substrate⁸⁶.

The silanes used as cross-linkers with a positive impact on bone regenerative process are several: 3-chloropropyl-(triethoxy)silane (CPTES)⁸⁷, 3-Methacryloxypropyltrimethoxysilane(MPS), 3-acryloxypropyltrimethoxysilane (APTMS), 3-isocyanatopropyltriethoxysilane (ICPTES), 3-

glycidoxypropyltrimethoxysilane (GPTMS), 3-mercaptopropyltrimethoxysilane (MPTMS) among others^{88,89}.

Many studies employ APTES (3-aminopropyltriethoxysilane) as a immobilization medium of biomolecules, the interest on this silane is the functional $-NH_2$ group with affinity to negatively charged species⁹⁰⁻⁹². A previous *in-vitro* study of APTES functional coating on titanium surface to covalently attach biomolecules revealed no promising results as HOS (human osteosarcoma) cell adhesion responses to the silane coating was poor; nevertheless, when L-Cysteine protein was incorporated to APTES coating the cell responses were similar to the ones verified on control samples⁹¹.

Although silanization is a simple technique and cost-effective there are many unknown parameters related with reaction conditions effects on the final structure, additionally, the stability of those coatings is scarcely studied on aqueous environments for long periods of time⁵⁶.

Other approach, not so extensively used as silanization, of chemical union between biomolecules and metallic substrate is the bonding between TiO_2 surface hydroxyl groups and phosphonates⁹. Bisphosphonates are species that affect bone resorption and soft tissue calcification, *in vitro* and *in vivo* studies validate their ability to alter the morphology of osteoclasts^{93,94}. Inhibiting the activity of osteoclasts, direct and interesting effects on bone regeneration and tissue-implant border establish another accessible strategy to dental implantology⁹⁵.

Micro-nano coatings, SAM's and hydrogels besides hold on biomolecules have many times a second purpose, be a scaffold and generate a suitable environment to adhesion and establishment of cells, proteins and other bioelements performers on bone regenerative process.

One of the main constituents of bone, about 70%, is an inorganic material with a similar chemical composition to hydroxyapatite (HA). Generate a stable and well adhered coating of this bioceramic on titanium dental implants surfaces is study subject of many researchers as it can act as a

INTRODUCTION

matrix for osteogenic cell attachment and growth besides own proven biocompatibility^{10,59,44,96}. To hold on HA to the titanium passive surface several techniques were investigated, plasma spraying, sol-gel coating, electrophoretic deposition, ion implantation, biomimetic precipitation, pulsed laser deposition and grid blasting^{62,59}. The coatings of HA and calcium phosphates are techniques used to trap noncollagenous proteins (fibronectin) and peptide sequences (BMP's) on a porous scaffold^{9,97,98}. An example of a multifunctional layer is the one proposed by Durrieu et al. that developed a biomimetic strategy to attach RGD onto HA surfaces by silanization with APTES⁹⁹.

Another strategy for biochemical modification is the use of organic nanoscale self-assembly monolayers (SAM's). Alkanephosphonic acids easily react with metal oxide surfaces and form a layer of ordered alkane chains making easy the reaction with organic bioactive elements^{100,89,9,101}. The alkylsilanes also show strong adhesion to metal surfaces due to chemisorption of metal alkoxide on a hydroxylated substrate, besides the reactive functional organic groups attached on silanes can show a positive outcome on cellular behaviour⁸⁹.

Hydrogels are usually three-dimensional polymer networks that retain large proportions of water and swell remaining insoluble due to chemical/physical cross links established by individual polymer chains^{59,102,103}. There are many natural polymers and synthetic monomers used on hydrogels production (Table 1.7) attached on metal surfaces; nevertheless, they differ from each other by water absorption abilities, hydrophobic and hydrophilic grade, degradation rate and mild fabrication conditions. Natural hydrogel polymers also termed "biopolymers" (some of them upper cited as ECM elements used as biomimetic tactic on metallic surfaces treatments) offer some advantages as biocompatibility, biodegradability, scaffolds for supporting cellular activity and ability to incorporate biomolecular cues, however, many times they do not show a strong and mechanically stable structure to support the incorporation of

bioactive molecules. On the other hand, synthetic monomers can be designed with defined structures, degradation rate and functionality grade^{103,59}. Polyethylene glycol (PEG) is one of the most extensively studied polymers, the interest about this hydrogel started on the 1960's and 1970's due to its good results on biocompatibility and resistance to protein adsorption^{59,102,104}. Many cell adhesive peptides have been incorporated to PEG hydrogels in order to endow the polymer network with biologic activity. Some of them with origin on the ECM proteins: a) fibronectin - RGD, KQAGDV, REDV, PHSRN, b) laminin - YIGSR, LGTIPG, IKVAV, PDGSR, LRE, LRGDN, IKLLI, c) collagen – DGEA, GFOGER and d) elastin – VAPG. In addition, enzymes (enzyme-sensitive peptides sequences) have been incorporated to PEG hydrogels to regulate the hydrolytic degradation and growth factors (GF's) as VEGF, bFGF, EGF, TGF- β , BMP, and many other bioactive elements with specific effects on biologic mechanisms of bone healing and implant attachment¹⁰⁴. Due to the long study period about PEG hydrogels and their bioactive modification as a strategy to award the passive metallic surfaces with biologic undertakings many positive results were achieved on biologic experiments *in vitro* and *in vivo*, for further information the reader is referred to a review on the subject¹⁰⁴.

Table 1.7 – Hydrogel natural polymers and synthetic monomers¹⁰³.

Hydrogel polymers origin	
Natural	Synthetic
Chitosan	Hydroxyethyl methacrylate (HEMA)
Alginate	<i>N</i> -(2-hydroxypropyl) methacrylate (HPMA)
Fibrin	<i>N</i> -vinyl-2-pyrrolidone (NVP)
Collagen	<i>N</i> -isopropyl acrylamide (NIPAAm)
Gelatin	Vinyl acetate (VAc)
Hyaluronic acid	Acrylic acid (AA)
Dextran	Methacrylic acid (MAA)
	Polyethylene glycol acrylate/methacrylate (PEGA/PEGMA)
	Polyethylene glycol diacrylate/dimethacrylate (PEGDA/PEGDMA)

INTRODUCTION

As a final approach on biochemical surface modification of titanium and alloys, the external coatings applied for transportation and delivering of drugs, for instance used as prevention practice against biofilm formation and periodontal diseases as periodontitis that can lead up to implant failure. The development of a surface with antibacterial and osteoconductive properties remains a challenge for biomaterials Scientifics, currently there are two main strategies based on materials that eliminate adherent bacteria or materials that repel bacteria.

The use of local disinfectants on titanium surfaces as antibiotics, fluorine, zinc oxide and silver ions are some of the additives used to eliminate bacteria. In a previous work about a zinc oxide (ZnO) and titanium oxide (TiO₂) coating, the antimicrobial performance of the contact surfaces was analysed and the results show a decrease adhesion of *S. epidermidis* and an increasing on osteoblast activity on both coatings making them suitable for their use on implants^{105,59}. Recent studies with silver based antimicrobials applied as coatings show promising results. Nanoscale modification of titanium with a sol-gel coating based on silver nanoparticles was studied and it was evaluated the antibacterial activity of the coating against *Aggregatibacter actinomycetemcomitans* (pathogen of dental pathology periimplantitis). As a result, the authors refer long term antibacterial properties and suggest the developed nanoscale surface modification as a promising strategy to prevent periodontal pathologies¹⁰⁶. Otherwise, it has been reported in a previous study about titanium surface modification performed with ion implantation with Ca⁺, N⁺ and F⁺ that F⁺ exhibited effective antibacterial activity against *Phorphyromonas gingivalis* (pathogen associated with dental periimplantitis) and *Actinobacillus actinomycetemcomitans* with no appreciated decrease on fibroblasts proliferation (L929 cellular medium)^{107,59}.

Much work was developed with vancomycin (antibiotic) attachment to titanium surfaces in order to improve the implants antibacterial properties. One of the suggested approach was the use of a PEG coating with incorporation of vancomycin, the coating was bactericidal against

Staphylococcus epidermidis through a release mechanism of unattached antibiotic species and direct bacterial elimination by covalently attached vancomycin^{108,59}.

Another strategy to prevent bacteria adhesion is the regulation of hydrophilicity associated with surface energy presented by some synthetic polypeptides that affects in some way the adhesion of early colonizers¹¹. An innovative peptide coating linked to a Ti surface by a silane structure (GL 13K obtained from parotid secretory protein) with antimicrobial properties was evaluated *in vitro* against *Phorphyromonas gingivalis* and show a clear decrease on bacteria in comparison with the control (uncoated eTi). The researchers attributed the antimicrobial effect to the electrostatic interference of the membrane of bacteria that show positively charged lysine residues and to the low surface energy presented on the coated Ti surface¹⁰⁹. Nevertheless it seems a delicate process as many other critical biologic mechanisms on bone regenerative process are affected by hydrophilicity, surface energy and surface electrostatic forces.

Nowadays, only a few nano-topographic surface modifications have been used to improve bone responses at commercial dental implants because of their ease of use and reproducibility^{48,44}.

On 2011 was published on Journal of Oral Implantology¹¹⁰ a study about the chemical and morphological surface properties of 14 dental implants available on market. The types of implants, manufacturers, surface treatment, morphological and chemical surface characteristics are listed in Table 1.8.

Table 1.8– Information of manufacturer and surface properties of 14 dental implants available on market.¹¹⁰

Type of implant	Manufacturer	Surface treatment	Morphological characteristics	Chemical characteristics
TiUnite	Nobel Biocare, Gothenburg, Sweden	Anodized surface	Microporosity. Smooth on nanoscale.	High quantity of phosphorus detected. Fluoride and sulfate contamination.
Ospol	Ospol, Höllviken, Sweden	Anodized surface	Microporosity. Smooth on nanoscale.	Calcium, sodium and phosphorus contamination.

INTRODUCTION

Kohno HRPS	Sweden & Martina, Due Carrare, Italy	Plasma spraying	Maximum microroughness. Smooth on nanoscale.	Fluoride, sulphur (as sulfate) and phosphorus (as phosphate) contamination.
Osseospeed	AstraTech, Mo" Indal, Sweden	Blasting with TiO ₂ particles and acid etching with hydrofluoric acid.	Moderated microroughness. Nanoroughness.	Residual levels of fluoride. Residual TiO ₂ particles.
Ankylos	Dentsply Friadent, Mannheim, Germany	Blasted and etched surface.	Moderated microroughness. Smooth on nanoscale. Heterogeneous surface.	Alumina particles (Al ₂ O ₃). Calcium, sodium, phosphorus (as phosphate), sulphur (as sulfate), fluoride, zinc and chloride contamination.
MTX	Zimmer, Carlsbad, Calif	Blasting with HA on a grade 5 titanium core.	Minimum microroughness. Smooth on nanoscale.	Calcium phosphate (CaP) impregnated at low level. Silicon contamination.
Promote	Camlog, Basel, Switzerland	Blasted and etched surface.	Moderated microroughness. Smooth on nanoscale. Homogeneous surface.	Zinc and calcium contamination.
BTI Interna	Biotechnology Institute, Vitoria, Spain	Etched surface.	Smooth on microscale. Smooth on nanoscale.	High levels of organic carbon species.
EVL Plus	SERF, Decines, France	Blasted and etched surface.	Minimal microroughness. Smooth on nanoscale.	Residual CaP. Alumina particles (Al ₂ O ₃). Residual fluoride contamination.
Twinkon Ref	Tekka, Brignais, France	Blasting on a grade 5 titanium core.	Minimal microroughness. Smooth on nanoscale.	Calcium impregnation. Alumina particles (Al ₂ O ₃). Organic carbon species. Silicon, sulphur (as sulfate), zinc and chloride contamination.
Ossean	Intra-Lock, Boca Raton, Fla	Blasted and etched surface with unknown postprocessing.	Minimal/moderate microroughness. Nanoroughness.	Calcium phosphate (CaP) impregnated at low level.
NanoTite	Biomet 3I, Palm Beach Gardens, Fla	Etched surface on a grade 5 titanium core and a final CaP discontinuous coating.	Smooth and flat on microscale. Nanoroughness (adhered nanoparticles). Heterogeneous surface.	Sulphur and fluoride contamination.
SLActive	ITI Straumann, Basel, Switzerland	Blasted and etched surface with final immersion in a sodium chloride (NaCl) physiological solution.	Moderate microroughness and rugged surface. Outside the casing the solution dries quickly on the surface and generates NaCl crystals causing a	NaCl crystals. Potassium, fluoride, calcium and phosphate contamination.

			nanotextured surface. Heterogeneous surface.	
Integra-CP/NanoTite	Bicon, Boston, Mass	Blasted and etched surface with a final coating with calcium phosphate ion-beam assisted deposition.	Flat on microscale. Smooth on nanoscale.	CaP layer. Sulphur and fluoride contamination.

The key mechanisms that explain the clinical success of titanium dental implants still unclear, however, it is accepted by scientific community that parameters as surface topography and chemical properties are crucial on the regenerative process of bone on dental implantation¹¹.

SOL-GEL COATINGS FOR BONE REMODELING

Sol-gel technique is an interesting technology to deposit nanoparticles and retain bioactive elements onto biologically passive surfaces, as titanium dental implants.

Some authors describe the sol-gel process as the “transformation of the molecular precursor into the final oxidic compound involving chemical condensation reactions in a liquid phase under mild conditions”¹¹¹. Some concepts definition related with sol-gel process are necessary for a better understanding of this technique.

A *sol* is a stable dispersion of colloidal particles (suspension of solid particles of 1-1000nm with interactions mediated by short-range forces such van der Waals and surface charges) in a liquid¹¹².

A *gel* is a continuous three dimensional network (agglomeration of colloidal particles) that encloses a liquid phase¹¹².

Sol-gel coatings were developed as protective layers for metallic materials, additionally, the integration of organic groups gave them flexibility generating films perfectly adhered to the surfaces without micro-

INTRODUCTION

cracks^{113,114}. This methodology gives place to amorphous or crystalline oxide coatings depending on the chemical reactions that takes place and the heat treatment used; all the same it is accepted as a simply process with mild production conditions.

The basic materials used to prepare the *sol* are usually metal-organic compounds with a structure $M(OR)_n$ where M represents the central network metal element and the most common are Si, Ti, Zr, Al and B¹¹⁵.

Although biomaterials research fall on the metallic compounds Ti and Si in an appreciable way, in this work Si compounds will be emphasized because is the base of the materials developed on the present work.

Silicon alkoxides with chemical composition $Si(OR')_4$ and $R_nSi(OR')_{n-1}$ are chosen monomers due to their ease and rapid hydrolysis. Organosilanes with non-hydrolysable organofunctional termination R_n (phenyl, amino, carboxyl, among others) are used as organically modified silicate materials (also known as ORMOSILs) and are the base of a creative development of new materials capable of solving relevant problems in many scientific fields as optics, catalysis, molecular recognition, chromatography, chemistry of conductive materials and many other applications^{116,113}.

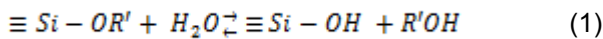
Due to the immiscibility between alkoxy silanes and water, an alcohol solvent is most of the times used as homogenizing element, though, it is possible to prepare gels without any external solvent as alcohol is a sub-product of the hydrolysis reaction preventing the liquid-liquid phase separation that may occur on the initial stages (eq. 1). The election of the solvent is usually related with the polarity, dipole moment and availability of labile protons. Water, alcohol or formamide are some examples of protic solvents (contain a removable proton) used to solvate polar tetrafunctional silicate species. Aprotic solvents (less polar) as dioxane and tetrahydrofuran are preferable in alkyl-substituted systems or incompletely hydrolyzed systems. Ether alcohols present both character, polar and nonpolar, what makes it appropriate when there are polar and nonpolar species in solution.¹¹²

The most common basic steps to deposit an organic-inorganic hybrid dense layer on substrates are the following (Figure 1.11):

Step 1 - Sol formation.

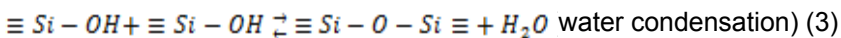
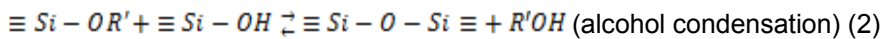
On this stage, mechanical mixing of low molecular weight alkoxysilanes in a solvent forms a colloidal suspension. The polycondensation of alkoxysilanes require hydrolysis and condensation reactions.

Hydrolysis



R' are alkyl hydrolysable groups C_xH_{2x+1}

Condensation



With reactions advancement Si-O-Si bonds are gradually formed and a colloidal submicrometer suspension or sol state is achieved. The size of colloidal particles and the type of network formed depends notably on pH, alcohol used as solvent and on alkyl hydrolysable groups ratio and type (R') on precursors structure¹¹⁷. For example, it was found on previous studies that tetraethylorthosilicate precursor on ethanol-water environment leads to silica particles on the range 1 - 50 nm^{118,119}.

Step 2 - Deposition of sol on a substrate. Gelation and drying.

Dip-coating method requires the dip of a support object into the colloidal liquid (sol) in totally well-defined conditions (speed, immersion time). The sol drainage during emerging leads to *gelation*, as the viscosity of the sol changes due to the interconnection of the colloidal species forming a continuous, rigid and porous network and achieving gel state. Although the dip coating is the preparation method emphasized on this work, other coating techniques can be used, as spin coating and spray coating to set

INTRODUCTION

sol-gel films on metallic surfaces¹¹⁵. On gelation stage, the final events are related with water and organic solvent evaporation from the cavities of the new formed solid mass, decreasing its volume. At this point, the shrank solid matrix acquires a new classification, *xerogel* or dried gel. During the drying phase usually larger pores are cleared but the smaller ones remain covered by solvent. This success is the cause of many irregularities on sol-gel coatings and monoliths, as the stress caused by pores internal pressure gradients leads to cracks and rupture of the solid network¹¹⁷.

Step 3 - Temperature treatments and densification.

Although the final propose of many sol-gel synthesized materials is the *xerogel* state it is necessary a final temperature treatment for densification of coatings, improvement of their characteristics and structure stabilization. On this stage pores are eliminated producing pore-free ceramic and this process is dependent on the treatment temperature, dimensions of the pore network, connectivity between pores and surface area. The used temperature must be high enough to cause sintering as the main objective of this final treatment is to collapse the pores driven by surface energy^{117,112}.

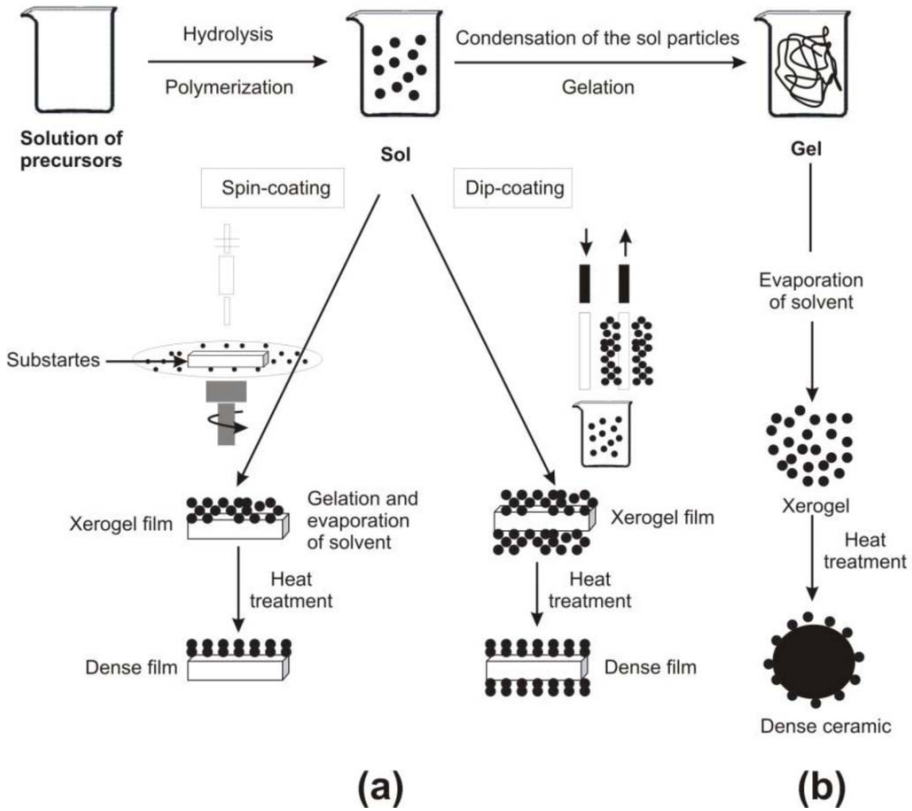
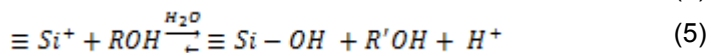
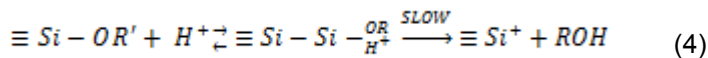


Figure 1.11 - Sol-gel process steps to make (a) dense films deposited on substrates and (b) dense ceramics.¹¹²

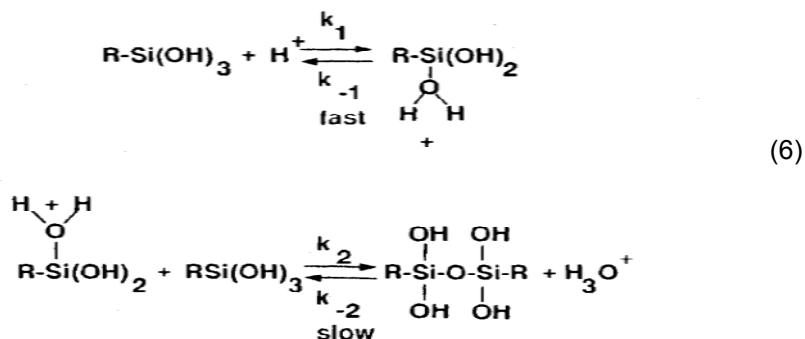
The *pH* is a process parameter that affects significantly the progress of hydrolysis and condensation reactions as H_3O^+ and OH^- ions apparently have a catalytic effect on tetraalkoxy- and organoalkoxysilanes altering their steric behavior¹¹².

Under acidic conditions ($pH < 2$), in a first step the alkoxide group is rapidly protonated (eq. 4) what expedite the liberation of the alcohol (origin on alkoxide linked to silicon) during hydrolysis to equilibrate charges¹¹².



INTRODUCTION

Furthermore, acid catalyzed condensation seems to affect the silanol species as the protonation of the silanol induce electrophilic character to silicon allowing nucleophilic attack. Consequently to the foregoing, condensation reactions preferentially will take place between neutral species and protonated silanols (monomers, end groups of chains, others).¹¹²



In the light of the issue, acid catalysis increase hydrolysis of alkoxide monomers and condensation rates. It also seems to originate dense and low-surface area materials¹²⁰.

On the other hand, higher pH cause water dissociation and consequent nucleophilic hydroxyl anions that will attack silicon atom causing the displacement of OR^- groups so hydrolysis occurs by displacement of an alkoxide anion encouraged by hydrogen bonding of the alkoxide anion with the solvent¹¹². During base catalyzed hydrolysis steric (spatial factors) and inductive effects mark the reactions course, as above mentioned for acid catalyzed hydrolysis, however steric factors have more influence over hydrolysis because silicon acquires little charge in the transition state¹¹².

Moreover, the proposed mechanism for condensation reaction under basic pH using alcohol as solvent refers an approximation of nucleophiles to silicon and consequent displacement of their hydroxyl anion. This

conditions increase deprotonation and surface charges accelerating on this way hydrolysis and condensation steps¹²⁰.

It was stated on bibliography that acid-catalysed conditions are desirable for promoting hydrolysis reaction on organically modified alkoxysilanes due to inductive effects, otherwise it was found that condensation rate is minimized at about 1,5 pH and maximized at neutral pH¹¹².

Another important parameter on sol-gel process is the $H_2O:Si$ ratio. In high $H_2O:Si$ ratios alkoxide hydrolysis is favored, the aggregation phenomenon decrease while the porosity and surface area of silica xerogel increase. If stoichiometric ratio is less than 4 the polymerization mechanism is controlled by condensation reaction. Low $H_2O:Si$ ratios generate polymeric structures with high content on residual organic material due to unhydrolysed alkoxy groups.¹²⁰

In view of the above cited low pH ratios promote hydrolysis instead condensation reaction and low $H_2O:Si$ ratios slow down hydrolysis reaction^{120,112}.

Technically, one of the most promising aspects of sol-gel processing is that the different states allow the production of thin films by ease processes as dipping, spinning or spraying among many other configurations as porous ceramics, monolith blocks, fibers and spherical monodispersions¹²⁰. The fluid sol is ideal for controlling the deposition of the films, to be exact, microstructure, surface area, among others. Thin films (<1 μm) usually shrink and detach during drying process, besides, thicker films require multiple layers or lower polymerization degree. Some procedures as particulate processing or incorporation of organoalkoxysilane monomers are suggested as options to minor the cracking on thin films.

INTRODUCTION

The grafting mechanism between silanes and a metal oxide surface as titanium dental implants is based on the alkoxy silanes reaction with –OH groups on the support metal oxide surface through a condensation reaction mechanism^{121,56}. This reaction leads to the establishment of a stable bonding with the metallic surface (Figure 1.12).

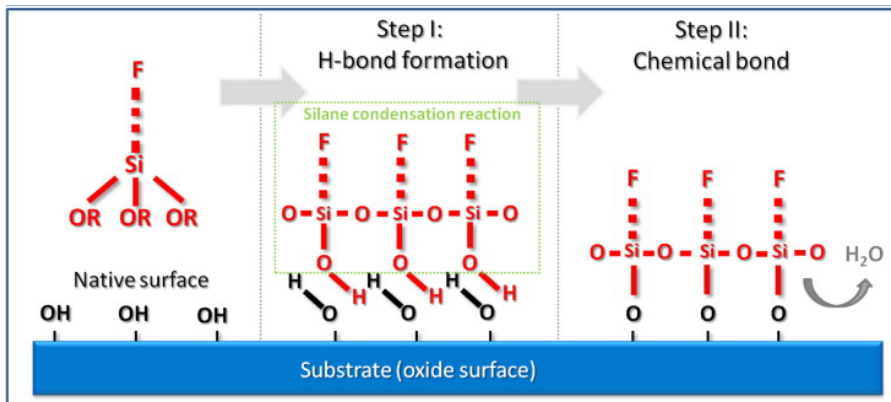


Figure 1.12 – Schematic view of the condensation reaction between alkoxy silanes and an oxide metallic surface (F - silane organo-functional group; OR – silane organic hydrolysable group).⁵⁶

The design of new hybrid biomaterials depends on the organofunctional characteristics of the alkoxy silanes used on the sol-gel process, the production conditions and the final purpose of the material as *versatility* is the word that best describes this new technology.

THE ROLE OF SILICON ON THE OSSEOINTEGRATIVE PROCESS

To better express the role of silicates in physiological environment, it is important to define the different states that silicon can acquire:

Silicon (Si) – pure silicon is rarely found on nature as it is thermodynamically unstable as ion.

Silicate – is a silicon containing anion and can present several configurations, the most usual configuration is SiO_4^{4-} .

Silica – is a silicate with chemical formula SiO_2 .

Silicates have low dissolution rate but can easily form silicic acid - $\text{Si}(\text{OH})_4$ or uncharged molecules in order to dissolve. At low concentrations (<2 mM) and pH range 7-9, Si acquires the stable form of soluble $\text{Si}(\text{OH})_4$.

Connective tissues are the main holders of silicon on human body as it is a component of the glycosaminoglycans (a category of long linear polysaccharide chains distributed in the ECM that virtually surround cell surfaces and generate a physiological environment to support several cellular events¹²²) and their protein complexes.^{123,124}

Silica based materials have diverse applications on medical practice/devices and biotechnology and due to their biocompatibility and bioactivity are one of the most investigated materials for tissue regeneration over the past decades⁵⁶.

One of the suggested strategies to enhance the biological behaviour of silica based materials is the incorporation of calcium and phosphate ions (or apatite) within the silica matrix, by this way the surface reactivity and degradation rate may be changed and controlled. For instance, the incorporation of calcium and phosphate oxides into xerogels may encourage the formation of a bioactive carbonated apatite layer with clear effects on biodegradation rate of the material¹²⁵. On the whole, this before cited strategy has two different concept ideas; on one hand calcium phosphate ceramics is a suitable substrate for bone tissue growth but lacks of inductive properties to proliferate bone cells, on the other hand, xerogel matrix form a structure capable of sustain calcium phosphate oxides and carry biomolecules improving the short release time registered on single ceramic materials.

The high porosity and surface area obtained on silica-based materials represent an opportunity for drug delivery systems and many works were published on the subject^{125-137,138}.

A study published on 2012 by Hernández-Escolano and co-workers¹³⁹ suggest a methodology to achieve a sol-gel coating for the release of

INTRODUCTION

active molecules. The Si based hybrid coating was prepared with triethoxyvinylsilane (VTES) and tetraethyl-orthosilicate (TEOS) and the physical-chemical properties and degradation rate was evaluated. It was stated that the developed sol-gel coating is suitable for its use as drug controlled released system, additionally, it was found a relation between the TEOS content and the releasing kinetics.

Also the work developed by Pandis and co-workers¹⁴⁰ on 2014 about chitosan-silica hybrid membranes refer the use of TEOS and GPTMS (3-(glycidoxypropyl) trimethoxysilane) as silica precursors and reinforcing elements of chitosan scaffolds. The results show that a continuous layer covers the walls of chitosan scaffold pores without altering in a significant way the porosity, also revealed that establishing precise TEOS/GPTMS ratios the porosity and mechanical properties can be adapted to the specific needs of the biomaterial.

On the same year, Juan-Díaz and co-workers¹³⁸ developed a multi-layered functional coating produced by sol-gel technology using several molar ratios of methyl-triethoxysilane (MTMOS) and TEOS. As stated on Hernández-Escolano and co-workers¹³⁹ upper cited work the TEOS content is also the key factor for controlling the degradation rate and it was proved by in-vitro degradation experiments and electrochemical impedance spectroscopy (EIS) tests.

Besides the above cited hybrid materials, additional biopolymer-silica materials have recently been subject of many research studies as they present clear biocompatibility with living matter and have apparent controllable biodegradation rates.

The special interest on gelatine as an additive to inorganic nano-biomaterials is due to its biodegradable character, bioadhesive properties and multifunctional properties¹⁴¹. From a biologic point of view, gelatine is a hydrolysed form of collagen (major constituent of the ECM of many tissues) easily recognizable by many cells¹⁴².

On 2001, Ren and co-workers¹⁴³ developed a hybrid material incorporating gelatine to 3-(glycidoxypropyl) trimethoxysilane (GPTMS) through sol-gel processing grafting the nucleophilic active groups of gelatine with the organic non-hydrolysable epoxy end of alcoxysilane (Figure 1.13). As conclusions, they stated that the gel formation, matrix structure, cross linking degree and phase separation are dependent on parameters as molecular composition and fraction of silane used on synthesis.

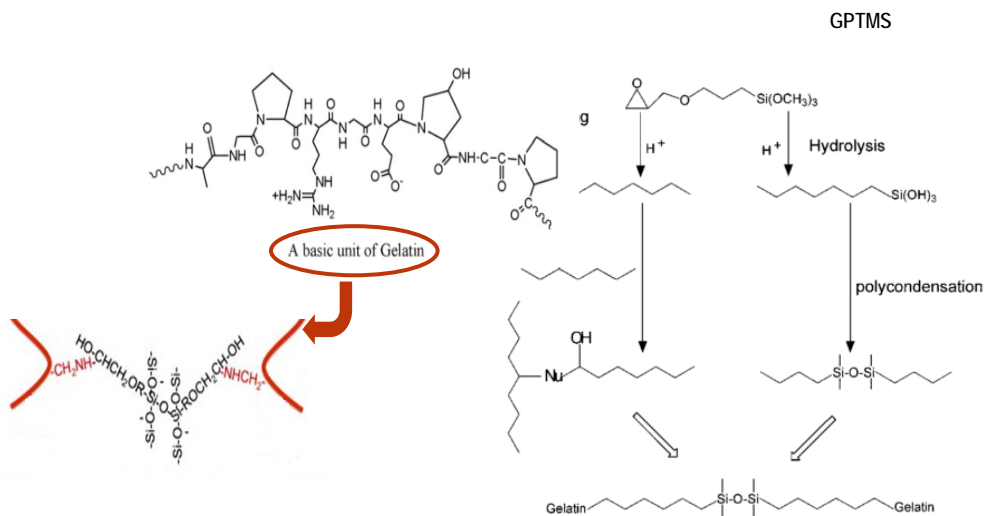


Figure 1.13 – Schematic representation of epoxy ring opening of GPTMS silane with gelatine (Nu-nucleophilic active groups on the side of the amino acid residues).¹⁴³

Later, Smitha et al.¹⁴¹ develop a silica-gelatine hybrid material synthesised by a sol-gel process. Colloidal silica was mixed with 2wt.% gelatine in water under constant stirring, then methyltrimethoxysilane (MTMOS) was added to the mixture to prepare a support matrix for the silica-MTMOS-gelatine hybrid. The sol was coated on glass sides by dip coating and dried at 70°C.

Many other silica based hybrid materials with incorporation of bioaditives can be found on bibliography, however on this work only a few examples are referred to demonstrate the versatility of this approach.

INTRODUCTION

Besides the clear advantages of silica-based xerogels as biocompatible carriers of bioactive additives and as strategic element to improve the mechanical properties of some biopolymers as gelatine, there is the direct effect of silicon on the biologic mechanisms of bone healing.

Carlisle¹⁴⁴ time ago made a microanalysis study and found silicon in active areas of early calcification; mouse and rats were used as animal model and modified the tibial bones. It was stated that silicon and calcium have the same increasing trend on the range of low calcium concentrations, nevertheless, when the calcium proportion achieves the HA composition the silicon concentration falls below the detection limit. Taking into account the before cited results, it was suggested that silicon is associated with calcium in an early stage of calcification on the bone remodelling process¹⁴⁴. However, phosphorus has a close $K\alpha$ peak position to silicon (electronic microanalysis) what could affect significantly the detection limit and presented results on this study¹²³.

Latter, Gatti and Zaffe carry out an experiment with granules of silica bioglass implanted on bone defects in jaws of sheep and detected silicon ions in the surrounding tissues. However it was not defined the role of silicon on the bone regenerative process or the mechanisms on which participates^{145,123}.

On 2011 was published on the Journal of Structural Biology a study on the role of silicon in the early stages of biocalcification. The results show that biocalcification processes in evolutionarily distant organisms make use of aggregate silica in calcifying organic matrices as general biochemical principle involved in mineralization¹⁴⁶.

The parallelism between the biocalcification process in evolutionary distant organisms and active growth areas in the young bone vertebrates in the initial phases of calcification seems to put on evidence the silicon presence as a key element at the organic-inorganic interface, even if the final results are different polymorphscalcite in lacustrine mineral

precipitation and crustacean cuticles and hydroxyapatite in vertebrate bones¹⁴⁶.

Reffitt and co-workers studied the *invitro* effects of orthosilicic acid (0 - 50 μ M) on collagen type 1 synthesis using human osteosarcoma cell line (MG-63), primary osteoblast-like cells (human bone marrow stromal cells) and an immortalized human early osteoblastic cell line (HCCI). They concluded that orthosilicic acid at physiological concentrations stimulates collagen type 1 synthesis in human osteoblast-like cells and enhances osteoblastic differentiation¹⁴⁷.

Later, on 2006, Arumugam and co-workers experiments about the effect of orthosilicic acid - Si(OH)_4 on collagen type 1, alkaline phosphatase (ALP) and osteocalcin mRNA expression in human bone derived osteoblasts show that Si(OH)_4 promote osteoblast proliferation, extracellular matrix differentiation, increase alkaline phosphatase activity and gene expression^{148,149}.

A study on the effect of biosilica on the expressions of osteoprotegerin (OPG) and the receptor activator for *NF- κ B* ligand (RANKL) in the SaOS-2 cell model revealed that biosilica is a selective inducer of OPG expression leading to an increase on synthesis and release rate of the cytokine in the ECM. Nonetheless, it was suggested that OPG might bind to RANKL and block its function to activate osteoclast differentiation¹⁴⁹.

Another recent study on the subject demonstrate that biosilica (enzymatically synthesized from ortho-silicate) and polyphosphate (likewise enzymatically synthesized polymer consisting of 10 to >100 phosphate residues linked by high-energy phosphoanhydride bonds) applied as Ca^{2+} salts increases mineralization of osteogenic cells and also show morphogenetic potential. The gene expression studies revealed a relevant increasing on the expression of bone morphogenetic protein 2 (BMP-2) and ALP in osteogenic cells. Besides, on the expression of collagen type 1 on osteogenic cells promising results were obtained, but not in chondrogenic cellular medium. On the other hand, the up regulation

INTRODUCTION

on the steady state level of collagen 2 transcripts in chondrogenic cells is stronger than in osteogenic cellular medium. These results sustain the proposal of the two biopolymers, biosilica and polyphosphate, as morphogenetically active additives for the otherwise biologically inert alginate polymer to develop a suitable biomaterial promoter of growth and differentiation of human multipotent stromal cells (hMSCs).¹⁵⁰

Mladenović and co-workers¹⁵¹ intended to study the silicon (Si) regulatory effects on osteoclast activity. They used as source of silicon bioglass, bioglass dissolution extracts and Si containing cell culture medium in mouse bone marrow culture medium and RAW264.7 cell culture medium. The results show that Si interferes on inter and intra cellular signalling pathways and consequently inhibits osteoclast formation and bone resorption, however, the suitable amount of silicon in bone tissue stills unknown and the physiological relevance of Si still not clear.

At the present time, the precise mechanism of orthosilicic acid action on molecular biology remains undefined. Nevertheless, many research works show that silicon affects several biologic functions in the human body, have an effect on cell molecular biology and produces direct and indirect outcome on the extra cellular matrix (ECM).

Silicon used as bioadditive increases the bioactivity of several materials without affecting the mechanical properties or inducing cytotoxicity so its use on future new biomaterials seems to be promising.

REFERENCES

1. d'Aquino, R., Rosa, A. De & Lanza, V. Human mandible bone defect repair by the grafting of dental pulp stem/progenitor cells and collagen sponge biocomplexes. *Eur Cell ...* **18**, 75–83 (2009).
2. Kolk, A. *et al.* Current trends and future perspectives of bone substitute materials - from space holders to innovative biomaterials. *J. Craniomaxillofac. Surg.* **40**, 706–18 (2012).
3. Heest, V. & Swiontkowski. in *Lancet* **353**, S128–S129 (1999).
4. Burg, K. J. ., Porter, S. & Kellam, J. F. Biomaterial developments for bone tissue engineering. *Biomaterials* **21**, 2347–2359 (2000).
5. Arcos, D. & Vallet-Regí, M. Sol-gel silica-based biomaterials and bone tissue regeneration. *Acta Biomater.* **6**, 2874–88 (2010).
6. Hench, L. L. & Polak, J. M. Third-generation biomedical materials. *Science* **295**, (2002).
7. Langer, R. & Vacanti, J. P. Tissue engineering. *Science (80-.).* **260**, 920–926 (1993).
8. Chen, Q. & Thouas, G. A. Metallic implant biomaterials. *Mater. Sci. Eng. R Reports* **87**, 1–57 (2015).
9. Tejero, R., Anitua, E. & Orive, G. Toward the biomimetic implant surface: Biopolymers on titanium-based implants for bone regeneration. *Prog. Polym. Sci.* **39**, 1406–1447 (2014).
10. Le Guéhennec, L., Soueidan, A., Layrolle, P. & Amouriq, Y. Surface treatments of titanium dental implants for rapid osseointegration. *Dent. Mater.* **23**, 844–54 (2007).
11. Shibata, Y. & Tanimoto, Y. A review of improved fixation methods for dental implants. Part I: Surface optimization for rapid osseointegration. *J. Prosthodont. Res.* **59**, 20–33 (2014).

INTRODUCTION

12. Holzapfel, B. M. *et al.* How smart do biomaterials need to be? A translational science and clinical point of view. *Adv. Drug Deliv. Rev.* **65**, 581–603 (2013).
13. Williams, D. F. On the nature of biomaterials. *Biomaterials* **30**, 5897–909 (2009).
14. Navarro, M., Michiardi, A., Castaño, O. & Planell, J. A. Biomaterials in orthopaedics. *J. R. Soc. Interface* **5**, 1137–58 (2008).
15. Kokubo, T. Apatite formation on surfaces of ceramics, metals and polymers in body environment. *Acta Mater.* **46**, 2519–2527 (1998).
16. Takahashi, Y., Yamamoto, M. & Tabata, Y. Osteogenic differentiation of mesenchymal stem cells in biodegradable sponges composed of gelatin and beta-tricalcium phosphate. *Biomaterials* **26**, 3587–96 (2005).
17. Ginebra, M. P., Traykova, T. & Planell, J. A. Calcium phosphate cements as bone drug delivery systems: a review. *J. Control. Release* **113**, 102–10 (2006).
18. S. Abramson, H. Alexander, S. Best, J.C. Bokros, J.B. Brunski, A. Colas, S.L. Cooper, J. Curtis, A. Haubold, L.L. Hensch, R.W. Hergenrother, A.S. Hoffman, J.E. Hubbel, J.A. Jansen, M.W. King, J. Kohn, N.M.K. Lamba, R. Langer, C. Migliaresci, R.B. More, N., I. V. Y. in *Biomaterials Science: An Introduction to Materials in Medicine* (ed. B.D. Ratner, A.S. Hoffmann, F.J. Schoen, J. E. L.) 67–137 (Elsevier Academic Press, 2004).
19. Witte, F. The history of biodegradable magnesium implants: a review. *Acta Biomater.* **6**, 1680–92 (2010).
20. Bhat, S. & Kumar, A. Biomaterials and bioengineering tomorrow's healthcare. *Biomatter* 1–12 (2013). at <<http://www.landesbioscience.com/journals/biomatter/2013BIOMATTER0008R.pdf>>

21. Brown, B. N. & Badylak, S. F. Expanded applications, shifting paradigms and an improved understanding of host-biomaterial interactions. *Acta Biomater.* **9**, 4948–55 (2013).
22. Douglas J. DiGirolamo, T. L. C. & S. K. The skeleton as an endocrine organ. *Nat. Rev. Rheumatol.* **8**, 647–683 (2012).
23. Brydone, a S., Meek, D. & Maclaine, S. Bone grafting, orthopaedic biomaterials, and the clinical need for bone engineering. *Proc. Inst. Mech. Eng. Part H J. Eng. Med.* **224**, 1329–1343 (2010).
24. Doblaré, M., García, J. M. & Gómez, M. J. Modelling bone tissue fracture and healing: a review. *Eng. Fract. Mech.* **71**, 1809–1840 (2004).
25. Fridez, P. Modélisation de l'adaptation osseuse externe. (EPFL Lausanne, 1996).
26. Marsell, R. & Einhorn, T. A. The biology of fracture healing. *Injury* **42**, 551–5 (2011).
27. Puleo, D. A. & Nanci, A. Understanding and controlling the bone–implant interface. *Biomaterials* **20**, 2311–2321 (1999).
28. Sansone, V., Pagani, D. & Melato, M. The effects on bone cells of metal ions released from orthopaedic implants. A review. *Clin. cases Miner. ...* **10**, 34–40 (2013).
29. Nichols, K. G. & Puleo, D. A. Effect of metal ions on the formation and function of osteoclastic cells in vitro. *J. Biomed. Mater. Res.* **35**, 265–71 (1997).
30. Hoppe, A., Güldal, N. S. & Boccaccini, A. R. A review of the biological response to ionic dissolution products from bioactive glasses and glass-ceramics. *Biomaterials* **32**, 2757–74 (2011).
31. Stegen, S., van Gestel, N. & Carmeliet, G. Bringing new life to damaged bone: The importance of angiogenesis in bone repair and regeneration. *Bone* **70**, 19–27 (2014).

INTRODUCTION

32. Gaviria, L., Salcido, J. P., Guda, T. & Ong, J. L. Current trends in dental implants. *J. Korean Assoc. Oral Maxillofac. Surg.* **40**, 50–60 (2014).
33. Anderson, J. M. Inflammatory response to implants. *ASAIO Trans* **34**, 101–107 (1988).
34. Nyary, T. & Scammell, B. E. Principles of bone and joint injuries and their healing. *Surg.* **33**, 7–14 (2015).
35. Walsh, J. S. Normal bone physiology, remodelling and its hormonal regulation. *Surg.* **33**, 1–6 (2015).
36. Duong, L. T., Lakkakorpi, P., Nakamura, I. & Rodan, G. A. Integrins and signaling in osteoclast function. *Matrix Biol.* **19**, 97–105 (2000).
37. Dimitriou, R., Tsiridis, E. & Giannoudis, P. V. Current concepts of molecular aspects of bone healing. *Injury* **36**, 1392–404 (2005).
38. Albrektsson, T., Sennerby, L. & Wennerberg, A. State of the art of oral implants. *Periodontol.* **2000** **47**, 15–26 (2008).
39. Pye, A. D., Lockhart, D. E. A., Dawson, M. P., Murray, C. A. & Smith, A. J. A review of dental implants and infection. *J. Hosp. Infect.* **72**, 104–110 (2009).
40. Ratner, B. D. The biocompatibility manifesto: biocompatibility for the twenty-first century. *J. Cardiovasc. Transl. Res.* **4**, 523–7 (2011).
41. Williams, D. F. On the mechanisms of biocompatibility. *Biomaterials* **29**, 2941–53 (2008).
42. Baggi, L., Cappelloni, I., Di Girolamo, M., Maceri, F. & Vairo, G. The influence of implant diameter and length on stress distribution of osseointegrated implants related to crestal bone geometry: a three-dimensional finite element analysis. *J. Prosthet. Dent.* **100**, 422–31 (2008).

43. Long, M., Rack, H. Titanium alloys in total joint replacement-a materials science perspective. *Biomaterials* **19**, 1621–39 (1998).
44. Mendonça, G., Mendonça, D. B. S., Aragão, F. J. L. & Cooper, L. F. Advancing dental implant surface technology – From micron- to nanotopography. *Biomaterials* **29**, 3822–3835 (2008).
45. Jones, F. H. Teeth and bones: applications of surface science to dental materials and related biomaterials. *Surf. Sci. Rep.* **42**, 75–205 (2001).
46. Steinemann, S. G. Titanium - The material of choice? *Periodontol.* **2000** **17**, 7–21 (1998).
47. Schwartz, Z. & Boyan, B. D. Underlying mechanisms at the bone-biomaterial interface. *J. Cell. Biochem.* **56**, 340–7 (1994).
48. Subramanian, K., Tran, D. & Nguyen, K. T. in *Emerging Nanotechnologies in Dentistry* 113–136 (William Andrew Publishing, 2012). doi:10.1016/B978-1-4557-7862-1.00008-0
49. Diebold, U. The surface science of titanium dioxide. *Surf. Sci. Rep.* **48**, 53–229 (2003).
50. Yue, C. & Yang, B. Bioactive Titanium Surfaces with the Effect of Inhibiting Biofilm Formation. *J. Bionic Eng.* **11**, 589–599 (2014).
51. Liu, X., Chu, P. K. & Ding, C. Surface modification of titanium, titanium alloys, and related materials for biomedical applications. *Mater. Sci. Eng. R Reports* **47**, 49–121 (2004).
52. Singh, R. & Dahotre, N. B. Corrosion degradation and prevention by surface modification of biometallic materials. *J. Mater. Sci. Mater. Med.* **18**, 725–51 (2007).
53. Rezwan, K., Chen, Q. Z., Blaker, J. J. & Boccaccini, A. R. Biodegradable and bioactive porous polymer/inorganic composite scaffolds for bone tissue engineering. *Biomaterials* **27**, 3413–31 (2006).

INTRODUCTION

54. Almeida, J. C. *et al.* Structural characterization of PDMS–TEOS–CaO–TiO₂ hybrid materials obtained by sol–gel. *Mater. Chem. Phys.* **143**, 557–563 (2014).
55. Shi, X., Xu, L. & Wang, Q. Porous TiO₂ film prepared by micro-arc oxidation and its electrochemical behaviors in Hank's solution. *Third Spec. Issue Dedic. to Plasma Electrolysis Plasma Electrolysis Inc. Pap. from 'EUROMAT 2009' Congr. Adv. Mater. Process. 7–10 Sept. 2009, Glas. UK* **205**, 1730–1735 (2010).
56. Treccani, L., Yvonne Klein, T., Meder, F., Pardun, K. & Rezwan, K. Functionalized ceramics for biomedical, biotechnological and environmental applications. *Acta Biomater.* **9**, 7115–7150 (2013).
57. NIINOMI, M. Fatigue characteristics of metallic biomaterials. *Int. J. Fatigue* **29**, 992–1000 (2007).
58. Arzt, E. Biological and artificial attachment devices: Lessons for materials scientists from flies and geckos. *Mater. Sci. Eng. C* **26**, 1245–1250 (2006).
59. Subramani, K. & Mathew, R. T. in *Emerging Nanotechnologies in Dentistry* 85–102 (William Andrew Publishing, 2012). doi:10.1016/B978-1-4557-7862-1.00006-7
60. Gittens, R. A. *et al.* The effects of combined micron-/submicron-scale surface roughness and nanoscale features on cell proliferation and differentiation. *Biomaterials* **32**, 3395–403 (2011).
61. Albrektsson, T, Wennerberg, A. Oral implant surfaces: Part 2-review focusing on clinical knowledge of different surfaces. *Int. J. Prosthodont.* **17**, 544–564 (2004).
62. Bauer, S., Schmuki, P., von der Mark, K. & Park, J. Engineering biocompatible implant surfaces. *Prog. Mater. Sci.* **58**, 261–326 (2013).
63. Roşu, R. A., Şerban, V.-A., Bucur, A. I. & Dragoş, U. Deposition of titanium nitride and hydroxyapatite-based biocompatible

- composite by reactive plasma spraying. *Appl. Surf. Sci.* **258**, 3871–3876 (2012).
64. Buser, D., Schenk, R. , Steinemann, S., Fiorellini, J., Fox, C., Stich, H. Influence of surface characteristics on bone integration of titanium implants. A histomorphometric study in miniature pigs. *J Biomed Mater Res* **25**, 889–902 (1991).
 65. Taba Junior, M. , Novaes Junior, A.B. , Souza, S.L. , Grisi, M.F., Palioto, D.B., Pardini, L. C. Radiographic evaluation of dental implants with different surface treatments: an experimental study in dogs. *Implant Dent* **12**, 252–258 (2003).
 66. Wennerberg, A. Experimental study of turned and grit-blasted screw-shaped implants with special emphasis on effects of blasting material and surface topography. *Biomaterials* **17**, 15–22 (1996).
 67. Abron, A., Hopfensperger, M., Thompson, J. & Cooper, L. F. Evaluation of a predictive model for implant surface topography effects on early osseointegration in the rat tibia model. *J. Prosthet. Dent.* **85**, 40–6 (2001).
 68. Trisi, P., Lazzara, R., Rebaudi, A., Rao, W., Testori, T., Porter, S. S. Bone-implant contact on machined and dual acid-etched surfaces after 2 months of healing in the human maxilla. *J Periodontol.* **74**, 945–956 (2003).
 69. Cochran, D.L., Buser, D., ten Bruggenkate, C.M., Weingart, D., Taylor, T.M., Bernard, J.P., Peters, F., Simpson, J. P. The use of reduced healing times on ITI A implants with a sandblasted and acid-etched (SLA) surface : Early results from clinical trials on ITI A SLA. *Clin Oral Implant. Res.* **13**, 144–153 (2002).
 70. Cooper, L. F. *et al.* Fluoride modification effects on osteoblast behavior and bone formation at TiO₂ grit-blasted c.p. titanium endosseous implants. *Biomaterials* **27**, 926–36 (2006).
 71. Jungner, M., Lundqvist, P. & Lundgren, S. Oxidized titanium implants (Nobel Biocare TiUnite) compared with turned titanium implants (Nobel Biocare mark III) with respect to implant failure in

INTRODUCTION

- a group of consecutive patients treated with early functional loading and two-stage protocol. *Clin. Oral Implants Res.* **16**, 308–12 (2005).
72. Su, I. Y.T., Johansson, C., Wennerberg, A., Cho, L.R., Chang, B.S., Albrektsson, T. Optimum surface properties of oxidized implants for reinforcement of osseointegration: surface chemistry, oxide thickness, porosity, roughness, and crystal structure. *Int J Oral Maxillofac Implant.* **20**, 349–359 (2005).
 73. Wang, X.-X., Hayakawa, S., Tsuru, K. & Osaka, A. Bioactive titania gel layers formed by chemical treatment of Ti substrate with a H₂O₂/HCl solution. *Biomaterials* **23**, 1353–1357 (2002).
 74. Ttachment, A. *et al.* Oxidation of titanium, RGD peptide attachment, and matrix mineralization rat bone marrow stromal cells. *J Oral Implant.* **30**, 343–349 (2004).
 75. Chauvy, P.-F., Hoffmann, P. & Landolt, D. Applications of laser lithography on oxide film to titanium micromachining. *Appl. Surf. Sci.* **208-209**, 165–170 (2003).
 76. Çelen, S. & Özden, H. Laser-induced novel patterns: As smart strain actuators for new-age dental implant surfaces. *Appl. Surf. Sci.* **263**, 579–585 (2012).
 77. Holloway, J. L., Ma, H., Rai, R. & Burdick, J. a. Modulating hydrogel crosslink density and degradation to control bone morphogenetic protein delivery and in vivo bone formation. *J. Control. Release* **191**, 63–70 (2014).
 78. Von der Mark, K. & Park, J. Engineering biocompatible implant surfaces. *Prog. Mater. Sci.* **58**, 327–381 (2013).
 79. Lodish, H., Berk, A., Zipursky, S.L., et al. in *Molecular Cell Biology* (Freeman, W. H., 2000). at <<http://www.ncbi.nlm.nih.gov/books/NBK21493/>>
 80. Rahmany, M. B. & Van Dyke, M. Biomimetic approaches to modulate cellular adhesion in biomaterials: A review. *Acta Biomater.* **9**, 5431–7 (2013).

81. Morris, A. H. & Kyriakides, T. R. Matricellular proteins and biomaterials. *Matrix Biol.* **37**, 183–91 (2014).
82. Scharnweber, D. *et al.* Mineralization behaviour of collagen type I immobilized on different substrates. *Biomaterials* **25**, 2371–2380 (2004).
83. Bierbaum, S. *et al.* Modification of Ti6AL4V surfaces using collagen I, III, and fibronectin. II. Influence on osteoblast responses. *J. Biomed. Mater. Res. A* **67**, 431–438 (2003).
84. Bierbaum, S., Beutner, R., Hanke, T., Scharnweber, D., Hempel, U., Worch, H. Modification of Ti6Al4V surfaces using collagen I, III, and fibronectin. I. Biochemical and morphological characteristics of the adsorbed matrix. *J. Biomed. Mater. Res. A.* **67**, 421 (2003).
85. Guo, K.-T., Scharnweber, D., Schwenzer, B., Ziemer, G. & Wendel, H. P. The effect of electrochemical functionalization of Ti-alloy surfaces by aptamer-based capture molecules on cell adhesion. *Biomaterials* **28**, 468–74 (2007).
86. Shin-Etsu. Silane Coupling Agents. (2014). at http://www.silicone.jp/e/catalog/pdf/SilaneCouplingAgents_e.pdf
87. Marín-Pareja, N., Salvagni, E., Guillem-Martí, J., Aparicio, C. & Ginebra, M.-P. Collagen-functionalised titanium surfaces for biological sealing of dental implants: effect of immobilisation process on fibroblasts response. *Colloids Surf. B. Biointerfaces* **122**, 601–10 (2014).
88. Lung, C. Y. K. & Matinlinna, J. P. Aspects of silane coupling agents and surface conditioning in dentistry: an overview. *Dent. Mater.* **28**, 467–77 (2012).
89. Advincula, M., Fan, X., Lemons, J. & Advincula, R. Surface modification of surface sol-gel derived titanium oxide films by self-assembled monolayers (SAMs) and non-specific protein adsorption studies. *Colloids Surf. B. Biointerfaces* **42**, 29–43 (2005).

INTRODUCTION

90. Yang, C., Cheng, K., Weng, W. & Yang, C. Immobilization of RGD peptide on HA coating through a chemical bonding approach. *J. Mater. Sci. Mater. Med.* **20**, 2349–2352 (2009).
91. Pegg, E. C., Walker, G. S., Scotchford, C. a., Farrar, D. & Grant, D. Mono-functional aminosilanes as primers for peptide functionalization. *J. Biomed. Mater. Res. - Part A* **90**, 947–958 (2009).
92. Von Walter, M. *et al.* In vitro behavior of a porous TiO₂/perlite composite and its surface modification with fibronectin. *Biomaterials* **26**, 2813–26 (2005).
93. Miller, S. C. & Jee, W. S. S. The effect of dichloromethylene diphosphonate, a pyrophosphate analog, on bone and bone cell structure in the growing rat. *Anat. Rec.* **193**, 439–461 (1979).
94. R. Schenk, W.A. Merz, R. Muhlbauer, R.G.G. Russell, H. F. Effect of ethane1-hydroxy-1,1-diphosphonate (EHDP) and dichloromethylene diphosphonate (Cl₂MDP) on the calcification and resorption of cartilage and bone in the tibial epiphysis and metaphysis of rats. *Calcif Tissue Res* **11**, 196–214 (1973).
95. Yoshinari, M. Immobilization of bisphosphonates on surface modified titanium. *Biomaterials* **22**, 709–715 (2001).
96. Hung, K.-Y. *et al.* Titanium surface modified by hydroxyapatite coating for dental implants. *Surf. Coatings Technol.* **231**, 337–345 (2013).
97. Chen, C., Lee, I.-S., Zhang, S.-M. & Yang, H. C. Biomimetic apatite formation on calcium phosphate-coated titanium in Dulbecco's phosphate-buffered saline solution containing CaCl₂ with and without fibronectin. *Acta Biomater.* **6**, 2274–81 (2010).
98. Liu, Y., Enggist, L., Kuffer, A. F., Buser, D. & Hunziker, E. B. The influence of BMP-2 and its mode of delivery on the osteoconductivity of implant surfaces during the early phase of osseointegration. *Biomaterials* **28**, 2677–86 (2007).

99. Durrieu, M., Pallu, S. & Guillemot, F. Grafting RGD containing peptides onto hydroxyapatite to promote osteoblastic cells adhesion. *J. Mater. ...* **5**, 779–786 (2004).
100. Gawalt, E. S., Avaltroni, M. J., Koch, N. & Schwartz, J. Self-Assembly and Bonding of Alkanephosphonic Acids on the Native Oxide Surface of Titanium. *Langmuir* **17**, 5736–5738 (2001).
101. Helmy, R. & Fadeev, A. Self-assembled monolayers supported on TiO₂: comparison of C₁₈H₃₇SiX₃ (X= H, Cl, OCH₃), C₁₈H₃₇Si (CH₃)₂Cl, and C₁₈H₃₇PO (OH)₂. *Langmuir* **3**, 8924–8928 (2002).
102. Buwalda, S. J. *et al.* Hydrogels in a historical perspective: From simple networks to smart materials. *J. Control. Release* **190**, 254–273 (2014).
103. Lin, C.-C. & Metters, A. T. Hydrogels in controlled release formulations: network design and mathematical modeling. *Adv. Drug Deliv. Rev.* **58**, 1379–408 (2006).
104. Zhu, J. Bioactive modification of poly(ethylene glycol) hydrogels for tissue engineering. *Biomaterials* **31**, 4639–56 (2010).
105. Colon, G., Ward, B. C. & Webster, T. J. Increased osteoblast and decreased Staphylococcus epidermidis functions on nanophase ZnO and TiO₂. *J. Biomed. Mater. Res. Part A* **78A**, 595–604 (2006).
106. Massa, M. A. *et al.* Synthesis of new antibacterial composite coating for titanium based on highly ordered nanoporous silica and silver nanoparticles. *Mater. Sci. Eng. C. Mater. Biol. Appl.* **45**, 146–53 (2014).
107. Yoshinari, M., Oda, Y., Kato, T. & Okuda, K. Influence of surface modifications to titanium on antibacterial activity in vitro. *Biomaterials* **22**, 2043–2048 (2001).
108. Lawson, M. C., Bowman, C. N. & Anseth, K. S. Vancomycin Derivative Photopolymerized to Titanium Kills S. epidermidis. *Clin. Orthop. Relat. Res.* **461**, (2007).

INTRODUCTION

109. Holmberg, K. V *et al.* Bio-inspired stable antimicrobial peptide coatings for dental applications. *Acta Biomater.* **9**, 8224–31 (2013).
110. Dohan Ehrenfest, D. M., Vazquez, L., Park, Y.-J., Sammartino, G. & Bernard, J.-P. Identification Card and Codification of the Chemical and Morphological Characteristics of 14 Dental Implant Surfaces. *J. Oral Implantol.* **37**, 525–542 (2011).
111. Niederberger, M., Pinna, N. in *Metal Oxide Nanoparticles in Organic Solvents Synthesis* 217 (2009).
112. C. J. Brinker; G. W. Scherer. *Sol–Gel Science: The Physics and Chemistry of Sol–Gel Processing*. Elsevier (Academic Press, 1990).
at
<<http://scholar.google.com/scholar?hl=en&btnG=Search&q=intitle:No+Title#0>>
113. Kirtay, S. Preparation of hybrid silica sol–gel coatings on mild steel surfaces and evaluation of their corrosion resistance. *Prog. Org. Coatings* **77**, 1861–1866 (2014).
114. Pepe, A., Galliano, P., Ceré, S., Aparicio, M. & Durán, A. Hybrid silica sol–gel coatings on Austempered Ductile Iron (ADI). *Mater. Lett.* **59**, 2219–2222 (2005).
115. Catauro, M., Papale, F. & Bollino, F. Characterization and biological properties of TiO₂/PCL hybrid layers prepared via sol–gel dip coating for surface modification of titanium implants. *J. Non. Cryst. Solids* **415**, 9–15 (2015).
116. Pagliaro, M., Ciriminna, R., Wong Chi Man, M. & Campestrini, S. Better chemistry through ceramics: the physical bases of the outstanding chemistry of ORMOSIL. *J. Phys. Chem. B* **110**, 1976–88 (2006).
117. Hench, L. L. & West, J. K. The sol-gel process. *Chem. Rev.* **90**, 33–72 (1990).

118. Stöber, Werner, Fink, A. Controlled growth of monodisperse silica spheres in the micron size range. *J. Colloid Interface Sci.* **26**, 62–69 (1968).
119. Lindberg, R., Sjöblom, J. & Sundholm, G. Preparation of silica particles utilizing the sol-gel and the emulsion-gel processes. *Colloids Surfaces A Physicochem. Eng. Asp.* **99**, 79–88 (1995).
120. Lev, O., Tsionsky, M., Rabinovich, L., Glezer, V., Sampath, S., Pankratov, I., Gun, J. Organically Modified Sol-Gel Sensors. *Anal. Chem.* **67**, 22A–30A (1995).
121. Neouze, M.-A. & Schubert, U. Surface Modification and Functionalization of Metal and Metal Oxide Nanoparticles by Organic Ligands. *Monatshefte für Chemie - Chem. Mon.* **139**, 183–195 (2008).
122. Mikami, T. & Kitagawa, H. in *Glycoscience: Biology and Medicine SE - 116-1* (eds. Endo, T., Seeberger, P. H., Hart, G. W., Wong, C.-H. & Taniguchi, N.) 1–7 (Springer Japan, 2014). doi:10.1007/978-4-431-54836-2_116-1
123. Habibovic, P. & Barralet, J. E. Bioinorganics and biomaterials: bone repair. *Acta Biomater.* **7**, 3013–26 (2011).
124. Henstock, J. R., Canham, L. T. & Anderson, S. I. Silicon: The evolution of its use in biomaterials. *Acta Biomater.* (2014). doi:10.1016/j.actbio.2014.09.025
125. Radin, S., El-Bassyouni, G., Vresilovic, E. J., Schepers, E. & Ducheyne, P. In vivo tissue response to resorbable silica xerogels as controlled-release materials. *Biomaterials* **26**, 1043–1052 (2005).
126. Radin, S., Ducheyne, P., Kamplain, T. & Tan, B. H. Silica sol-gel for the controlled release of antibiotics. I. Synthesis, characterization, and in vitro release. *J. Biomed. Mater. Res.* **57**, 313–320 (2001).
127. Santos, E. M., Radin, S. & Ducheyne, P. Sol-gel derived carrier for the controlled release of proteins. *Biomaterials* **20**, 1695–1700 (1999).

INTRODUCTION

128. Aughenbaugh, W., Radin, S. & Ducheyne, P. Silica sol-gel for the controlled release of antibiotics. II. The effect of synthesis parameters on the in vitro release kinetics of vancomycin. *J. Biomed. Mater. Res.* **57**, 321–326 (2001).
129. Radin, S., Falaize, S., Lee, M. H. & Ducheyne, P. In vitro bioactivity and degradation behavior of silica xerogels intended as controlled release materials. *Biomaterials* **23**, 3113–3122 (2002).
130. Radin, S. & Ducheyne, P. Sol-gel formulations for the controlled delivery of growth factors and proteins. in *8th World Biomaterials Congress 2008* **1**, 484 (2008).
131. Radin, S. & Ducheyne, P. Controlled release of vancomycin from thin sol-gel films on titanium alloy fracture plate material. *Biomaterials* **28**, 1721–1729 (2007).
132. Radin, S., Parvizi, J. & Ducheyne, P. Thin sol-gel films on fracture fixation material for the controlled release of antibiotics. *Key Engineering Materials* **309-311 II**, 759–762 (2006).
133. Radin, S., Chen, T. & Ducheyne, P. The controlled release of drugs from emulsified, sol gel processed silica microspheres. *Biomaterials* **30**, 850–858 (2009).
134. Falaize, S., Radin, S. & Ducheyne, P. In vitro behavior of silica-based xerogels intended as controlled release carriers. *J. Am. Ceram. Soc.* **82**, 969–976 (1999).
135. Radin, S., El-Bassyouni, G., Vresilovic, E. J., Schepers, E. & Ducheyne, P. Tissue reactions to controlled release silica xerogels carriers. *R.Z. LeGeros, J.P. LeGeros (Eds.), World Sci. New York* **11**, 529 (1998).
136. Radin, S. *et al.* In vitro and in vivo bactericidal effect of sol-gel/antibiotic thin films on fixation devices. *Key Engineering Materials* **330-332 II**, 1323–1326 (2007).
137. Prokopowicz, M. Bioactive silica-based nanomaterials for doxorubicin delivery: evaluation of structural properties

- associated with release rate. *Mater. Sci. Eng. C. Mater. Biol. Appl.* **33**, 3942–50 (2013).
138. Juan-Díaz, M. J. *et al.* Study of the degradation of hybrid sol–gel coatings in aqueous medium. *Prog. Org. Coatings* **77**, 1799–1806 (2014).
 139. Hernández-Escolano, M. *et al.* The design and characterisation of sol–gel coatings for the controlled-release of active molecules. *J. Sol-Gel Sci. Technol.* **64**, 442 (2012).
 140. Pandis, C. *et al.* Chitosan-silica hybrid porous membranes. *Mater. Sci. Eng. C. Mater. Biol. Appl.* **42**, 553–61 (2014).
 141. Smitha, S., Shajesh, P., Mukundan, P., Nair, T. D. R. & Warriar, K. G. K. Synthesis of biocompatible hydrophobic silica–gelatin nano-hybrid by sol–gel process. *Colloids Surfaces B Biointerfaces* **55**, 38–43 (2007).
 142. Mahony, O. *et al.* Silica-Gelatin Hybrids with Tailorable Degradation and Mechanical Properties for Tissue Regeneration. *Adv. Funct. Mater.* **20**, 3835–3845 (2010).
 143. Ren, L., Tsuru, K., Hayakawa, S. & Osaka, A. Synthesis and characterization of gelatin-siloxane hybrids derived through sol-gel procedure. *J. Sol-Gel Sci. Technol.* **21**, 115–121 (2001).
 144. Carlisle, E. M. Silicon: A possible factor in bone calcification. *Science (80-.)*. **167**, 279–280 (1970).
 145. Gatti, A. M. & Zaffe, D. Long-term behaviour of active glasses in sheep mandibular bone. *Biomaterials* **12**, 345–350 (1991).
 146. Matsko, N. B. *et al.* Silicon: The key element in early stages of biocalcification. *J. Struct. Biol.* **174**, 180–6 (2011).
 147. Reffitt, D. M. *et al.* Orthosilicic acid stimulates collagen type 1 synthesis and osteoblastic differentiation in human osteoblast-like cells in vitro. *Bone* **32**, 127–135 (2003).

INTRODUCTION

148. Arumugam, M.Q., Ireland, D.C., Brooks, R.A., Rushton, N., Bonfield, W. The effect of orthosilicic acid on collagen type I, alkaline phosphatase and osteocalcin mRNA expression in human bone-derived osteoblasts in vitro. *Key Eng Mater* **32**, 309–311 (2006).
149. Wiens, M. *et al.* The role of biosilica in the osteoprotegerin/RANKL ratio in human osteoblast-like cells. *Biomaterials* **31**, 7716–25 (2010).
150. Wang, X. *et al.* The marine sponge-derived inorganic polymers, biosilica and polyphosphate, as morphogenetically active matrices/scaffolds for the differentiation of human multipotent stromal cells: Potential application in 3D printing and distraction osteogenesis. *Mar. Drugs* **12**, 1131–1147 (2014).
151. Mladenović, Ž. *et al.* Soluble silica inhibits osteoclast formation and bone resorption in vitro. *Acta Biomater.* **10**, 406–18 (2014).

CHAPTER 2. OBJECTIVES

RESEARCH PROPOSAL

STATEMENT OF THE PROBLEM

Tooth loss is a very common problem and the implantation of titanium (Ti) dental implants is a frequent clinical practice to treat this pathology.

Commercially pure titanium (cp Ti) has proved biocompatibility and osseointegrative skills, presents relatively high stiffness and has good corrosion resistance due to the oxide surface (TiO₂) that spontaneously forms in contact with air or aqueous medium. This oxide layer is the real contact surface with the physiological environment and the control of the surface characteristics are imperative for a successful osseointegrative process.¹⁻³

As referenced in the previous chapter, the knowledge and control of surface parameters (as morphology, topography, roughness, chemical composition, surface energy, residual stress, impurities, thickness of TiO₂ film) that affect the tissue response to the implant that consequently increase or decrease the healing times and affect the bone regenerative process are the main objective of many actual studies. Although titanium presents excellent osteoconductive skills and promotes a good mechanical anchorage with bone, it lacks of osteoinductive properties and is biologically inactive at a molecular level.

The actual strategy used by the majority of manufacturers to modify titanium dental implants surface is mechanical-chemical treatments, as most commercial dental implants have a microroughened surface in a range 0,5 - 1 μm achieved by techniques as grit blasting, plasma spraying and/or acid etching. Even though surface roughness can stimulate some positive cellular responses and induce changes on orientation, locomotion, cell shape and function, for commercial products there is no standard for the roughness of dental implants.^{1, 4-6}

OBJECTIVES

The interest on new strategies to endow bioactivity to titanium surfaces is relevant to dental implants manufacturers. Moreover, a viable method with reproducible results must be achieved for a proper industrial implementation. The application of external coatings is a good alternative to provide bioactivity to titanium dental implants surface and improve its success. This type of modification can have two purposes, its use as scaffold for cellular and protein adhesion and as a vehicle able to retain and release drugs *in situ*.

The biomaterial developed on this work is a synthetic hybrid silicon based external coating, synthesized by the sol-gel technology. The thin and well adhered layer should be biodegradable and not trigger any undesirable biologic reaction on the host and, in addition, must be compatible with biomolecules and organic elements without affecting the proved skills of the metallic substrate (Ti) of commercial dental implants. The most important advance may be to provide titanium surface with osteoinductive ability, thereby reducing the healing time and accelerating the bone regenerative process with an appropriate bone-implant contact.

Currently there are no commercial products available with a similar approach, but the real challenge is the development of biocompatible coatings, biodegradable and correctly adhered to the metal surface with proved enhancement of the actual benefits of titanium dental implants (osseointegration).

OBJECTIVES

The main objective of this study is the production of a silica based nano-hybrid material coated on titanium dental implants that improve its bioactivity. This coating must be biocompatible, with controlled biodegradability and should provide bioactive properties to titanium inert medical devices. As a consequence it must provide osseoinductive properties to titanium dental implants and represent a new technology for controlled drug delivery in the injured area (originated by implantation). This new aptitude could improve the success of titanium devices integration in patients with poor bone regenerative capability and reduce the actual bone healing times.

To achieve the previously cited general objective several specific objectives will be accomplished:

1. Synthesis of coatings with biodegradable characteristics capable to act as vehicles for bioactive molecules.

To achieve this first objective two types of composition vectors will be use to modify the reference material of 50%MTMOS:50%GPTMS, on one hand introducing TEOS silane for degradation regulation, on the other hand, changing GPTMS content (coupling agent for bioactive molecules). This will keep the initial sol-gel silica based coating's characteristics of biocompatibility and homogeneity and seek the improvement of the initial coating properties (reference material 50MTMOS:50GPTMS).

2. Selection of the coating with the best performance and suggestion of a final prototype. To achieve this goal a complete material characterization will be made to study the structural properties of the coatings and correlate it with the degradation

OBJECTIVES

profiles and aqueous medium uptake. In addition, some surface properties will be measured to corroborate if they are appropriate for the cellular proliferation and mineralization processes. The barrier effect of the coatings against metal corrosion will be evaluated as well to verify the coatings ability to block possible exchange of corrosion products (from the implant metal substrate) that may affect bone regenerative biologic mechanisms.

3. Biological tests will be made to ascertain the biocompatibility of each of the new developed biomaterials and finally select a prototype.

To achieve this specific objective, *in vitro* experiments will be made to evaluate the first stage of biocompatibility, recognize the cellular proliferation in contact with the sol-gel coatings and optimize mineralization rates.

On the other hand, the *in vivo* evaluation will be made to confirm the biocompatibility of the sol-gel coatings and verify its successful osteoinductive effect compared with the titanium metal substrate and reference material 50%MTMOS:50%GPTMS.

INNOVATIVE CONTRIBUTION OF THE RESEARCH WORK

As referenced previously in the Introduction chapter, the actual interest of many research groups on silica based xerogels is its use as vehicle for carrying drugs and biomolecules.⁷⁻¹⁸

However, the use of silicon (Si) as an additional bioelement to promote osseointegration and osteoblastic activity represents another advantage of silica based xerogels and has been used under many different forms on bone regeneration. Silicon is widely used for orthopaedics and is usually applied in the form of biosilica particles, also denominated bioglass (SiO_2) for bone replacement. Nevertheless, it has been found that the low silica content is essential to the function of the bioactive glass and it affects the softening temperature and increases the thermal expansion of the glass with negative implications for its use as bioactive coatings on metal implants.¹⁹

Another source of Si can be its use directly as orthosilicic acid ($\text{Si}(\text{OH})_4$) as silicates are poorly soluble and usually form silicic acid or uncharged molecules in order to dissolve.^{20,21,22,23,24,25}

The employment of a bio-absorbable osteoconductive coating on different kinds of prosthesis that release silicon during its degradation process represents an extra strategy to provide silicon to the bone damage area stimulating osteoblastic activity.

Besides the above mentioned advantage, the versatility of silica based biocoatings enables its use as a guide for the remodeling process acting on strategic moments of the biologic process of bone regeneration. This active feature of the biomaterial improves the passive behavior of metal dental implants surfaces.

This work proposal to develop sol-gel silica based coatings biodegradable and consequently as a source of silicon, an element that positively affects osteoblast activity, extracellular matrix (ECM) differentiation, alkaline phosphatase (ALP) activity and gene expression intend to provide

OBJECTIVES

bioactivity to the inactive titanium surface of commercial dental implants. Additionally, the proposed silica based coatings intend to act as a barrier that prevents the exchange of ionic corrosion subproducts between the implant metallic surface and the damaged tissues preventing their interference in bone regenerative biologic mechanisms.

This proposal is of great importance to the dental implants industry; it represents a noteworthy progress in surface technology that at the moment falls upon mechanical-morphological treatments and coatings based on calcium phosphates and other inorganic materials.²⁶

A productive method with mild conditions and ease to put on commercial dental implants opens up a wide range of possibilities to provide bioactivity to titanium dental implants. Besides, makes possible the incorporation of strategic biomolecules to guide the bone regenerative process on the metal passive surface. Therefore the real goal of this research work is the development of a biomaterial with the properties cited above.

APPROACH AND METHODOLOGY

This research work is part of a INNPACTO project entitled “Development of coatings obtained via sol-gel for dental prostheses of metal alloys - SOLDENT” with financial support provided by the Spanish Ministry of Economy and Competitiveness and the ERDF (IPT-010000-2010-004) in partnership with Universidad Jaume I, Universidad del País Vasco and an industrial partner Ilerimplant S.L.. The present thesis is part of a multidisciplinary team work with members specialized in different fields and the experiments were performed at different places due to the availability of analysis instruments. The biologic experiments were carried out by the team biologist member of Centro de Biomateriales e Ingeniería Tisular at Universidad Politécnica de Valencia.

The present research work arises from three previous PhD Theses on the subject.

In 2011, Miriam Hernández Escolano presented her PhD work about a degradable coating synthesized by the sol gel process applied to dental implants to enhance cell adhesion, mineralization and proliferation. It was used as silicon precursors in the research project TEOS, MTMOS, VTES and GPTMS and initially some experiments were carried out to define the properties of each alkoxide by means of physico-chemical tests, degradation kinetics definition and biological performance (*in vitro* experiments). The obtained results motivated the use of two groups of materials, one formed by VTES-TEOS and another one made with VTES-GPTMS with different interests based on the hydrophilic properties of each group, biologic performance and possibility of its use as vehicle for transportation of drugs or biomolecules. The obtained results showed that VTES and MTMOS were the metal alkoxides that promoted the best coatings to protect against corrosion phenomenon, moreover, the biological studies with osteoblasts demonstrated an improvement of cellular proliferation compared to the control (titanium).

OBJECTIVES

Later, in 2013, M^a Jesus Juan Díaz worked with the same alcoxides (TEOS, MTMOS, VTES and GPTMS) and studied the variation of physico-chemical properties of the MTMOS film applied to metallic dental implants when combined with TEOS managing the hydrophilic behavior and degradation kinetic and, on the other hand, combined with GPTMS to increase the organic content of the implant, thereby enabling the chemical bonding with bioactive elements and promoting different degradation rates. Finally, the material composed by 70%MTMOS:30%TEOS resulted the most appropriated material to improve the titanium surface performance on the initial stages accelerating the osseointegrative process.

Recently, in 2015, Irene Lara Sáez evaluated the biological performance of the coatings developed in the above cited PhD Theses. The results show that the composition 70%MTMOS:30%TEOS is the most degradable coating *in vitro* and *in vivo* and consequently release the greatest amount of silicon. The biomaterial made with 50%MTMOS:50%GPTMS induced high osteoblast differentiation, nevertheless, during the *in vivo* experimental time (8 weeks) did not disappear completely and motivated the formation of a fibrous capsule between the bone and implant.

Taking into account the previous works results, the hypothesis of improving the biological performance of the biomaterial composed by 50%MTMOS:50%GPTMS emerges and represents an opportunity in the biomaterials field as a source of silicon (element that affects bone healing process) and/or vehicle to biomolecular carrying due to the organic functionality provided by GPTMS. The handicap of the formation of a fibrous tissue surrounding all the coated implant (no biocompatible) verified in *in vivo* experiments will be an important target of the present research work.

To meet the previously cited proposed objectives of this research work the subsequent structure was followed:

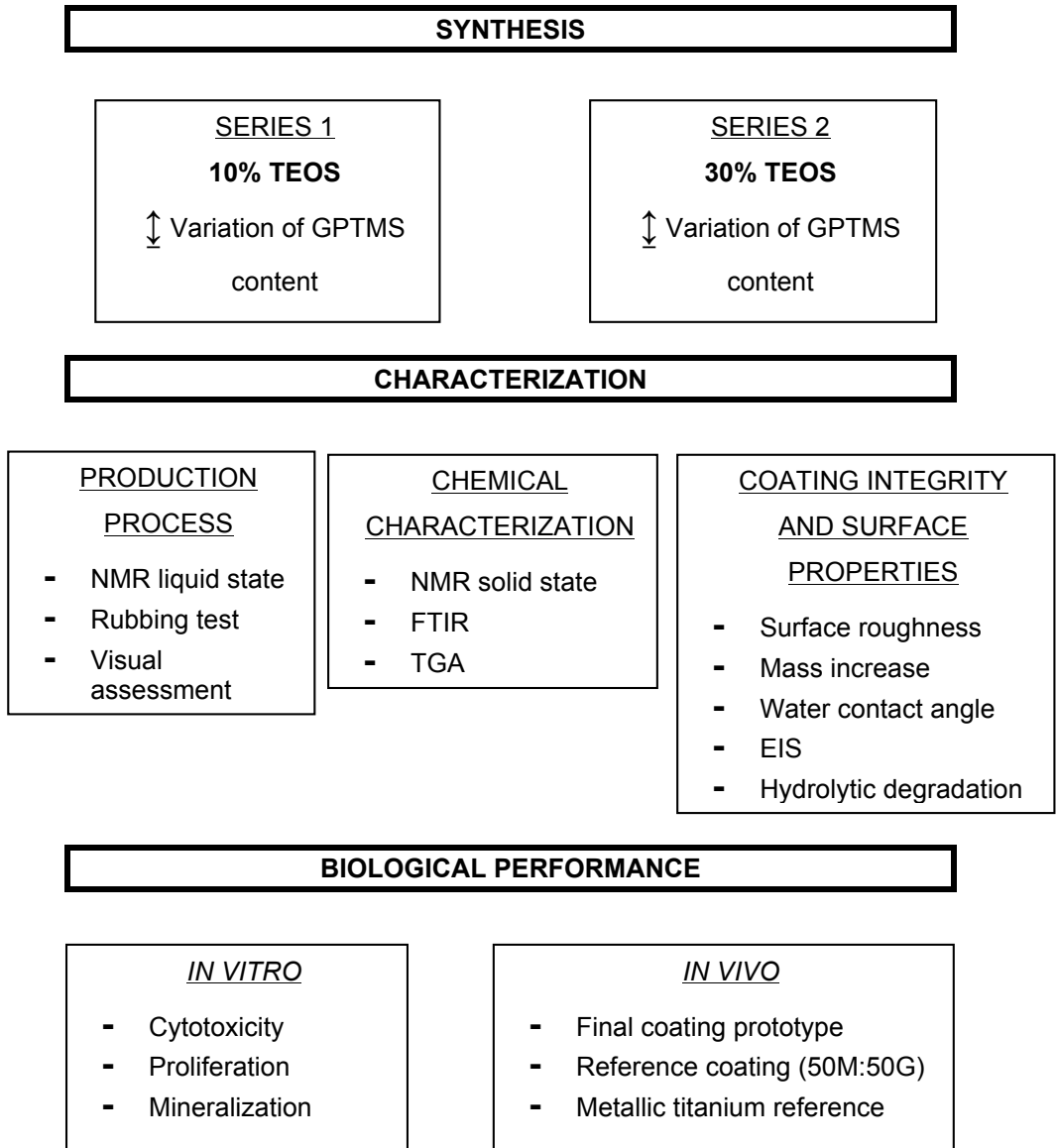


Figure 2. 1 - Schematic representation of the experimental tactic to achieve the proposed objectives.

The structure of this document is presented in five main chapters. The first chapter will explain this work's motivation and concepts related to dental implantology, bone regenerative processes, the sol-gel method, among others. Then a second chapter where the statement of the

OBJECTIVES

problem will be presented, will explain this work's main objectives, innovative contribution and finally the approach and methodology used. The third chapter where it will report the materials and methods used to perform the experimental work. Next, the fourth chapter where the production process of the new biomaterials will be delineated and its chemical characterization will also be completed. This characterization consists of the evaluation of the polysiloxanic matrix structure and visual assessment of the sol-gel coatings. Additionally, some surface properties of the coatings will be studied as well as the hydrolytic degradation profiles and barrier effectiveness against possible release of corrosive metal products in simulated biological fluids. Also the success of the incorporation of a biomolecule (gelatin) to the coatings will be evaluated. Gelatin-siloxane hybrids stability and degradation profiles will be studied. A final prototype will be selected taking into account the *in vitro* cellular assay results for the evaluation under *in vivo* conditions. Lastly, the fifth chapter will describe some final conclusions.

REFERENCES

1. Gaviria, L., Salcido, J. P., Guda, T. & Ong, J. L. Current trends in dental implants. *J. Korean Assoc. Oral Maxillofac. Surg.* **40**, 50–60 (2014).
2. Albrektsson, T., Sennerby, L. & Wennerberg, A. State of the art of oral implants. *Periodontol.* **2000** **47**, 15–26 (2008).
3. Pye, A. D., Lockhart, D. E. A., Dawson, M. P., Murray, C. A. & Smith, A. J. A review of dental implants and infection. *J. Hosp. Infect.* **72**, 104–110 (2009).
4. Mendonça, G., Mendonça, D. B. S., Aragão, F. J. L. & Cooper, L. F. Advancing dental implant surface technology – From micron- to nanotopography. *Biomaterials* **29**, 3822–3835 (2008).
5. Riccardis, D. E. *et al.* Comparative investigation of the surface properties of commercial titanium dental implants. Part I: chemical composition. *Innovation* **3**, 535–548 (2002).
6. Dohan Ehrenfest, D. M., Vazquez, L., Park, Y.-J., Sammartino, G. & Bernard, J.-P. Identification Card and Codification of the Chemical and Morphological Characteristics of 14 Dental Implant Surfaces. *J. Oral Implantol.* **37**, 525–542 (2011).
7. Radin, S. & Ducheyne, P. Controlled release of vancomycin from thin sol-gel films on titanium alloy fracture plate material. *Biomaterials* **28**, 1721–1729 (2007).
8. Radin, S., Parvizi, J. & Ducheyne, P. Thin sol-gel films on fracture fixation material for the controlled release of antibiotics. *Key Engineering Materials* **309-311 II**, 759–762 (2006).
9. Radin, S., El-Bassyouni, G., Vresilovic, E. J., Schepers, E. & Ducheyne, P. In vivo tissue response to resorbable silica xerogels as controlled-release materials. *Biomaterials* **26**, 1043–1052 (2005).
10. Radin, S. *et al.* In vitro and in vivo bactericidal effect of sol-gel/antibiotic thin films on fixation devices. *Key Engineering Materials* **330-332 II**, 1323–1326 (2007).
11. Radin, S., El-Bassyouni, G., Vresilovic, E. J., Schepers, E. & Ducheyne, P. Tissue reactions to controlled release silica xerogels

OBJECTIVES

- carriers. *R.Z. LeGeros, J.P. LeGeros (Eds.), World Sci. New York* **11**, 529 (1998).
12. Falaize, S., Radin, S. & Ducheyne, P. In vitro behavior of silica-based xerogels intended as controlled release carriers. *J. Am. Ceram. Soc.* **82**, 969–976 (1999).
 13. Radin, S., Ducheyne, P., Kamplain, T. & Tan, B. H. Silica sol-gel for the controlled release of antibiotics. I. Synthesis, characterization, and in vitro release. *J. Biomed. Mater. Res.* **57**, 313–320 (2001).
 14. Radin, S. & Ducheyne, P. Sol-gel formulations for the controlled delivery of growth factors and proteins. in *8th World Biomaterials Congress 2008* **1**, 484 (2008).
 15. Juan-Díaz, M. J. *et al.* Study of the degradation of hybrid sol–gel coatings in aqueous medium. *Prog. Org. Coatings* **77**, 1799–1806 (2014).
 16. Hernández-Escolano, M. *et al.* The design and characterisation of sol–gel coatings for the controlled-release of active molecules. *J. Sol-Gel Sci. Technol.* **64**, 442 (2012).
 17. Kortesus, P. *et al.* Silica xerogel as an implantable carrier for controlled drug delivery—evaluation of drug distribution and tissue effects after implantation. *Biomaterials* **21**, 193–198 (2000).
 18. Kortesus, P. *et al.* In vitro release of dexmedetomidine from silica xerogel monoliths: effect of sol-gel synthesis parameters. *Int. J. Pharm.* **221**, 107–114 (2001).
 19. Henstock, J. R., Canham, L. T. & Anderson, S. I. Silicon: The evolution of its use in biomaterials. *Acta Biomater.* (2014). doi:10.1016/j.actbio.2014.09.025
 20. Habibovic, P. & Barralet, J. E. Bioinorganics and biomaterials: bone repair. *Acta Biomater.* **7**, 3013–26 (2011).
 21. Carlisle, E. M. Silicon: A possible factor in bone calcification. *Science (80-.)*. **167**, 279–280 (1970).
 22. Gatti, A. M. & Zaffe, D. Long-term behaviour of active glasses in sheep mandibular bone. *Biomaterials* **12**, 345–350 (1991).

23. Reffitt, D. M. *et al.* Orthosilicic acid stimulates collagen type 1 synthesis and osteoblastic differentiation in human osteoblast-like cells in vitro. *Bone* **32**, 127–135 (2003).
24. Wiens, M. *et al.* The role of biosilica in the osteoprotegerin/RANKL ratio in human osteoblast-like cells. *Biomaterials* **31**, 7716–25 (2010).
25. Wang, X. *et al.* The marine sponge-derived inorganic polymers, biosilica and polyphosphate, as morphogenetically active matrices/scaffolds for the differentiation of human multipotent stromal cells: Potential application in 3D printing and distraction osteogenesis. *Mar. Drugs* **12**, 1131–1147 (2014).
26. Le Guéhennec, L., Soueidan, A., Layrolle, P. & Amouriq, Y. Surface treatments of titanium dental implants for rapid osseointegration. *Dent. Mater.* **23**, 844–54 (2007).

PROPUESTA DEL TRABAJO DE INVESTIGACIÓN

PLANTEAMIENTO DEL PROBLEMA

La pérdida de dientes es un problema muy común y la reposición de piezas dentales mediante implantes de titanio (Ti) es una práctica clínica recurrente para tratar esta patología.

El titanio comercial puro (cp Ti) está reconocido como altamente biocompatible con propiedades osteointegradoras por sus cualidades mecánicas como densidad y módulo elástico y alta resistencia a la corrosión. La resistencia a la corrosión característica del cp Ti se debe a la formación de una capa superficial de óxido (TiO_2) que se forma de manera instantánea cuando el material está expuesto al aire o medios acuosos. Esta capa superficial de óxido de titanio es la real superficie de contacto de los implantes de titanio con el medio fisiológico y por consiguiente el control de sus propiedades resulta ser muy importante para el éxito del proceso de osteointegración de los implantes.¹⁻³

Como se ha explicado en el apartado anterior, el conocimiento y control de las características superficiales de los implantes (como morfología, topografía, rugosidad, composición química, energía superficial, módulo elástico, impurezas, espesor de la capa de óxido) que afectan la respuesta de los tejidos y consecuentemente afectan el proceso de regeneración ósea constituyen el foco de atención de muchos trabajos de investigación actuales. Aunque el titanio presenta magníficas cualidades y comprobadas propiedades osteoconductoras reflejadas en el correcto anclaje mecánico establecido entre el implante y el tejido óseo carece de capacidad osteoinductiva y es biológicamente inactivo a nivel molecular (material inerte).

OBJETIVOS

Las estrategias actuales utilizadas por la mayoría de los fabricantes de implantes de titanio para mejorar sus características superficiales se basan en tratamientos mecánicos y químicos. La mayoría de implantes dentales comerciales presentan micro-rugosidad de aproximadamente 0,5 - 1 μm obtenida a través de tratamientos superficiales como granallado, deposición de titanio por plasma *spray* y/o tratamientos ácidos, entre otros.

Aunque estas modificaciones superficiales estimulan la respuesta celular induciendo modificaciones en la orientación, locomoción, forma y función celular no existe hasta la actualidad un estándar de rugosidad superficial para los implantes dentales comerciales.^{1, 4-6}

El estudio de nuevas estrategias para conferir a las superficies de titanio propiedades bioactivas es relevante para los fabricantes de implantes dentales. Para una aplicación industrial adecuada es importante encontrar un proceso de fabricación viable y reproducible. Por ello, la aplicación de recubrimientos externos representa una interesante estrategia para mejorar la bioactividad de los implantes dentales de titanio y mejorar su tasa de éxito como tratamiento clínico. Este tipo de modificación se puede idear con dos propósitos, por una parte como matriz para la adhesión celular y por otro como vehículo capaz de retener y liberar biomoléculas y fármacos *in situ*.

El biomaterial desarrollado en este trabajo es un recubrimiento externo orgánico-inorgánico de base silicio aplicado sobre implantes metálicos y sintetizado vía sol-gel. La capa depositada debe ser biodegradable y no debe provocar ninguna reacción indeseable en el huésped. Además, debe ser compatible con la incorporación de biomoléculas y elementos orgánicos sin afectar las propiedades osteoconductoras ampliamente comprobadas de los actuales implantes dentales comerciales de titanio. Esta tecnología resulta interesante especialmente por proporcionar a la superficie de titanio (biológicamente inerte e inactiva) capacidad osteoinductora, reflejándose en una reducción del tiempo de recuperación

del tejido dañado y establecimiento de un contacto hueso-implante adecuado.

Actualmente no existen productos comerciales disponibles en el mercado con un enfoque similar, así que el verdadero reto es el desarrollo de recubrimientos biocompatibles, biodegradables y correctamente adheridos a la superficie metálica de los implantes con comprobada mejoría de las características de los implantes dentales de titanio (osteointegración).

OBJETIVOS

OBJETIVO DE LA INVESTIGACIÓN

El principal objetivo de esta investigación es la producción de un recubrimiento híbrido de base silicio para aplicación en implantes dentales de titanio capaz de mejorar su bioactividad. Esta capa externa debe ser biocompatible, biodegradable y debe proporcionar a los dispositivos médicos de titanio propiedades bioactivas. Consecuentemente, proporcionará a los implantes dentales de titanio propiedades osteoinductoras representando una innovadora tecnología para la administración específica de fármacos en el área lesionada (originada por la implantación). Esta propiedad añadida constituye una alternativa para mejorar el éxito de la integración de los implantes de titanio en pacientes con poca capacidad de regeneración ósea y reducir los tiempos de recuperación de la intervención clínica.

Para lograr el objetivo genérico anteriormente propuesto, diversos objetivos específicos se plantean:

1. Síntesis de recubrimientos con características biodegradables capaces de actuar como vehículo de transporte para moléculas bioactivas.

Para lograr cumplir este primer objetivo específico dos vectores composición se aplicarán para modificar el material referencia 50%MTMOS:50%GPTMS (50M:50G), por una parte se introducirá TEOS (silano) para regular los perfiles de degradación y por otra parte, se variará el contenido en GPTMS que actúa como elemento compatibilizador de las biomoléculas. Esta estrategia mantendrá las características de los implantes, como la biocompatibilidad y además procurará mejorar las características del revestimiento sol-gel usado como referencia (50M:50G)

2. Selección del recubrimiento con mejores propiedades y sugerencia de un prototipo final.

Para lograr cumplir este objetivo específico se realizará una caracterización completa de cada material para estudiar sus propiedades estructurales y se relacionarán los resultados obtenidos con los perfiles de degradación y absorción del medio. Además, se estudiarán algunas propiedades superficiales para comprobar si las características son apropiadas para el desarrollo de los procesos de proliferación y mineralización celular. El estudio del efecto barrera de los recubrimientos contra el intercambio de productos derivados de la corrosión del sustrato metálico que pueden afectar los mecanismos biológicos de regeneración del hueso también se efectuará.

3. Evaluación biológica de cada uno de los nuevos biomateriales para determinar su biocompatibilidad y seleccionar un prototipo final.

Para lograr este objetivo específico se realizarán estudios biológicos *in vitro* y se evaluará en un primero estudio la biocompatibilidad, la proliferación celular en contacto con los recubrimientos sol-gel y se optimizarán las tasas de mineralización.

Por otra parte, se realizará la evaluación *in vivo* de los recubrimientos para comprobar su biocompatibilidad en contacto con los tejidos vivos y verificar su efecto osteoinductivo en comparación con el sustrato metálico (inerte y solamente osteoconductor) y con el material sol-gel usado como referencia (50M:50G).

OBJETIVOS

APORTACIONES ORIGINALES

Actualmente, el interés de muchos grupos de investigación en los xerogeles de base silicio se basa en su utilización como vehículos de transporte de medicamentos y biomoléculas.⁷⁻¹⁸

Sin embargo, el uso del silicio (Si) como bioelemento adicional capaz de promover la osteointegración y la actividad osteoblástica representa otra ventaja de los compuestos de base silicio y se ha aplicado en distintas formas.

El silicio se utiliza ampliamente en ortopedia y por lo general se aplica en forma de biosilica, también denominado biovidrio (SiO_2), para la sustitución de hueso. Además, se ha detectado que el bajo contenido en sílice es esencial para la correcta función del biovidrio y su presencia en cantidades pequeñas altera la temperatura de reblandecimiento y aumenta la expansión térmica del vidrio con consecuencias negativas para su utilización como recubrimiento bioactivo en implantes metálicos.¹⁹

Otra fuente de Si es su uso directo como ácido ortosilícico ($\text{Si}(\text{OH})_4$), una vez que los silicatos son poco solubles y por lo general forman ácidos silícicos o moléculas eléctricamente neutras para disolución.^{20,21,22,23,24,25}

El empleo de un revestimiento osteoconductor biológicamente absorbido en diferentes tipos de prótesis capaces de liberar silicio durante el proceso de degradación representa una estrategia adicional para proporcionar silicio a la zona ósea dañada estimulando la actividad osteoblástica.

Además de la ventaja anteriormente referenciada, la versatilidad de los recubrimientos de base silicio permiten su uso como guía en el proceso de remodelación ósea capaz de actuar en momentos específicos del proceso biológico de regeneración ósea. Esta funcionalidad del recubrimiento se traducirá en la mejora del comportamiento pasivo de las superficies metálicas de los implantes.

La propuesta de este trabajo de desarrollo de recubrimientos biodegradables de base silicio y por lo tanto fuente de silicio, elemento que afecta de forma positiva la actividad osteoblástica, la diferenciación de la matriz extracelular (ECM), la actividad de la fosfatasa alcalina (ALP) y la expresión génica, procura proporcionar bioactividad a la superficie de titanio de los implantes dentales comerciales que son inertes y biológicamente inactivos. Además, los recubrimientos propuestos se diseñan con la intención de actuar como barrera que impida el intercambio de subproductos de la corrosión entre la superficie metálica del implante y los tejidos dañados y así prevenir posibles interferencias de esos elementos en los mecanismos biológicos iniciales del proceso de regeneración ósea.

Esta propuesta resulta interesante para la industria de los implantes dentales representando un notable avance en la tecnología de tratamientos superficiales que actualmente reace sobre tratamientos mecánicos-morfológicos y recubrimientos basados en fosfatos cálcicos u otros materiales inorgánicos.²⁶

Conseguir un método de producción con procesado sencillo y de fácil aplicación en los implantes dentales comerciales genera una serie de posibilidades para proporcionar bioactividad a los implantes dentales de titanio. Además, posibilita la incorporación de biomoléculas estratégicamente seleccionadas capaces de guiar el proceso de regeneración del hueso en las superficies metálicas pasivas.

Por lo tanto, el verdadero reto de este trabajo de investigación es el desarrollo de un biomaterial con las propiedades anteriormente citadas capaz de reducir los tiempos de integración de los implantes y permitir su utilización en pacientes con deficiente regeneración ósea.

PLANTEAMIENTO Y METODOLOGÍA

Este trabajo de investigación se encuadra en un proyecto INNPACTO titulado “Desarrollo de recubrimientos obtenidos vía sol-gel para prótesis dentales de aleaciones metálicas (SOLDENT)” financiado por el Ministerio Español de Economía y Competitividad y el FEDER realizado entre 2010-2013. Dicho proyecto se realizó por un gran equipo multidisciplinar en colaboración con la Universitat Jaume I (UJI), Universidad del País Vasco (EHU) y un socio industrial, ILERIMPLANT S.L.. Los diversos experimentos de este trabajo se realizaron en diferentes lugares (UJI, EHU e ILERIMPLANT) según disponibilidad de instrumentos de análisis. A parte, los experimentos biológicos han tenido lugar en el Centro de Biomateriales e Ingeniería Tisular de la Universidad Politécnica de Valencia y fueron realizados por miembros expertos del equipo de investigación (biólogos).

Este trabajo proviene de tres tesis doctorales en el tema anteriormente defendidas.

En 2011, Miriam Hernández Escolano presentó su trabajo sobre recubrimientos degradables sintetizados vía sol-gel aplicados sobre implantes dentales para mejorar la adhesión celular, la mineralización y la proliferación. Utilizó como precursores de silicio el tetraetil-ortosilicato (TEOS), metil-trimetoxisilano (MTMOS), vinil-trietoxisilano (VTES) y glicidoxipropil-trimetoxisilano (GPTMS) y realizó algunos experimentos para definir las propiedades de cada alcóxido por medio de ensayos físico-químicos, definir la cinética de degradación y rendimiento biológico (ensayos *in vitro*). Los resultados obtenidos motivaron el establecimiento de las mezclas de precursores VTES-TEOS y VTES-GPTMS definidas por distintos intereses, por una parte controlar las propiedades hidrófilas y por otra la posibilidad de transporte de fármacos y biomoléculas. A parte, los resultados obtenidos sugieren que los recubrimientos formados por VTES o MTMOS presentan los revestimientos más protectores frente a la corrosión y los estudios

biológicos con osteoblastos indican la mejora de la proliferación celular en comparación con el control de titanio.

Más tarde, en 2013, M^a Jesús Juan Díaz trabajó con los mismos alcóxidos (TEOS, MTMOS, VTES y GPTMS) y estudió la variación de las propiedades físico-químicas de películas de MTMOS-TEOS y MTMOS-GPTMS para controlar el comportamiento hidrófilo de los recubrimientos y aumentar el contenido orgánico del recubrimiento (permitiendo la unión química con elementos bioactivos) alcanzando distintos grados de degradación, respectivamente. Como conclusión, la mezcla 70%MTMOS:30%TEOS resultó ser el material más apropiado para mejorar las características de la superficie de titanio en la fase inicial del proceso de osteointegración.

Recientemente, en 2015, Irene Lara Sáez evaluó el rendimiento biológico de los recubrimientos desarrollados en los trabajos doctorales anteriormente citados. Los resultados obtenidos muestran que el recubrimiento de composición 70%MTMOS:30%TEOS es el más degradable *in vitro* e *in vivo* y consecuentemente libera la mayor cantidad de silicio. El biomaterial constituido por 50%MTMOS:50%GPTMS provoca una elevada diferenciación osteoblástica, no obstante, la experimentación animal *in vivo* muestra la formación de una capsula fibrosa que recubre toda la superficie del implante que se mantuvo durante las 8 semanas de duración del ensayo experimental indicando el fallo de la osteointegración del implante recubierto con esta formulación.

Teniendo en cuenta las conclusiones de los trabajos anteriormente comentados, la hipótesis de mejorar el rendimiento biológico del material 50%MTMOS:50%GPTMS resulta interesante y constituye una oportunidad de estudio en el campo de los biomateriales de base silicio con funciones de vehículo de transporte de biomoléculas debido a la funcionalidad orgánica proporcionada por el precursor GPTMS. La

OBJETIVOS

desventaja detectada para esta doble mezcla de alcóxidos de formación de tejido fibroso alrededor de todo el implante (no existe biocompatibilidad) en los ensayos in vivo constituye un importante reto para el presente trabajo de investigación descrito en este documento.

Para cumplir con los objetivos propuestos en este trabajo se siguió la siguiente estructura de planificación de la investigación:

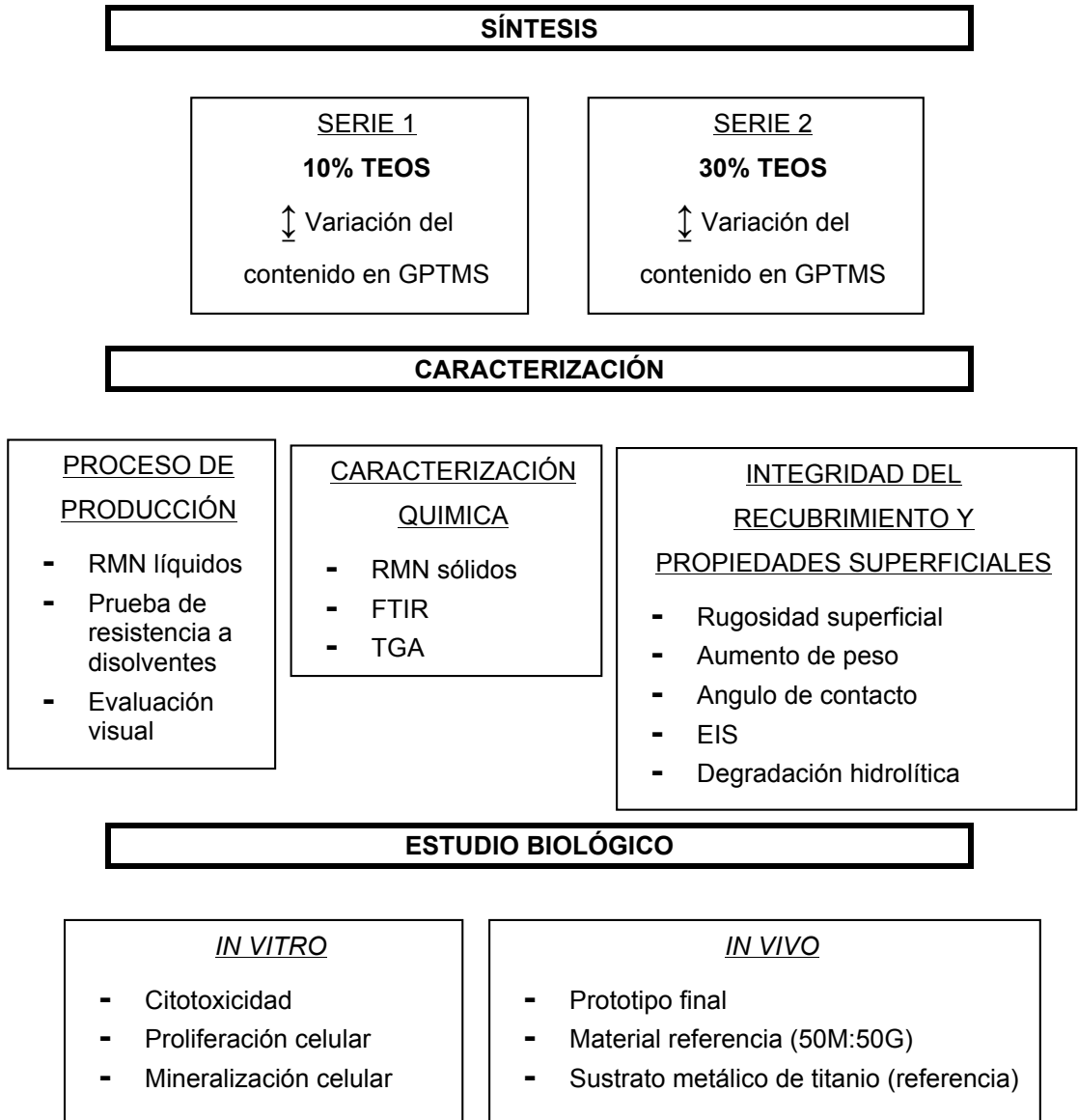


Figura 2. 1 - Esquema del diseño experimental para cumplimiento de los objetivos propuestos.

La estructura de este documento se distribuye en cinco capítulos principales.

OBJETIVOS

En el primer capítulo se explicará la motivación de realización del trabajo y los conceptos relacionados con la implantología dental, proceso de regeneración del hueso, el método sol-gel, entre otros.

A continuación, en el segundo capítulo se presentará el planteamiento del problema, se definirán los principales objetivos de este trabajo, las aportaciones originales y por fin el planteamiento y metodología utilizados.

El tercer capítulo, presentará información sobre los materiales y métodos utilizados para realizar el trabajo experimental.

A continuación se desarrolla el cuarto capítulo dónde se explicará el proceso de producción de los nuevos biomateriales y su caracterización química. Esta caracterización consiste básicamente en la evaluación de la estructura de la matriz polisiloxánica formada y la evaluación visual de los recubrimientos sol-gel. Además, se estudiarán algunas propiedades superficiales, perfiles de degradación hidrolítica y efecto barrera de los recubrimientos contra la posible liberación de subproductos de la corrosión metálica en medios salinos. Se evaluará, además, el éxito de incorporación de biomoléculas (gelatina) a los recubrimientos. Se estudiará la estabilidad de estos híbridos (silano+gelatina) y sus perfiles de degradación. Aún en este capítulo, se seleccionará con base en los resultados celulares *in vitro* y resultados fisico-químicos un prototipo final para evaluación *in vivo*.

Por último, en el quinto capítulo se definirán algunas conclusiones finales del trabajo realizado.

BIBLIOGRAFÍA

1. Gaviria, L., Salcido, J. P., Guda, T. & Ong, J. L. Current trends in dental implants. *J. Korean Assoc. Oral Maxillofac. Surg.* **40**, 50–60 (2014).
2. Albrektsson, T., Sennerby, L. & Wennerberg, A. State of the art of oral implants. *Periodontol.* **2000** **47**, 15–26 (2008).
3. Pye, A. D., Lockhart, D. E. A., Dawson, M. P., Murray, C. A. & Smith, A. J. A review of dental implants and infection. *J. Hosp. Infect.* **72**, 104–110 (2009).
4. Mendonça, G., Mendonça, D. B. S., Aragão, F. J. L. & Cooper, L. F. Advancing dental implant surface technology – From micron- to nanotopography. *Biomaterials* **29**, 3822–3835 (2008).
5. Riccardis, D. E. *et al.* Comparative investigation of the surface properties of commercial titanium dental implants. Part I: chemical composition. *Innovation* **3**, 535–548 (2002).
6. Dohan Ehrenfest, D. M., Vazquez, L., Park, Y.-J., Sammartino, G. & Bernard, J.-P. Identification Card and Codification of the Chemical and Morphological Characteristics of 14 Dental Implant Surfaces. *J. Oral Implantol.* **37**, 525–542 (2011).
7. Radin, S. & Ducheyne, P. Controlled release of vancomycin from thin sol-gel films on titanium alloy fracture plate material. *Biomaterials* **28**, 1721–1729 (2007).
8. Radin, S., Parvizi, J. & Ducheyne, P. Thin sol-gel films on fracture fixation material for the controlled release of antibiotics. *Key Engineering Materials* **309-311 II**, 759–762 (2006).
9. Radin, S., El-Bassyouni, G., Vresilovic, E. J., Schepers, E. & Ducheyne, P. In vivo tissue response to resorbable silica xerogels as controlled-release materials. *Biomaterials* **26**, 1043–1052 (2005).
10. Radin, S. *et al.* In vitro and in vivo bactericidal effect of sol-gel/antibiotic thin films on fixation devices. *Key Engineering Materials* **330-332 II**, 1323–1326 (2007).
11. Radin, S., El-Bassyouni, G., Vresilovic, E. J., Schepers, E. & Ducheyne, P. Tissue reactions to controlled release silica xerogels

OBJETIVOS

- carriers. *R.Z. LeGeros, J.P. LeGeros (Eds.), World Sci. New York* **11**, 529 (1998).
12. Falaize, S., Radin, S. & Ducheyne, P. In vitro behavior of silica-based xerogels intended as controlled release carriers. *J. Am. Ceram. Soc.* **82**, 969–976 (1999).
 13. Radin, S., Ducheyne, P., Kamplain, T. & Tan, B. H. Silica sol-gel for the controlled release of antibiotics. I. Synthesis, characterization, and in vitro release. *J. Biomed. Mater. Res.* **57**, 313–320 (2001).
 14. Radin, S. & Ducheyne, P. Sol-gel formulations for the controlled delivery of growth factors and proteins. in *8th World Biomaterials Congress 2008* **1**, 484 (2008).
 15. Juan-Díaz, M. J. *et al.* Study of the degradation of hybrid sol-gel coatings in aqueous medium. *Prog. Org. Coatings* **77**, 1799–1806 (2014).
 16. Hernández-Escolano, M. *et al.* The design and characterisation of sol-gel coatings for the controlled-release of active molecules. *J. Sol-Gel Sci. Technol.* **64**, 442 (2012).
 17. Kortesus, P. *et al.* Silica xerogel as an implantable carrier for controlled drug delivery—evaluation of drug distribution and tissue effects after implantation. *Biomaterials* **21**, 193–198 (2000).
 18. Kortesus, P. *et al.* In vitro release of dexmedetomidine from silica xerogel monoliths: effect of sol-gel synthesis parameters. *Int. J. Pharm.* **221**, 107–114 (2001).
 19. Henstock, J. R., Canham, L. T. & Anderson, S. I. Silicon: The evolution of its use in biomaterials. *Acta Biomater.* (2014). doi:10.1016/j.actbio.2014.09.025
 20. Habibovic, P. & Barralet, J. E. Bioinorganics and biomaterials: bone repair. *Acta Biomater.* **7**, 3013–26 (2011).
 21. Carlisle, E. M. Silicon: A possible factor in bone calcification. *Science (80-.)*. **167**, 279–280 (1970).
 22. Gatti, A. M. & Zaffe, D. Long-term behaviour of active glasses in sheep mandibular bone. *Biomaterials* **12**, 345–350 (1991).

23. Reffitt, D. M. *et al.* Orthosilicic acid stimulates collagen type 1 synthesis and osteoblastic differentiation in human osteoblast-like cells in vitro. *Bone* **32**, 127–135 (2003).
24. Wiens, M. *et al.* The role of biosilica in the osteoprotegerin/RANKL ratio in human osteoblast-like cells. *Biomaterials* **31**, 7716–25 (2010).
25. Wang, X. *et al.* The marine sponge-derived inorganic polymers, biosilica and polyphosphate, as morphogenetically active matrices/scaffolds for the differentiation of human multipotent stromal cells: Potential application in 3D printing and distraction osteogenesis. *Mar. Drugs* **12**, 1131–1147 (2014).
26. Le Guéhennec, L., Soueidan, A., Layrolle, P. & Amouriq, Y. Surface treatments of titanium dental implants for rapid osseointegration. *Dent. Mater.* **23**, 844–54 (2007).

OBJETIVOS

CHAPTER 3. MATERIALS AND METHODS

MATERIALS AND METHODS

Here, the materials and experimental methods used to produce the new biomaterials and evaluate their properties, as own materials and as hybrid coatings on metallic substrates.

MATERIALS

Three silane derivatives have been used as precursors for materials production; concretely, tetraethoxysilane, trimethoxymethylsilane and (3-glycidyloxypropyl)trimethoxysilane (from now onwards simplified as TEOS, MTMOS and GPTMS, respectively). All these reagents were supplied by Sigma-Aldrich, have analytical grade and were used as received. Their chemical structures are presented in Figure 3.1.

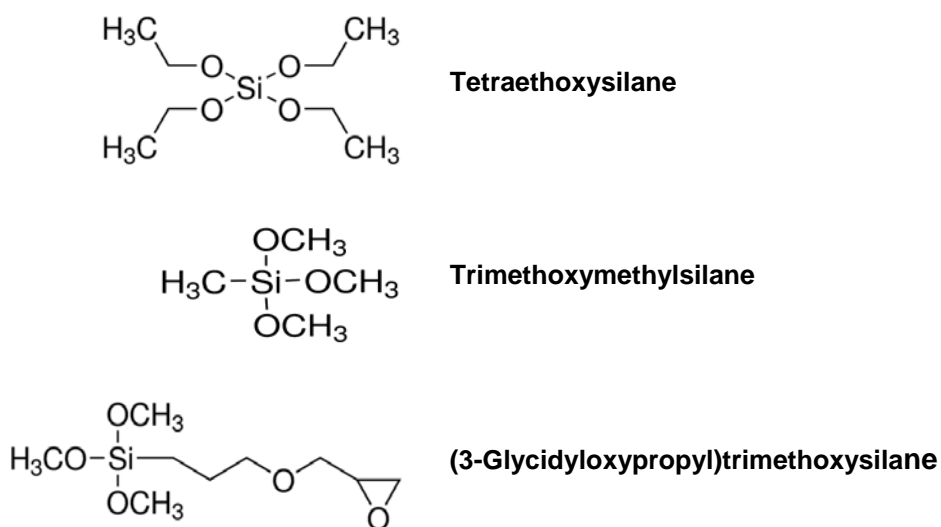


Figure 3.1 – Chemical structure of silane derivatives used on synthesis of hybrid coatings: Tetraethoxysilane (TEOS), Trimethoxymethylsilane (MTMOS) and (3-Glycidyloxypropyl)trimethoxysilane (GPTMS).

MATERIALS AND METHODS

Silane molecules are compounds that contain a general structure $X_n\text{-Si-OR}'_{(4-n)}$ and usually present two types of functional groups characterized into different categories according to their reactivity. On one hand, there are alkoxy groups that participate on the hydrolysis reactions, such as $-(\text{OR}')_4$ in TEOS situation or $-\text{OR}'_{(4-n)}$ on MTMOS and GPTMS molecules, capable of forming chemical bonds with inorganic materials. On the other hand, there are alkyl groups generally expressed as X_n groups,

such as $-\text{CH}_3$ on MTMOS and $-(\text{CH}_2)_3\text{OCH}_2\text{CH}-\text{CH}_2$ on GPTMS, that can bond with organic compounds.

The biomaterials that have been developed in this work are combinations of the three selected alkoxy silanes. They have been specifically selected as each one of them may contribute to obtain a final material with specific properties. For instance, taking into account preceding works by Hernández-Escolano^{1,2,3} and Juan-Díaz⁴, MTMOS helps generating a network with suitable organic-inorganic contents, with proper intermolecular spaces and with good biologic results (*in vitro* assay). GPTMS, otherwise, is a key element for functionalizing implant surfaces. Finally, TEOS is the most inorganic component of these three as it has four alkoxy chains which are susceptible of reacting with water by hydrolysis reaction. Moreover, it is one of the most important constituents to control some of the polysiloxanic matrix properties.^{1,2,3,4}

SAMPLES PREPARATION

This work is based on the fabrication of five different types of samples. Apart from that, four different substrates were used to assess the performance of these biomaterials in the cases they are produced as coatings.

The substrates used to put on the sol and obtain a coating were:

- **Stainless steel AISI 316-L plates** (50 mm length, 50 mm width, 1 mm thickness) supplied by Ramón Navarrete Soria S.A.
- **Microscope glass slides** (26 mm length x 76 mm width) from Labbox Labware S.L.
- **CP grade 4 Titanium Machined Discs** (12 mm diameter and 1,2 mm thick) **treated with ADS® surface treatment** (Advanced Double-Grip Surface) developed by Ilerimplant® S.L. – GMI S.L., consisting of a combination of white corundum micro-bubble treatment and acid etching treatment.
- **Commercial Dental Implantsⁱ: Frontier®** solid screw (3,75 mm outer diameter, 8 mm implanted segment) developed by Ilerimplant® S.L. – GMI S.L. **machined from CP Grade 4 Titanium treated with ADS® surface treatment** (Advanced Double-Grip Surface) that combines a white corundum micro-bubble treatment and acid etching from Ilerimplant® S.L. – GMI S.L.

Prior to their use the stainless steel plates were cleaned with acetone in order to remove impurities resulting from the machining process. Furthermore, a polishing treatment was made to the metal surface with sandpaper (grit size 1200 particles/cm²) followed by deionized (DI) water and acetone cleaning.

The microscope glass slides were washed under sonication for 20 minutes in HNO₃ 25% V/V solution followed by 20 minutes sonication into deionized water. Each of the sonication steps ended with slides being rinsed under deionized water. Finally, these substrates were dried for 2h at 120°C.

ⁱ <http://www.ilerimplant.com/en/ic-frontier-implants.html>

MATERIALS AND METHODS

Titanium discs and dental implants are used as received without any further cleaning protocol. According to the supplier information, these substrates are packaged in a clean room and sterilized with gamma radiation according to their regulations.

Apart from being used as coatings, the silane biomaterials were also obtained as free films. To do so, Teflon cylindrical moulds were used in order to obtain 1 mm thick dry films.

SYNTHESIS AND FILM DEPOSITION

The sol-gel technology used to synthesize the xerogel is based on the methodology proposed by Hernández-Escolano¹. Briefly, it consists on a one-step acid catalyzed sol-gel process at room temperature.

The basic mixture of substances used on sol synthesis is: Co-solvent + Reagents + Catalyst (Figure 3.2).

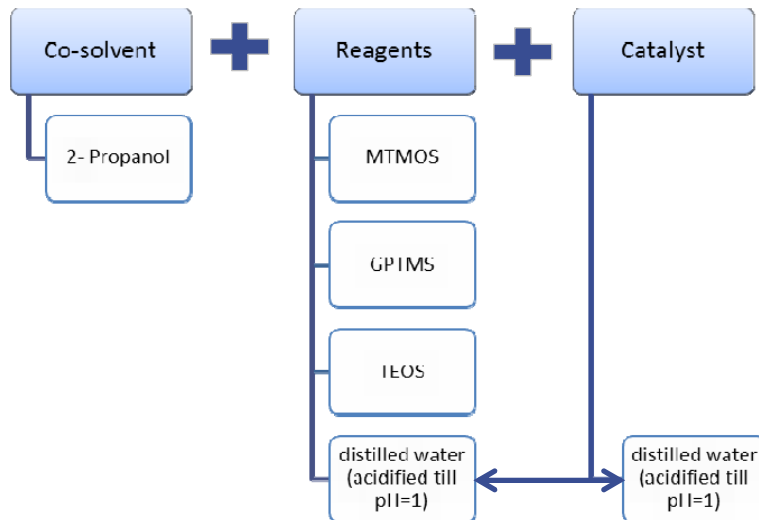


Figure 3.2 – Schematic representation of synthesis reactives.

The volumetric ratio between 2-propanol and alkoxy silanes was fixed on 1:1. In addition, acidified water was used as catalyst to promote alkoxy silanes hydrolysis. To do so, distilled water was used in stoichiometric amounts and, then, acidified with 0,1 N HNO₃ up to pH=1.¹ The obtained solution were stirred for one hour and subsequently set still for another hour at room temperature prior to coating substrates. The room temperature was fixed all the time at 20 - 25 degrees Celsius and the relative humidity was kept at 30 - 40%.

Silanes molar proportions used to make each biocoating are displayed in Table 3.2.

Table 3.2 – Molar ratios of silanes used to prepare the biomaterials.

Material	MTMOS	GPTMS	TEOS
90(M:G):10T	45	45	10
	76	14	
	83	7	
	86,5	3,5	
70(M:G):30T	35	35	30
	56	14	
	63	7	
	66,5	3,5	

A dip coating technique was used to cover the substrates with the *sol*. This methodology requires the substrate to be dipped into the *sol* and withdrawn at constant speed to enable the *sol* drainage (accompanied by solvent evaporation and furtherance of condensation reactions) and its instantaneous gelation (Figure 3.3). The withdrawal speed and *sol* viscosity are key parameters that affect in an important way the film thickness and morphology.⁵

In this work, cleaned substrates were immersed on the previously obtained colloidal suspension using a dipping device (KSV instrument-

MATERIALS AND METHODS

KSV DC). The immersion speed was fixed at $100 \text{ cm}\cdot\text{min}^{-1}$. The substrate was left submerged into the *sol* for 1 min and finally levered up also at a speed of $100 \text{ cm}\cdot\text{min}^{-1}$.

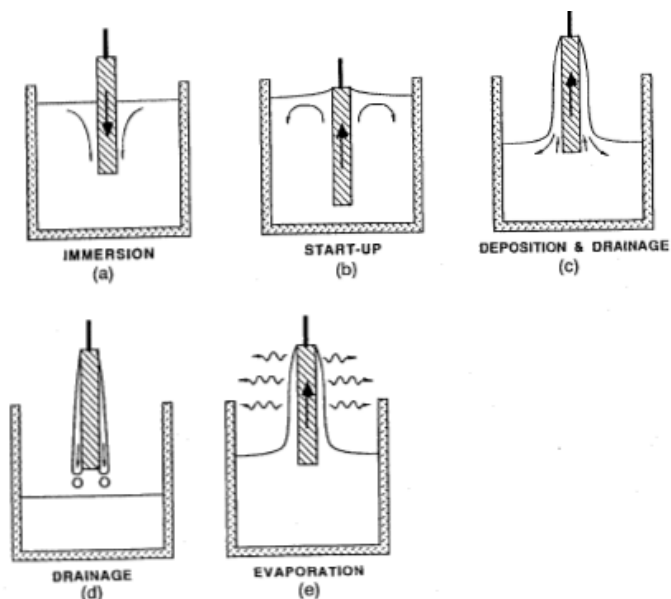


Figure 3.3 – Schematic representation of the dip coating batch process.⁶

Afterwards, xerogels were dried by thermally treating them in order to encourage solvent evaporation and condensation of residuary $-\text{OH}$ groups, thus originating a final thick coating. The conditions of the thermal processes that have been used, according to the biomaterial that was produced, are described in Table 3.3.

Table 3.3 – Thermal treatments used to produce the biocoatings.

Material	90(M:G):10T		70(M:G):30T
Temperature (°C)	50	100	80
Time (min)	15	105	120

The thermal treatment of series 90(M:G):10T materials follows a progressive temperature raising profile, it starts 15 minutes at 50°C followed by 105 minutes at 100°C (120 minutes total treatment). On the other hand, series 70(M:G):30T materials thermal treatment consists of 120 minutes at 80°C during all the treatment.

The production of the free films follows the same synthesis process and thermal treatment as coatings, however, after the *sol* production an appropriate quantity of *sol* was poured into the moulds to obtain a final dry film thickness of 1mm.

To sum up, Figure 3.4 depicts the global process that has been followed in order to obtain the biomaterials used in this work.

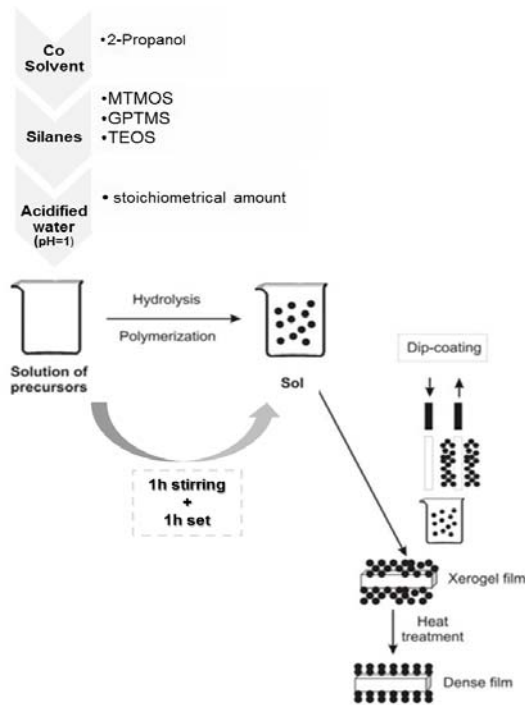


Figure 3.4 – Schematic representation of the global productive method of biomaterials.

ANALYSIS TECHNIQUES

COATING INTEGRITY AND SURFACE PROPERTIES

Scanning electron microscopy (SEM)

Scanning electron microscopy has been used to study the morphology and thickness of the biocoatings, as well as to perform elements' analyses to the coatings samples.

Scanning electron microscope (SEM) is one of the most useful instruments for examination and analysis of microstructure morphology and chemical composition determination on nanomaterials. This technique has its origin on the replacement of the light source of optical microscopes with high-energy electron beam. The equipment is prepared to scan electron beam across the sample surface and collect scattered electrons for imaging. The most popular SEM imaging method used is secondary electron imaging (SEI), it is possible to attain good resolution imaging down to 10 nm with a large depth of field and topographic contrast, a very important feature to study surface topography, texture and roughness. When primary beam strikes sample surface and origin ionization of specimen atoms, loosely bound electrons may be emitted and those are known as secondary electrons. These secondary electrons have low energy, typically 3 – 5 eV and can only escape from regions within a few nanometers of the material surface.

The images can also be achieved by means of backscattered signals (BSE) associated with electrons that escape from the surface with an energy greater than 50eV, on this case the sample need to be conductive to prevent charging. Besides, backscattered electrons are many times scattered by samples elastically what can be related to atomic number near the surfaces as well as crystallographic orientation of the surface. In addition to those signals used to generate an image,

other signals are produced when an electron beam strikes a sample as X-rays, Auger electrons and cathodoluminescence. Many times, backscattered electrons, together with characteristic X-rays, are often used to identify chemical composition and the base concept associated with this technology is the fact that wavelength of the characteristic X-ray is directly related with the energy delta between the outer and inner shells, besides is intrinsic to each element. Characteristic X-rays have been widely used in SEM and is usually called energy-dispersive X-ray spectroscopy (EDX).^{7,8}

Samples were examined in a *Leica-Zeiss LEO 440* scanning electron microscope equipped with an *INCA 250 (Oxford)* energy dispersive X-ray spectroscopy (EDX) microanalytical system and software. Samples were coated with carbon for elemental microanalysis and with platinum for surface morphologic characterization. The operating conditions were: 20 kV acceleration potential, 22 - 26 mm working distance, 2000 A specimen current for BSE and 100 A specimen current for SE.

Mechanical Profilometry

Surface roughness profiles were acquired by mechanical profilometry.

The applications of surface profilometry cover roughness and waviness estimation and step height measurements. The base of mechanical profilometry stands on contact measurements of the sample; a stylus is moved across the surface to detect the vertical displacement and is converted to a height value in Z axis equivalent to the step height in the sample. The hardware that comprises this analysis is mechanical and electronic devices in order to register the surface topography and convert the data. During the surface scanning, the vertical displacement of the stylus respect to a conventional zero value is converted into a electrical signal and then amplified, digitalized and analyzed in order to achieve a line profile according to the international standards.⁹

MATERIALS AND METHODS

Measurements were carried out with a *Dektack 6* equipment (*Veeco*) and the data analysis was assisted by *standard Dektak 6M software* version 8.30.005.

In this work analysis, the cursor displacement was of 10 mm and the following local surface irregularities were recorded and amplified to get a line profile.

Six records were measured for each sample, corresponding with the positions and displacements shown in Figure 3.5. The tracking force used was 15 mg, which was known from preliminary tests to be suitable to obtain accurate data but not excessively intense to damage the coating and modify the original texture. Each scanned line was acquired with a resolution of $1,11\mu\text{m}/30\text{sec}$ and were used cut-off wavelength filters up to 1 mm or 4 mm.

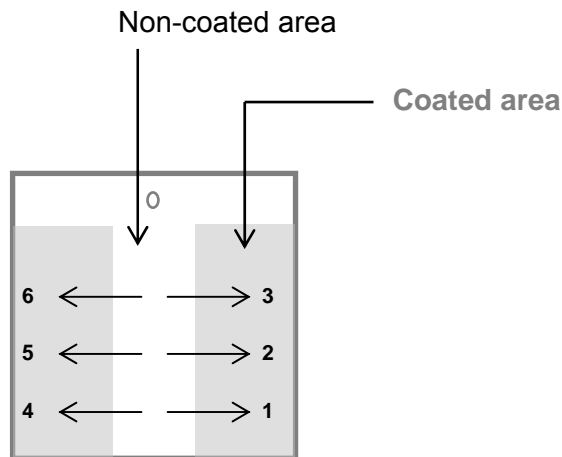
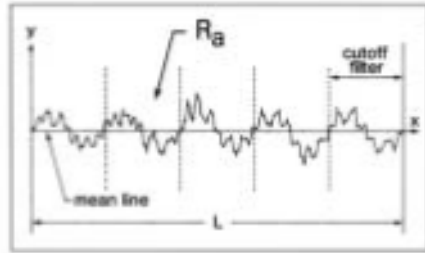


Figure 3.5 – Schematic representation of linear profiles acquired on coated samples.

Average roughness (R_a) was used for measuring surface texture. This parameter is defined as the arithmetic average deviation from the mean value of high along the distance covered during the test (Figure 3.6).



R_a is the arithmetic average deviation from the mean line within the assessment length (L).

$$R_a = \frac{1}{L} \int_{x=0}^{x=L} |y| dx$$

Figure 3.6 - Average roughness (R_a) analytical function.¹⁰

Contact Angle (Wettability)

The contact angle was measured to quantify the wettability of the coatings surfaces. Two situations can be well-defined from a thermodynamic point of view, complete or partial wetting. The complete wetting gives place to a thin film above the solid surface, on the other hand, partial wetting with contact angles $>90^\circ$ are generally attributed to “non-wetting” surfaces and the partial wetting results $<90^\circ$ contact angles sustain an equilibrium of three interfacial tensions, solid/vapor (γ_{sv}), solid/liquid (γ_{sl}) and liquid-vapor (γ_{lv}) (see Figure 3.7). The mechanical equilibrium at the contact point of the three phases determines the value of the parameter contact angle (θ_e) used for measuring wettability according to Young’s correlation:

$$\cos \theta_e = \frac{\gamma_{sv} - \gamma_{sl}}{\gamma_{lv}} \quad .^{11}$$

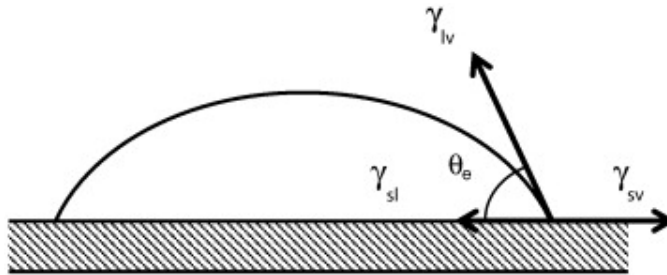


Figure 3.7 – Schematic representation of equilibrium contact angle and the interfacial tensions associated with the system.

The wettability of the sol-gel coatings was characterized by measuring the contact angle of a water drop after 21 seconds contact with the polymeric surface with a Dataphysics OCA20 (Dataphysics Corp.) analyzer. A syringe was used to place a drop of 10 μl (velocity 27,5 $\mu\text{l/s}$) of DI water on the sol-gel surface. The results correspond with the mean values of the measurements from 30 distinct drops placed at different points of each coated sample, based on stainless steel plates (15 drops in each side of the plates). All experiments were performed at room temperature $\approx 23^\circ\text{C}$ and relative humidity of 50%.

Electrical Impedance Spectroscopy (EIS)

Electrochemistry is the study of the chemical response of a system to an electrical stimulation and is associated with the reduction and oxidation reactions that a material undergoes during that stimulus.

Electrical impedance spectroscopy (EIS) is the measurement of a material resistance to the flow of alternating current (AC). It can be used to measure electrical resistance of biological tissues (dental tissues, bone and skin), structural ceramics and some polymers, besides, it is a non-destructive and very sensitive method to study not only conductive materials (metals and alloys) but also insulating materials. Conductive properties are strongly affected by a material microstructure and

impedance measurement can be related with changes in a material microstructure caused by many different causes.¹²

Some concepts of electrical circuit theory and electrochemistry are necessary to clarify for better understanding EIS technique.¹³⁻¹⁵

The classical definition of electrical resistance is related with Ohm's law and is expressed by the relation between voltage (E) and current (I)

$$R = \frac{E}{I}$$

where R is resistance in ohms, E is voltage in volts and I is current in amperes. Nevertheless, in the real world systems are quite more complex than the classical resistor behavior associated with Ohm's law. For that reason arises a new concept to measure the ability of a circuit to resist the flow of electrical current, impedance (Z), this time not affected by some of the limitations associated with the ideal resistor (Ohm's law relationship is valid for all current and voltage levels, the resistance value is independent of frequency, alternating current (AC) and voltage signals though resistors are in phase with each other). The mathematical expression used to define impedance is function of the magnitude (Z_0) and the phase shift (φ).

$$Z = \frac{E(t)}{I(t)} = \frac{E_0 \cdot \cos(\omega t)}{I_0 \cdot \cos(\omega t - \varphi)} = Z_0 \frac{\cos(\omega t)}{\cos(\omega t - \varphi)}$$

where $E(t)$ (excitation signal) and $I(t)$ (response signal) are voltage and current on instant (t), E_0 and I_0 are voltage and current of the signal, ω represents the radial frequency (expressed in radians/second) also defined as $\omega = 2\pi f$, f is frequency (expressed in hertz) and finally φ is the phase shift (expressed in degrees). The impedance is therefore expressed in terms of a magnitude - Z_0 and a phase shift - φ .

MATERIALS AND METHODS

The ratio of amplitudes of the induced signal and the response signal as well as the phase shift between both signals defines impedance. In a linear system, the current response to a sinusoidal potential signal will be also a sinusoidal response at the same frequency but shifted in phase. (Figure 3.8)

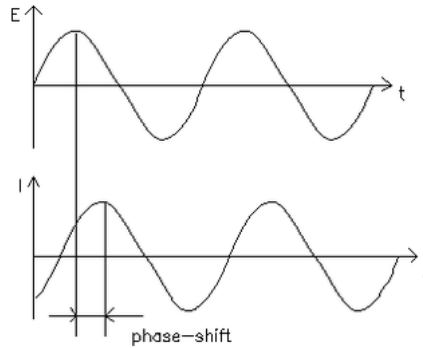


Figure 3.8 - Sinusoidal current response in a linear system.¹³

With Euler's relationship it is possible to express the impedance as a complex function.

$$\exp(i\theta) = \cos\theta + i \sin\theta$$

Where $i^2 = -1$ is the imaginary number and θ is the angle.

Although the sinusoidal perturbation of the potential and consequent response is represented by two vectors in the complex plane, the associated impedance can be represented by a sum vector of the real and imaginary part. As a result, the impedance is then represented as a complex number characterized by a modulus Z_0 and a phase shift φ :

$$Z = \frac{E_0 \exp(j\omega t)}{I_0 \exp(j\omega t - j\varphi)} = Z_0 \exp(j\varphi) = Z_0 (\cos\varphi + j\sin\varphi)$$

$$Z = Z_{Re} + j Z_{Im}$$

Using appropriate mathematical relations, impedance modulus can be calculated by

$$|Z| = \sqrt{Z_{Re}^2 + Z_{Im}^2}$$

And phase shift

$$\theta = \arctan\left(\frac{Z_{Im}}{Z_{Re}}\right)$$

The usual data presentations are the forms: Nyquist diagram or Bode plot (Figure 3.9). When impedance is represented in the complex plane with the real part plotted on the X-axis and the imaginary part plotted on the Y-axis of a chart for different frequencies the attained graphic is called “Nyquist diagram”. On the other hand, if impedance is represented by its modulus p (logarithmic scale) (Y axis) and phase shift (secondary Y axis) as function of frequency f (logarithmic scale) is usually called “Bode plot”.

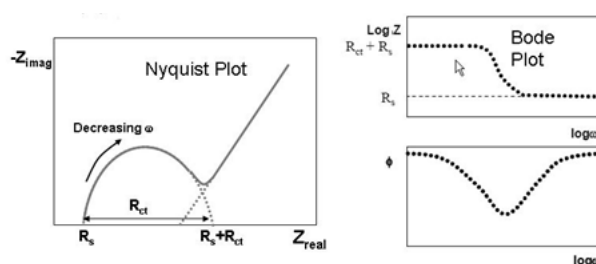


Figure 3.9 - Nyquist diagram (left) and Bode plot (right) of impedance data for a simple equivalent circuit (Randles circuit).

It is very important to achieve reliable impedance results for the accomplishment of linearity of the electrochemical system. A linear system was described by Oppenheim and Willsky¹⁶ as a system that presents the property of superposition, this mean that if input is the

MATERIALS AND METHODS

weighted sum of several signals then the output must be the weighted sum of the responses of the system to each of the signals. Electrochemical systems can be classified as pseudo-linear if a small AC signal, 1-10 mV, is applied to the cell. Another important condition to achieve valid EIS results is the accomplishment of steady state systems, that is to say, the system must be at a steady state throughout the time required to measure EIS spectrum.

The analysis of impedance spectra results requires the data translation to electrical models that best fits with the physico-chemical phenomenon that occur on the studied system.

Some of the electrical elements commonly used to describe electrochemical mechanisms and properties of the systems are listed in Table 3.4.

Table 3.4 - Electrical elements used to fit EIS experimental results, physico-chemical meaning and corresponding impedance expression.

Electrical element	Physico-chemical meaning	Impedance expression
Resistance (R)	Describes charge transfer across certain interface (for example metal/electrolyte).	R
Capacitance (C)	It is characteristic to charge structures (double layers) if considering these layers as parallel plate condensers.	$-\frac{i}{\omega \cdot C}$
Inductor (L)	It is related with adsorption-desorption processes occurring in the formation of layers (passive film).	$i \cdot \omega \cdot L$
Warburg (infinite)	It represents linear diffusion processes under semi-finite conditions. Also assumes the diffusion layer to possess an infinite thickness.	$-\frac{1}{Y_0 \sqrt{i \cdot \omega}}$ where Y_0 is admittance
Warburg (finite)		$\frac{\tanh(B \cdot \sqrt{i \cdot \omega})}{(Y_0 \cdot \sqrt{i \cdot \omega})}$ where B is a diffusion parameter

The simplest equivalent circuit used to fit EIS experimental results is Randles circuit of the electrode-electrolyte interface (Figure 3.10),

where R_s is solution or electrolyte resistance, C_{dl} is the double layer capacitance and R_{ct} is charge transfer resistance (also referred as R_p due to polarization phenomenon).

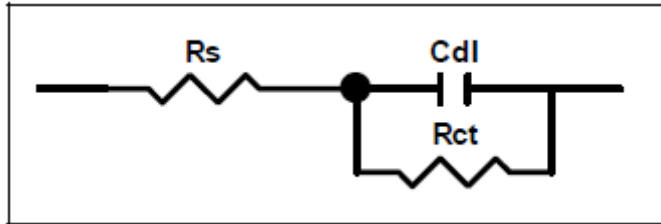


Figure 3.10 - Equivalent Randless electric circuit used to fit electrode-electrolyte interface.

The impedance mathematical expression used to define a system behavior that fits on a Randless equivalent circuit is:

$$Z(\omega) = R_s + \left(\frac{1}{\frac{1}{R_{ct}} + i \cdot \omega \cdot C_{dl}} \right)$$

The impedance results of the analysis of a system translated to a Randless circuit are similar to the ones represented on Figure 3.9 where it can be seen that at high frequencies $|Z|$ shows a tendency to stabilization at a constant value with a phase shift close to 0° when frequency increases. This resistive behavior and impedance data are usually associated to R_s (electrolyte resistance). In the range medium-lower frequencies a linear relationship between $\log|Z|$ and $\log f$ becomes visible. For an ideal capacitive behavior the slope (n) is approximately -1. In the case of a non-ideal system far-off an ideal capacitive behavior, different and lower value of the slope and lower phase angles fits better with that behavior. A constant phase angle element (CPE) replaces the capacitive element on the system to better describe the non-ideal conduct that can be induced by many physical phenomenons as surface

MATERIALS AND METHODS

roughness, impurities, dislocations or grain boundaries. CPE is mathematically defined as

$$Z(\omega) = Z_0 (i\omega)^{-n}$$

Where Z_0 is the CPE constant and n is the CPE exponent. The n value determinates if the appropriate electrical element is a resistance ($n=0$ and $Z_0=R$), a capacitive element ($n=1$ and $Z_0=C$) or a Warburg impedance ($n=0,5$ and $Z_0=W$). If n is within a range 0,5-1 the CPE represents a distribution of dielectric relaxation times in the frequency scanning.

Capacitance, C , is an important parameter and it is related to the film/coating thickness as it can be seen on the mathematical expression used to estimate its value

$$C = \varepsilon \cdot \varepsilon_0 \cdot \frac{A}{d}$$

Where ε is related with the relative dielectric constant of the layer, ε_0 represents the vacuum permittivity ($8,85 \times 10^{-14}$ F.cm⁻¹), A is the active area (cm²) and finally d represent film thickness (cm).

1. A minimum number of electrical elements employed to describe the electrochemical system in study
2. Chi-squared value (χ^2) should be less than 10^{-4}
3. The errors associated with each electrical element by itself must not be greater than 5%.

The special case of EIS of coated metals follows a specific behavior, after a certain contact period of time with electrolyte the liquid penetrates into the coating and gives place to a new liquid-metal interface under the coating and corrosion phenomena can happen at this new interface. Besides, while organic coatings are in contact with electrolyte the

capacitance will present changes with time as the coating swells or absorbs liquid. To quantify the physical and chemical processes that take place on a system established as “coated metals” it is necessary to find a proper equivalent circuit. The most frequently used electrical circuit to describe the system of an organic coating on a metallic substrate is the one illustrate in Figure 3.11.

The first element, referred in Figure 3.11 as uncompensated resistance (R_s), also called electrolyte resistance, represents the resistance between the working electrode and reference electrode produced by electrolyte presence. In the study case of organic coatings the electrolyte is very conductive ($R = 1 - 50 \Omega$) and its resistance can be ignored in many situations. Usually R_s remains relatively constant and for 3,5wt% NaCl electrolyte is about $17\Omega^{12}$, on the other hand, for Hank’s solution stays around $9,5\Omega^{17}$.

The next circuit element, named coating capacitance (C_c) is associated with coating permeability. The mathematical expression used to estimate a pure capacitive behavior (C_c) is

$$C_c = \varepsilon \cdot \varepsilon_0 \cdot \frac{A}{d}$$

where ε is the dielectric constant of the coating, ε_0 refers to free space dielectric constant and is $8,85 \times 10^{-14}$ Farads/cm, A is the contact area with electrolyte (cm^2) and d is the thickness of the coating (cm). The relation between capacitance and the magnitude of the impedance $|Z|$ is established by

$$|Z| = \frac{1}{2 \cdot \pi \cdot f \cdot C_c}$$

where f is the frequency of the applied AC voltage.

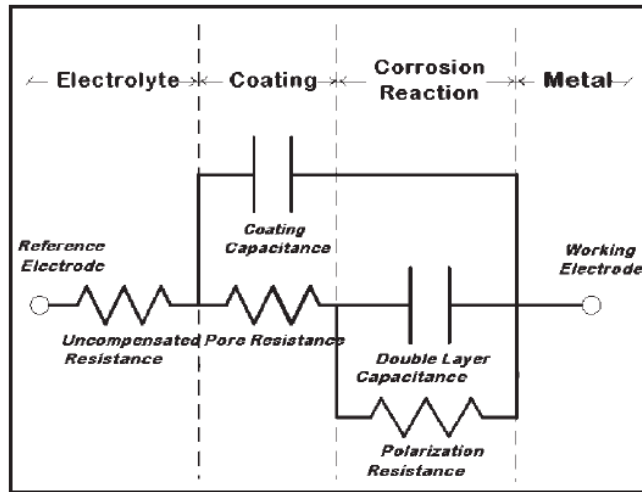


Figure 3.11 – Equivalent circuit of an organic coating overlaid on a metal substrate.¹⁸

Pore resistance (R_{po}) is related with the penetration of electrolyte into the micropores of the coating.

A third resistance closer to the metal, called polarization resistance (R_p) is associated with the corrosion rate of the metal substrate beneath the coating. The polarization resistance is inversely proportional to the corrosion rate. This parameter must be normalized since it is electrode area dependent.

The final circuit element, double layer capacitance (C_{dl}), arises from the metal-electrolyte interface formed due to the different charges registered on the work electrode (metal substrate) and on the electrolyte. When a coating is strongly adhered to the metal surface does not allow metal-electrolyte direct contact, so C_{dl} can be related to delamination of the coating. C_{dl} must be normalized since it is electrode area dependent.

The two circuit elements that typically most interfere on impedance results are the coating capacitance (C_c) and the pore resistance (R_{po}). However, when a coating is damage by electrolyte attack, changes in the EIS response are detected and circuit elements may modify.

The corrosion resistance and electrochemical exchange of coated stainless steel plates were evaluated by means of electrochemical measurements carried out at room temperature in a Faraday cage, in contact with 25ml of naturally aerated 3,5wt% NaCl solution and Hank's Balanced Salt Solution (Ref. H 9269 from Sigma-Aldrich). The electrolyte was stirred during 20 minutes before each measurement and the exposed area of coated surface to the solutions was of 3,14 cm² (diameter = 20 mm). The coated surface (working electrode) was adapted in a three electrode cell using as reference electrode Ag/AgCl and a graphite sheet as counter electrode (Figure 3.12).

The electrochemical impedance spectroscopy (EIS) tests were carried out using a potentiostat-galvanostat AUTOLAB ECO CHEMIE, model PGSTAT30. The EIS measurements were acquired for several immersion times (0h, 1.30h, 3h, 4h, 6h, 8h, 10h, 24h, 48h, 7 days and 14 days) and performed applying a 10mV sinusoidal perturbation signal, from 0,01 Hz to 100 000 Hz recording 5 points per frequency decade.

For quantitative analysis the results were associated with electrical equivalent circuits and fitted with Z-view® program.

MATERIALS AND METHODS

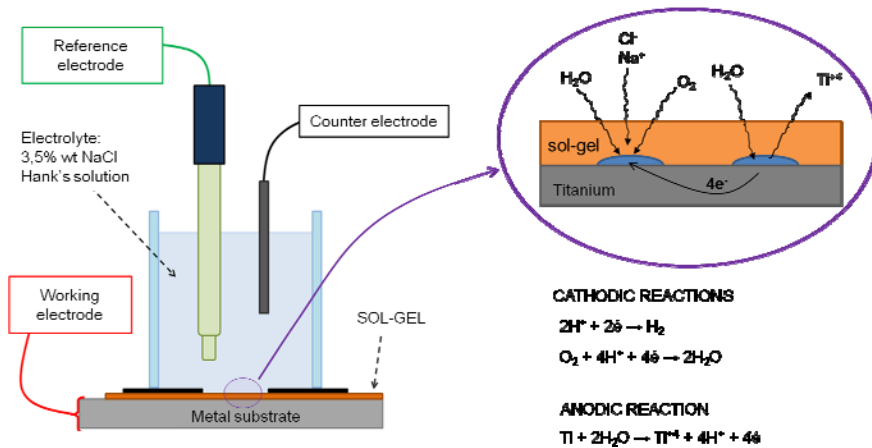
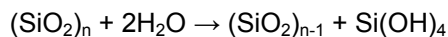


Figure 3.12 - Schematic representation of the three electrode cell used on electrochemical impedance spectroscopy (EIS) measurements.

Hydrolytic Degradation

The hydrolytic degradation of the silica based coatings was evaluated by means of indirect measurement of weight loss. With that purpose, a test was developed taking into account the standard directive on "Biological evaluation of medical devices. Part 13: Identification and quantification of degradation products from polymeric medical devices" - ISO 10993-13:2010.

The chemical reaction of silica dissolution in the presence of water and consequent formation of orthosilicic acid follows the scheme:



The degradation measurement was performed by soaking microscope glass slides coated with silica based sol-gel by flow-coating in distilled water at 37°C. The weight loss was measured at 7, 14, 28, 42 and 63 days of immersion in 100 ml of distilled water (enough quantity to avoid medium saturation). After completion of each of the selected times' analysis, each sample was removed and dried in an oven at 50°C for

24h, followed by vacuum drying at 50°C for another 24h. Finally the samples are left on a desiccator until weighing. Three samples were tested per time period and, after being weighed, the samples were retired from the study. The water uptake, as an average value for every set of these 3 samples, was calculated as:

$$W(\%) = \frac{m_f - m_i}{m_i} \times 100$$

where m_f and m_i are samples' weights after and before immersion, respectively.

PHYSICO-CHEMICAL PROPERTIES

Fourier Transform Infrared Spectroscopy (FTIR)

Fourier transform infrared (FTIR) spectroscopy is a useful technique to study the chemical interactions between the organic and inorganic structural units of hybrid gels. FTIR spectroscopy is a technique based on the vibrations of the atoms. The spectrum is usually obtained by passing infrared radiation through a sample and determining what fraction of the incident radiation is absorbed at a specific energy. The peaks that rise at a specific energy range in spectrum correspond to the vibration frequency of a part of a sample molecule.

For a molecule to show infrared absorptions must present a change on electric dipole moment during the vibration (stretching and bending movements). The larger this change, more intense will be the absorption band on spectrum.²³

The acquirement of a spectrum is based on the interferences on the radiation between two beams and achievement of an *interferogram*, defined as a signal produced as a function of the change path length

MATERIALS AND METHODS

between the two beams. The two domains, distance and frequency, are convertible by the mathematical method of Fourier-transformation.

The emerging radiation from the source system passes through an interferometer to the sample before reaching a detector. Then, the signal is amplified and filtered to finally get data translation to digital form and transference to the computer. The common spectra record percentage transmittance over a linear wavelength range. It is commonplace to have the choice of absorbance or transmittance as a measure of band intensity.

Structural and chemical characteristics of the hybrid coatings, on the form of free films, were characterized with an Equinox 55 FTIR spectrometer. All spectra were recorded on the attenuated total reflectance (ATR) mode in the range of $600\text{-}4000\text{ cm}^{-1}$, at a nominal resolution of 4 cm^{-1} using 32 scans. The results were normalized against a background scan collected at room temperature.

Nuclear Magnetic Resonance (NMR)

Nuclear magnetic resonance (NMR) is one of the most extensively studied and used magnetic resonance techniques; it is non-destructive and allows structural elucidation and quantification of single atoms and molecules.

NMR spectroscopy is based on the use of an electromagnetic radiation to force the α orientated nuclei into β state, when energy stimulation stops the excited nuclei relax and return to α state (Figure 3.13). The fluctuation of the magnetic field generated on the relaxation process is called resonance and with appropriate equipment is detected and converted into a NMR spectrum.

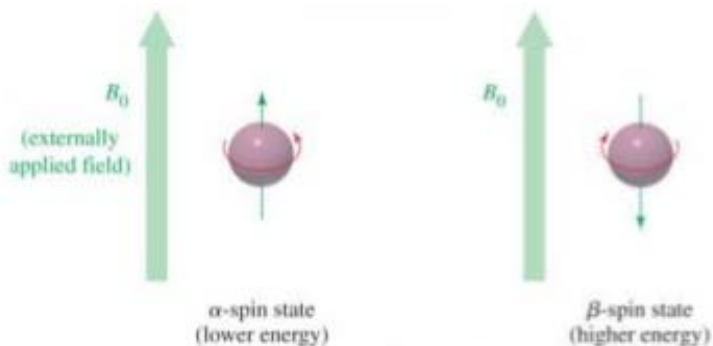


Figure 3.13 – Schematic diagram of α spin state and β spin state.

Usually the NMR spectrum is a plot of absorbance versus frequency (δ (ppm), parts per million chemical shift) (Figure 3.14).²⁴

$$\text{chemical shift } (\delta) = \frac{\left(\begin{array}{l} \text{frequency of absorbed} \\ \text{electromagnetic radiation} \\ \text{by sample nucleus in Hz} \end{array} \right) - \left(\begin{array}{l} \text{frequency of absorbed} \\ \text{electromagnetic radiation by} \\ \text{TMS standard in Hz} \end{array} \right)}{\text{Spectrometer frequency in MHz} \\ \text{(This accounts for magnet strength)}}$$

reported as parts per million (ppm) shift downfield from the TMS standard

Note that the absorbed frequencies are in Hz and the spectrometer frequency is in MHz, meaning there is a millionfold difference in frequencies here, hence the term "parts per million (PPM)".

Figure 3.14 – Equation that defines chemical shift (δ) used on NMR spectrum.

²⁹Si NMR solid spectroscopy was carried out to evaluate the degree of cross linking of the coatings after heat treatment. The samples, under the form of free film, were yield to a Bruker 400 AVANCE II WB PLUS spectrometer, coupled to a CP-MAS (cross polarization magic angle spinning) probe. The sample spinning speed was fixed on 7,0 kHz and the pulse sequence followed was Bruker standard, frequency was 79,5 MHz, spectral width was 55 kHz, contact time was 2 ms and delay time was 5 s.

MATERIALS AND METHODS

^{29}Si NMR liquid spectroscopy was performed to investigate the evolution of the hydrolysis and condensation steps of the sol reaction process. Samples were analyzed on a FT-NMR Bruker 400 Avance spectrometer at a frequency of 79,47 MHz. In order to have a reliable measure of chemical shift, tetramethyl silane (TMS, $(\text{CH}_3)_4\text{Si}$) was used as internal reference and $2,5 \cdot 10^{-3}\text{M}$ of chromium (III) acetylacetonate was used as relaxation agent. Spectra were acquired under the following conditions: 384 scans were collected for each sample with a repetition time between pulses of 2,8 s.

The first spectrum acquired was a mixture of solvent and silanes only, then acidified water (catalyst) was added and a new spectrum obtained. In order to follow hydrolysis and condensation reactions' progress, a first spectrum was acquired over the mixture of solvent and silanes, in each case, then, acidified water (catalyst) was added and a new spectrum was recorded. Finally a spectrum was recorded each hour until stabilization.

Thermogravimetric Analysis (TGA)

Thermogravimetric analysis (TGA) is a technique that measure samples weight variation as a function of temperature or time as the sample specimen is subjected to a controlled and well defined temperature program in a controlled atmosphere.

This analysis enables the quantification of loss of water, loss of solvent, decarboxylation, pyrolysis, oxidation, decomposition, amount of metallic residue remaining among others.

Usually, the TGA thermal curve is displayed as weight (mg) or weight percent (%) versus time or temperature.

TGA was conducted by a TG-STDA Mettler Toledo (model: TGA/SDTA851e/LF/1600) equipment coupled to a quadrupole mass spectrometer PFEIFFER VACCUM (model: THERMOSTAT). Xerogel

samples (20 mg) were placed on platinum crucibles and heated at a rate of 10°C/min from 50°C until 900°C in N₂ atmosphere. A thermal treatment of 50°C during 10 min was made to all samples before thermogravimetric analysis.

BIOLOGICAL PERFORMANCE

In vitro

The impact of the developed sol-gel coatings on cells' phenotype and metabolism is necessary as their final application requires cellular adhesion and differentiation into specific cells that are the real performers of the bone regenerative process. With that purpose, biological *in vitro* experiments were made as a first study of the biological performance of the new biomaterials. MC3T3 cell lines from mouse calvaria (Riken Cell Bank, Tokyo) were used to measure cellular proliferation and mineralization.

Measurement of the cellular cytotoxicity

The measurement of cellular viability was made through MTS (3-(4,5-dimethylthiazol-2-yl)-5-(3-carboxymethoxyphenyl)-2-(4-sulfophenyl)-2H-tetrazolium) assay. This colorimetric method is based on the reduction of MTS tetrazolium compound by viable cells to generate a blue colored formazan product soluble in cell culture medium. The formazan dye produced by viable cells can be quantified by measuring the absorbance at 490-500nm.

The used detection method was the extract test and the protocol followed is in agreement with ISO 10993-5 related with medical devices.

MATERIALS AND METHODS

This assay allows the quantification of cytotoxicity and was assessed using CellTiter 96[®] Aqueous One Solution Assay (Promega, Wisconsin;EEUU).

To do so, 0,5 g of study materials were sterilized by ultraviolet light (UV) and were incubated for 24 hours at 37°C and 5%CO₂ with 1ml of DMEM (Dulbeco's Modified Eagle's medium) (2ml/1g) (Gibco[®]-Invitrogen, California;EEUU). The same process was followed to prepare the positive control (commercial latex) for *in vitro* cytotoxicity test and as negative control was used the polystyrene cell culture dish without extract.

MC3T3 cells were plated (24 well plate) at an initial density of 18.000 cells/cm² during 24h in DMEM medium with 10% FBS (Fetal Bovine Serum) (ThermoFisherScientific, MassachusettsEEUU) and 1% P/S (penicillin/streptomycin) (Lonza,Basilea; Switzerland). Afterwards, cellular medium was removed and materials' extract was added to a wells plate. After 24 hours incubation the medium was removed and 1:5 MTS and DMEM solution (Sigma-Aldrich, Missouri;EEUU) was added. Finally, it was incubated for 3h at 37°C and 5%CO₂ in light absence and the absorbance was measured at 490 nm with a standard microplate reader Victor3 Multilabel plate reader (Perkin-Elmer). The quantity of formazan product, as measured by the amount of 490 nm absorbance, is directly proportional to the number of living cells in culture. Each experiment was done in triplicate.

Measurement of the cellular proliferation

The Alamar Blue[®] assay was selected as methodology because it has been widely use in many studies of cell viability and cytotoxicity, apart from its ability to quantify cell proliferation. Alamar blue (AB) reagent acts as a cell health indicator and its use stands on cellular response to

resazurin, the active ingredient of the reagent. Resazurin, is a non-toxic cell permeable compound, originally blue and non-fluorescent. Upon entering into cells, it is reduced to resofurin, a red compound which is fluorescent. As viable cells continuously convert resazurin to resofurin the fluorescence and color of the media change and the absorbance of the cellular medium can be measured on a spectrophotometer. Finally, the results are translated to a plot absorbance/fluorescent signal versus compound concentration and correlated with cellular proliferation.²⁵

The Alamar Blue® assay was carried out on coated cp Ti discs. Each biocoating experiment was conducted in triplicate and all samples were sterilized by exposition to ultraviolet (UV) light during 20 min (focal distance to source 80-100 cm). The coated discs, after sterilization, were incubated with 1 ml growth medium (DMEM, Gibco®, Invitrogen) for 16h at 37°C with 5% CO₂.

Then, MC3T3 cells were plated (24 well plate) onto coated Ti discs at an initial density of 35.000 cells/well (1 ml medium with 10% FBS (Fetal Bovine Serum) (ThermoFisherScientific, MassachusettsEEUU) and 1% P/S (penicillin/streptomycin) (Lonza,Basilea; Switzerland)) and grown under standard conditions (37°C and 5% CO₂). Cellular proliferation was studied after culturing for 1, 3, 7 and 14 days at 37°C; the cellular medium was changed every 2 days for longer culturing times (7 and 14 days) and once only for the other culturing times.

After incubation time, cellular medium was removed, samples were rinsed with Dulbeco's phosphate buffered saline (DPBS) solution and 1 ml of growth medium with 10% of filtered Alamar Blue (AB) Cell Viability Reagent (DAL1100, Invitrogen) was added to each well, where samples rested for incubation for 16 hours at 37°C. Then, 3 replicates of 200 µl of medium were taken and AB absorbance was measured at an emission wavelength of 570 nm (normalized at 600 nm) using a Victor3 multilabel plate reader (PerkinElmer). The final result corresponds to the average

MATERIALS AND METHODS

of the 3 replicates values read on 3 different wells (3 absorbance measurements x 3 different wells for each biocoating). The results are displayed as optical density (OD) defined as:

$$OD = \frac{\text{absorbance}}{\text{thickness of sample}} = \frac{\frac{\text{intensity of light before it enters the sample}}{\text{transmitted light}}}{\text{thickness of sample}}$$

and the OD registered depends on the resorufin concentration measured at 570 nm and is proportional to the viable cells.

Measurement of the cellular mineralization

The alkaline phosphate activity (ALP) assay was used to assess cellular mineralization. ALP catalyzes the hydrolysis of *p*-nitrophenol phosphate (PNPP) into *p*-nitrophenol and phosphate in the presence of magnesium ions, for that reason the ALP content can be correlated with *p*-nitrophenol detection and quantified by monitoring light absorbance.²⁶

Coated and sterilized discs (exposition to UV light during 20 min), were incubated with 1 ml growth medium (DMEM, Gibco®, Invitrogen) for 16h at 37°C with 5% CO₂. Then, MC3T3 cells were plated (24 well plate) onto coated Ti discs at an initial density of 35.000 cells/well (1 ml growth medium with 10% FBS (Fetal Bovine Serum) (ThermoFisherScientific, MassachusettsEEUU) and 1% P/S (penicillin/streptomycin) (Lonza,Basilea; Switzerland)) and incubated for 24h at 37°C with 5% CO₂. Afterwards, growth medium was removed from wells and substituted by osteogenic differentiation medium (medium with 10% FBS (ThermoFisherScientific, MassachusettsEEUU) and 1% P/S (penicillin/streptomycin) (Lonza,Basilea; Switzerland), 1% ascorbic acid 5mg/ml (SigmaAldrich) and 0,21% β-glycerol phosphate 1M (Fluka)). Until achievement of the experimental time of 7 and 14 days, differentiation medium was changed every 2 days.

The ALP activity in the cells was assayed at the end of each experimental period and the supernatant was used to its measure *via* BCA assay kit Micro BCA™ Protein Assay Kit (Invitrogen). To do so, cellular medium was removed, samples were rinsed with Dulbecco's phosphate buffered saline (DPBS) solution (three times), 200 µl of lysis buffer were added to each well and placed on ice for 10 min for incubation.

Then, 100 µl of supernatant were used to detect ALP activity. In a first step, the aliquot exposed to high-frequency sound waves (sonication) during 2 min and refrigerated. After centrifugation of the sample at 14000 rpm for 7 min at 4°C the supernatant was removed. 100 µl of *p*-nitrophenol phosphate (PNPP) were added and gently shaken. After that, the reaction media was incubated at 37°C during 2 hours. The reaction was stopped by adding 50 µl of 1M NaOH and subsequently 100 µl were deposited on each wheel to absorbance reading.

Previously, serial dilutions of *p*-nitrophenol in NaOH solution were prepared and used as standards. Finally, the optical density was measured at 405 nm using a Victor3 Multilabel plate reader (Perkin-Elmer). ALP results were normalized to the total amount of protein (BCA or bicinchoninic acid assay) at a specific time.

Total protein concentration was measured by means of BCA (bicinchoninic acid) assay kit, by using a Micro BCA™ protein assay kit (Invitrogen). BCA protein assay is based on the reduction process of Cu^{2+} to Cu^{1+} executed by protein in an alkaline medium through detection of Cu^{1+} by BCA. The purple colour intensity of the reaction product can be related with the number of peptide bonds interveners in the reduction reaction.²⁶

MATERIALS AND METHODS

In a 96 well plate, 75 µl of reactive prepared following manufacturer instructions where on each well containing 75 µl of supernatant and incubated at 37°C for 2h. Afterwards, proteins' concentration was finally measured using a spectrophotometric microplate reader (Victor3 Multilabel plate reader (Perkin-Elmer)) at wavelength of 550 nm (1s). The total protein amount (µg/ml) was achieved using a standard curve with patterns of albumin (BSA) in lysis buffer. Finally the mineralization rate will be calculated as:

$$\text{Mineralization rate} = \frac{\text{nM p-nitrophenol/h (related with ALP)}}{(\mu\text{g/ml})(\text{related with total protein})}$$

In vivo implantation

According to ISO 10993-2 (2006), it is necessary animal experimentation to test new biomedical devices and validate hypothesis and results obtained on *in vitro* assay.²⁷ The animal model was selected considering some factors as the research objectives, required time to obtain results and laboratory constraints.

In vivo experiments were conducted at Instituto de Biomecánica de Valencia (IBV) with New Zealand white rabbits (*Oryctolagus cuniculus*) with 18 weeks lifetime. The experiment protocol respected the rules of ethical committee of the R.D. 1201/2005 of 10th October and order of 13th October, about surgical procedures with animals, pain control, standards of living and appropriated death. All coated dental implants, with dimensions 3,75 mm diameter and 8 mm length, used on the experiment were previously sterilized with gamma radiation. Taking into account that an implant can be osseointegrated on a rabbit bone in 6 weeks²⁷, the selected experimental times were 1 and 2 weeks since previous works showed that *in vivo* experiments for up to 8 weeks exhibited significant modifications at implantations on this periods²⁸. Implantation was made in the proximal tibias of rabbits (Figure 3.15),

using both legs and it was introduced one implant on each leg. Four replicas were used for each material; all the samples were used both on the osseointegration analysis and the biocompatibility study by optical microscopy (OM).

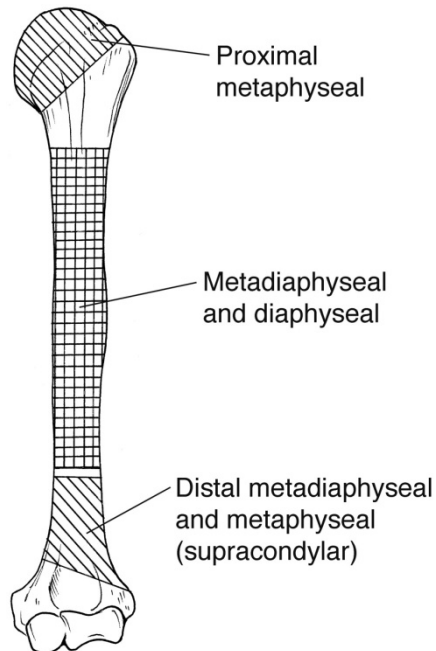


Figure 3.15 - Schematic representation of the parts of a tibia bone.

Animals were pre-anesthetized with ketamine hydrochloride 17 mg/kg (Imalgene[®], Merial, Georgia, USA) and xylazine 2,5mg/kg (Rompun[®] 2%, Bayer Hispania S.L., Barcelona, Spain) by intramuscular injection. After 15 minutes the animals were finally anesthetized by intravenous injection with 3mg/kg of propofol (Propofol[®], B.Braun Medical S.A., Melsungen, Germany). The maintenance regimen was adjusted with Propofol[®] continuous administration of 21mg/kg/h.

The surgery surface was cleaned with antiseptic soap and the implantation site was exposed. Two holes of around 3,5 mm diameter and 8,0 mm depth were drilled at low speed at the proximal tibia. Coated

MATERIALS AND METHODS

and uncoated (control) implants were placed by press fit into the rabbit bone. After implantation, the wound was closed by suturing with Vicryl® 4/0 (Ethicon, EEUU): for internal tissues simple points were used and the skin was closed by intradermal suture to prevent a possible reopening of the wound by animal actions. Flunixin meglumin (Finadyne® 50 mg/ml, Schering-Plough S.A., Spain) was used as antiinflammatory agent and 1mg/ml was subcutaneously administrated. The antibiotic and analgesic procedure was maintained for three days with daily intramuscular administration of 3,5 mg/kg of Baytril® and 0,4 mg/kg of Torbugesic® respectively.

The animals were sacrificed at the end of the experimental periods by overdose of sodium pentobarbital (Dolethal®, Vetoquinol S.A., Spain) administrated via intravenous injection in the marginal vein handset. After proved absence of vital signs, the proximal tibia region was cleaned and an osteotomy was performed.

The retrieved samples were cleaned from surrounding soft tissues and fixed on ethanol 40% (4°C). After that, they were dehydrated on several alcohol-water dissolutions (with increasing alcohol content) followed by methacrylate solution and, finally, embedded in methyl methacrylate (MMA) solution and polymerized for 3 days at 38°C. The methodology followed for MMA embedding of bone biopsies was the one suggested by Peris (1993)²⁹. This polymer, methyl methacrylate, was chosen due to its stiffness very similar to bone and possibility to stain samples with significant size.

The MMA embedded blocks were cut into thin slices with an EXAKT® (EXAKT® Vertriebs, Norderstedt, Germany) system and dyed for histological evaluation. EXAKT® thin section cutting technology allows the cutting of samples up to 100 µm thick without affecting the composition, surface or structure during samples' processing, which

explains the choice of that methodology for preparing the *in vivo* extracted samples for histological studies.³⁰

Dye processing of the samples is described elsewhere²⁸. Briefly, the cut samples were rehydrated with decreasing alcohol content on several alcohol-water dissolutions. Then, Gomori's trichrome was used as dye solution to identify woven bone and calcified bone. To do so, the cuts were dehydrated with anhydrous ethanol 95% followed by a cleaning process based on a 10 minute submersion in xylene. Coverslips were mounted with Canada balsam (Sigma-Aldrich) and dried at 37°C for 12h.

This staining procedure makes osteoids acquire red colour whereas mature bone shows a bluish hue. Fibrous tissue will also present red colour as well as cellular cytoplasm.

For histological study of the *in vivo* samples a vertical Eclipse 80i optical microscope (Nikon) operating on bright field was used.

DESCRIPTION OF THE SAMPLES USED ON THE DIFFERENT ANALYSIS

A brief description of the samples used on the different analysis made on the actual research work can be seen in Table 3.1.

Table 3.1 – Samples used on the different analysis performed on the research work.

Sample	Substrate	Form	Analysis
Coating	Stainless steel plates	Coating	EIS, Morphology, Wettability
	CP Ti discs	Coating	<i>In vitro</i> assay, Morphology
	Implants	Coating	<i>In vivo</i> assay, Morphology
	Microscope glass slides	Coating	Hydrolytic degradation
Powder	--	Free film	TGA, RMN, FTIR

#

REFERENCES

1. Escolano, M. H. Desarrollo de Recubrimientos Híbridos Osteoinductores para Implantes Dentales. (Universidad Politécnica de Valencia, 2011).
2. Hernández-Escolano, M. *et al.* The design and characterisation of sol–gel coatings for the controlled-release of active molecules. *J. Sol-Gel Sci. Technol.* **64**, 442 (2012).
3. Hernández-Escolano, M., Ramis, X., Jiménez-Morales, A., Juan-Díaz, M. & Suay, J. Study of the thermal degradation of bioactive sol-gel coatings for the optimization of its curing process. *J. Therm. Anal. Calorim.* 1–10 (2011). at <<http://www.scopus.com/inward/record.url?eid=2-s2.0-79953865234&partnerID=40&md5=aa6d90dd94750012586baf1be74d7c3c>>
4. Juan-Díaz, M. J. *et al.* Study of the degradation of hybrid sol–gel coatings in aqueous medium. *Prog. Org. Coatings* **77**, 1799–1806 (2014).
5. Catauro, M., Papale, F. & Bollino, F. Characterization and biological properties of TiO₂/PCL hybrid layers prepared via sol–gel dip coating for surface modification of titanium implants. *J. Non. Cryst. Solids* **415**, 9–15 (2015).
6. C. J. Brinker; G. W. Scherer. *Sol–Gel Science: The Physics and Chemistry of Sol–Gel Processing.* Elsevier (Academic Press, 1990). at <<http://scholar.google.com/scholar?hl=en&btnG=Search&q=intitle:No+Title#0>>
7. Zhen Guo, L. T. *Fundamentals and Applications of Nanomaterials.* (2009).
8. Zhou, W., Apkarian, R., Wang, Z. & Joy, D. in *Scanning Microscopy for Nanotechnology SE - 1* (eds. Zhou, W. & Wang, Z.) 1–40 (Springer New York, 2007). doi:10.1007/978-0-387-39620-0_1
9. Franceschinis, G. Surface Profilometry as a tool to Measure Thin Film Stress, A Practical Approach. 1–5 (2005).

10. Kowalski, C. Dektak 6M Manual Document Revision History: Dektak 6M Manual. *Scanning* **000**, (2002).
11. Grundke, K. *et al.* Experimental studies of contact angle hysteresis phenomena on polymer surfaces - Toward the understanding and control of wettability for different applications. *Adv. Colloid Interface Sci.* (2014). doi:10.1016/j.cis.2014.10.012
12. Xu, Z., Neoh, K. G. & Kishen, A. Monitoring acid-demineralization of human dentine by electrochemical impedance spectroscopy (EIS). *J. Dent.* **36**, 1005–12 (2008).
13. Brockman, S. Basics of Electrochemical Impedance Spectroscopy. *Application note* 1–13 (2012).
14. Vidal, C. V. & Muñoz, A. I. in *Materials Science* (2006).
15. Loveday, D., Peterson, P. & Rodgers, B. Evaluation of Organic Coatings with Electrochemical Impedance Spectroscopy Part 1: Fundamentals of Electrochemical Impedance Spectroscopy. *Jctr* 88–93 (2004).
16. Oppenheim, Alan V.; Willsky, A. S. *Signals and systems*. (Prentice Hall, 1997).
17. Shi, X., Xu, L. & Wang, Q. Porous TiO₂ film prepared by micro-arc oxidation and its electrochemical behaviors in Hank's solution. *Third Spec. Issue Dedic. to Plasma Electrolysis Plasma Electrolysis Inc. Pap. from 'EUROMAT 2009' Congr. Adv. Mater. Process. 7–10 Sept. 2009, Glas. UK* **205**, 1730–1735 (2010).
18. Loveday, D. *et al.* Evaluation of organic coatings with electrochemical impedance spectroscopy. Part 2: application of EIS to coatings. *JCT CoatingsTech* **1**, 88–93 (2004).
19. Fernández-Sánchez, C., McNeil, C. J. & Rawson, K. Electrochemical impedance spectroscopy studies of polymer degradation: Application to biosensor development. *TrAC - Trends Anal. Chem.* **24**, 37–48 (2005).
20. Hou, D., Ma, H., Li, Z. & Jin, Z. Molecular simulation of 'hydrolytic weakening': A case study on silica. *Acta Mater.* **80**, 264–277 (2014).

MATERIALS AND METHODS

21. Zhu, T., Li, J., Lin, X. & Yip, S. Stress-dependent molecular pathways of silica–water reaction. *J. Mech. Phys. Solids* **53**, 1597–1623 (2005).
22. Leboda, R., Mendyk, E. & Tertykh, V. A. Effect of the hydrothermal treatment method in an autoclave on the silica gel porous structure. *Mater. Chem. Phys.* **42**, 7–11 (1995).
23. Stuart, B. *Infrared Spectroscopy: Fundamentals and Applications*. (Wiley).
24. James, T. L. in *Biophysics Textbook Online* (ed. Biophysical Society) 1–31 (1998).
25. Bonnier, F. *et al.* Cell viability assessment using the Alamar blue assay: a comparison of 2D and 3D cell culture models. *Toxicol. In Vitro* **29**, 124–31 (2015).
26. Tripathi, G. & Basu, B. A porous hydroxyapatite scaffold for bone tissue engineering: Physico-mechanical and biological evaluations. *Ceram. Int.* **38**, 341–349 (2012).
27. Alzarea, B. K. Selection of animal model in dentistry: State of Art, Review Article. *J. Anim. Vet. Adv.* **13**, 1080–1085 (2014).
28. Sáez, I. L. Evaluación biológica de nuevos recubrimientos osteoinductores sintetizados vía sol-gel para aplicación en implantología dental. (Universidad Politécnica de Valencia, 2015).
29. Peris, J. L., Prat, J., Comin, M., Dejoz, R. & Vera, I. R. P. Técnica histológica para la inclusión en metil- metacrilato de muestras óseas no descalcificadas. *Rev. Española Cirugía Osteoartic.* **28**, 231–238 (1993).
30. EXAKT Advanced Technologies GmbH. at <<http://www.exakt.de/en/products/thin-section-cutting-technology/general.html>>

CHAPTER 4. RESULTS

RESULTS

The clinical goal of dental implantation is the substitution of a lost tooth and recovery of the biomechanical function of the system. To accomplish the proposed objective the establishment of an adequate interface between tissues and implantable materials is imperative in order to obtain a long term secure bone anchorage capable of sustain dynamic and static loads caused by mastication and other phenomena. Biomaterials surface characteristics are very important on the management of tissue-implant interaction. Taking into account, from previous studies and results¹, that the silica based materials produced with 50% MTMOS:50% GPTMS (50M:50G) does not show good results *in-vivo* as it remain adhered to implants surface until 8 weeks due to the dense fibrous capsule formed between the material and the surrounding tissue, the addition of TEOS (T) precursor arise as an interesting strategy to improve the biocompatibility of the biomaterial and enhance its biodegradability. In that way, the triple system developed on the present research work, with triple silane composition MTMOS:GPTMS:TEOS (M:G:T) represent a new biomaterial applied as a coating on titanium dental implants that dispense silicon on bone-biomaterial interface, an element with proven positive effects on cellular metabolism and differentiation^{2,3,4}, otherwise than make possible biomolecules incorporation with a bioactive role on bone regeneration process. The GPTMS (G) is used to functionalize the silica base structure and as coupling agent to covalently link with biomolecules. Accordingly, its content variation on the new developed compositions will be maximum 45% or 35%, besides, previous works results⁵ show that pure GPTMS is potentially cytotoxic so it is not appropriate the incorporation of high amounts of this silane.

Surface reactivity determines the bonding ability of biomaterials and their performance as osteoinductive elements. As after implantation several molecular processes take place at the material-tissue interface that lead to time-dependent biologic changes, the study of surface morphology,

RESULTS

surface reactivity, chemical properties, structure arrangement and degradation rate of the biomaterials is necessary, as well as the analysis of biomaterials effects on cellular attachment, proliferation and mineralization. Thereby, at the present work the surface properties and integrity of the new triple system biomaterials were evaluated and a comparative study between developed materials and reference (50M:50G) will be made in order to verify the improvement on the biological performance of 50M:50G.

PRODUCTION PROCESS OF HYBRID MATERIALS AND CHEMICAL CHARACTERIZATION

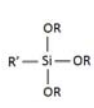
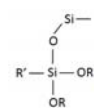
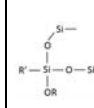
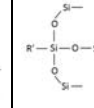
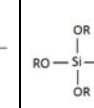
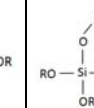
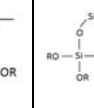
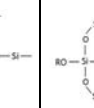

The hydrolysis of alkoxy silane groups and consequent condensation to form the silica based network, otherwise than the opening reaction of the epoxy ring of 3-glycidoxypropyltrimetoxysilane (GPTMS) may be affected by several factors: type of solvent (presence of nucleophiles), amount of water, catalyst employed, temperature and nature of the alkoxy groups bounded to the silicon atom⁶.

A first approach on hydrolysis and condensation degree achieved on the sol synthesis was made by means of Nuclear Magnetic Resonance (NMR) spectroscopy in liquid phase.

To better understand NMR results, a nomenclature widely referred on bibliography was taking up^{6,7,8}. **T^w** corresponds to a Si atom with a Si-C bond and three reactive methoxy groups, that is to say, is the definition of different condensation degrees adopted by MTMOS and GPTMS with w = 1, 2 or 3 condensed alkoxy groups. In addition, **Q^w** corresponds to a Si atom bond with four alkoxy reactive groups predisposed to participate on hydrolysis and later condensation reactions (where w can adopt values 1, 2, 3 or 4), condition of TEOS alkoxy silane.

The typical ²⁹Si chemical shift (δ) registered for TEOS, MTMOS and GPTMS different species along hydrolysis and condensation process are collected in Table 4.1.

Table 4. 1 - ²⁹Si chemical shift (δ) of TEOS, MTMOS and GPTMS different species.

									
Material	T⁰ δ (ppm)	T¹ δ (ppm)	T² δ (ppm)	T³ δ (ppm)	Q⁰ δ (ppm)	Q¹ δ (ppm)	Q² δ (ppm)	Q³ δ (ppm)	Q⁴ δ (ppm)
TEOS	--	--	--	--	≈ -82	≈ -84	≈ -91	≈ -99	$\approx -110^7$
MTMOS	≈ -40	≈ -46	≈ -57	≈ -64	--	--	--	--	--
GPTMS	≈ -42	≈ -49	≈ -59	≈ -66	--	--	--	--	--

RESULTS

^{29}Si NMR studies were performed on all the materials of both series, 90(M:G):10T and 70(M:G):30T, and the recorded spectra are depicted in Figure 4.1 - Figure 4.8.

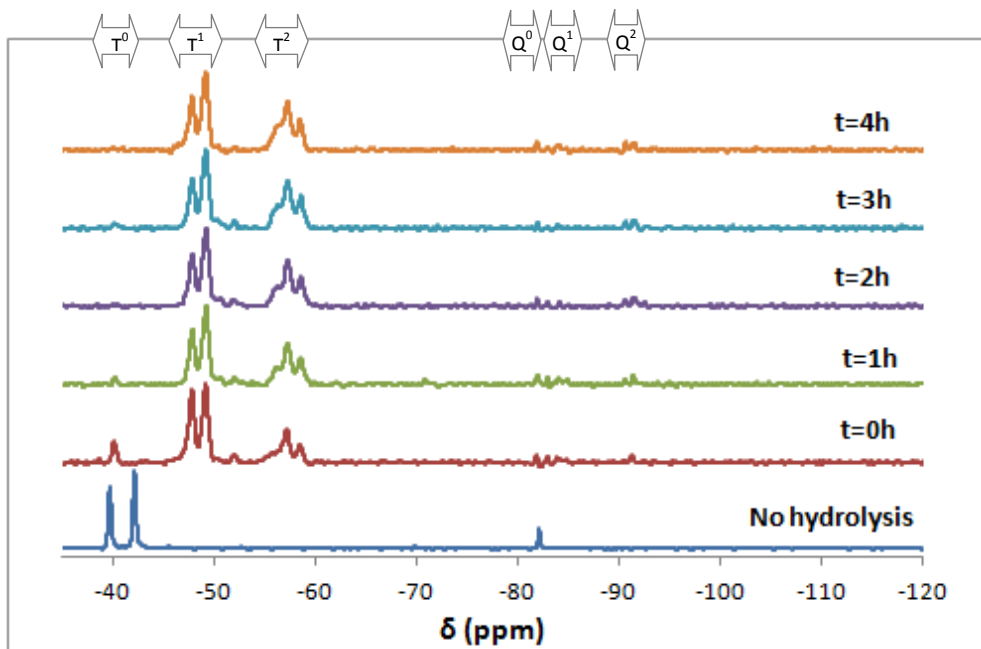


Figure 4.1 - ^{29}Si NMR spectra of the hydrolysis and condensation of 45M:45G:10T during sol synthesis.

It can be seen on Figure 4.1 two separate groups of Si structural units, one with chemical shifts between -40 and -59 ppm, assigned to T structural units, and another with chemical shifts between -80 and -91 ppm assigned to Q structural units.

Time evolution shows that consecutive and parallel hydrolysis and condensation reactions take place, as it is observable the coexistence of species T^0 and Q^0 with species T^1 , T^2 , Q^1 and Q^2 for $t=0\text{h}$ and $t=1\text{h}$ spectra.

The results show that in the first 2 hours of synthesis the system change as species T^0 tend to disappear and give rise to species T^1 and T^2 . MTMOS and GPTMS silanes reach an intermediate condensation degree

suggesting that still remain Si-OH groups available to react during the subsequently heat treatment. On the other hand, Q species seems stable since the beginning of hydrolysis with no modifications on spectra with time evolution. The spectra shows Q^0 , Q^1 and Q^2 species from TEOS silane, in fact the silicon atoms still preserve many Si-OH groups able to react. The appointed synthesis time, $t=2h$, was appropriate for the synthesis of 45M:45G:10T since the condensation degree does not evolve significantly from 1h to 2 h of reaction.

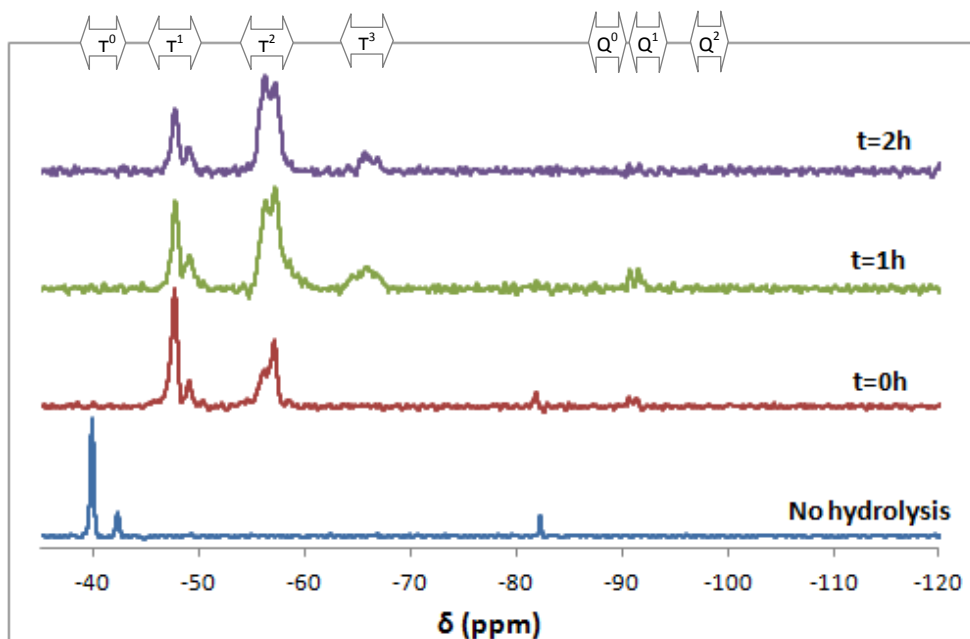


Figure 4.2 - ^{29}Si NMR spectra of the hydrolysis and condensation of 76M:14G:10T during sol synthesis.

The ^{29}Si NMR spectroscopic data registered for 76M:14G:10T (Figure 4.2) illustrate the existence of new species T^3 . Otherwise, in this case, the spectra show some variation on species Q^0 as they disappear after 1 hour synthesis. MTMOS and GPTMS structural units reveal the achievement of higher condensation level; on the other hand, Q species still preserve low bridging oxygen bonding Si-O-Si. The appointed synthesis time, $t=2h$, was

RESULTS

appropriate for synthesis of 76M:14G:10T since the condensation degree does not evolve significantly from 1h to 2 h reaction time.

It is important to notice that for the same synthesis time ($t=2h$), lesser content on GPTMS seems to promote higher condensation level on sol.

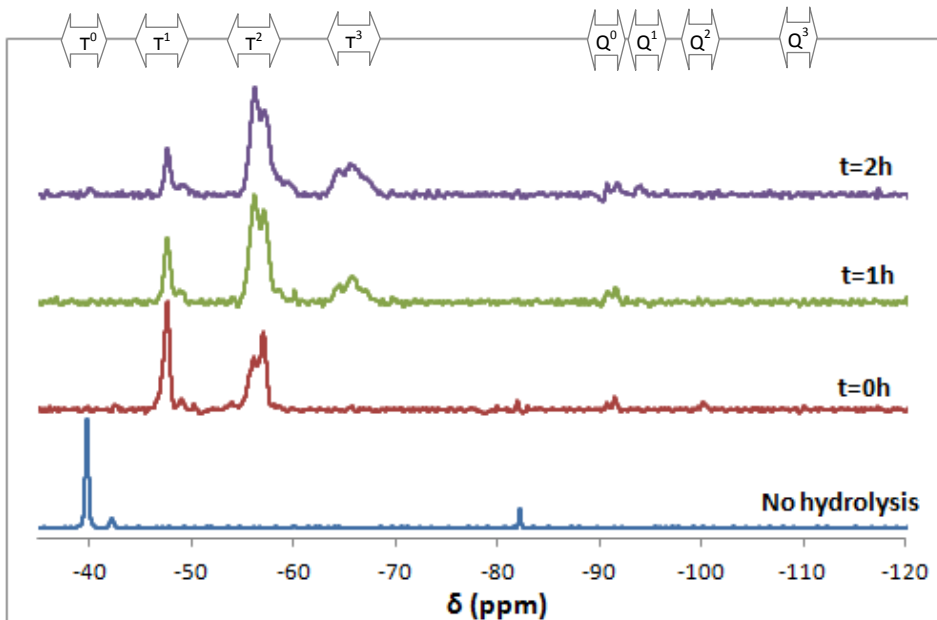


Figure 4.3 - ^{29}Si NMR spectra of the hydrolysis and condensation of 83M:7G:10T during sol synthesis.

The spectra registered for 83M:7G:10T (Figure 4.3) illustrate an increase in the number of T^3 species. Besides, Q^3 species started to show immediately after addition of catalyst ($t=0h$). Once more, lesser content on GPTMS seems to promote higher condensation level on sol for the same time of synthesis.

It was not noticeable any variation in spectra from 1h to 2h reaction time.

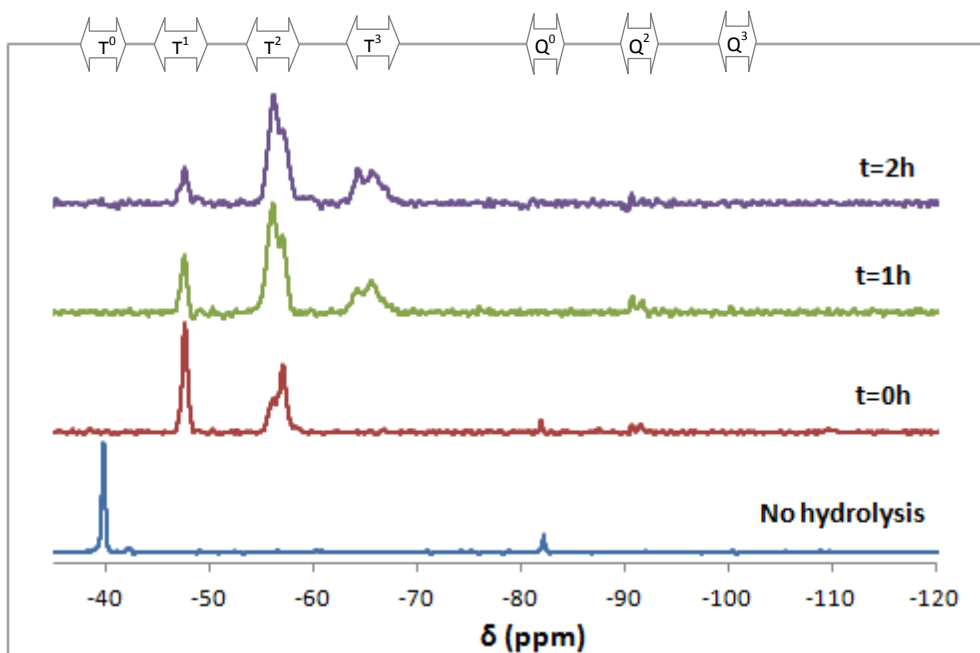


Figure 4.4 - ^{29}Si NMR spectra of the hydrolysis and condensation of 86,5M:3,5G:10T during sol synthesis.

Figure 4.4 show the analysis of the structural units obtained after 2 hours synthesis of 86,5M:3,5G:10T silane combination. The peaks associated with T^1 , T^2 and T^3 units in T region is in agreement with the results obtained for 83M:7G:10T (Figure 4.3). Nevertheless, in the Q region only Q^2 units are detected indicating that the decrease on GPTMS content is not followed by a correspondent increasing on Si-O-Si bonding of silicon atoms derived from TEOS silane. Almost certainly silane combinations with higher content on MTMOS affect and decrease the number of Q^3 structural units from TEOS.

The synthesis fixed time of 2h was appropriate for 86,5M:3,5G:10T since it was not detected significant spectra alteration from 1h to 2h reaction.

RESULTS

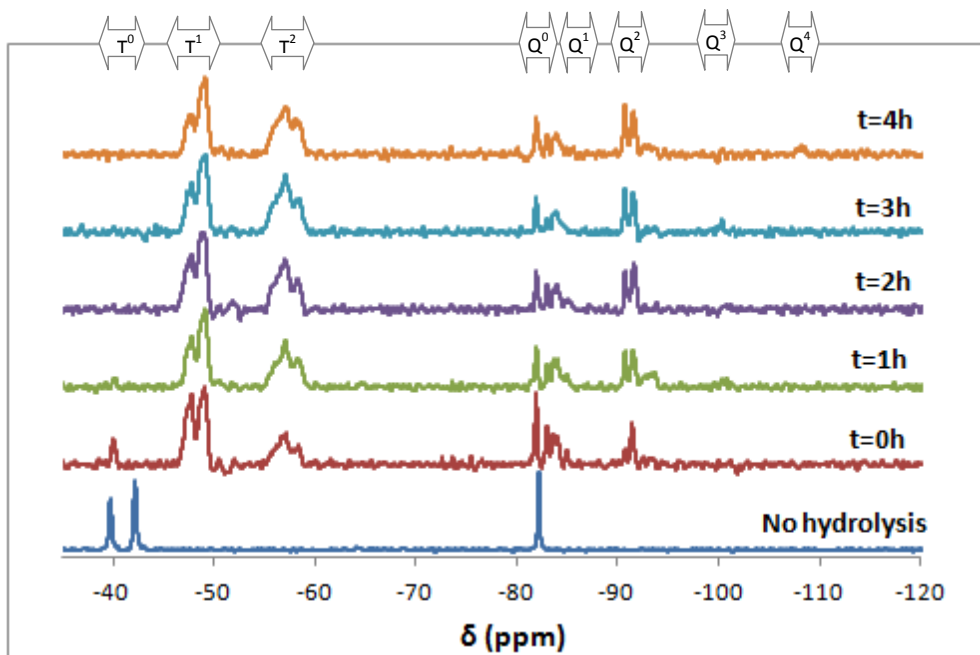


Figure 4.5 - ^{29}Si NMR spectra of the hydrolysis and condensation of 35M:35G:30T during sol synthesis.

In Figure 4.5 (related with 30% TEOS content series materials) two separate groups of Si structural units can be identified, one with chemical shifts between -40 and -59 ppm, assigned to T structural units, and another with chemical shifts between -80 and -110 ppm assigned to Q structural units.

Time evolution shows that consecutive and parallel hydrolysis and condensation reactions take place, as it is observable the coexistence of T^0 species with T^1 and T^2 structural units ($t=0$ and $t=1\text{h}$) and Q^0 species with Q^1 , Q^2 , Q^3 and Q^4 structural units ($t=1 - 4\text{h}$).

The results show that in the first two hours synthesis the system change as species T^0 tend to disappear leading to species T^1 and T^2 . MTMOS and GPTMS silanes reach an intermediate condensation degree suggesting that still remain Si-OH groups available to react during the subsequent heat treatment. On the other hand, Q region show predominance of Q^0 , Q^1 and Q^2 units in all time analysis, nevertheless, for synthesis times $t=1\text{h}$,

2h and 3h Q^3 units can be detected otherwise than Q^4 structural units in $t=4h$ spectra. Doubtless the silicon atoms still preserve many Si-OH groups able to react because the signals detected for high Si-O-Si bonding structures (T^3 , Q^3 and Q^4) are slight.

The fixed synthesis time of 2h, was acceptable for synthesis of 35M:35G:30T since the attained condensation degree does not show major variations, only slight signals of species Q^3 and Q^4 at higher synthesis times.

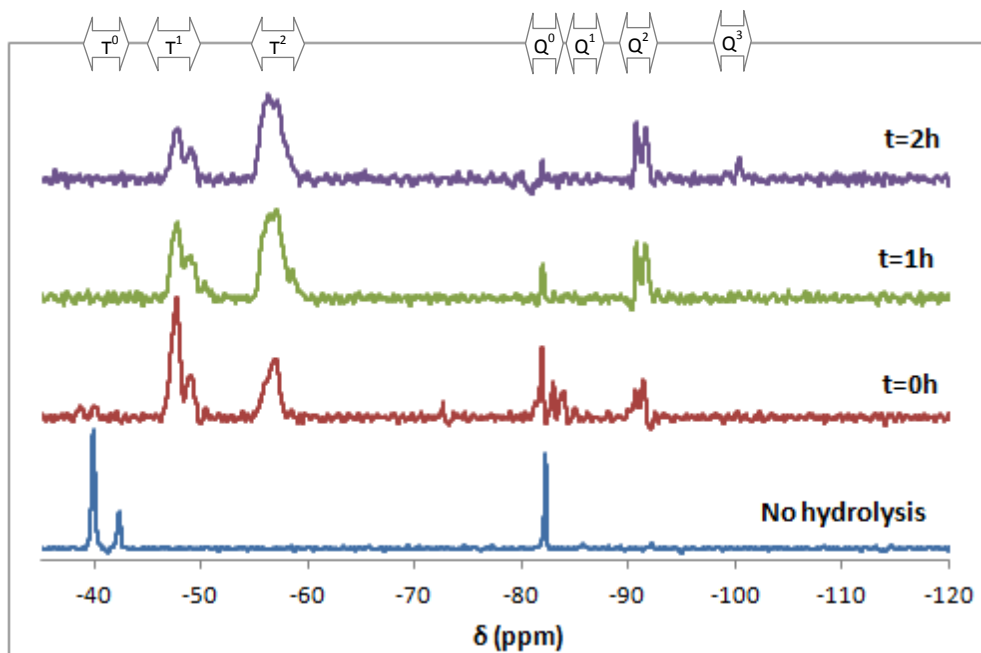


Figure 4.6 - ^{29}Si NMR spectra of the hydrolysis and condensation of 56M:14G:30T during sol synthesis.

The ^{29}Si NMR spectroscopic data registered for 56M:14G:30T (Figure 4.6) show a crosslinking intermediate level. The structures with higher bridging oxygen bonding Si-O-Si on species T and Q were T^2 and Q^3 . It is detectable a signal of species Q^0 in Q region from TEOS monomer in all registered spectra ($t=0h$ until $t=2h$). Once again, the results show that consecutive and parallel hydrolysis and condensation reactions take place.

RESULTS

The synthesis fixed time of 2h was appropriate for 86,5M:3,5G:10T since it was not detected significant spectra alteration from 1h to 2h reaction time.

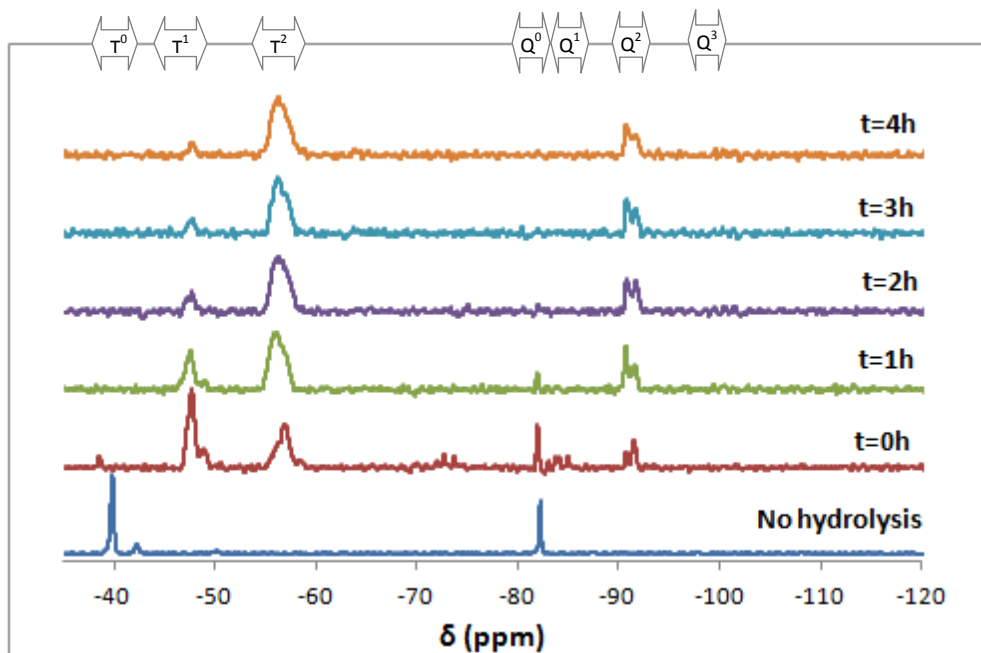


Figure 4. 7 - ^{29}Si NMR spectra of the hydrolysis and condensation of 63M:7G:30T during sol synthesis.

The spectra registered for 63M:7G:30T (Figure 4.7) illustrate an increase in the number of T^2 species, also in Q region Q^2 species present the most intense peaks. Apparently, this series lesser content on GPTMS seems to favour hydrolysis, nevertheless, does not stimulate high condensation level of alkoxy groups bonded to Si metal atom ($w_{\text{max}}=2$ on both spectra regions).

It was not perceptible any variation in spectra from 1h to 2h synthesis time, therefore the fixed 2h synthesis time was appropriate.

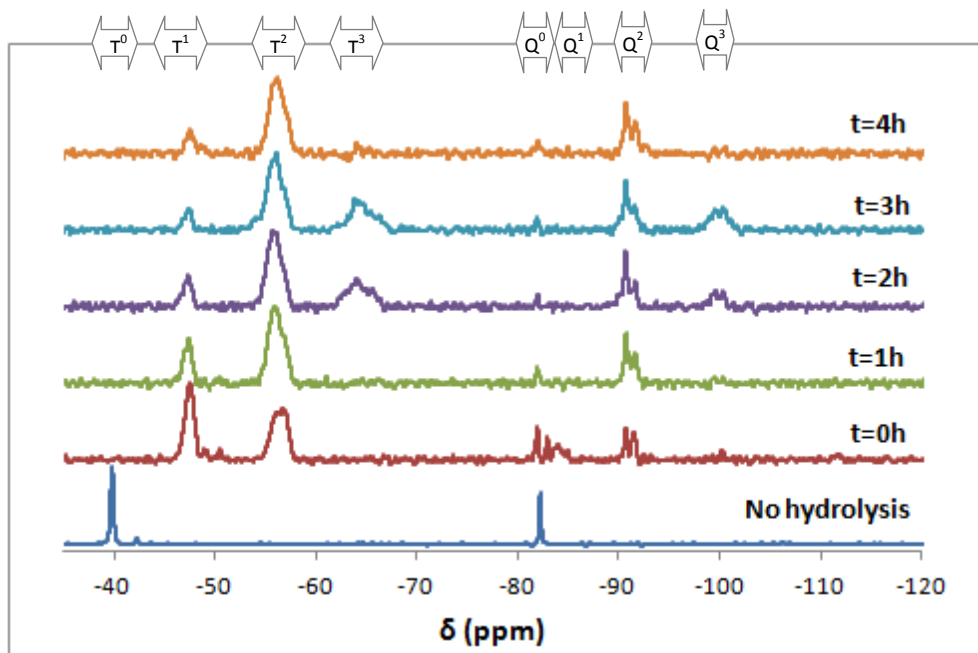


Figure 4.8 - ^{29}Si NMR spectra of the hydrolysis and condensation of 66,5M:3,5G:30T during sol synthesis.

Figure 4.8 show the analysis of the structural units obtained after 3 hours synthesis of 66,5M:3,5G:30T silane combination. There are peaks associated with T^1 , T^2 and T^3 units in T region with predominance of T^2 units. Nevertheless, in the Q region Q^2 signals become visible since $t=0\text{h}$ and Q^3 units emerge at $t=1\text{h}$ spectra.

In this special silane combination, the low content on GPTMS favour Si-O-Si bonding of silicon atoms derived from TEOS. Perhaps the special characteristics of GPTMS molecule and the presence of the alkyl epoxy group affects TEOS reactivity, reducing intermolecular closeness and molecular synergy.

The synthesis fixed time of 2h was appropriate for 66,5M:3,5G:30T since it was not detected a significant spectra alteration from 1h to 2h reaction time.

RESULTS

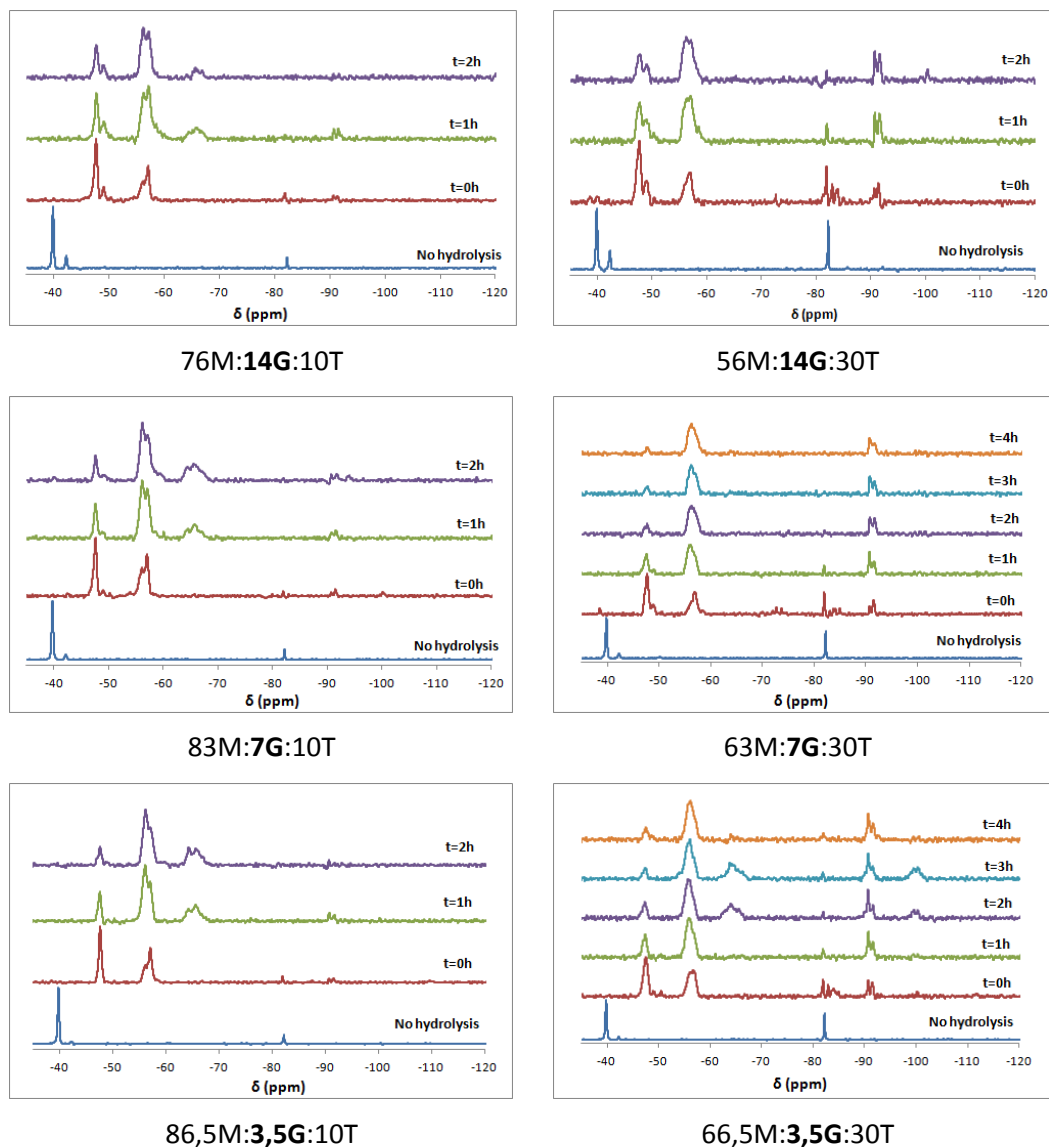


Figure 4.9 - ^{29}Si NMR spectra of the hydrolysis and condensation of silane combinations with similar content on GPTMS (left - series with 10% TEOS, right - series with 30% TEOS) during sol synthesis.

It is clear, analysing Figure 4.9 spectra, the high intensity peaks of Q region on the series with 30% TEOS (spectra in evidence on the right side). Q species show total hydrolysis (absence of Q⁰ species) when

added to MTMOS and GPTMS in a molar rate of 10%, on the other hand, when the silane molar combination has 30% TEOS only the material with 63M:7G:30T show complete hydrolysis of the silicon-alkoxy groups at synthesis time 4h. In previous works^{9,10} was stated that sol-gel synthesis under acidic conditions promote faster hydrolysis than condensation and trialkoxysilanes hydrolyse faster than tetralkoxysilane. The suggested reason for faster hydrolysis of trialkoxysilanes was attributed to the special character of alkyl groups as better electron donors than alkoxy groups on the hydrolysis process of silicon alkoxides (acidic conditions hydrolysis follows a first protonation of alkoxide group, then S_N2 attack with water molecules as nucleophile finally guiding Si atom to a transitional state of penta-coordinated configuration).⁹ Apparently, from the spectra analysis exposed in Figure 4.6, is possible to distinguish an almost complete peaks stabilization since the first instant (0h - 1h) of trialkoxysilanes species. Nevertheless, peaks associated with tetralkoxysilane species show more noticeable changes until complete stabilization (1h - 2h). These results are in agreement with the above cited studies and conclusions^{9,10}.

On 90(M:G):10T series, is possible to identify species T³ in all silane combinations, nevertheless for 14% GPTMS content (76M:14G:10T) a slight peak show up at chemical shifts (δ) -64 and -66 ppm. The main species present in all silane combinations was T², this demonstrate the medium condensation level of the synthesized sols and the availability of Si-OH groups to react subsequently during the heat treatment.

In addition, 70(M:G):30T series, show a lower condensation rate of T species as only in the spectra of the silane combination with 3,5% GPTMS content is observable a peak at chemical shift (δ) -64 and -66 ppm, signals of T³ structural units. What's more, this special silane combination 66,5M:3,5G:30T show the highest signals related with Q³ species. These results motivate the consideration of a special micro organization between GPTMS and TEOS monomers, that is to say, similar contents on GPTMS and TEOS does not encourage hydrolysis

RESULTS

and condensation reaction during synthesis maybe due to a higher content on Si-OH groups that repeal each other.

After the sol analysis, it was necessary the establishment of a minimum threshold of coatings integrity on the sol-gel condition.

It is a current practice in organic coatings industry the use of solvents as abrasive medium to evaluate the crosslinking degree of coatings in order to achieve the desired properties of the polymeric layers. At the present work and according to Standard UNE-EN 13523-11, methyl ethyl ketone (MEK) was used as solvent and it was set as minimum requirement the coating resistance to 120 double-rubs with a cotton swab soaked in MEK. The results are reported in Table 4.2 and Table 4.3.

The establishment of a proper thermal treatment for each series (10%TEOS and 30%TEOS) was set in order to rubbing test results of the biocoatings with the maximum content on GPTMS, that is to say, 45M:45G:10T and 35M:35G:30T. Although the new proposed materials follow the same production methodology as the reference material 50%MTMOS:50%GPTMS, the incorporation of a third reactive, TEOS, may alter the synergy and reactivity between components. Taking that into account it is necessary a final heat treatment adjustment of the new sol-gel coatings to attain a relative dense structure with proper solvent evaporation and substantial volume contraction in order to achieve favourable final properties. Previous studies^{7,5} with similar process of synthesis and application using silanes MTMOS and GPTMS propose the thermal treatments at 100°C and 140°C for coatings made of 100% MTMOS and 100% GPTMS respectively. Accordingly, temperature range tested for polymerization degree of the biomaterials developed on this research work was 60°C until 140°C.

Table 4.2 - Biocoatings resistance, series 90(M:G):10T, to double-rubs with a cotton swab soaked in MEK submitted to different thermal treatments to promote cross-linking.

Material	MTMOS:GPTMS:TEOS (molar ratio)	Thermal treatment (time = 2h)				
		60°C	80°C	100°C	120°C	140°C
90(M:G):10T	45:45:10	--	<100	>120	--	--
	76:14:10	--	--	>120	--	--
	83:7:10	--	--	>120	--	--
	86,5:3,5:10	--	--	>120	--	--
Reference ¹¹	50:50:0	--	--	--	--	>120

The elected thermal treatment to achieve acceptable coatings on series 90(M:G):10T was 100°C and positive results (resistance to 120 double-rubs with a cotton swab soaked in MEK) were achieved to all molar ratios (Table 4.2). It was considered the accomplishment of enough network crosslinking to acquire acceptable structure integrity.

Table 4.3 - Biocoatings resistance, series 70(M:G):30T, to double-rubs with a cotton swab soaked in MEK submitted to different thermal treatments to promote cross-linking.

Material	MTMOS:GPTMS:TEOS (molar ratio)	Thermal treatment (time = 2h)				
		60°C	80°C	100°C	120°C	140°C
70(M:G):30T	35:35:30	<10	>120	--	--	--
	56:14:30	--	>120	--	--	--
	63:7:30	--	<40	--	--	--
	66,5:3,5:30	--	<119	--	--	--
Reference ¹¹	50:50:0	--	--	--	--	>120

The selected thermal treatment to achieve acceptable coatings on series 70(M:G):30T was 80°C as 35M:35G:30T passed the test of resistance to 120 double-rubs with a cotton swab soaked in MEK. The molar ratios of 35% and 14% on GPTMS passed the test as well, however, the lower contents 7% and 3,5% failed.

RESULTS

After thermal treatment stipulation were considered successful the coatings or biomaterials that after the production and application process show homogeneous semblance, without particles or agglomerates, transparent and clear of pores and fissures perceptible to the naked eye. In view of that, all obtained biocoatings have homogenous and bright surface, free of imperfections with a layer thickness ranging from 0,5 - 1 μm (a few examples are shown in Figure 4.10 and Figure 4.11).



Figure 4.10 - Images of some biomaterials coated on stainless steel plates. Material with molar silane composition 45M:45G:10T (left), material with molar silane composition 86,5M:3,5G:10T (center) and material with molar silane composition 35M:35G:30T (right).

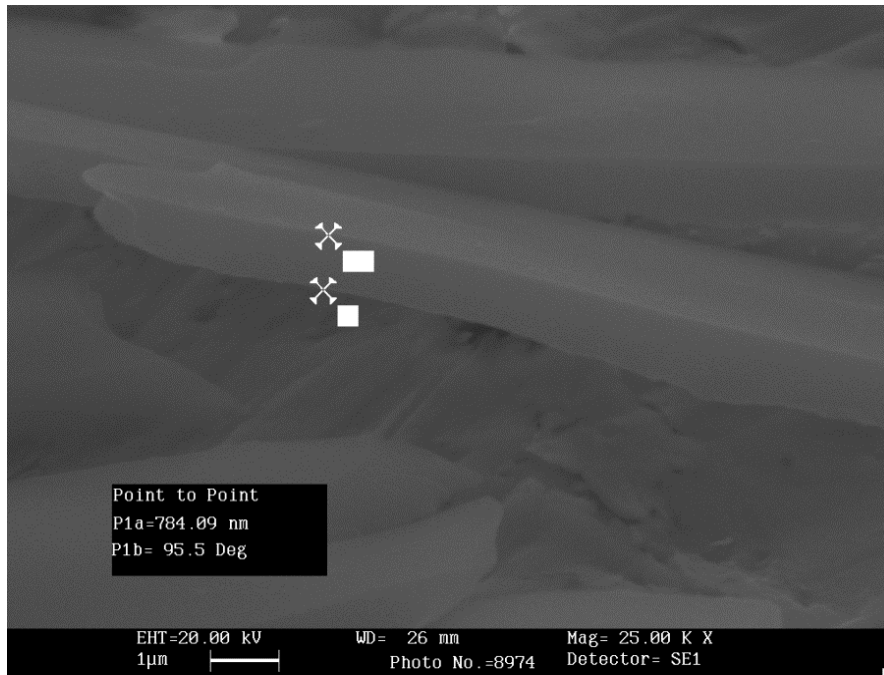


Figure 4. 11 - Microscope image (SEM) of 56M:14G:30T.

Finally solid state ^{29}Si NMR spectroscopy of samples, specifically compositions with the highest and lowest contents on GPTMS, was concluded to evaluate the achieved cross linking density after the final heat treatment. The NMR peak assignments will follow the data above cited in Table 4. 1.

Figure 4.12 show the obtained signals for reference sol-gel composition, 50%MTMOS:50%GPTMS, with special predominance of T^2 and T^3 units.

RESULTS

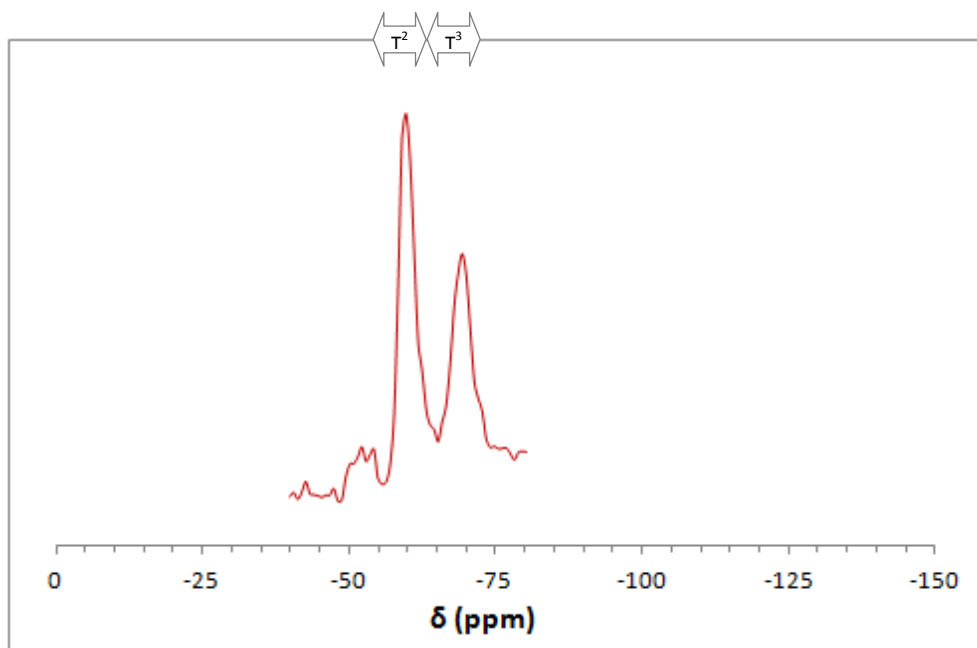


Figure 4.12 - Solid state ^{29}Si NMR spectra of 50M:50G (reference biomaterial).

When TEOS was incorporated in 10% to a composition with equivalent parts of MTMOS and GPTMS, i. e. 45M:45G:10T, in addition to T signals from trialkoxysilanes, new signals come into view nearby -99 and -110 ppm assigned to Q^3 and Q^4 species from tetraalkoxysilane - TEOS (Figure 4.13). The predominance of T^3 , Q^3 and Q^4 structures validates the achievement of a medium-high crosslinked matrix as predicted in the resistance to solvents test (Standard UNE-EN 13523-11) before cited.

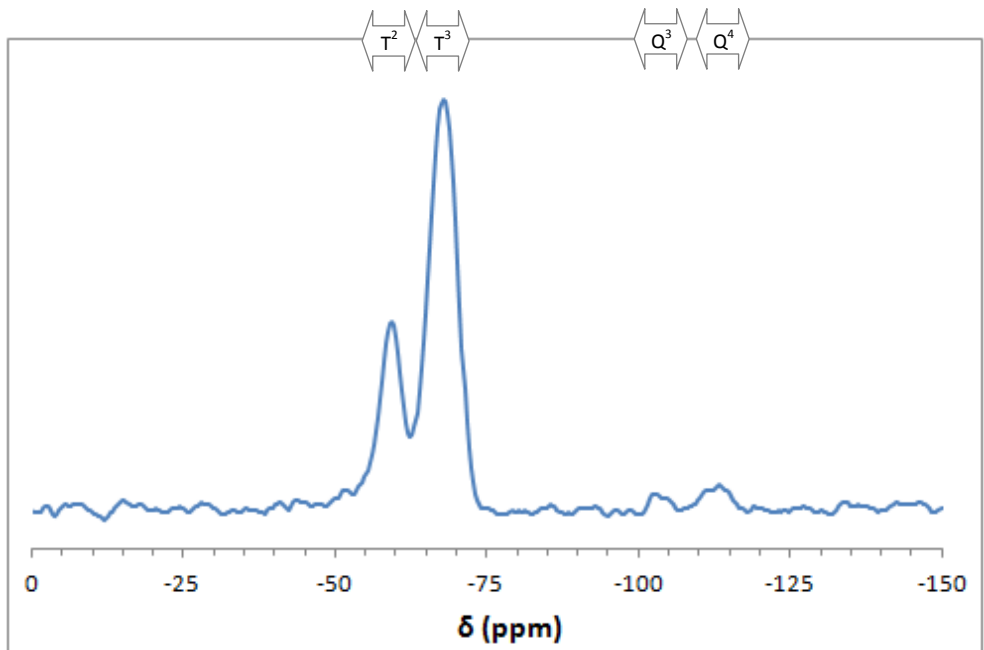


Figure 4. 13- Solid state ^{29}Si NMR spectra of 45M:45G:10T.

The crosslinking degree of 86,5M:3,5G:10T biocoating was also evaluated (Figure 4.14). The spectra show the presence of species T^2 and T^3 . Besides, strong signals were detected at -91, -99 and -110 ppm assigned to Q^2 , Q^3 and Q^4 species with higher intensity of Q^3 structure.

The predominance of structures with high crosslinking degree (T^2 and T^3 , Q^2 , Q^3 and Q^4) validates the achievement of a medium-high crosslinked matrix and these results agree with the resistance to solvents test (Standard UNE-EN 13523-11) results before cited.

RESULTS

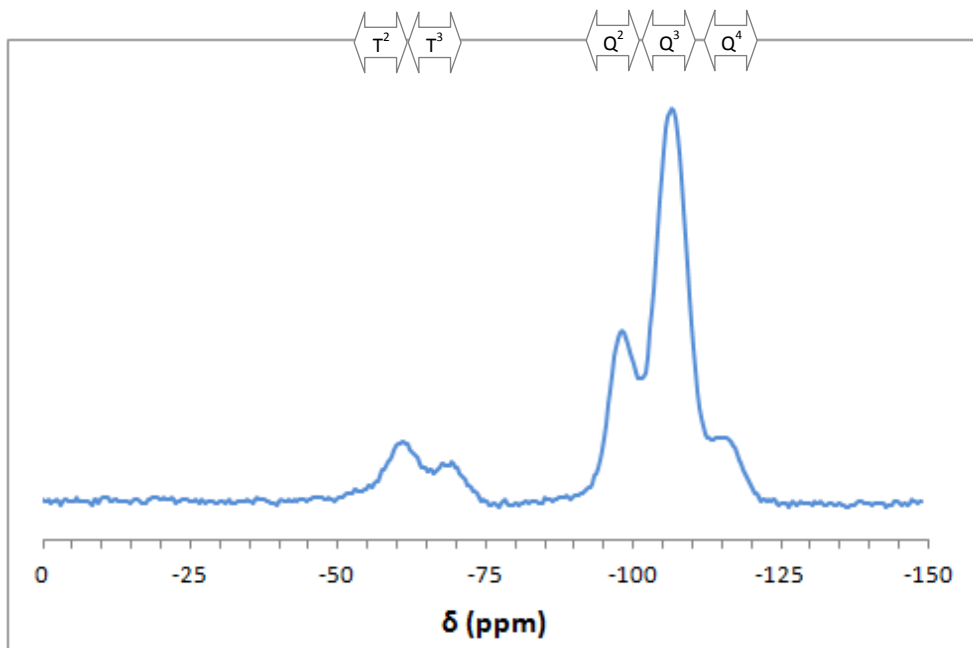


Figure 4. 14- Solid state ^{29}Si NMR spectra of 86,5M:3,5G:10T.

The spectra of 35M:35G:30T (Figure 4.15) shows the presence of T^1 , T^2 and T^3 units, with higher intensity signal detected between - 64 and - 66 ppm (T^3 structural units) from trialkoxysilanes (MTMOS and GPTMS) and Q^2 , Q^3 and Q^4 units from tetraalkoxysilane (TEOS).

The predominance of T^3 and Q^3 structures validates the achievement of a medium-high crosslinked matrix as predicted in the resistance to solvents test (Standard UNE-EN 13523-11) before cited.

It is important to notice as well the signal associated with T^1 species, not detected in any of the analysed materials of series with 10% TEOS (Figure 4.13 and Figure 4.14).

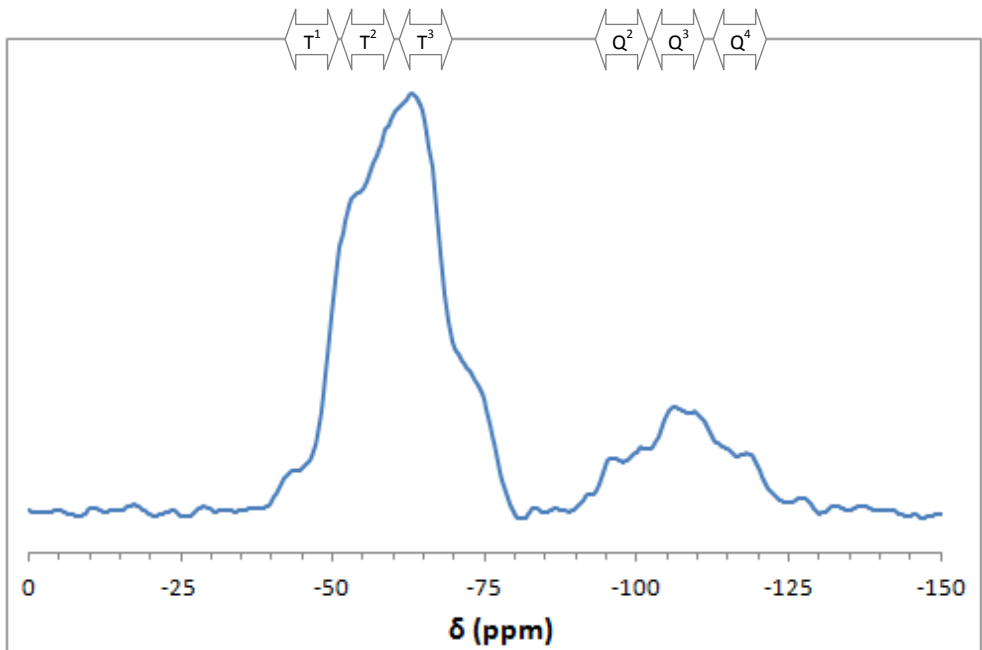


Figure 4.15 - Solid state ^{29}Si NMR spectra of 35M:35G:30T.

Figure 4.16 shows the solid state ^{29}Si NMR spectra of 66,5M:3,5G:30T biomaterial where it can be identified the presence of T¹, T² and T³ units, with higher intensity signal detected for T² structural units. Q species show structures Q², Q³ and Q⁴ with high intensity detected for Q³ units.

The predominance of T² and Q³ structures validates the achievement of a medium crosslinked matrix. The medium crosslinking degree and the detection of T¹ species are in agreement with the results predicted in the resistance to solvents test (Standard UNE-EN 13523-11) about the lower polymerization degree achieved for the materials of series 70(M:G):30T with lesser content on GPTMS.

RESULTS

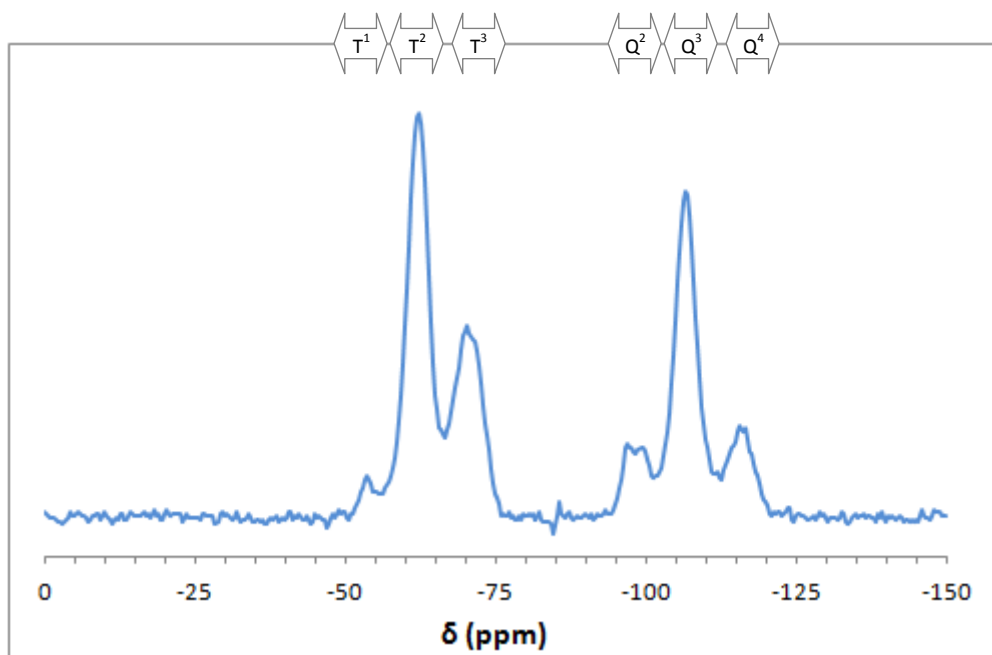


Figure 4. 16- Solid state ^{29}Si NMR spectra of 66,5M:3,5G:30T.

In Table 4.4 are collected the peak intensity proportion between T species and Q species of the biomaterials evaluated by ^{29}Si solid NMR analysis. Absorption intensity in RMN can be determined by peak area, nonetheless, when the signal is acute matches with relative accuracy with the relation between peaks height.¹²

Table 4.4 - ^{29}Si solid NMR peak intensity proportion of materials of series 90(M:G):10T and 70(M:G):30T.

Composition	MTMOS:GPTMS:TEOS (molar ratio)	Peak intensity proportion	
		$\text{T}^1/\text{T}^2/\text{T}^3$	$\text{Q}^2/\text{Q}^3/\text{Q}^4$
90(M:G):10T	45:45:10	-/56/109	-/13/16
	86,5:3,5:10	-/15/9	42/99/16
70(M:G):30T	35:35:30	9/99/33	22/25/13
	66,5:3,5:30	9/100/47	17/80/22
Reference	50:50:0	-/48/52 ¹¹	--

X. Rios and co-workers⁹ have studied the role that an ethyl group has as matrix modifier of an inorganic network of pure tetraethoxysilane (TEOS). They observed and concluded that the existence of a new alkyl group on the matrix decreases the condensation rate due to several possible causes: a) cancel one of the four condensation sites of silicon atom; b) reduces the positive net charge of the silicon atom (by inductive effect) affecting the nucleophilic condensation process; c) increase sterical restrictions and d) intramolecular reactions require more thermal energy and are slower than polymerization (intermolecular reactions). This study can help in understand the special behaviour of 70(M:G):30T series and the differences detected between compositions with high content in GPTMS (35M:35G:30T and 56M:14G:30T) and less GPTMS content (63M:7G:30T and 66,5M:3,5G:30T).

In fact, the incorporation of TEOS to the double composition reference material (50M:50G) generate a reduction on the thermal energy necessary to promote the polymerization process and that is clear on the resistance to solvents test (Standard UNE-EN 13523-11) results (Table 4.2 and Table 4.3) and solid state ²⁹Si NMR (Figure 4.13 - Figure 4.16) spectra. The thermal treatment of 140°C used to promote condensation reactions of reference biomaterial was reduced to 100°C when 10% TEOS was incorporated and to 80°C when 30% TEOS was incorporated. Nevertheless, interestingly the thermal treatment of 30% TEOS series biomaterials does not result equally effective to all the series sol-gel coatings.

Although the higher content on TEOS (30%) promote higher condensation rate (corroborated by the mild thermal treatment necessary to attain satisfactory final products) there is another factor related with the MTMOS content on coatings composition that affects in an important manner the structural properties of the sol-gel matrix. It is strange that GPTMS, a trialkoxysilane as MTMOS, does not induce so marked changes on the polymerization rate of the tricomposition coatings. This phenomenon may be explained by a previous study where it was proposed that the epoxy

RESULTS

group in the GPTMS silane is highly reactive and may open in acid environments (Figure 4.17). The resultant -CH-OH and -CH₂-OH may co-condensate with Si-OH, leading to more condensate networks with lesser free silanols¹³.

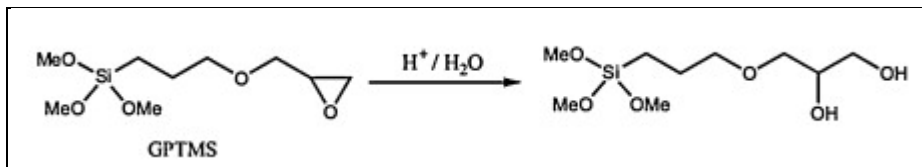


Figure 4. 17- Formation of hydroxyl functional alkoxy silane originated from GPTMS opening of epoxy ring¹⁴.

Taking into account all the before cited results and studies it is possible to make some suppositions:

- TEOS incorporation to double composition sol-gel biomaterials reduces the thermal energy necessary to promote the polymerization process (in agreement with X. Rios and co-workers⁹ findings);
- series 90(M:G):10T biomaterials achieve a similar crosslinking degree with the 100°C thermal treatment used;
- series 70(M:G):30T biomaterials does not achieve the same crosslinking degree with the 80°C thermal treatment used.

In the special case of series 70(M:G):30T coatings the balance between MTMOS:GPTMS content seems to be crucial. On one hand, GPTMS insert in the matrix a new alkyl group that may affect the condensation rate possibly due to the thermal energy consumption on the intramolecular rearrangements. Nevertheless this alkyl group is susceptible of reacting with available silanol groups converting this silane in a different structure with four condensation sites and possibly enhancing the condensation rate. On the other hand, MTMOS silane introduce in the polymer matrix a methyl group that may affect the condensation reactions by many motifs as inductive effects on the silicon atom or sterical restrictions (as stated on the X. Rios and co-workers⁹ study) among other synergic phenomenon's.

So, although GPTMS content on series 70(M:G):30T materials does not cause noticeable changes on crosslinking degree due to the equilibrium between favourable and adverse factors, the higher level of MTMOS content on the compositions (special case of 63M:7G:30T and 66,5M:3,5G:30T) affects in an important way the condensation rate leading to the thought that the methyl group impair the condensation rate of the sol-gel matrix.

Infrared Spectroscopy (FTIR) is another important tool to gather information about the macromolecular structure of sol-gel silica based materials developed in this work. The wavenumbers at which an organic molecule absorbs radiation gives information about the functional groups present in the materials.¹⁵

Table 4.5 includes the assignments of the bands appearing in the FTIR spectra of studied silica based materials, according to current literature.^{7,9}

Table 4.5 - Assignment of the most relevant bands in the FTIR spectra of sol-gel hybrid materials.

Wavenumber range (cm ⁻¹)	Structural unit assign
≈ 3400	-OH
≈ 3050	Aromatic C-H stretching
≈ 2873 - 2972	C-H stretching
≈ 1640	Adsorbed water
≈ 1270	C-H (epoxy opening)
≈ 1199	Si-CH ₂
≈ 1093	Si-O stretching
≈ 1024	Si-OH
≈ 906	Epoxy ring deformation
≈ 857 and 905	Si-OH
≈ 770	Si-O-Si

RESULTS

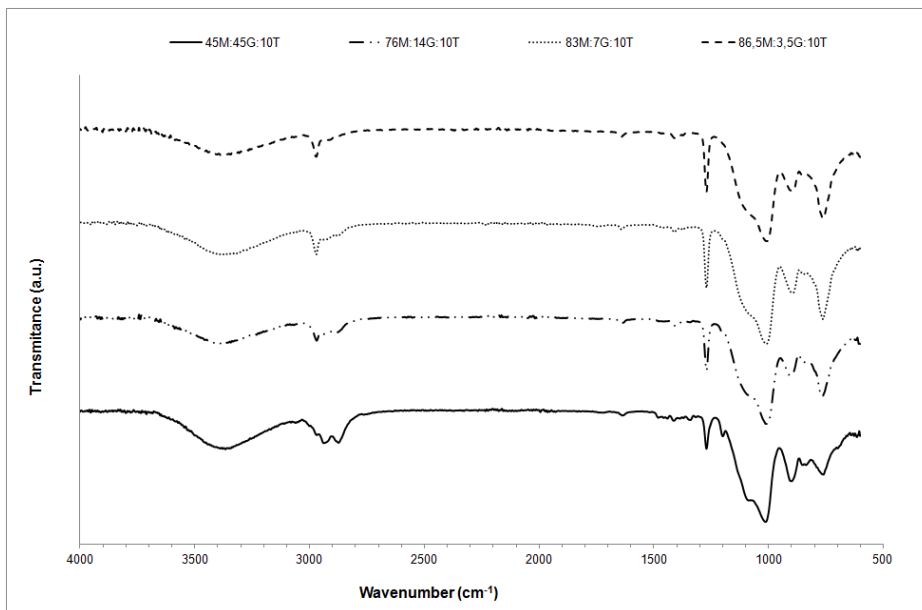


Figure 4.18 - FTIR spectra recorded for synthesized xerogels of series 90(M:G):10T.

Figure 4.18 show the FTIR spectra of samples 45M:45G:10T, 76M:14G:10T, 83M:7G:10T and 86,5M:3,5G:10T of series 90(M:G):10T. The broad band around 3400 cm^{-1} is assigned to the O-H stretching bonds of surface silanols, non removed solvents and by-products formed on chemical reactions.¹⁶ The weak peak registered at 1640 cm^{-1} was also associated with H_2O absorption in other previous works.¹⁷ Besides, bands detected at 857 and 905 cm^{-1} also offer important information about the network structure of the materials as they belong to silanol groups (Si-OH) stretching present on the hybrid matrix.¹⁸ Some authors infer that the intense band detected at 1024 cm^{-1} could be ascribed to hydrolyzed products between metalorganic compounds and silanol groups.¹⁸ The free silanols detected on FTIR analysis is in accordance with upper cited NMR results (Figure 4.13 and Figure 4.14) as it was identified a medium-high condensation degree but not total.

One of the most intense bands detected on all spectra is centred around 1093 cm^{-1} and corresponds to a vibration mode of the Si-O-Si silica network.^{9,18} Also at 770 cm^{-1} another band is detected on all hybrid films

spectra associated to a different vibration mode of the same silica matrix structure.⁹ As expected the bands 1093, 1024, 905 and 770 cm^{-1} attributed to the several vibration modes of the silica network were the most intense, these results are indicative of a correct formation of the inorganic structure Si-O-Si.

Bands identified at 906 cm^{-1} and 1270 cm^{-1} were related with GPTMS structural species, antisymmetric epoxide ring deformation and epoxide ring opening respectively.¹⁹ However, it is important to notice that the detection range of Si-O-Si bonding is between 1100-1300 cm^{-1} what could be a cause for the perceptible reduction on 1270 cm^{-1} peak intensity with increasing on GPTMS content of this series materials.

Peaks identified at 1413 cm^{-1} belong to C-H vibrations of the organic groups that remain on coatings structures after synthesis and thermal treatment. Peaks between 2873 and 2972 cm^{-1} are assigned to C-H stretching vibrations. The bands registered at 1199 cm^{-1} and 3050 cm^{-1} , only detectable for the highest GPTMS content composition 45M:45G:10T, are related to the vibration of Si-CH₂ bonding and aromatic C-H stretching from GPTMS alkyl group respectively.²⁰

The increase on the GPTMS content (3,5% → 7% → 14% → 45% GPTMS) generate the most visible changes on spectra nevertheless does not seems to affect the structure of the matrix supported by the Si-O-Si structural unit. Specifically, peaks related with GPTMS alkyl group identified at wavenumbers 1199 cm^{-1} , 2873 cm^{-1} , 2972 cm^{-1} and 3050 cm^{-1} changes its intensity with GPTMS content increase.

The infrared spectra of series 90(M:G):10T show some important structural characteristics of the hybrid materials, to be precise, the ability to hold the organic chains of MTMOS and GPTMS silanes, the formation of the inorganic skeleton by Si-O-Si bonding structures and the identification of silanol groups Si-OH that were not crosslinked.

RESULTS

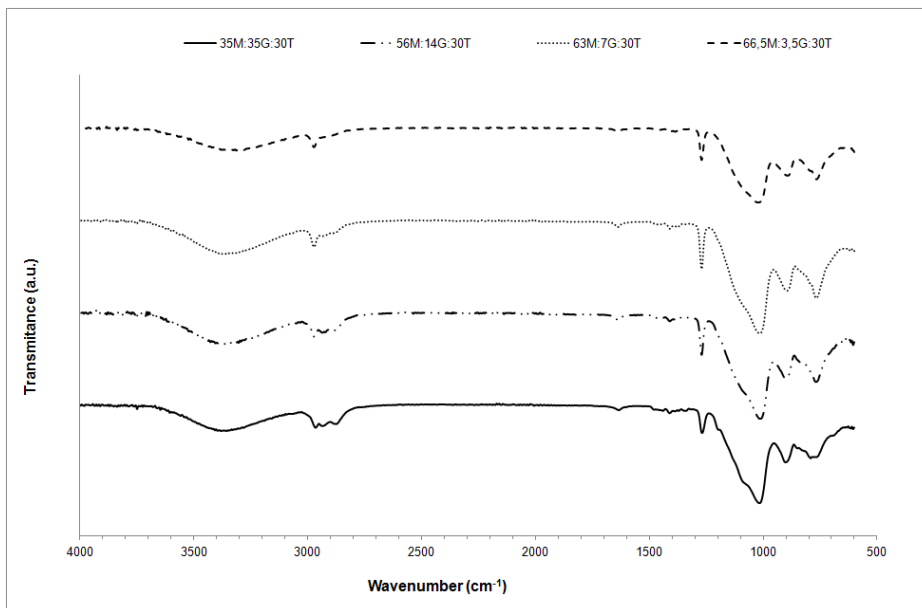


Figure 4. 19- FTIR spectra recorded for synthesized xerogels of series 70(M:G):30T.

Figure 4.19 show the FTIR spectra of samples 35M:35G:30T, 56M:14G:30T, 63M:7G:30T and 66,5M:3,5G:30T of series 70(M:G):30T. The results of the FTIR analysis are similar to the spectra registered for biomaterials of series 90(M:G):10T (Figure 4.15) as the bands attributed to the different vibration modes of the silica network, - OH group and organic groups from precursors were the most intense.

The broad band at 3400 - 3600 cm^{-1} belongs to H_2O and hydroxyl group vibrations. The weak peak registered at 1640 cm^{-1} was also related on literature with H_2O adsorption.^{16,17} The bands detected at 857 and 905 cm^{-1} were related to silanol groups (Si-OH) stretching present on the silica based coatings.¹⁸ Some authors suggest that the intense band detected at 1024 cm^{-1} could be ascribed to hydrolyzed products between metalorganic compounds and silanol groups.¹⁸ The FTIR results on the identification of free silanols are in accordance with upper cited NMR results (Figure 4.15 and Figure 4.16) where it was identified that not all Si-OH groups were crosslinked during the final thermal treatment.

The strong band detected at around 1093 cm^{-1} corresponds to a vibration mode of the Si-O-Si silica network.^{9,18} Above and beyond a different vibration mode of the same silica matrix structure was detected at 770 cm^{-1} .⁹ As expected the bands attributed to the several vibration modes of the silica network were perfectly identified and these results are indicative of a correct formation of the inorganic structure Si-O-Si.

The identification of bands at 906 cm^{-1} and 1270 cm^{-1} were related with GPTMS structural species, antisymmetric epoxide ring deformation and epoxide ring opening respectively.¹⁹ However, it is important to notice that the detection range of Si-O-Si bonding is between $1100\text{--}1300\text{ cm}^{-1}$ what could be the cause of the perceptible reduction on 1270 cm^{-1} peak intensity with increasing on GPTMS content.

Peaks identified at 1413 cm^{-1} belong to C-H vibrations of the organic groups that remain on coatings structures after synthesis and thermal treatment. Peaks between 2873 and 2972 cm^{-1} are assigned to C-H stretching vibrations. The band registered at 1199 cm^{-1} , specially visible for the highest GPTMS content composition 35M:35G:30T spectra, is related to the vibration of Si-CH₂ bonding from GPTMS alkyl group.²⁰

The GPTMS content (3,5% → 7% → 14% → 35% GPTMS) generate noticeable changes on spectra at specific wavenumbers related with the attached alkyl group identified at 1199 cm^{-1} , 2873 cm^{-1} , 2972 cm^{-1} and 3050 cm^{-1} . In fact, the intensity of those peaks is directly affected by GPTMS content. Nevertheless, changes on GPTMS content does not modify bands related with the structure of the matrix supported by an inorganic matrix of Si-O-Si bondings.

The infrared spectra of series 70(M:G):30T successfully used for studying hydrolysis and condensation of alkoxides revealed some important structural information of the complex hybrid matrix as: the ability to hold the alkyl groups of MTMOS and GPTMS silanes, the formation of the inorganic skeleton by Si-O-Si bonding structures and the identification of free silanol groups.

RESULTS

FTIR analysis provides evidences that the developed biomaterials matrix still preserve the alkyl organic chains of silica precursors and Si-O-Si bonding was clearly identified as the inorganic skeleton of the network.

The addition of different TEOS content (10% → 30%) to the silane compositions does not seem to affect the structure of the biomaterials as the bands identified on the FTIR spectra are very similar for the materials of both materials series. However, the different GPTMS content on compositions affect peaks intensity related with the GPTMS alkyl group attached on the networks.

Thermogravimetric analysis (TGA) was also performed to investigate the thermal decomposition of the silica based hybrid coatings with different organic content. Figure 4.20 and Figure 4.21 show TGA and differential weight loss (DTG or 1st derivate) curves for materials from series 90(M:G):10T and from series 70(M:G):30T, respectively.

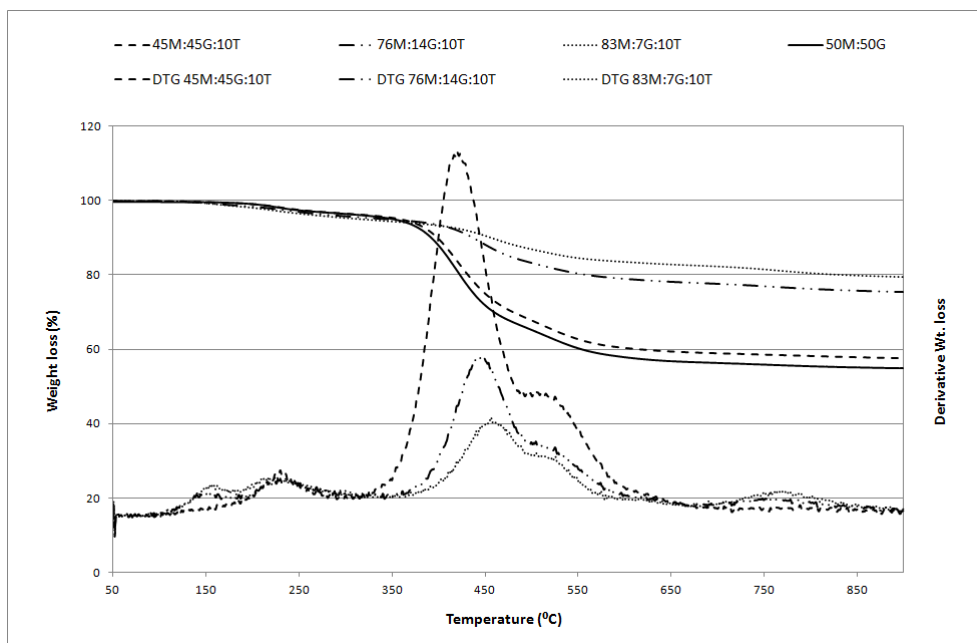


Figure 4.20 - TG and DTG profiles of the hybrid coatings of series 90(M:G):10T.

DTG curve of series 90(M:G):10T (Figure 4.20) show four main degradation stages. The first weight losses detected below 270°C might be related with loss of adsorbed water and evaporation of volatiles present in the hybrid matrix. Besides, between 350 - 500°C another weight loss is perceived and attributed to the volatilization of small molecular oligomers or unreacted precursors. Additionally, weight losses registered at 500 - 600 °C and 750 - 850°C are possibly related with the decomposition of the polymeric structure and the dehydration of silanol groups respectively.^{21-24,25}

The temperature related with each degradation stage registered to all compositions of this series is very similar suggesting that the changes on GPTMS content does not affect in an important manner the formation and stability of the matrix. However, there are appreciable differences on the lightweight loss registered at 150°C and 800 °C besides the pronounced weight loss of 45M:45G:10T registered between 400 - 600°C not so noticeable in the other compositions with lesser GPTMS content.

The weight loss registered at 150°C for compositions with lesser content on GPTMS was associated with the evaporation of physically adsorbed water and volatiles evaporation^{26,25}, this suggests that the GPTMS alkyl group attached on the network can affect the physical and chemical characteristics of the matrix and consequently water adsorption. In a previous study¹³ was stated that the unhydrolysable group of GPTMS silane is a long and flexible chain with the ability to fill the pores of the silica matrix leading to a more compact structure. In addition, in the same study was suggested that resulting -CH-OH and -CH₂-OH groups from epoxy ring opening may co-condensate with Si-OH leading to a higher crosslinking degree and decrease of available -OH hydrophilic groups. Both exposed situations may be the cause of the lightweight loss registered at ≈150°C for 76M:14G:10T (≈1,2%) and 83M:7G:10T (≈0,7%) compositions and almost imperceptible weight loss for 45M:45G:10T (≈0,5%).

RESULTS

At 230°C all the compositions registered a weight loss of $\approx 2\%$ associated with the evaporation of volatiles, as the volumetric ratio of alcohol:silanes was fixed on 1:1 it is expectable a similar retention degree of co-solvent on the hybrid matrix.

The most noticeable weight loss was registered at the range 350 - 450°C and according to previous studies²⁵ may be attributed to the volatilization of small molecular oligomers and unreacted silane precursors. 45M:45G:10T loses 25% weight at 420°C, 76M:14G:10T loses 12% weight registered at 442°C and finally 83M:7G:10T loses about 7% at 455°C. What is more, it was proposed that the evaporation of these volatile components may be affected by the presence of residual silanols²⁵, as the above cited RMN results (Figure 4.13) show a high and not total condensation degree provides evidence of non-condensed silanols on the network of biomaterials. DTG plot (Figure 4.20) show a hierarchy on GPTMS content, degradation temperature and amount of weight loss, that is to say, 45M:45G:10T starts degradation at 420°C and lose the greater weight amount, followed by 76M:14G:10T and finally composition with only 7% GPTMS degrade at 455°C and lose only 7% weight. These results suggest that GPTMS does not increase biomaterials thermal stability but enhance the amount of weight loss.

The third degradation thermal section takes place at 510°C and was assigned to pyrolysis of organic chains.²⁵ The weight losses registered for compositions 45M:45G:10T, 76M:14G:10T and 83M:7G:10T was 10%, 8% and 2% and is in accordance with the GPTMS content of each composition as higher organic content results in higher weight loss.

Finally, a lightweight loss of about 2% was detected at 765°C (stage 4) for biomaterials with lesser organic content 76M:14G:10T and 83M:7G:10T assigned to silanol groups dehydration.²⁵ Once again the results are in accordance with previous findings¹³ about the co-condensation of alkyl groups from epoxy ring opening leading to higher condensation degree and consequent decrease on available Si-OH.

Interestingly, the weight losses detected only for biomaterials with lesser organic content 76M:14G:10T and 83M:7G:10T at 150°C associated with

evaporation of adsorbed water and at 765°C attributed to silanol groups dehydration could be related with the available -OH groups and density of these coatings. That is to say; lesser GPTMS content reduce the availability of possible four linking possibilities of silicon atom (the ring opening may represent a fourth condensation point besides the three hydrolysable alkoxides) and consequently reduce the matrix density what in some way may be an advantage for water adsorption and absorption culminating in higher contents of adsorbed water.

The TGA thermograms also show that the final thermal treatment of 100°C used on the process to achieve a xerogel condition does not affect or destroy the organic groups provided by silanes precursors as the decomposition of the polymeric part of the coatings takes place above 400°C.

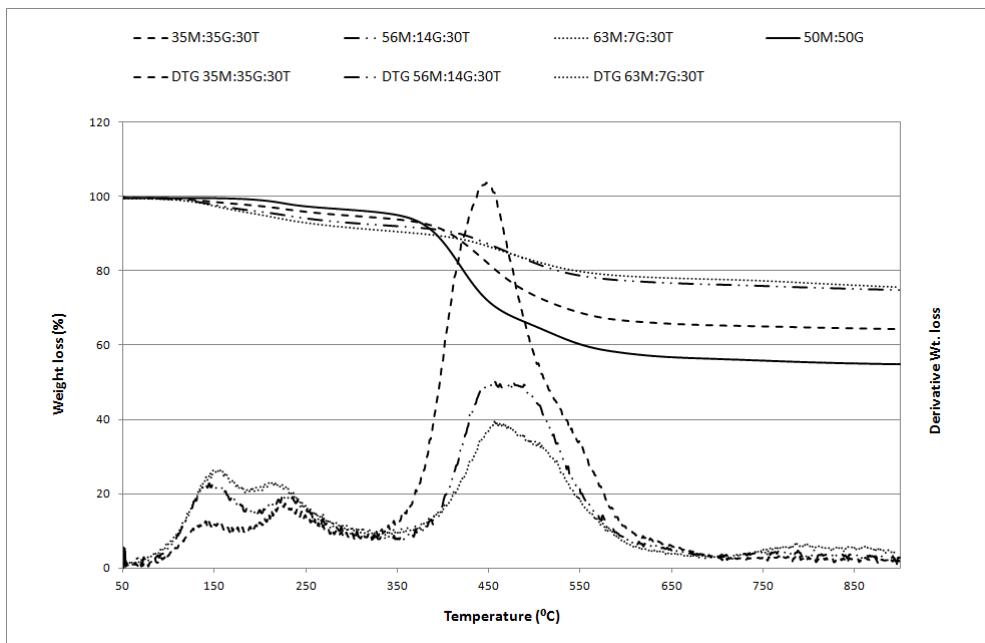


Figure 4.21 - TG and DTG profiles of the hybrid coatings of series 70(M:G):30T.

RESULTS

The TGA curves for series 70(M:G):30T materials (Figure 4.21) show a different profile from 90(M:G):10T series curves. Although the temperatures corresponding to each degradation stage remain practically the same, weight loss proportion undergo substantial changes. DTG curves show a pronounced inflection at about 450°C and two smaller inflection points between 100 - 270°C. Exceptionally, 63M:7G:30T composition show a slight inflection point above 730°C.

The first weight losses detected below 270°C were associated with loss of adsorbed water and volatiles evaporation. At the thermal degradation range 350 - 600°C a strong weight loss is noticeable and attributed to the evaporation of small molecular oligomers/unreacted precursors and decomposition of the polymeric structure. Additionally, weight loss registered for 63M:7G:30T composition above 730°C is related with dehydration of silanol groups.^{21-24,25}

At 150°C starts the weight loss with 0,6% for 35M:35G:30T, followed by 2% for 56M:14G:30T and 3% for 63M:7G:30T coating. Composition with highest GPTMS content, 35M:35G:30T, clearly lose lesser weight amount than other compositions (as verified for series 90(M:G):10T materials). The upper cited rationalization about the co-condensation of alkyl groups from epoxy ring opening leading to higher condensation degree and consequent decrease on available Si-OH could justify this result.¹³

The weight loss registered at ≈220°C could be attributed to alcohol (co-solvent) evaporation, the weight loss verified for 35M:35G:30T, 56M:14G:30T and 63M:7G:30T was: 3,2%, 2,7% and 3,9% respectively. The lower temperature (80°C) of the thermal treatment used in this series coatings production could be a reason for higher weight losses registered as the thermal energy available for alcohol volatilization is minor. It is interesting to refer that 63M:7G:30T show the highest weight loss related with volatiles evaporation suggesting higher retention of co-solvents in the matrix, on the other hand, results from rubbing test (Table 4.3) suggests the formation of an unstable hybrid structure. Both TGA and rubbing test results on 63M:7G:30T coating point to some synergic effects on this

composition that difficult the polymerization process and thermal treatment efficiency.

When temperature was increased from 330 to 600°C a large weight loss peak was marked in the spectra of all coatings. When content range of GPTMS on the different series materials increases from 7% to 14% and finally 35% the weight loss registered at $\approx 450^\circ\text{C}$ was: 5,1%, 12% and 27,5%. It is obvious a relation between the GPTMS amount on the hybrid coatings and the weight loss proportion.

In the case of series 90(M:G):10T in a temperature range between 330 - 600°C (Figure 4.20) two weight losses were easily recognized and attributed to the volatilization of small molecular oligomers and unreacted silane precursors ($\approx 450^\circ\text{C}$) and to pyrolysis of organic chains ($\approx 510^\circ\text{C}$). Nonetheless, series 70(M:G):30T DTG spectra (Figure 4.21) show a single wide peak maybe because there is a lower organic content and the pyrolysis of organic chains starts at lower temperature overlapping the volatilization of small molecular oligomers and unreacted precursors.

Finally, from 720°C to 850°C only 63M:7G:30T composition show a unimportant weight loss of 0,7%.

In a few words, DTG curve of series 90(M:G):10T (Figure 4.20) show four main degradation stages. The first weight losses detected below 270°C might be related with loss of adsorbed water and evaporation of volatiles present in the hybrid matrix. Between 350 - 500°C another weight loss is perceived and attributed to the volatilization of small molecular oligomers or unreacted precursors. Finally, weight losses registered at 500 - 600 °C and 750 - 850°C are possibly related with the decomposition of the polymeric structure and the dehydration of silanol groups respectively.^{21-24,25}

On the other hand, the TGA curves for series 70(M:G):30T materials (Figure 4.21) show only three main degradation stages. The DTG curves illustrate a pronounced inflection at about 450°C and two smaller inflection points between 100 - 270°C.

RESULTS

Table 4.6 show the weight loss (%) of series 90(M:G):10T and series 70(M:G):30T materials in each degradation stage.

Table 4.6 - Weight loss (%) of hybrid coatings of series 90(M:G):10T, 70(M:G):30T and reference material (50M:50G) in the degradation stages.

Biomaterial	Stage 1 ≈ 150°C (%)	Stage 1 ≈ 230°C (%)	Stage 2 ≈ 450°C (%)	Stage 3 ≈ 500°C (%)	Stage 4 ≈ 800°C (%)
45M:45G:10T	0,5	2,0	25,0	10,0	--
76M:14G:10T	1,2	2,5	12,0	8,0	2,0
83M:7G:10T	1,0	2,0	7,0	2,0	2,0
35M:35G:30T	0,6	3,2	5,1		--
56M:14G:30T	2,0	2,7	12,0		--
63M:7G:30T	3,0	3,9	27,5		0,7
50M:50G	--	2,8	21,7	11,1	--

COATING INTEGRITY AND SURFACE PROPERTIES

To investigate biocoatings surface properties, a first analysis of topography was made otherwise than the study of surface energy.

Roughness profiles were acquired with a mechanical profilometer and an example of the prepared samples is in evidence in Figure 4.22.



Figure 4.22 - Prepared sample for average roughness (R_a) measurement of 83M:7G:10T biocoating.

The topography of a biomaterial affects its macroscopic behaviour and the influence of surface topography on the biological response must be investigated to each specific case.

The metal plate substrate show an average roughness of $0,0503 \mu\text{m}$, nevertheless when coated with the reference material 50%MTMOS:50%GPTMS this average roughness is reduced to $0,0288 \mu\text{m}$. Therefore, it will be interesting the study of the changes motivated by the new sol-gel biomaterials as well.

Average roughness parameters estimated by profilometry of metal plates coated with series 90(M:G):10T and 70(M:G):30T materials are exposed in Figure 4.23 and Figure 4.24.

RESULTS

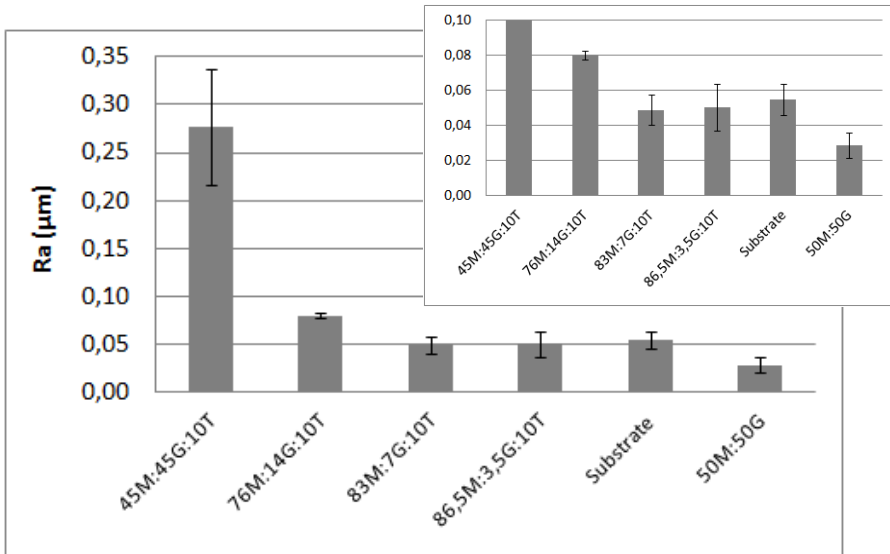


Figure 4.23 - Average roughness (R_a) of the four biocoatings of series 90(M:G):10T estimated by profilometry.

The coating with the highest content on GPTMS, 45M:45G10T, increase in an important manner the substrate average roughness (R_a) when compared with any of the other coatings of the series and reference material.

On the other hand, adhered layers with low content on GPTMS, 83M:7G:10T and 86,5M:3,5G:10T, reduce slightly the substrate roughness respecting the metallic base topography.

Taking into account the roughness results of series 90(M:G):10T, it is expected higher available surface area for 45M:45G:10T and easier access of surrounding fluids, followed by 76M:14G:10T in lower proportion. It is also clear that TEOS incorporation to reference material 50M:50G increases the surface average roughness.

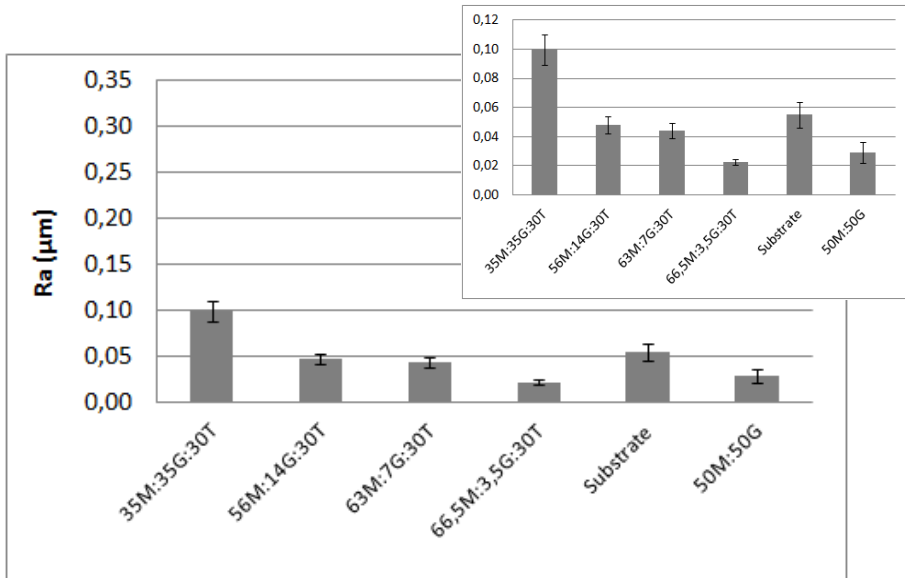


Figure 4.24 - Average roughness (R_a) of the four biocoatings of series 70(M:G):30T estimated by profilometry.

Figure 4.24 compiles the average roughness (R_a) of the four coatings of series 70(M:G):30T, the results show a certain hierarchy related with GPTMS content. Besides, the average roughness of reference material 50M:50G is increased by TEOS incorporation, exceptionally, 66,5M:3,5G:30T reduce the average roughness of reference coating.

The material with higher content on GPTMS, 35M:35G:30T, increase twice the substrate roughness, the intermediate contents 56M:14G:30T and 63M:7G:30T seems to keep up the roughness of metal substrate and finally the material with lower content on GPTMS, 66,5M:3,5G:30T, decrease surface roughness to half part of reference metallic surface.

In this series, the higher TEOS content (30%) on coatings composition cause smooth morphologies. On the other hand, as verified on series 90(M:G):10T, there is a clear correlation between GPTMS content and roughness. So it is expectable more available area for 35M:35G:30T coating and easier access of surrounding aqueous environment, on the other hand, more difficult access on adhered films with lower contents on GPTMS as 66,5M:3,5G:30T that result in a smoother surface.

RESULTS

To facilitate comparison between the triple silane coatings and reference double silane coating 50M:50G the difference between average roughness of the new developed coatings and reference material 50M:50G was estimated and the results are illustrated in Figure 4. 22.

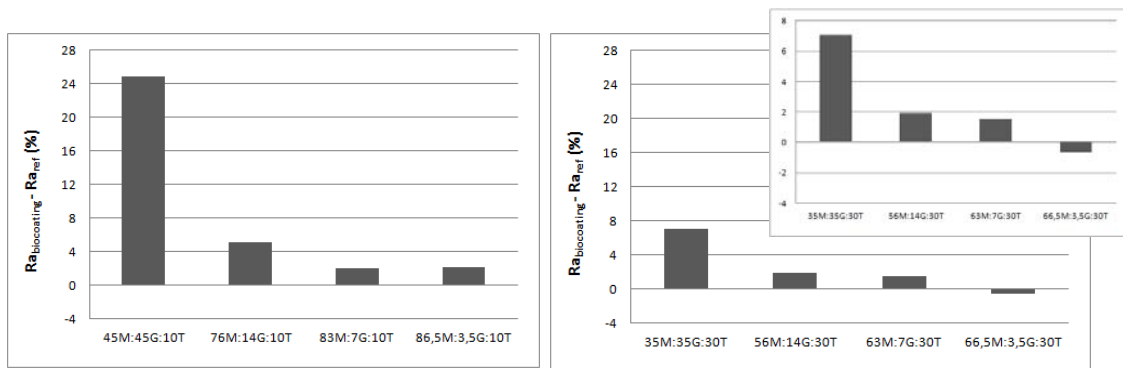


Figure 4. 25 - Δ Average roughness (R_a) in percentage of the biocoatings of series 90(M:G):10T (left) and 70(M:G):30T (right) in regard to reference material 50M:50G.

All the biocoatings of series 90(M:G):10T raise the reference material 50M:50G average roughness (R_a) as it can be verified in Figure 4.25 (left diagram), the highest increase is detected for 45M:45G:10T composition ($\approx 25\%$) followed by 76M:14G:10T in much lower proportion ($\approx 5\%$) and the compositions with less content on GPTMS surpass the reference R_a only about 2%. Perhaps, the higher spatial structure of GPTMS molecule and the condensation degree achieved for these materials (NMR solid state results in Table 4.4) represent the factors that most influence the surface roughness results, with a hierarchy trend verified with GPTMS content variation. On the other hand, clearly the TEOS content affects the average roughness of reference material 50M:50G increasing it.

On the other hand, the results registered for series 70(M:G):30T materials (Figure 4.25, right diagram) show the composition with highest content on GPTMS show the highest increase on R_a regarding reference material 50M:50G (7,1%) followed by 56M:14G:30T (1,9%) and 63M:7G:30T (1,5%). Nonetheless, the composition with lesser content on GPTMS,

66,5M:3,5G:30T, is the only coating that decrease on 0,64% the reference material average roughness showing a smoother surface.

Once again, apparently the incorporation of TEOS in 30% affects the average roughness of the reference double silane composition material, 50M:50G, increasing it (35M:35G:30T, 56M:14G:30T, 63M:7G:30T) or decreasing it (66,5M:3,5G:30T).

In the main, the 70(M:G):30T and 90(M:G):10T series results leads to the supposition of a high influence of GPTMS content on coatings surface roughness, as a hierarchy trend is detected for both series, higher GPTMS content leads to higher average roughness.

Finally, to ascertain if the GPTMS content and consequently its higher spatial structure affect the coatings thicker/surface roughness, a weight control of coated metal plates was made to all the materials. In Figure 4.26 and Figure 4.27 is exposed the mass increase of metal plates after coating with 90(M:G):10T and 70(M:G):30T series materials.

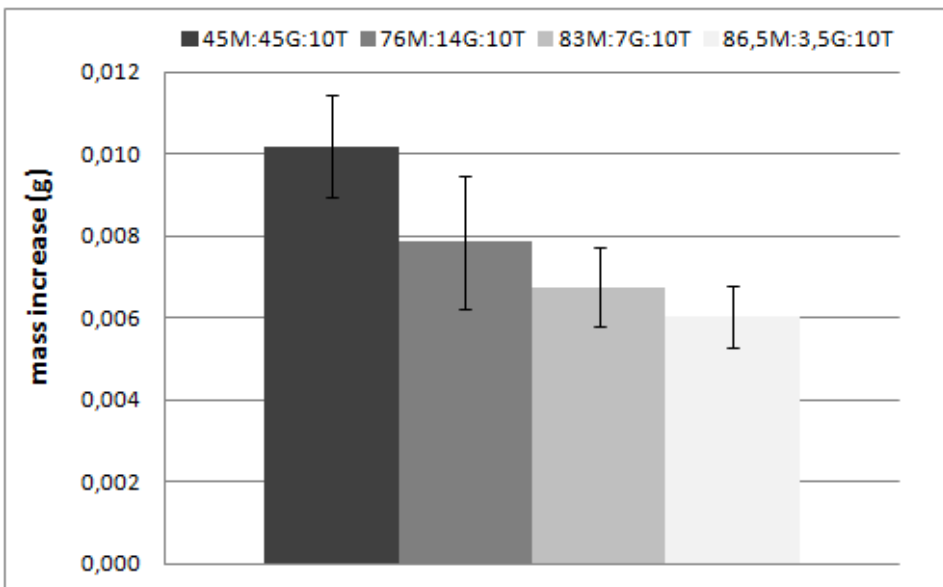


Figure 4.26 - Weight increase of metal substrate after coating with sol-gel - series 90(M:G):10T.

RESULTS

The results of weight increase on plates coated with 90(M:G):10T series materials show a clear effect of the GPTMS content on the mass gain in an organization ranked one above the other according to GPTMS content, varying in a range from 0,00603 g (3,5% GPTMS) to 0,0102 g (45% GPTMS). These results suggest that there is a mass increase of the films with the increasing of GPTMS content possibly due to the higher molecular weight of GPTMS.

An important issue is the way somehow the weight increase can affect coatings surface topography. Surface roughness results show that when GPTMS content is equal or greater than 14% (molar ratio) affect the metallic base surface roughness, increasing it (Figure 4.23). Possibly due to the thicker films adhered when there is an elevated proportion of GPTMS in the materials compositions. On the other hand, the possible thinner layers formed by materials with lower contents on GPTMS respect the metal base morphology. This hypothesis is corroborated by the weight increase results that show a clear mass augment with increasing GPTMS content.

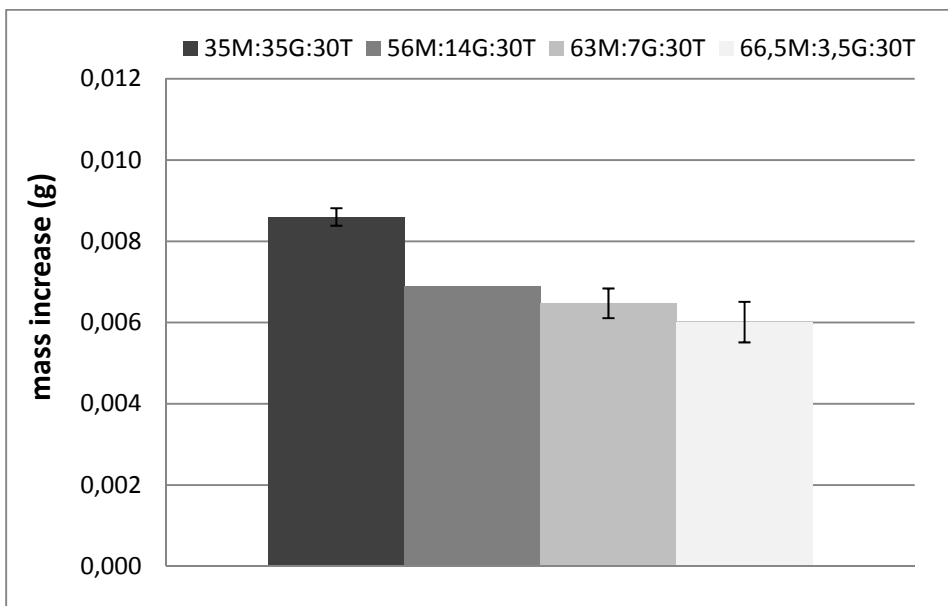


Figure 4.27 - Mass increase of metal substrate after coating with sol-gel - series 70(M:G):30T.

In Figure 4.27 can be found the mass gain of metal plates when coated with the materials of series 70(M:G):30T. As verified on series 90(M:G):10T, it is perceptible a hierarchy related with the content on GPTMS as 3,5% GPTMS (molar ratio) on silane combination results in 0,0060 g weight gain, a 7% GPTMS content in 0,0065 g weight gain, a 14% GPTMS content in 0,0069 g and finally the higher content on GPTMS of 35% marks 0,0086 g weight gain.

In this case, the higher content on TEOS (30%) plays a noticeable role and it is not so noticeable the alkyl group (GPTMS) influence on weight gain.

The average roughness results and mass increase measurements leads to the supposition that the GPTMS content affects the adhered films thickness on both series materials, as higher GPTMS content leads to higher average roughness and higher weight gain.

Continuing within the materials surface properties, surface energy (intimately related to wettability) represents a surface property that affects protein adsorption and cellular adhesion.

Hydrophilic surface characteristics results mostly from the balance between two important factors, surface roughness and surface energy.²⁷ Subsequently, a study about the influence that TEOS incorporation has on reference coating water contact angle will be made, otherwise than the evaluation on how GPTMS content affects the water contact angle of triple silane combination coatings.

The typical structure of the sol-gel after synthesis process will be a central silicon atom bond to silanol groups in condensed or free form and besides an alkyl group attached that remains available for interaction with other elements in the case of MTMOS and GPTMS that may alter surface wettability and reactivity.

Table 4.7 and Table 4.8 show the contact angles of water drops on the metal plates coated with the series 90(M:G):10T and 70(M:G):30T materials, respectively.

RESULTS

Table 4.7 - Contact angle (degrees) of the four silane combinations of coatings of series 90(M:G):10T.

Coating	Water contact angle (°)
45M:45G:10T	63,7±1,1
76M:14G:10T	73,4±1,0
83M:7G:10T	74,2±0,8
86,5M:3,5G:10T	75,5±1,0
50M:50G	69,6±0,6

It is expected that differences in surface roughness (related with surface area) may cause changes in wettability. Nevertheless, both properties: topography and wettability/surface chemistry show important regulatory effects on osseointegration by their own.^{28,29} Accordingly to roughness results, 45M:45G:10T with the highest R_a value of all series show the lowest contact angle, that is to say, higher wettability. Following the trend with decreasing GPTMS content on silane combinations increases the contact angle, more explicitly, diminish wettability. Besides the surface topography that affects wettability many other factors may play an important role on water contact angle results, in this system may exist a balance between surface topography and availability of free silanols (wettability promoters). It is important to say that 45M:45G:10T is the only material of all series that improves on the wettability result registered to the reference material 50M:50G (Table 4.7).

Table 4.8 - Contact angle (degrees) of the four silane combinations of coatings of series 70(M:G):30T.

Coating	Water contact angle (°)
35M:35G:30T	62,0±1,0
56M:14G:30T	68,1±0,6
63M:7G:30T	69,6±0,4
66,5M:3,5G:30T	70,7±0,5
50M:50G	69,6±0,6

As expected, due to the previous 90(M:G):10T series analysis, a clear hierarchy behaviour of water contact angle registered in Table 4.8 related with GPTMS content and R_a results can be perceived. Silane combination with higher GPTMS content, 35M:35G:30T, show the lowest water contact angle, what is the same highest wettability and highest roughness. The results show a tendency between GPTMS content and wettability/roughness, decreasing behaviour of both characteristics is noticeable with reduction on GPTMS content in the consequent silane combination of the series. At the end, the silane combination with lowest content on GPTMS, 66,5M:3,5G:30T has the lowest roughness and lowest wettability.

It is important to make reference that 35M:35G:30T is the material of all series that most improve the wettability results registered for reference material 50M:50G. This is an important parameter as it is expectable that wettability affects siloxane matrix degradability and consequential Si release. It is also perceptible from water contact angle results (Figure 4.28) of series 70(M:G)30T that the water contact angle does not achieve so higher values as on series with lesser TEOS content (10%), this may lead to a reflection about a potential effect of TEOS on the free available silanols. The additional content on silanols introduce by TEOS (fully hydrolysable alkoxy silane) may generate more free available silanols on surface and it is noticeable on lower water contact angle values of series 70(M:G)30T directly related with higher wettability.

It was stated in bibliography that cellular adhesion is maximized on surfaces with an intermediate wettability (50° - 70° water contact angle)³⁰ so the materials 45M:45G:10T and all series 70(M:G):30T represent the most suitable options to stimulate cellular adhesion (see Figure 4.28).

RESULTS

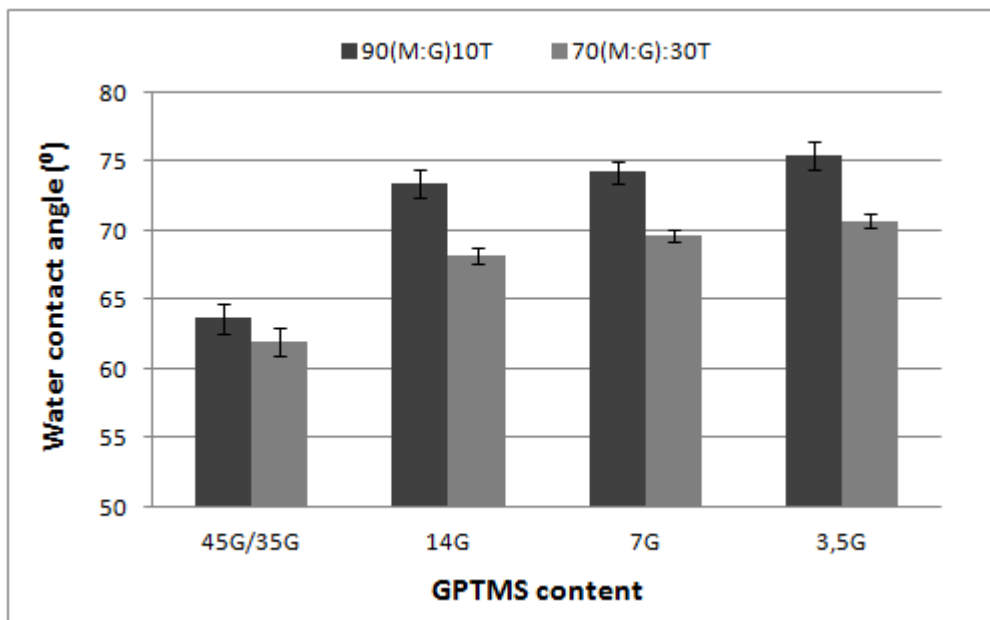


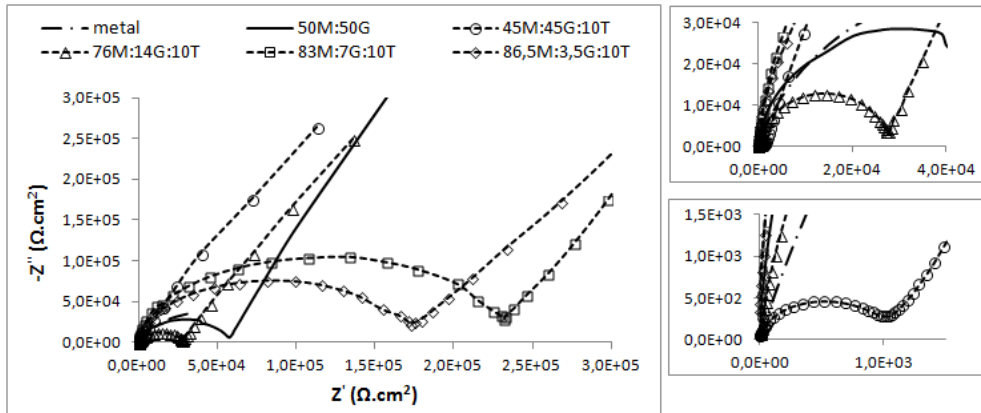
Figure 4.28 - Contact angle of the four silane combinations of both series 90(M:G):10T and 70(M:G):30T.

The analysis of deterioration processes taking place on polymer coated metal substrates under controlled experimental conditions by means of impedance measurement is an interesting study to better understand the access and diffusion of liquid environment through the coatings. Otherwise than ascertain its barrier effect against possible release of ions and corrosion metal products from metal substrate due to possible physiological fluids movement and cellular displacement on biomaterial surface during osseointegration biological process.

The versatility of Electrochemical Impedance Spectroscopy (EIS) allows its application to study the different stages of coatings degradation, hydrolysis of the side chains and detection of some defects, among others.

The EIS diagrams obtained at 0h immersion on NaCl 3,5wt.% solution for coated samples with 90(M:G):10T and 70(M:G):30T series materials are exposed in Figure 4.29 and Figure 4.30.

(a)



(b)

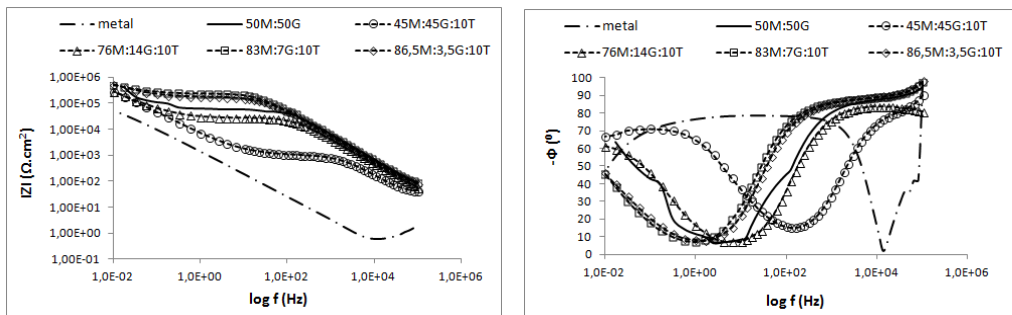


Figure 4.29 - Nyquist diagram (a) and Bode plots (b) for the materials of series 90(M:G):10T, reference material and metal substrate after 0h immersion on NaCl 3,5wt. % solution.

Series 90(M:G):10T coatings impedance, at 0h time contact with NaCl solution electrolyte, is depicted in Figure 4.29.

For the first instants of metal substrate immersion (metal sample), Bode plots show one time constant in the medium-high frequency range, associated with the passive top layer formed by corrosion products that generate a capacitive spectrum.³¹

However, after coating with sol-gel two time constants can be recognized in the spectra, one at low-medium frequency range related with the corrosion process of metal substrate and another one at medium-high frequency range associated with the coating properties as a barrier against penetration of electrolyte through pores or cracks.

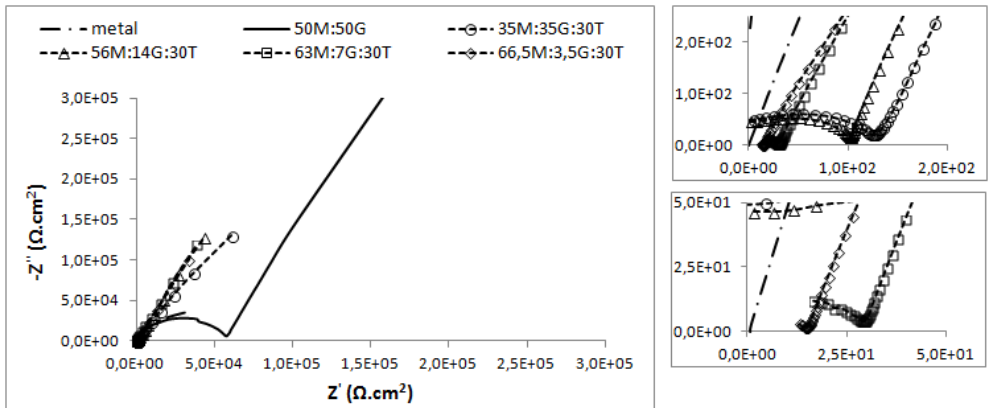
RESULTS

45M:45G:10T coating show the lowest values of impedance modulus and a decreasing phase angle detected at high frequency range.

On the other hand, the high impedance modulus of materials with less content on GPTMS (83M:7G:10T and 86,5M:3,5G:10T) reveal higher impedance. At last, 76M:14G:10T bode plot show a intermediate behaviour between the higher content on GPTMS coating and the lowest contents (83M:7G:10T and 86,5M:3,5G:10T), as it is noticeable the displacement of phase angle to higher frequency range with more perceptible signs of corrosion phenomena predicting the worse barrier properties registered for 45M:45G:10T.

The impedance results registered at 0h time contact with the electrolyte reveal that reference material (50M:50G) is affected by TEOS incorporation as well as the presence of high contents of GPTMS on sol-gel coating compositions affect coatings behaviour. Both deteriorate the barrier properties registered for reference material 50M:50G. In contrast, if the GPTMS content in sol-gel coatings of series 90(M:G):10T is lesser than 14% improves the barrier performance results recorded for reference material (50M:50G).

(a)



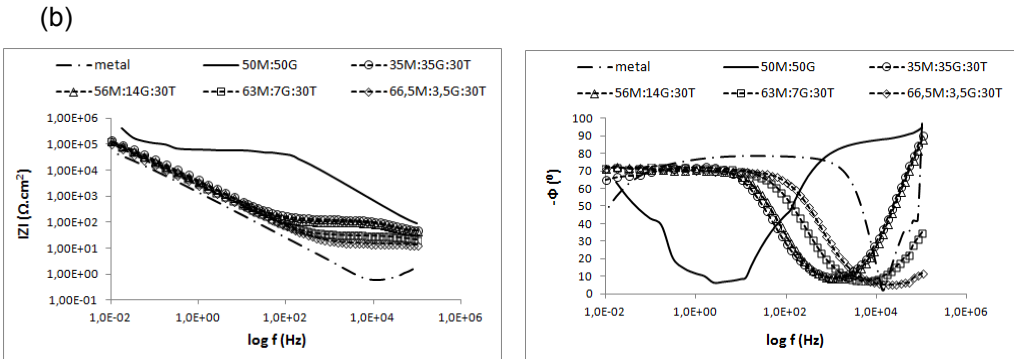


Figure 4.30 - Nyquist diagram (a) and Bode plots (b) for the materials of series 70(M:G):30T, reference material and metal substrate after 0h immersion on NaCl 3,5wt. % solution.

It can be seen in Figure 4.30 the EIS spectra obtained for 50M:50G (reference material), 35M:35G:30T, 56M:14G:30T, 63M:7G:30T and 66,5M:3,5G:30T coatings after 0h immersion in NaCl solution. Considering the bode plots results of series 70(M:G):30T materials two time constants are detected, one at higher frequencies associated with the barrier properties of the coatings and another one at medium-low range frequencies related to the corrosion process that takes place at the metal-coating interface.

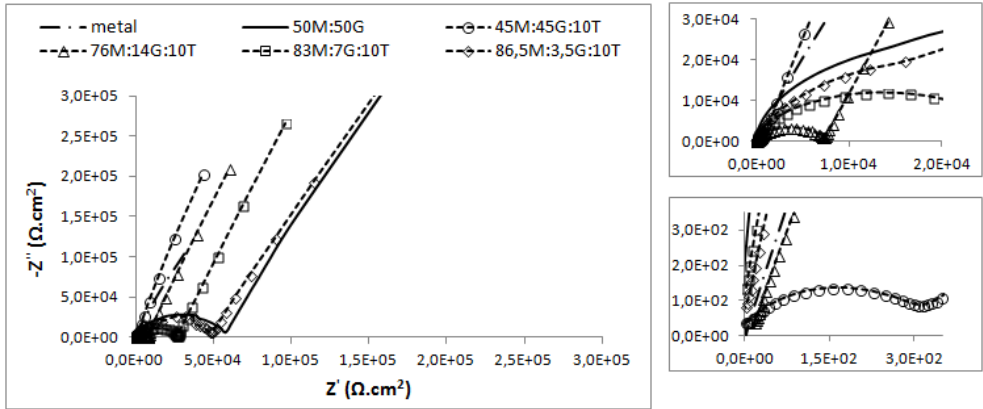
The coating resistance properties remained nearly the same for all tested materials suggesting low variation to water uptake and no significant influence of coating composition on its resistive properties. The Z modulus bode plot show that materials with 30% TEOS incorporation are significantly less resistive than the reference material 50M:50G, proved by the reduced impedance modulus registered at high frequency range.

Previous studies^{32,33,34} about the influence of TEOS on the corrosion resistance of coatings recognize that this silane addition to coatings leads to more permeable structures, suggesting a more porous film that consequently affects water uptake (increasing it).

The EIS diagrams obtained at 48h immersion on NaCl 3,5wt.% solution for coated samples with 90(M:G):10T and 70(M:G):30T series materials are exposed in Figure 4.31 and Figure 4.32.

RESULTS

(a)



(b)

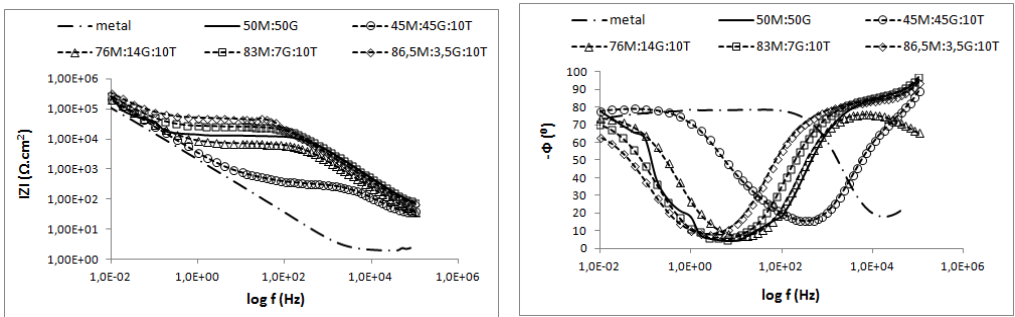


Figure 4.31 - Nyquist diagram (a) and Bode plots (b) for the materials of series 90(M:G):10T, reference material and metal substrate after 48h immersion on NaCl 3,5wt. % solution.

After 48h immersion the metal substrate (stainless steel) show one time constant in the medium-high frequency range, certainly due to passive top layer.

Figure 4.31 Bode diagrams obtained after 48h immersion in NaCl solution of metal substrate coated with siloxane films 50M:50G (reference material), 45M:45G:10T, 76M:14G:10T, 83M:7G:10T and 86,5M:3,5G:10T show similar impedance spectra. Two time constants can be recognized in the spectra, one at low-medium frequency range related with the corrosion processes and another one at medium-high frequency range attributed to the barrier properties of silane coatings. Series 90(M:G):10T spectra (Figure 4.31 -b)) show a gradient of electrolyte uptake identified at medium frequencies, also a

progressive decrease of the impedance values in the resistive plateau occur as the GPTMS content increase.

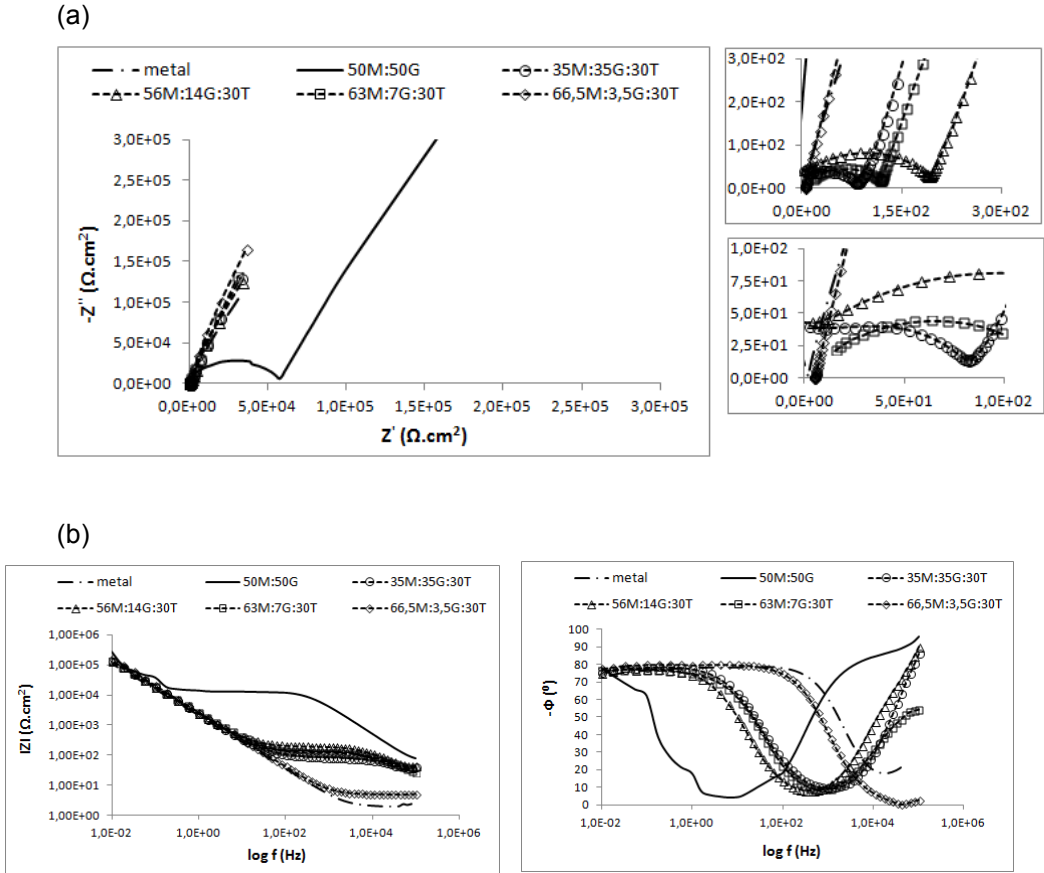


Figure 4.32 - Nyquist diagram (left) and Bode plots (right) for the materials of series 70(M:G):30T, reference material and metal substrate after 48h immersion on NaCl 3,5wt. % solution.

Figure 4.32 depicts the EIS spectra obtained for 50M:50G (reference material), 35M:35G:30T, 56M:14G:30T, 63M:7G:30T and 66,5M:3,5G:30T coatings after 48h immersion in NaCl solution. The worse impedance modulus was obtained for 66,5M:3,5G:30T as it was not detected a high frequency time constant, suggestive of a very porous coating that no longer protects the substrate. This result is coherent with previous outcome verified on resistance to solvent test (Standard UNE-EN 13523-

RESULTS

11) where this silane composition does not pass the minimum requirement of 120 double rubs (see Table 4.3) revealing poor crosslinking degree. The other series materials, 35M:35G:30T, 56M:14G:30T and 63M:7G:30T show two time constants at medium-high frequency range attributed to the electrolyte-metal interaction and to the barrier properties of the silane coatings, and point up to a characteristic spectra of a damaged coating system.

The impedance results illustrate that this series materials does not afford so good protection to the substrate as series 90(M:G):10T materials neither as the reference material 50M:50G. The coating impedance versus frequency remained nearly the same for all tested materials suggesting low variation to water uptake and no significant influence of coating composition (GPTMS content) in the electrochemical response. Other authors^{32,33,34} have worked with TEOS and have found similar results, they state that this silane addition to coating materials leads to more permeable structures, suggesting an irregular surface coverage and poor corrosion protection.

In order to better understand the deterioration mechanism of the coatings, EIS results were fitted using equivalent circuits. The equivalent circuits that best describes the impedance behaviour of the different materials immersed on NaCl 3,5wt.% solution are the ones illustrated in Figure 4.33. The different parameters acquired with impedance data fitting are collected in Table 4.9 and Table 4.10.

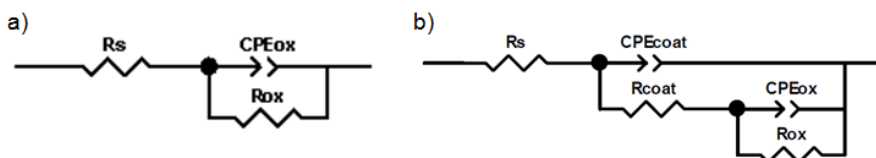


Figure 4. 33- Equivalent circuits that best describes the impedance behaviour of the systems sol-gel - metal substrate developed in this work in contact with saline solution.³² - a) Equivalent circuit that best represent the system stainless steel substrate, b) Equivalent circuit that best describe the system metal substrate coated with sol-gel.

For uncoated stainless steel metal plates only one time constant is detected, comprehensively related with oxides layer physically formed by many metal materials in contact with aqueous environments. The model used as representative of the oxide layer system developed when stainless steel is in contact with NaCl 3,5wt.% solution (Figure 4.33 - a)) results in the solution resistance (R_s) connected in series with capacitive-resistive elements (CPE_{ox} , R_{ox}) associated in parallel.

On the other hand, for the sol-gel coatings systems two time constants were used to fit the experimental EIS data on medium-high frequencies (Figure 4.33 - b)). The first time constant related with the sol-gel film can be identified at high frequency range correlated with the barrier properties of the silane coatings, and another one at medium-low frequency range can be attributed to the substrate activation and oxide layer generated.

Although the entire impedance spectra is important to describe the processes that take place at the sol-gel coated metal substrate in contact with the electrolyte, the degradation process of the coating is the real study subject so the medium-high frequency results (semicircle of Nyquist diagram) are the ones studied with more interest.

When stainless steel is coated with a sol-gel layer (reference material or any of the triple composition materials) the equivalent circuit that best describes this new system is represented as a solution resistance (R_s) connected in series with capacitive-resistive elements (CPE_{coat} , R_{coat}) related with the sol-gel coating capacitance and pore resistance associated in parallel joined in series with other capacitive-resistive elements (CPE_{ox} , R_{ox}) associated in parallel related with the stainless steel oxide layer (Figure 4.33 - b)).

In all the electrical equivalent circuits the coating capacitance (associated with adsorption processes) was replaced by a constant phase element (CPE) to take the non-ideality of the hybrid films into account.

The CPE impedance is expressed as:

RESULTS

$$Z_{CPE} = 1/Y_0(j\omega)^n$$

Where, ω is the frequency and Y_0 is the capacitance of the system. A value of exponent $n=1$ match with a smooth surface, for that reason CPE should be substituted by an ideal capacitor (C); $n=0,5$ suggests a response of diffusion or porous material and $0,5 < n < 1$ is associated with heterogeneous, rough or non-homogeneous current distribution.^{33,31} R_s is the electrolyte resistance usually $\approx 17 \Omega \cdot \text{cm}^2$ for NaCl solution, R_{coat} (or R_{po}) and CPE_c (or CPE_{coat}) represent high frequency range phenomenon associated with the coating degradation. CPE_{ox} and R_{ox} also show up at medium-high frequency range and are related with corrosion phenomenon.

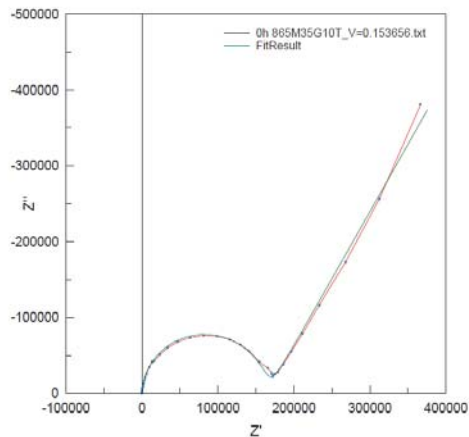


Figure 4.34 - Nyquist diagram and fitting curve obtained for 86,5M:3,5G:10T biocoating at 0h contact time with saline solution (NaCl 3,5wt.%).

Very good correlation was observed between experimental results and the equivalent circuit fitting model, as the Chi-squared (χ^2) calculated values were lower than 10^{-2} . An example of a typical fitting curve is exposed in Figure 4.34.

The parameters acquire from the fitting method are in evidence in Table 4.9 and Table 4.10.

Table 4.9 - Parameters of the equivalent circuits (EC) used to describe the physical-chemical phenomenon of series 90(M:G):10T materials in contact with NaCl 3,5wt. % solution from 0h until 48h - a) 45M:45G:10T; b) 76M:14G:10T; c) 83M:7G:10T; d) 86,5M:3,5G:10T.

a) 45M:45G:10T							
t (h)	Time constants	Rcoat ($\Omega.cm^2$)	CPEcoat ($F.cm^2$)	n	Rox ($\Omega.cm^2$)	CPEox ($F.cm^2$)	n
0	2	1016	3,76E-7	0,87	1,0E20	3,82E-5	0,77
1,5	2	699	4,00E-7	0,87	1,0E20	4,42E-5	0,79
3	2	623	4,06E-7	0,87	1,0E20	4,60E-5	0,80
4	2	596	4,09E-7	0,87	1,0E20	4,75E-5	0,80
6	2	500	3,56E-7	0,90	1,0E20	5,03E-5	0,80
8	2	484	3,65E-7	0,90	1,0E20	5,20E-5	0,82
10	2	466	4,15E-7	0,87	1,0E20	5,42E-5	0,81
24	2	343	3,65E-7	0,90	1,0E20	5,44E-5	0,81
48	2	341	3,75E-7	0,86	1,0E20	5,68E-5	0,82

b) 76M:14G:10T							
t (h)	Time constants	Rcoat ($\Omega.cm^2$)	CPEcoat ($F.cm^2$)	n	Rox ($\Omega.cm^2$)	CPEox ($F.cm^2$)	n
0	2	27248	6,34E-8	0,94	1,0E20	2,81E-5	0,75
1,5	2	14409	8,87E-8	0,93	1,0E20	3,24E-5	0,80
3	2	11829	9,63E-8	0,92	1,0E20	3,46E-5	0,82
4	2	10104	9,90E-8	0,92	1,0E20	3,62E-5	0,82
6	2	8841	1,03E-7	0,92	1,0E20	3,85E-5	0,83
8	2	8272	1,07E-7	0,92	1,0E20	4,04E-5	0,84
10	2	7121	1,12E-7	0,92	1,0E20	4,30E-5	0,84
24	2	7433	1,30E-7	0,91	1,0E20	4,61E-5	0,85
48	2	7352	1,81E-7	0,91	1,0E20	4,92E-5	0,86

RESULTS

c) **83M:7G:10T**

t (h)	Time constants	Rcoat ($\Omega.cm^2$)	CPEcoat ($F.cm^2$)	n	Rox ($\Omega.cm^2$)	CPEox ($F.cm^2$)	n
0	2	222840	3,75E-8	0,97	1,0E20	1,58E-5	0,71
1,5	2	62809	4,85E-8	0,95	1,0E20	2,76E-5	0,80
3	2	50553	4,85E-8	0,95	1,0E20	2,78E-5	0,80
4	2	45280	5,14E-8	0,95	1,0E20	3,18E-5	0,83
6	2	41220	5,14E-8	9,95	1,0E20	3,19E-5	0,83
8	2	32748	5,63E-8	0,94	1,0E20	3,31E-5	0,82
10	2	32728	5,63E-8	0,94	1,0E20	3,31E-5	0,82
24	2	31473	6,21E-8	0,94	1,0E20	3,52E-5	0,84
48	2	26561	6,62E-8	0,94	1,0E20	3,73E-5	0,84

d) **86,5M:3,5G:10T**

t (h)	Time constants	Rcoat ($\Omega.cm^2$)	CPEcoat ($F.cm^2$)	n	Rox ($\Omega.cm^2$)	CPEox ($F.cm^2$)	n
0	2	162520	3,83E-8	0,97	1,0E20	1,42E-5	0,65
1,5	2	87982	4,29E-8	0,96	1,0E20	1,78E-5	0,70
3	2	75766	6,15E-8	0,94	1,0E20	2,00E-5	0,74
4	2	68506	5,97E-8	0,94	1,0E20	2,12E-5	0,76
6	2	56998	6,05E-8	0,94	1,0E20	2,32E-5	0,77
8	2	49805	6,41E-8	0,94	1,0E20	2,59E-5	0,80
10	2	49790	6,41E-8	0,93	1,0E20	2,60E-5	0,80
24	2	50134	1,01E-7	0,91	1,0E20	2,93E-5	0,82
48	2	50140	1,01E-7	0,92	1,0E20	2,93E-5	0,82

Table 4.10 - Parameters of the equivalent circuits (EC) used to describe the physical-chemical phenomenon of series 70(M:G):30T materials in contact with NaCl 3,5wt. % solution from 0h until 48h - a) 35M:35G:30T; b) 56M:14G:30T; c) 63M:7G:30T; d) 66,5M:3,5G:30T.

a) 35M:35G:30T							
t (h)	Time constants	Rcoat ($\Omega.cm^2$)	CPEcoat ($F.cm^2$)	n	Rox ($\Omega.cm^2$)	CPEox ($F.cm^2$)	n
0	2	124	6,47E-8	1,00	1,0E20	6,64E-5	0,82
1,5	2	98	6,50E-8	1,00	1,0E20	6,90E-5	0,82
3	2	76	3,87E-7	0,86	1,0E20	7,16E-5	0,84
4	2	95	3,84E-7	0,86	1,0E20	7,30E-5	0,84
6	2	67	4,11E-7	0,86	1,0E20	7,51E-5	0,85
8	2	87	4,07E-7	0,86	1,0E20	7,56E-5	0,84
10	2	97	6,78E-7	0,80	1,0E20	7,71E-5	0,85
24	2	86	4,06E-7	0,85	1,0E20	7,53E-5	0,89
48	2	80	3,24E-6	0,72	1,0E20	5,25E-5	0,91

b) 56M:14G:30T							
t (h)	Time constants	Rcoat ($\Omega.cm^2$)	CPEcoat ($F.cm^2$)	n	Rox ($\Omega.cm^2$)	CPEox ($F.cm^2$)	n
0	2	97	4,00E-8	1,05	1,0E20	6,54E-5	0,81
1,5	2	103	9,09E-8	0,99	1,0E20	7,36E-5	0,83
3	2	110	9,12E-8	0,99	1,0E20	7,37E-5	0,84
4	2	116	1,12E-7	0,97	1,0E20	7,52E-5	0,84
6	2	119	1,44E-7	0,95	1,0E20	7,92E-5	0,84
8	2	129	1,45E-7	0,95	1,0E20	7,93E-5	0,84
10	2	79	2,83E-7	0,89	1,0E20	9,04E-5	0,86
24	2	201	3,34E-7	0,89	1,0E20	8,41E-5	0,85
48	2	195	3,87E-7	0,88	1,0E20	9,74E-5	0,86

RESULTS

c) **63M:7G:30T**

t (h)	Time constants	R _{coat} (Ω.cm ²)	CPE _{coat} (F.cm ²)	n	R _{ox} (Ω.cm ²)	CPE _{ox} (F.cm ²)	n
0	2	26	1,54E-7	0,93	1,0E20	7,79E-5	0,82
1,5	2	91	3,10E-7	0,87	1,0E20	8,75E-5	0,83
3	2	146	2,20E-7	0,90	1,0E20	8,51E-5	0,82
4	--	--	--	--	--	--	--
6	2	148	4,11E-7	0,85	1,0E20	8,71E-5	0,83
8	2	150	4,37E-7	0,84	1,0E20	8,62E-5	0,83
10	2	134	5,50E-7	0,83	1,0E20	8,58E-5	0,84
24	--	--	--	--	--	--	--
48	2	116	7,78E-7	0,81	1,0E20	7,89E-5	0,86

d) **66,5M:3,5G:30T**

t (h)	Time constants	R _{coat} (Ω.cm ²)	CPE _{coat} (F.cm ²)	n	R _{ox} (Ω.cm ²)	CPE _{ox} (F.cm ²)	n
0	2	14	7,94E-6	0,57	1,0E20	7,78E-5	0,82
1,5	2	33	2,15E-7	0,91	1,0E20	8,84E-5	0,82
3	--	--	--	--	--	--	--
4	2	53	9,55E-7	0,8	1,0E20	9,23E-5	0,83
6	2	50	1,01E-6	0,8	1,0E20	1,02E-4	0,83
8	2	54	3,69E-6	0,69	1,0E20	9,58E-5	0,85
10	2	55	4,80E-6	0,67	1,0E20	8,96E-5	0,85
24	--	--	--	--	--	--	--
48	1	Δ	Δ	Δ	1,0E20	7,24E-5	0,90

Δ - no data because it is not detected the presence of the layer.

The water uptake in coatings can be monitored by the increase of CPE_{coat} as well as R_{coat} or R_{po} can be correlated with the compactness of the coating³², therefore diagrams of temporal evolution of the upper cited parameters are exposed in Figure 4.35 and Figure 4.36.

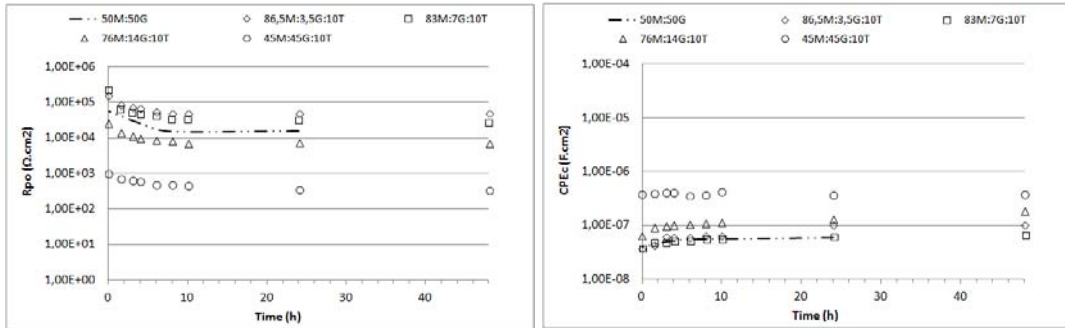


Figure 4.35 - Evolution of dielectric properties R_{coat} (left) and CPE_{coat} (right) with immersion time for samples of series 90(M:G):10T and reference material (50M:50G) immersed in NaCl 3,5wt. % solution from 0h until 48h.

The high frequency time constants R_{coat} (or R_{po}) and CPE_{coat} are ascribed to the properties of the sol-gel coatings, for that reason time evolution of films 45M:45G:10T, 76M:14G:10T, 83M:7G:10T and 86,5M:3,5G:10T are in evidence in Figure 4.35.

The figured results for compositions with higher GPTMS content (45M:45G:10T and 76M:14G:10T) show a slight decrease of R_{po} . Systems 83M:7G:10T and 86,5M:3,5G:10T with lesser content on GPTMS of series 90(M:G):10T show the highest resistance at the beginning of immersion followed by an important R_{coat} drop on the first 6h.

It is interesting to refer that even though 45M:45G:10T and 76M:14G:10T coatings do not experiment a major deterioration during immersion time evolution, the R_{coat} values are significantly inferior than the results of reference coating (50M:50G) revealing a worse barrier effect.

On the other hand, a very slight increase of CPE_{c} was registered for 76M:14G:10T, 83M:7G:10T and 86,5M:3,5G:10T. 45M:45G:10T CPE_{c} remains fairly constant during all exposition time. Also CPE_{coat} results show higher amount of absorbed water for 76M:14G:10T than reference material as ΔCPE_{coat} of reference 50M:50G was $2,45E-8 \text{ F.cm}^2$ and ΔCPE_{coat} of 76M:14G:10T was $1,2E-7 \text{ F.cm}^2$ suggesting that this coating matrix is more porous and allows greater amounts of water uptake (Table 4. 11). ΔCPE_{coat} of 45M:45G:10T was about $1,0E-9 \text{ F.cm}^2$ indicative of the poorest absorption (Table 4. 11).

RESULTS

Table 4. 11 - Variation of CPE_{coat} (between 0h and 48h) of samples coated with 90(M:G):10T materials in contact with NaCl 3,5wt. % solution.

Coating	ΔCPE_{coat} ($F.cm^2$)
45M:45G:10T	1,0E-9
76M:14G:10T	1,2E-7
83M:7G:10T	2,9E-8
86,5M:3,5G:10T	6,3E-8
50M:50G	2,45E-8

Finally, it is important to notice that GPTMS content in series 90(M:G):10T biomaterials affects in a perceptible manner the coatings behaviour. Explicitly, GPTMS content increase causes a diminishment in R_{coat} indicative of more imperfections on the sol-gel layers, besides, GPTMS content also affects CPE_{coat} related with water uptake, augmenting it. On the other hand, TEOS addition in 10% does not cause apparently a clear effect on coatings barrier effect, it is only noticeable higher water uptake (higher CPE_{coat}) in comparison with the double reference material (50M:50G).

It is important to note that, from a degradation point of view, compositions 45M:45G:10T and 76M:14G:10T (with higher GPTMS content) are the most suitable to test in vivo as they reveal higher water uptake therefore are good candidates to improve on biodegradability of reference biomaterial (50M:50G).

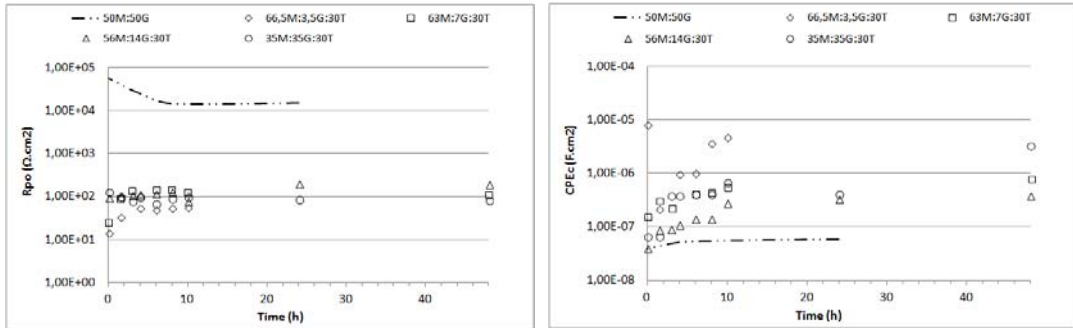


Figure 4.36 - Evolution of dielectric properties R_{coat} (left) and CPE_{coat} (right) with immersion time for samples of series 70(M:G):30T immersed in NaCl 3,5wt. % solution from 0h until 48h.

The evolution of resistance (R_{coat}) and water uptake (CPE_{coat}) of the sol-gel 70(M:G):30T series coatings is presented in Figure 4.36. The values of resistance are evidently minor than the reference sol-gel coating 50M:50G revealing worse barrier effect of the new biomaterials 35M:35G:30T, 56M:14G:30T, 63M:7G:30T and specially 66,5M:3,5G:30T.

The evolution of coating pore resistance to the passing of electrolyte (R_{coat} or R_{po}) follows a similar trend for the biomaterials 35M:35G:30T and 56M:14G:30T and remains fairly constant during all exposition time. On the other hand, coatings with less GPTMS content (63M:7G:30T and 66,5M:3,5G:30T) show a significant increase on R_{coat} in the first 3h contact time followed by a quite stable resistance until the end of the experiment. These results suggest that initially some corrosion products may be produced reducing the interstitial matrix space, subsequently for longer immersion periods a possible equilibrium is established.

Resistance magnitude is very similar to all this series materials with 30% TEOS addition, revealing that the factor that most affects this coatings behaviour is the TEOS content that promotes more porous matrices with worse barrier effect and higher water uptake content.

CPE_{coat} results show higher amount of absorbed solution for series 70(M:G):30T materials than reference material, besides an increasing evolution is detected for 70(M:G):30T series coatings suggesting the

RESULTS

water uptake and coating degradation. To better identify water uptake evolution ΔCPE_{coat} was estimated for all the biomaterials (Table 4. 12).

Table 4. 12 - Variation (between the highest and lowest value) of CPE_{coat} (between 0h and 48h) of samples coated with 70(M:G):30T materials in contact with NaCl 3,5wt. % solution.

Coating	ΔCPE_{coat} ($F.cm^2$)
35M:35G:30T	3,18E-6
56M:14G:30T	3,43E-7
63M:7G:30T	6,24E-7
66,5M:3,5G:30T	4,58E-6
50M:50G	1,95E-8

Materials 66,5M:3,5G:30T and 35M:35G:30T show an increasing evolution of CPE_{coat} in all the experiment, suggesting higher ability to water uptake. On the other hand, 56M:14G:30T and 63M:7G:30T show a noticeable increasing of CPE_{coat} until 10h contact time with saline solution and continue in a constant profile until the end of the experiment.

At last, GPTMS content in series 70(M:G):30T does not show a clear effect in coatings behavior as Rpo profiles and magnitude are fairly analogous. On the other hand, CPE_{coat} results do not show any perceptible correlation between GPTMS content and water uptake.

In another way, TEOS incorporation of 30% clearly results in a big drop of the barrier effect of the coatings, accompanied by an important CPE_{coat} rise. Occurrence of lower Rpo and higher CPE_{coat} (in comparison with reference biomaterial and series 90(M:G):10T biomaterials) indicates a coating with more imperfections attributed to higher TEOS content incorporation to biocoatings composition.

Taking into account the before cited, from a degradation point of view, all this series compositions are suitable to test in vivo (even more appropriate then the before suggested 45M:45G:10T and 76M:14G:10T) as they reveal worse barrier effect of the coating and higher water uptake.

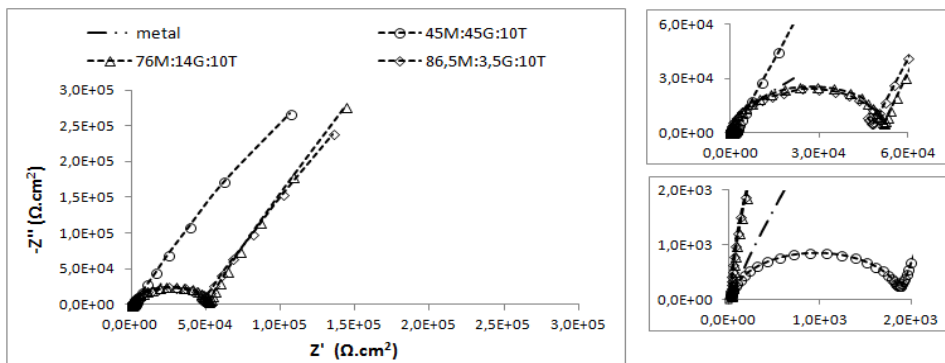
In order to better reproduce the physiological medium conditions on the EIS degradation study, the experiment was replicated using Hank's Balanced Salt Solution as electrolyte for immersion of sol-gel coated metal samples. This solution resembles the physiological fluids because it combines several inorganic salts (plus NaCl) and carbohydrates (see Table 4. 13).

Table 4. 13 - Composition of Hank's balanced salt solution used as electrolyte on EIS experiments.

	Component	Concentration g/L
Inorganic salts	CaCl ₂ ·2H ₂ O	0,185
	MgSO ₄ (anhyd)	0,09767
	KCl	0,4
	KH ₂ PO ₄ (anhyd)	0,06
	NaHCO ₃	0,35
	NaCl	8,0
	Na ₂ HPO ₄ (anhyd)	0,04788
Other	D-Glucose	1,0

The EIS diagrams acquired at 0h immersion on Hank's solution for coated samples with 90(M:G):10T and 70(M:G):30T series biomaterials are exposed in Figure 4.37 and Figure 4.38.

a)



RESULTS

b)

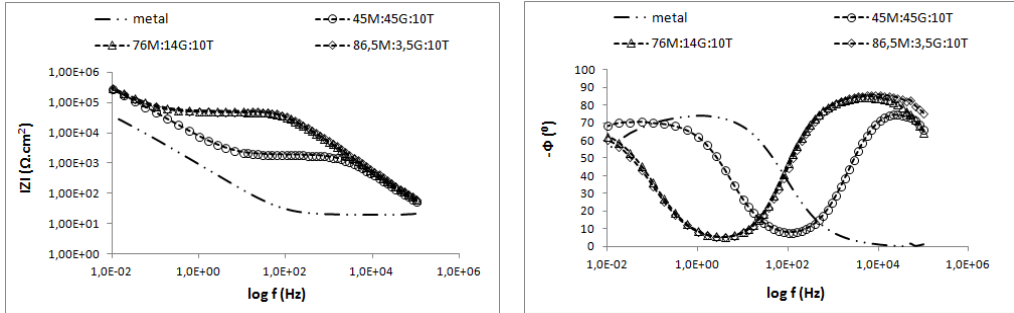


Figure 4.37- Nyquist diagram (a) and Bode plots (b) of materials of series 90(M:G):10T after 0h immersion in Hank's solution.

It can be seen in Figure 4.37 the EIS spectra registered for 45M:45G:10T, 76M:14G:10T and 86,5M:3,5G:10T coatings in the first contact instant with the electrolyte Hank's solution.

It is interesting to note that three time constants were observed, one at high frequency range, besides the two time constants identified at medium-low frequency range, which were related to the coating and passive oxide layer of stainless steel. This new time constant (high frequency) could be associated with an external deposition layer of salts.

45M:45G:10T bode impedance plots show a minor capacitive behavior at high frequency range correlated with the extent of water uptake and low impedance modulus in comparison with the other series materials.

On the other hand, 76M:14G:10T and 86,5M:3,5G:10T show higher impedance than 45M:45G:10T and a displacement of phase angle to lower frequency range.

The impedance results registered at 0h time contact with Hank's electrolyte reveal that the GPTMS content affects the barrier properties of the coatings. Interestingly, the same tendency was observed in NaCl solution experiments (Figure 4.29).

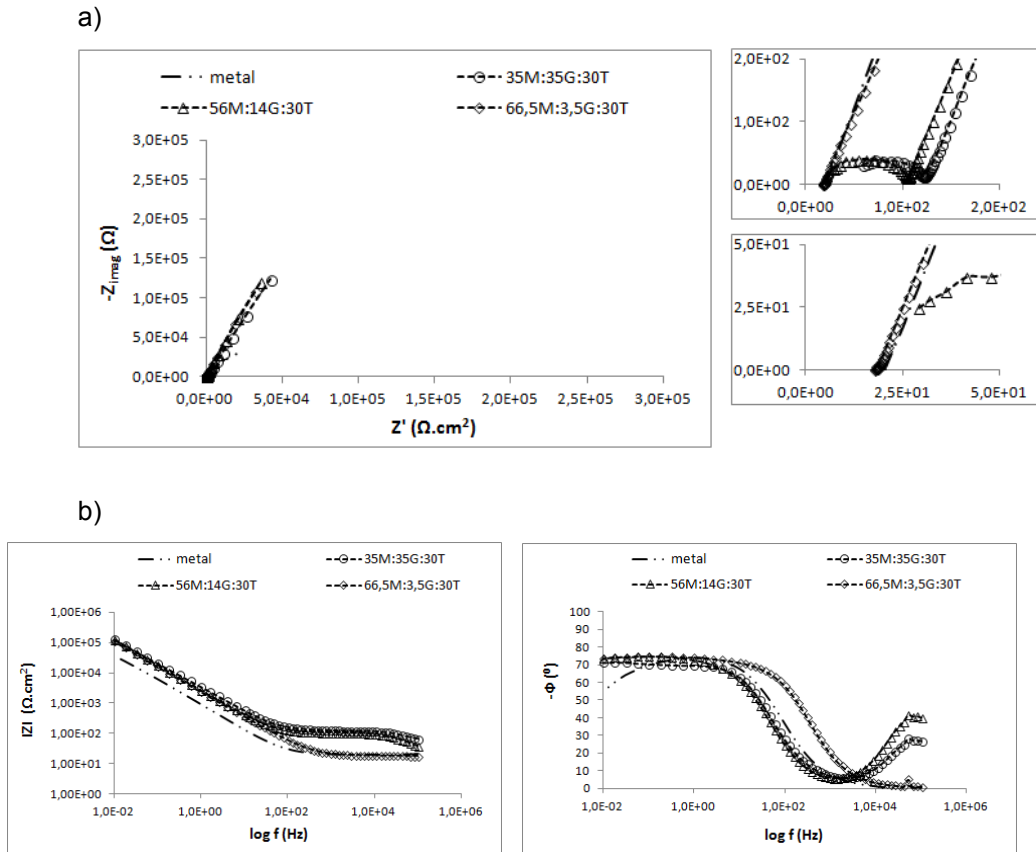


Figure 4. 38- Nyquist diagram (a) and Bode plots (b) for the materials of series 70(M:G):30T after 0h immersion in Hank's solution.

Figure 4.38 shows representative complex plane and Bode plots recorded for 35M:35G:30T, 56M:14G:30T and 66,5M:3,5G:30T coatings in Hank's solution at 0h immersion time. All the compositions follow the same trend with a clear resistive behavior at high frequency range, as well as the metal substrate in the same conditions. Two maxima can be identified in the Bode phase angle vs. frequency plot, one at medium frequency range and another one at high frequency range related with the corrosion phenomenon and barrier properties of the coating respectively.

Worth to notice that 66,5M:3,5G:30T, composition with less GPTMS content, show the lowest resistance in the high frequency range suggesting worse barrier effect. Nevertheless, the factor that most affects

RESULTS

this series materials may be the 30% TEOS incorporation that is intimately related with the compactness/ barrier effect of the sol-gel layers produced.

The EIS diagrams acquired at 48h immersion on Hank's solution for coated samples with 90(M:G):10T and 70(M:G):30T series biomaterials are exposed in Figure 4.39 and Figure 4.40.

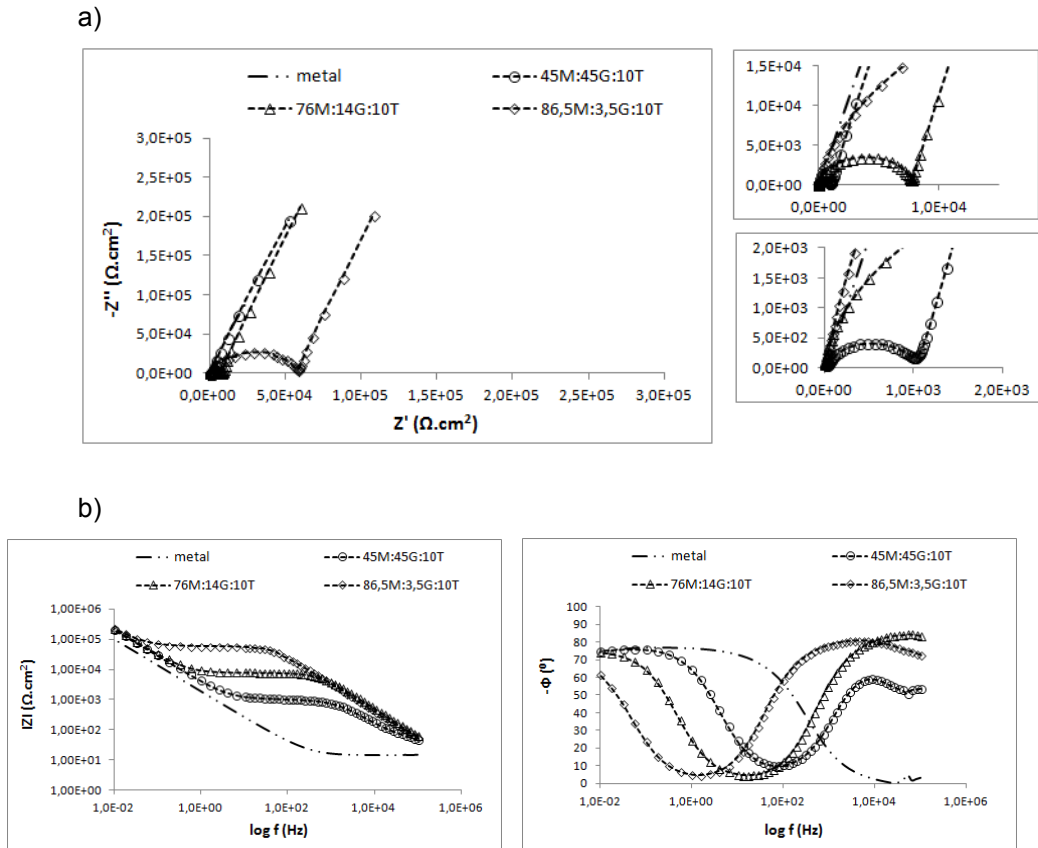


Figure 4. 39 - Nyquist diagram (a) and Bode plots (b) of materials of series 90(M:G):10T after 48h immersion on Hank's solution.

Figure 4.39 shows EIS spectra registered for 45M:45G:10T, 76M:14G:10T and 86,5M:3,5G:10T coatings after 48h immersion in Hank's solution. Three time constants were observed, one at high frequency range and another two time constants identified at medium-high and medium-low

frequency range, which were related to a possible external layer of mineral deposits, the coating properties and passive oxide layer of stainless steel respectively.

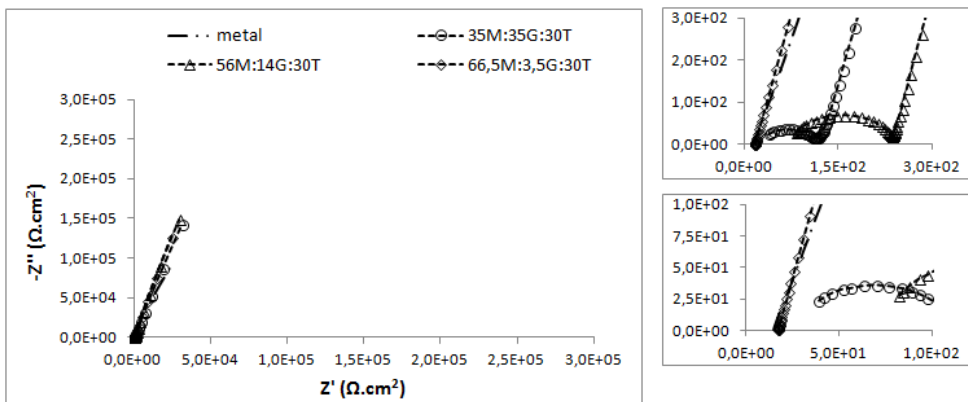
Bode plots show that 45M:45G:10T present the lowest impedance correlated with the extent of water uptake and consequently the lowest coating resistance.

On the other hand, 86,5M:3,5G:10T show the higher impedance modulus values and 76M:14G:10T Bode plot show an intermediate behavior between the before cited compositions (with 45% GPTMS and 3,5% of GPTMS).

The displacement of phase angle from lower to medium frequency range according to GPTMS increase suggest that the activation of the metal substrate corrosion and reduction of coating barrier properties/resistance may be instigated by GPTMS.

These results put on evidence the effect of GPTMS content on the barrier effect of coatings of series 90(M:G):10T and the same trend was detected in the experiment made with NaCl solution where the electrolyte uptake and impedance values follow the GPTMS gradient (Figure 4.31).

a)



RESULTS

b)

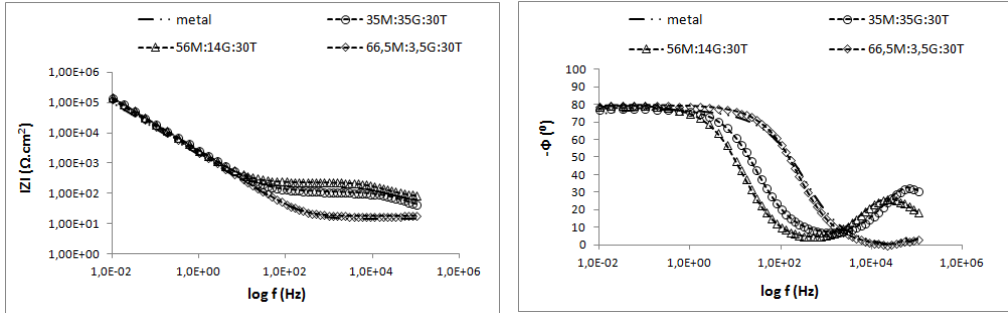


Figure 4. 40- Nyquist diagram (a) and Bode plots (b) of materials of series 70(M:G):30T after 48h immersion on Hank's solution.

Figure 4.40 depicts EIS spectra obtained for 35M:35G:30T, 56M:14G:30T and 66,5M:3,5G:30T coatings after 48h immersion in Hank's solution.

Compositions with higher GPTMS content, 35% and 14%, show two time constants, at medium-high frequency range attributed to electrolyte-metal interaction and to the barrier properties of sol-gel coatings. Nevertheless, for 66,5M:3,5G:30T only one time constant is detected and the displacement of the time constant from medium to high frequency range suggest a strong coating degradation and a low resistive behavior supported specially by the oxide layer of metal substrate.

As verified on the same series coatings experiment made for 0h contact time, the imperfections of the coatings matrices must prevail and mitigate any sign of GPTMS content variation or possible external layer created by mineral deposits. The factor that most affects this series materials may be the 30% TEOS incorporation that cause more porous and less compact matrices.

In order to corroborate the suspicion of formation of a deposits external layer on the coated samples in contact with Hank's solution, a visual assessment was made and registered.

Figure 4.40 shows images of sol-gel coated samples with 45M:45G:10T and 35M:35G:30T before and after two weeks immersion in NaCl and Hank's solution. Figure 4.41 -b) show the 45M:45G:10T coating after 2 weeks immersion in NaCl 3,5wt. %, suggesting a non uniform layer of

sodium chloride crystals. Previous experiments made with titanium coated with sol-gel coatings immersed in NaCl 3,5wt. % solution at room temperature for 14 days revealed the presence of NaCl crystals. The analysis of microstructure and chemical composition of the above cited samples was made with SEM (scanning electron microscope) and leads to the suspicion of an external layer of NaCl crystals formed in stainless steel coated with sol-gel as well.

Figure 4.41 - c) show the 45M:45G:10T coating after 2 weeks immersion in Hank's solution and illustrate a well-covered surface by an uniform film. On the other hand, Figure 4.41 - e) show the 35M:35G:30T coating after 2 weeks contact time with NaCl 3,5wt. %, suggesting a non uniform layer of sodium chloride crystals much more dispersed than the crystals layer found for 45M:45G:10T coating. Figure 4.41 - f) show the 35M:35G:30T coating after 2 weeks immersion in Hank's solution and illustrate a non-uniform layer of deposits. This non-uniform layer suggests the presence of the same deposits nature on both compositions (with 10% TEOS and 30% TEOS) nevertheless 35M:35G:30T external layer show signs of dissolution and discontinuity.

Upon visual assessment, the differences appreciated on both compositions, 45M:45G:10T and 35M:35G:30T, suggest that although the nature of crystals detected on NaCl samples and depositions on Hank's samples seems to be the same for both composition the films detected on 35M:35G:30T coatings is not so dense, present interruptions and more imperfections. Accordingly, perhaps the base sol-gel structure in which these deposits will fall (35M:35G:30T sol-gel coating) is more unstable and follow a fast degradation kinetics leading to a difficult process of formation of a dense and uniform deposition film.

These differences could explain the time constants detected on EIS results, as in 10% TEOS series materials were identified three time constants (Figure 4.37 and Figure 4.39) and in 30% TEOS series materials were identified two time constants (Figure 4.38 and Figure 4.40).

RESULTS

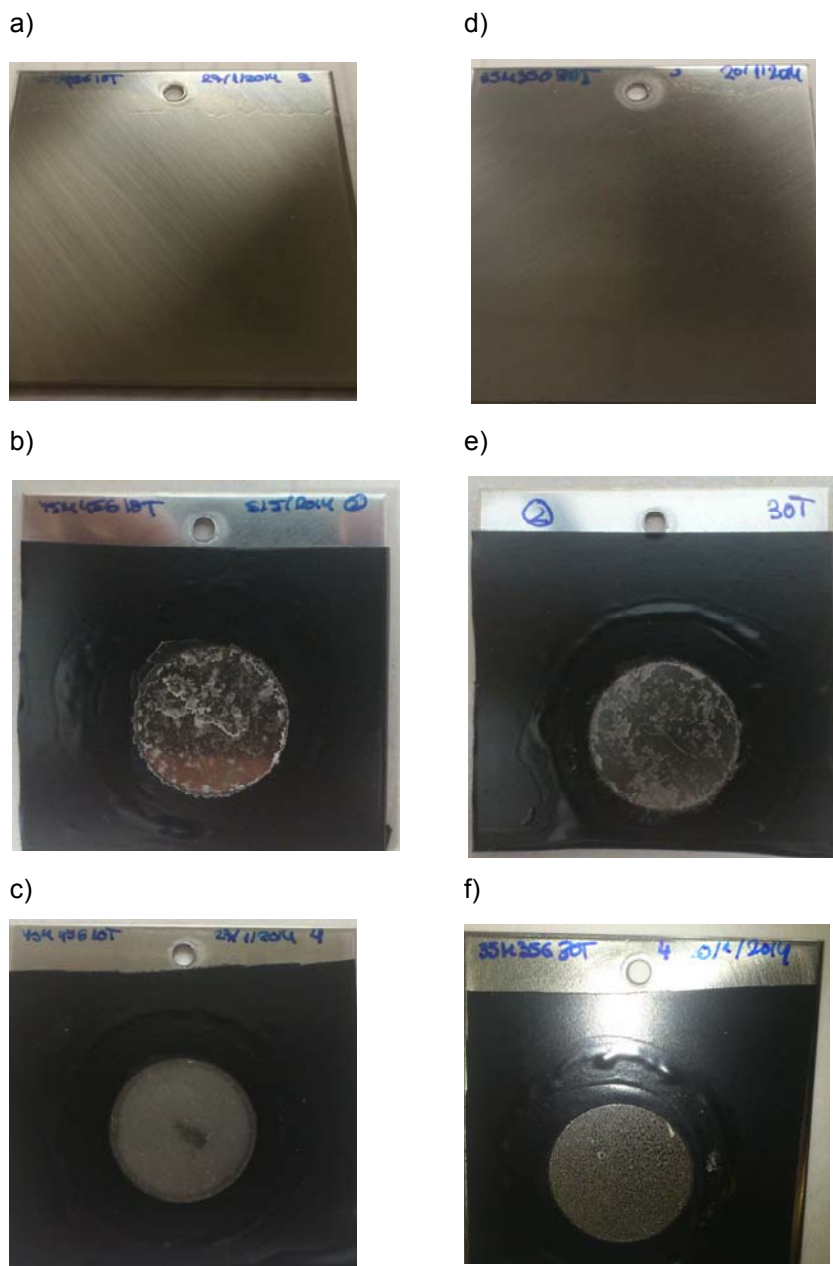


Figure 4. 41 - Images of the coatings 45M:45G:10T and 35M:35G:30T before immersion in electrolyte (a) and d)), after 2 weeks immersed in NaCl 3,5wt. % solution (b) and e)) and after 2 weeks immersed in Hank's solution (c) and f)).

Reviewing the results of EIS experiment in Hank's solution, 45M:45G:10T and all the biomaterials of series 70(M:G):30T are good options to improve on the degradability of the reference material 50M:50G.

In order to study the deterioration mechanisms and response of the new developed coatings in a medium more similar to physiological fluid (Hank's solution), the EIS results were fitted to equivalent electrical circuits. The equivalent circuits that best describe the resistive behavior of the biomaterials immersed in Hank's solution are the ones illustrated in Figure 4.42.

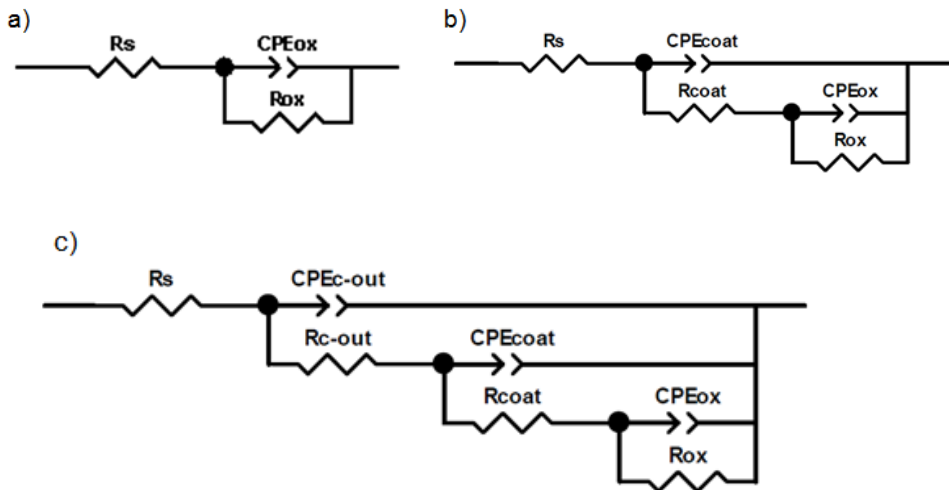


Figure 4. 42 - Equivalent circuits that best describe the impedance behaviour of the systems sol-gel - metal substrate developed in this work in contact with Hank's solution. - a) Equivalent circuit that best represent the system stainless steel substrate, b) Equivalent circuit that best describe the system metal substrate coated with sol-gel and c) Equivalent circuit that best describe the system metal substrate coated with sol-gel and with formation of an external film of precipitates.

The equivalent circuit that best represents the systems generated by materials of series 90(M:G):10T in contact with Hank's solution is the one identified as c) in Figure 4.42. The suspicion of an external dense film formation for 90(M:G):10T series materials is confirmed upon visual assessment (Figure 4.41). Besides, three time constants are identified on

RESULTS

the Bode plots, at low, medium and high frequency range attributable to metal substrate oxide layer, barrier properties of the coatings and an external film formed by mineral crystals depositions among others (see Figure 4.37 and Figure 4.39). Accordingly when stainless steel is coated with a sol-gel layer of series 90(M:G):10T the equivalent circuit that best describes this new system is represented as a solution resistance (R_s) connected in series with capacitive-resistive elements (CPE_{c-out} , R_{c-out}) related with the external film capacitance and resistance to the electrolyte inlet associated in parallel joined in series with capacitive-resistive elements (CPE_{coat} , R_{coat}) related with the sol-gel coating capacitance and pore resistance associated in parallel also joined in series with other capacitive-resistive elements (CPE_{ox} , R_{ox}) associated in parallel related with the stainless steel oxide layer (Figure 4.42 - c)).

For the 70(M:G):30T coatings systems two time constants were used to fit the experimental EIS data. The first time constant related with the sol-gel film can be identified at high frequency range correlated with the barrier properties of the silane coatings, and another one at medium frequency range that can be attributed to the metal substrate activation (oxide layer generated). The equivalent circuit that best describes this systems is represented as a solution resistance (R_s) connected in series with capacitive-resistive elements (CPE_{coat} , R_{coat}) related with the sol-gel coating capacitance and pore resistance associated in parallel joined in series with other capacitive-resistive elements (CPE_{ox} , R_{ox}) associated in parallel related with the stainless steel oxide layer (Figure 4.42 - b)).

Exceptionally, 66,5M:3,5G:30T biocoating for long time contact with Hank's solution (24h and 48h) and at 0h and 8h only reveal one time constant identified at high frequency range, signal of a very damaged sol-gel coating and strong metal substrate activation. The model used as representative of this system is illustrated in Figure 4.42 - a) and is represented by a solution resistance (R_s) connected in series with capacitive-resistive elements (CPE_{ox} , R_{ox}) associated in parallel.

Constant phase elements (CPE) instead of capacitors were used in the equivalent circuit models to take into account the dispersive character of the time constants and inhomogeneous properties of the layers.³⁵

R_s is the electrolyte resistance usually $\approx 9,5 \Omega \cdot \text{cm}^2$ for Hank's solution³⁵, R_{c-out} and CPE_{c-out} represent the high frequency range phenomenon related with the external film of depositions, R_{coat} (or R_{po}) and CPE_c (or CPE_{coat}) represent medium-high frequency range phenomenon associated with the coating degradation. CPE_{ox} and R_{ox} also show up at medium frequency range and are related with corrosion phenomenon.

Very good correlation was observed between experimental results and the equivalent circuit fitting model, as the Chi-squared (χ^2) calculated values were lower than 10^{-2} .

The parameters acquired after fitting EIS results of coated samples in contact with Hank's solution with equivalent circuits models are exposed in Table 4. 14 and Table 4. 15.

Table 4. 14 - Parameters of the equivalent circuits used to describe the physical-chemical phenomenon of 90(M:G):10T series biomaterials in contact with Hank's solution from 0h until 48h - a) 45M:45G:10T; b) 76M:14G:10T; c) 86,5M:3,5G:10T.

a) 45M:45G:10T										
t (h)	Time constants	R_{c-out} ($\Omega \cdot \text{cm}^2$)	CPE_{c-out} ($F \cdot \text{cm}^2$)	n	R_{coat} ($\Omega \cdot \text{cm}^2$)	CPE_{coat} ($F \cdot \text{cm}^2$)	n	R_{ox} ($\Omega \cdot \text{cm}^2$)	CPE_{ox} ($F \cdot \text{cm}^2$)	n
0	3	461	5,16E-8	0,95	1399	1,27E-8	0,89	1,0E20	3,05E-5	0,81
1,5	3	206	4,19E-8	0,98	712	9,04E-8	0,86	1,0E20	4,24E-5	0,84
3	3	162	3,84E-8	0,98	627	9,52E-8	0,88	1,0E20	4,53E-5	0,85
4	3	147	5,24E-8	0,95	618	7,07E-8	0,90	1,0E20	4,59E-5	0,85
6	3	191	7,21E-8	0,94	459	1,06E-7	0,88	1,0E20	4,91E-5	0,85
8	3	160	6,80E-8	0,95	500	1,57E-7	0,90	1,0E20	4,92E-5	0,85
10	3	99	8,71E-8	0,91	555	1,91E-7	0,90	1,0E20	5,02E-5	0,85
24	3	157	2,02E-7	0,88	632	2,95E-7	0,84	1,0E20	5,29E-5	0,86
48	3	74	1,21E-7	0,87	981	4,05E-7	0,84	1,0E20	5,26E-5	0,87

RESULTS

b)

76M:14G:10T										
t (h)	Time constants	Rc-out ($\Omega \cdot \text{cm}^2$)	CPEc-out ($\text{F} \cdot \text{cm}^2$)	n	Rcoat ($\Omega \cdot \text{cm}^2$)	CPEcoat ($\text{F} \cdot \text{cm}^2$)	n	Rox ($\Omega \cdot \text{cm}^2$)	CPEox ($\text{F} \cdot \text{cm}^2$)	n
0	3	6955	3,23E-8	0,98	44454	1,06E-8	0,94	1,0E20	3,06E-5	0,80
1,5	3	3400	4,60E-8	0,96	16568	4,02E-8	0,65	1,0E20	3,74E-5	0,85
3	3	2634	5,03E-8	0,95	11381	1,04E-8	0,67	1,0E20	4,25E-5	0,86
4	3	1316	5,09E-8	0,95	10987	2,44E-8	0,68	1,0E20	4,32E-5	0,86
6	3	1286	5,22E-8	0,95	9521	1,49E-8	0,85	1,0E20	4,46E-5	0,86
8	3	925	5,22E-8	0,95	8507	1,32E-8	0,82	1,0E20	4,57E-5	0,86
10	3	865	5,79E-8	0,94	8184	1,64E-8	0,78	1,0E20	4,63E-5	0,86
24	3	520	6,26E-8	0,93	9395	1,68E-8	0,85	1,0E20	4,73E-5	0,86
48	3	310	4,00E-8	0,96	7427	5,16E-8	0,79	1,0E20	5,02E-5	0,87

c)

86,5M:14G:10T										
t (h)	Time constants	Rc-out ($\Omega \cdot \text{cm}^2$)	CPEc-out ($\text{F} \cdot \text{cm}^2$)	n	Rcoat ($\Omega \cdot \text{cm}^2$)	CPEcoat ($\text{F} \cdot \text{cm}^2$)	n	Rox ($\Omega \cdot \text{cm}^2$)	CPEox ($\text{F} \cdot \text{cm}^2$)	n
0	3	23443	3,72E-8	0,98	25456	2,38E-8	0,83	1,0E20	3,49E-5	0,80
1,5	3	12749	4,43E-8	0,97	11575	1,14E-7	0,76	1,0E20	4,65E-5	0,84
3	3	10686	4,46E-8	0,97	13338	8,77E-8	0,78	1,0E20	4,48E-5	0,85
4	3	12256	4,50E-8	0,97	12423	9,88E-8	0,79	1,0E20	4,85E-5	0,85
6	3	9029	5,92E-8	0,95	13391	8,51E-8	0,66	1,0E20	5,05E-5	0,85
8	3	8402	6,15E-8	0,94	11441	8,32E-8	0,67	1,0E20	5,11E-5	0,85
10	3	4853	5,39E-8	0,95	17404	6,08E-8	0,73	1,0E20	5,22E-5	0,85
24	3	2466	8,80E-8	0,91	36314	1,76E-8	0,86	1,0E20	5,44E-5	0,87
48	3	3794	9,48E-8	0,91	52609	2,60E-8	0,79	1,0E20	5,54E-5	0,88

Table 4. 15 - Parameters of the equivalent circuits used to describe the physical-chemical phenomenon of 70(M:G):30T series biomaterials in contact with Hank's solution from 0h until 48h - a) 35M:35G:30T; b) 56M:14G:30T; c) 66,5M:3,5G:30T.

a) **35M:35G:30T**

t (h)	Time constants	Rcoat ($\Omega.cm^2$)	CPEcoat ($F.cm^2$)	n	Rox ($\Omega.cm^2$)	CPEox ($F.cm^2$)	n
0	2	84	1,42E-7	0,91	1,0E20	6,89E-5	0,80
1,5	2	89	2,34E-7	0,87	1,0E20	7,41E-5	0,82
3	2	100	3,17E-7	0,85	1,0E20	7,59E-5	0,82
4	2	105	3,59E-7	0,84	1,0E20	7,61E-5	0,83
6	2	110	3,73E-7	0,84	1,0E20	7,64E-5	0,83
8	2	115	4,98E-7	0,81	1,0E20	7,74E-5	0,84
10	2	111	3,66E-7	0,85	1,0E20	7,74E-5	0,84
24	2	117	1,14E-6	0,71	1,0E20	7,64E-5	0,86
48	2	101	1,24E-6	0,74	1,0E20	7,53E-5	0,87

b) **56M:14G:30T**

t (h)	Time constants	Rcoat ($\Omega.cm^2$)	CPEcoat ($F.cm^2$)	n	Rox ($\Omega.cm^2$)	CPEox ($F.cm^2$)	n
0	2	89	1,73E-7	0,92	1,0E20	8,28E-5	0,84
1,5	2	158	1,53E-7	0,92	1,0E20	7,90E-5	0,86
3	2	170	1,64E-7	0,92	1,0E20	8,00E-5	0,86
4	2	174	1,66E-7	0,92	1,0E20	8,00E-5	0,86
6	2	178	1,68E-7	0,91	1,0E20	8,08E-5	0,87
8	2	198	1,82E-7	0,91	1,0E20	7,96E-5	0,87
10	2	228	2,13E-7	0,89	1,0E20	7,73E-5	0,87
24	2	154	3,26E-7	0,85	1,0E20	7,82E-5	0,88
48	2	174	6,23E-7	0,81	1,0E20	7,61E-5	0,89

RESULTS

c)

66,5M:3,5G:30T							
t (h)	Time constants	R _{coat} (Ω.cm ²)	CPE _{coat} (F.cm ²)	n	R _{ox} (Ω.cm ²)	CPE _{ox} (F.cm ²)	n
0	2	Δ	Δ	Δ	1,0E20	9,12E-5	0,83
1,5	2	21	3,93E-7	0,89	1,0E20	9,06E-5	0,85
3	2	--	--	--	--	--	--
4	2	20	4,81E-7	0,90	1,0E20	9,18E-5	0,85
6	2	25	1,61E-6	0,74	1,0E20	9,10E-5	0,86
8	2	Δ	Δ	Δ	1,0E20	9,35E-5	0,86
10	2	11	2,36E-6	0,81	1,0E20	9,03E-5	0,87
24	1	Δ	Δ	Δ	1,0E20	9,06E-5	0,87
48	1	Δ	Δ	Δ	1,0E20	8,97E-5	0,88

Δ - no data because it is not detected the presence of the layer.

The electrolyte uptake in coatings can be monitored by the analysis of CPE_{coat} time evolution; on the other hand, R_{coat} evolution can provide information about the barrier properties of the coatings. In view of the before cited, diagrams of temporal evolution of CPE_{coat} and R_{coat} are exposed in Figure 4.43 and Figure 4.44.

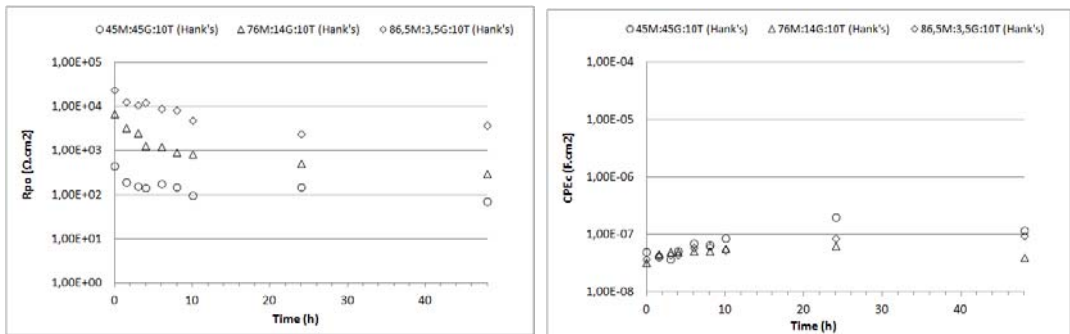


Figure 4. 43 - Evolution of sol-gel coating properties R_{coat} (left) and CPE_{coat} (right) with immersion time for 45M:45G:10T, 76M:14G:10T and 86,5M:3,5G:10T in Hank's solution from 0h until 48h.

R_{coat} results from fitting EIS data of series 90(M:G):10T materials are illustrated in Figure 4.43 - left diagram. A decreasing evolution can be identified for all the coatings immersed in Hank's solution, revealing a normal pattern of sol-gel coatings degradation with time evolution. Besides, a hierarchy behavior between GPTMS content and coating resistive properties can be identified. To be precise, the increase in GPTMS content cause a decrease in the coatings barrier properties as 45M:45G:10T show the weaker barrier properties and 86,5M:3,5G:10T coating the best pore resistance results.

On the other hand, when coatings performance in Hank's solution is compared with their performance in NaCl saline solution (Table 4. 16), although the pattern of increasing GPTMS content cause a decreasing in the coatings barrier properties is respected for both electrolytes, a clear decrease of the temporal evolution of R_{coat} is detected in Hank's solution. Probably the external deposits film act as a first barrier, preventing the full contact of the sol-gel coatings with the electrolyte requiring lesser barrier effect.

Table 4. 16 - R_{coat} time evolution of 45M:45G:10T, 76M:14G:10T and 86,5M:3,5G:10T in NaCl 3,5% wt. and Hank's solution.

t (h)	45M:45G:10T		76M:14G:10T		86,5M:3,5G:10T	
	Rcoat ($\Omega \cdot \text{cm}^2$)		Rcoat ($\Omega \cdot \text{cm}^2$)		Rcoat ($\Omega \cdot \text{cm}^2$)	
	NaCl	Hank's	NaCl	Hank's	NaCl	Hank's
0	1016	461	27248	6955	162520	23443
1,5	699	206	14409	3400	87982	12749
3	623	162	11829	2634	75766	10686
4	596	147	10104	1316	68506	12256
6	500	191	8841	1286	56998	9029
8	484	160	8272	925	49805	8402
10	466	99	7121	865	49790	4853
24	344	157	7430	520	50134	2466
48	341	74	7352	310	50140	3794

RESULTS

CPE_{coat} fitting equivalent circuit (EC) results of EIS data in Hank's solution (Figure 4.43 - right diagram) show a slight increase and follow a similar trend during all exposition time without a clear relation with GPTMS content.

A decreasing evolution of capacitance (detected for 45M:45G:10T and 76M:14G:10T after 24h contact with Hank's solution) is unusual for sol-gel systems as it is expected an increasing profile due to water uptake and hydrolytic degradation of the coatings, nevertheless this parameter may be affected by other factors as surface area or thickness of the layer.¹⁸ This discrepancy could also be related with the EC used as model and the synergic effects between the external deposits film and the coating.

All the same, if a comparison between the materials of series 90(M:G):10T exposed to Hank's and NaCl saline solution is made (Table 4. 17), the amount of absorbed solution is always lower in Hank's solution. This outcome may be originated by the containment effect that the external deposits film accomplishes, leading to lesser extent access of the electrolyte solution to the sol-gel coating.

Table 4. 17 - CPE_{coat} time evolution of 45M:45G:10T, 76M:14G:10T and 86,5M:3,5G:10T in NaCl 3,5% wt. and Hank's solution.

	45M:45G:10T		76M:14G:10T		86,5M:3,5G:10T	
	CPE_{coat} (F.cm ²)		CPE_{coat} (F.cm ²)		CPE_{coat} (F.cm ²)	
t (h)	NaCl	Hank's	NaCl	Hank's	NaCl	Hank's
0	3,76E-7	5,16E-8	6,34E-8	3,23E-8	3,83E-8	3,72E-8
1,5	4,00E-7	4,19E-8	8,87E-8	4,60E-8	4,29E-8	4,43E-8
3	4,06E-7	3,84E-8	9,63E-8	5,03E-8	6,15E-8	4,46E-8
4	4,09E-7	5,24E-8	9,90E-8	5,09E-8	5,97E-8	4,50E-8
6	3,56E-7	7,21E-8	1,03E-7	5,22E-8	6,05E-8	5,92E-8
8	3,65E-7	6,80E-8	1,07E-7	5,22E-8	6,41E-8	6,15E-8
10	4,15E-7	8,71E-8	1,12E-7	5,79E-8	6,41E-8	5,39E-8
24	3,65E-7	2,02E-7	1,30E-7	6,26E-8	1,01E-7	8,80E-8
48	3,75E-7	1,21E-7	1,81E-7	4,00E-8	1,01E-7	9,48E-8

It is important to notice that GPTMS content in series 90(M:G):10T biomaterials in contact with Hank's solution affects in a perceptible way the coatings performance. From a degradation improvement point of view, 45M:45G:10T is the most suitable coating to improve on degradation behaviour of the reference material and is in agreement with the results/conclusions find in NaCl saline solution experiments.

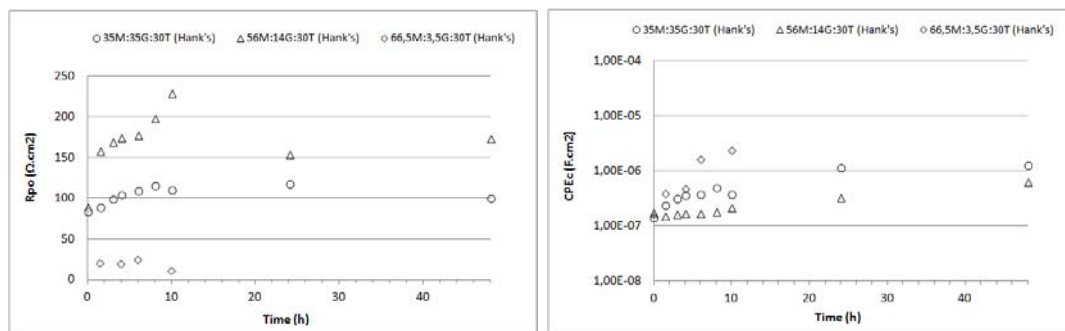


Figure 4. 44 - Evolution of sol-gel coating properties R_{coat} (left) and CPE_{coat} (right) with immersion time for 35M:35G:30T, 56M:14G:30T and 66,5M:3,5G:30T in Hank's solution and NaCl saline solution from 0h until 48h.

The time evolution of sol-gel series 70(M:G):30T coatings resistance (R_{coat}) and water uptake (CPE_{coat}) in contact with Hank's solution is revealed in Figure 4.44. The resistive evolution through time remains fairly constant and does not follow any hierarchy pattern related with the GPTMS content. To notice that 66,5M:3,5G.30T coating resistive properties is noticeably minor than the R_{coat} registered for the other compositions, probably related with a minor condensation degree achieved and verified with the resistance to solvents test (Table 4.3) and ^{29}Si NMR spectra (Figure 4.16). Also worth to note that, this coating performance in Hank's solution is worse than the performance registered in NaCl saline solution (Table 4. 18).

RESULTS

Table 4. 18 - R_{coat} time evolution of 35M:35G:30T, 56M:14G:30T and 66,5M:3,5G:30T in NaCl 3,5% wt. and Hank's solution.

t (h)	35M:35G:30T		56M:14G:30T		66,5M:3,5G:30T	
	Rcoat ($\Omega.cm^2$)		Rcoat ($\Omega.cm^2$)		Rcoat ($\Omega.cm^2$)	
	NaCl	Hank's	NaCl	Hank's	NaCl	Hank's
0	124	84	97	89	14	--
1,5	98	89	103	158	33	21
3	76	100	110	170	--	--
4	95	105	116	174	53	20
6	67	110	119	178	50	25
8	87	115	129	198	54	--
10	97	111	79	228	55	11,37
24	86	117	201	154	--	Δ
48	80	101	195	174	Δ	Δ

Δ - no data because it is not detected the presence of the layer.

CPE_{coat} results show an increasing evolution for all 70(M:G):30T series biomaterials, an expectable result with water uptake and coatings degradation with time evolution. It cannot be identified any relation between GPTMS content and water uptake as verified in the same experiment carried out in NaCl saline solution (Table 4. 19).

Table 4. 19 - CPE_{coat} time evolution of 35M:35G:30T, 56M:14G:30T and 66,5M:3,5G:30T in NaCl 3,5% wt. and Hank's solution.

t (h)	35M:35G:30T		56M:14G:30T		66,5M:3,5G:30T	
	CPE _{coat} (F.cm ²)		CPE _{coat} (F.cm ²)		CPE _{coat} (F.cm ²)	
	NaCl	Hank's	NaCl	Hank's	NaCl	Hank's
0	6,47E-8	1,42E-7	4,00E-8	1,73E-7	7,94E-6	--
1,5	6,50E-8	2,34E-7	9,09E-8	1,53E-7	2,15E-7	3,93E-7
3	3,87E-7	3,17E-7	9,12E-8	1,64E-7	--	--
4	3,84E-7	3,59E-7	1,12E-7	1,66E-7	9,55E-7	4,81E-7
6	4,11E-7	3,73E-7	1,44E-7	1,68E-7	1,01E-6	1,61E-6
8	4,07E-7	4,98E-7	1,45E-7	1,82E-7	3,69E-6	--
10	6,78E-7	3,66E-7	2,83E-7	2,13E-7	4,79E-6	2,36E-6
24	4,06E-7	1,14E-6	3,34E-7	3,26E-7	--	Δ
48	3,24E-6	1,24E-6	3,83E-7	6,23E-7	Δ	Δ

Δ - no data because it is not detected the presence of the layer.

Although the GPTMS content in series 70(M:G):30T biomaterials does not affect extensively the coatings resistive properties and water uptake, the higher TEOS content of this series causes important changes in the layer properties. The lowest R_{coat} and higher CPE_{coat} denote strong degradability of these coatings and consequently very defective matrices suggesting the TEOS incorporation as a good strategy to improve on the degradation performance of the reference material 50M:50G.

Besides the study on deterioration processes taking place on polymer coated metal substrates under controlled experimental conditions by means of impedance measurement it is very interesting the measurement of polysiloxanic matrix hydrolytic degradation. As the biomaterials will be on direct contact with a physiological aqueous medium, the study of the coatings degradation kinetics is a very important issue. Furthermore, if the main goal of this new dental implants coatings is the improvement of the osseointegration process by means of Si release (osteoinductor) and the establishment of a barrier effect against possible metal substrate

RESULTS

corrosion in the early stage of osteointegration, the hydrolytic degradation experiment will be an interesting study to provide information about the degradation rate and total degradation degree achieved. In addition, this study will demonstrate if the coatings are absorbable in a few weeks and leave the metal substrate in direct contact with the physiological medium after the initial osteoblastic response takes place.

Hydrolytic degradation behaviour of the silica based hybrid coatings was evaluated by measuring the weight loss as function of immersion time (until 63 days). Figure 4.45 and Figure 4.46 show the dissolution profiles of series 90(M:G):10T materials and series 70(M:G):30T materials respectively.

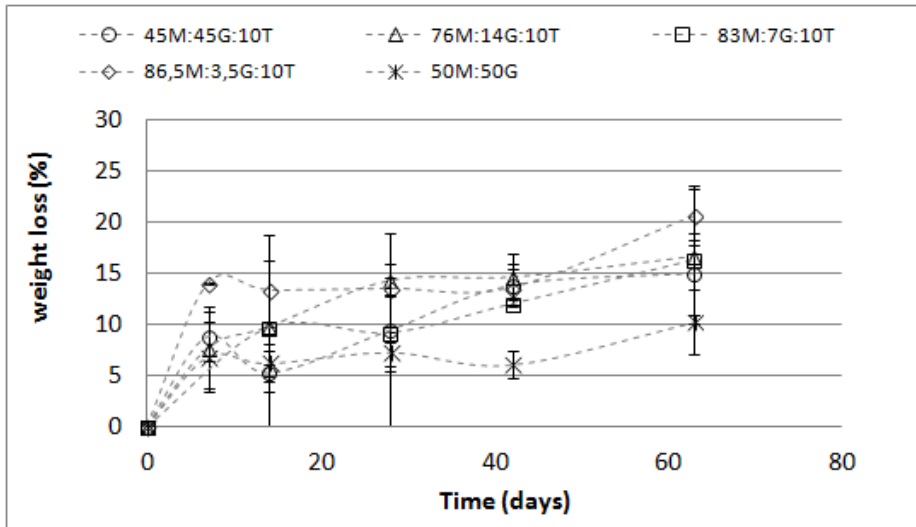


Figure 4.45 - Dissolution profiles (measured as weight loss in distilled water) of reference biomaterial 50M:50G and series 90(M:G):10T coatings.

The final weight loss of reference material (50M:50G) was strongly affected by TEOS incorporation to the hybrid matrix, increasing the weight loss from 10% to 15 - 20%.

Hydrolytic degradation of coatings show two different stages, a fast degradation rate identified in the first 7 days (1 - 2% weight loss/day) and a slower degradation second stage from 7 until 63 days (0,1 - 0,2% weight loss/day).

Hydrolytic degradation of silica based sol-gel particles was previously studied by many authors^{36,37,38} and all agree about the diffusion process control on silica based materials erosion. As the experiment was accomplished with plentiful water to avoid Si saturation the dissolution process depends in an important manner on the ability of the aqueous media to diffuse through the matrix.

It was stated on bibliography that the organic group γ -glycidoxypropyl of GPTMS show flexibility enough to fill the interstitial spaces on silica based network and fill some pores leading to a material categorized as compact¹³. In addition, the elasticity of the coating can be improved by the presence of organic groups that diminish stress and crack formation during the thermal treatment.³¹ Reducing the organic content in biomaterials compositions (incorporation of an inorganic element - TEOS) imperfections may appear in the coatings weakening its barrier effect and making easier aqueous medium diffusion through the matrix, consequently enhancing its degradation. Besides, the higher wettability (Table 4.7) and surface roughness (Figure 4.23 and Figure 4.25) caused by TEOS incorporation to reference composition 50M:50G may represent one cause (among others) for this hydrolytic degradation results.

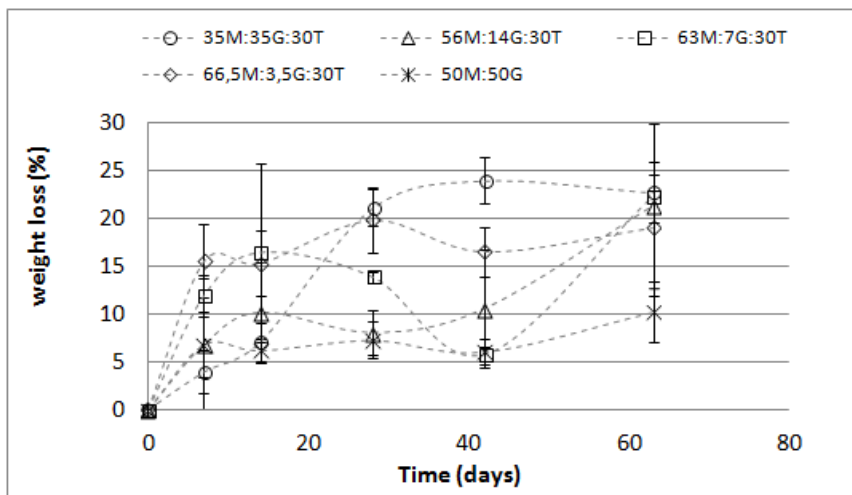


Figure 4.46 - Dissolution profiles (measured as weight loss in distilled water) of reference biomaterial 50M:50G and series 70(M:G):30T coatings.

RESULTS

Figure 4.46 show degradation data registered for series 70(M:G):30T materials and it is perceptible a dissolution profile similar to the one registered for series 90(M:G):10T materials (Figure 4.45). There are two degradation stages, a faster one registered on the initial 7-14 days (0,5 - 2% weight loss/day) and a slower degradation rate identified for 14 - 63 days period of time (0,1 - 0,3% weight loss/day).

Compositions with lesser GPTMS content, 63M:7G:30T and 66,5M:3,5G:30T, show very analogous dissolution rate with a fast degradation rate achieving almost the final weight loss at 7 days contact with aqueous medium. Nevertheless, a different behaviour is registered for the other compositions, 35M:35G:30T show high degradation rate until 28 days and 56M:14G:30T until 14 days, revealing a slower dissolution process for higher GPTMS content compositions. These results are in agreement with other research works^{13,31} conclusions about the effects of organic groups on the silica based networks, that is to say, γ -glycidoxypropyl of GPTMS may fill the interstitial spaces and difficult the diffusion process.

Again, final weight loss of reference material (50M:50G) was clearly affected by TEOS incorporation to the silica based matrix, increasing the weight loss from 10 to 20-23% (Figure 4.47). Surface roughness (Figure 4.24) may constitute one of the reasons for this water diffusion process issued by TEOS incorporation to the reference composition 50M:50G.

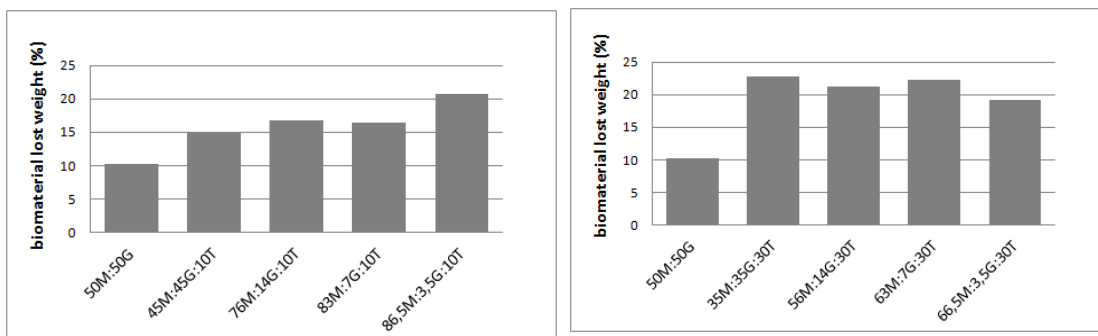


Figure 4.47 - Distribution of total weight loss at the end of 63 days contact with distilled water for series 90(M:G):10T (left chart) and series 70(M:G):30T (right chart) biomaterials and reference material 50M:50G.

The results of 90(M:G):10T series show direct weight loss dependence on GPTMS content as higher GPTMS content promotes lesser weight loss, reference material with 50%GPTMS lost 10% total weight, compositions with 45%, 14%, 7% and 3,5% GPTMS lost 15%, 16,7%, 16,3% and 21% total weight.

Acquired data for 70(M:G):30T series compositions does not show a relation between GPTMS content and total weight loss possibly due to the results dispersion of hydrolytic degradation experiment.

TEOS content clearly affects total weight loss of the coatings as all of the studied materials increase the reference material (50M:50G) weight loss. One of the reasons for these results may be the average roughness registered for the new triple silane coatings (Figure 4.23 and Figure 4.24) as the TEOS incorporation generally increase R_a that may result in easier aqueous medium access and diffusion, among other factors. The hydrolytic degradation results are in agreement with EIS measurements, as TEOS incorporation to 50M:50G reference matrix resulted in higher water uptake and higher matrix degradability.

Materials with 30% TEOS may be the most satisfactory to replace reference material 50M:50G as the best results on dissolution were registered for these coatings. The highest weight losses registered for 70(M:G):30T series materials suggest higher dissolution rate and consequently higher Si liberation due to silica network degradation what may cause reduction on coatings osseointegration time due to the positive effects of silicon on bone regeneration process^{2,3,4}.

It is important to note that the experimental conditions of hydrolytic degradation test do not reproduce *in vivo* situation in which silica saturation cannot be reached due to fluids constant movement. Besides, erosion phenomenon and biologic mechanisms may also affect coatings dissolution process *in vivo*.

RESULTS

COATING INTEGRITY AND SURFACE PROPERTIES OF GELATIN - SILOXANE HYBRIDS

It cannot be ignored the potential of silica based hybrid coatings developed on this research work as a support matrix for entrapment of biomolecules besides its direct effect on osseointegration biological mechanisms due to Si release.³⁹

Natural polymers as chitosan or gelatin have already been employed in clinics due to its bioresorption properties and flexibility⁴⁰ nevertheless they lack of bioactivity and show premature dissolution. New materials that assemble silica based bioactive structures with biodegradable and multifunctional natural polymers may represent an innovative group of biomaterials appropriate for tissues replacement and regeneration.

Gelatin-siloxane hybrids were synthesized and the stability of the hybrid coatings after gelatin incorporation and degradation was measured. Specific compositions of both series, 76M:14G:10T and 56M:14G:30T, were selected for the tests with gelatin incorporation because both have the same GPTMS proportion, 14%, and is the highest GPTMS content identical on both series. The production method followed was exactly the same as the one used for the pure silanes compositions (without gelatin), only important to refer the changes:

- temperature of the sol solution was fixed at 37°C
- gelatin (0,9 wt. % with respect to silanes) was incorporated to the acidified water (pH=1)

Gelatin-siloxane hybrids are suggested to form from hydrolysis and condensation of GPTMS with water and the ring-opening reaction of GPTMS with gelatin.⁴⁰

The amount of added gelatin to the silica based biomaterials was 0,9 wt.% as the goal of this experiments was to verify any properties modifications of the sol-gel coatings when the natural polymer was incorporated to the silica based network. In bibliography is possible to find studies about silica-gelatin hybrid materials with gelatin proportions of ≈ 2 wt.% or less.²²

RESULTS

After sol synthesis and metal coating with a dip-coater the production process ended with the thermal treatment to promote hydrolysis and condensation reactions, besides volatilization of dissolvent and water.

Visual assessment of coated stainless steel plates was made to ascertain the homogeneous semblance of the layer without particles or agglomerates, transparent and free of pores or fissures perceptible to the naked eye. Both coatings, 76M:14G:10T + 0,9wt.%gel and 56M:14G:30T + 0,9wt.%gel show homogeneous and bright surfaces free of imperfections with a layer thickness of $\approx 1,0 - 1,5 \mu\text{m}$ (some examples in Figure 4.48 and Figure 4.49).



Figure 4. 48 - Images of 76M:14G:10T+0,9wt.%gel (left) and 56M:14G:30T+0,9wt.%gel (right) biocoatings on stainless steel plates.

RESULTS

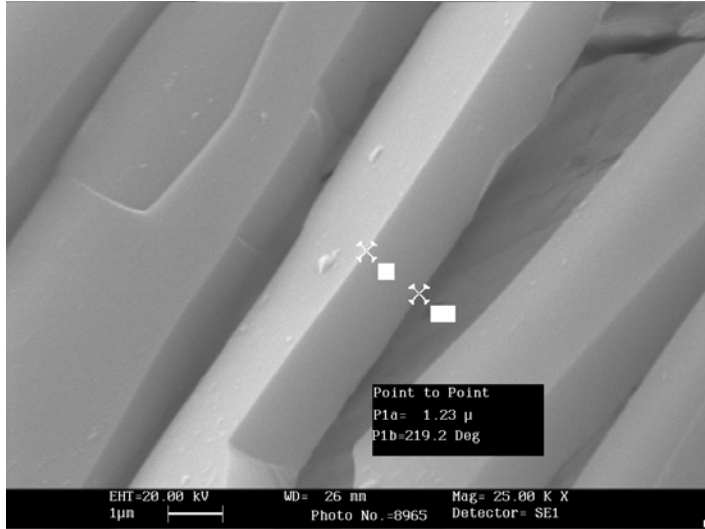


Figure 4. 49 - Microscope image (SEM) of 56M:14G:30T+0,9wt.%gel hybrid coating.

To evaluate the crosslinking degree of the sol-gel matrices with incorporation of gelatin, solid state ^{29}Si NMR spectroscopy was prepared. The NMR peak assignments will follow the above cited data in Table 4. 1.

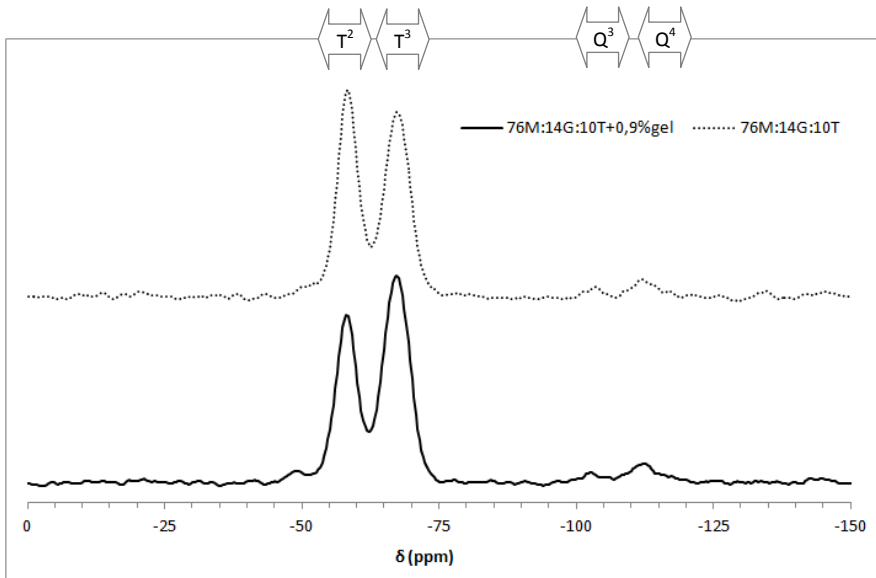


Figure 4. 50- Solid state ^{29}Si NMR spectra of 76M:14G:10T and 76M:14G:10T + 0,9wt. % gelatin.

To verify the condensation of silanol groups from 76M:14G:10T and 76M:14G:10T with 0,9wt. % gelatin incorporation that result from hydrolysis of methoxy silane groups (sol synthesis) ^{29}Si NMR spectra was registered (Figure 4.50). The predominance of T^2, T^3 and Q^3, Q^4 structures from MTMOS/GPTMS and TEOS, respectively, validates the achievement of a medium-high condensation degree on both compositions.

It is possible to detect that the incorporation of 0,9wt. % gelatin to the composition 76M:14G:10T did not affect in a perceptible way the crosslinking degree of the matrix. Only to notice a slight increase on the intensity of T^3 structural units signal (Table 4. 20).

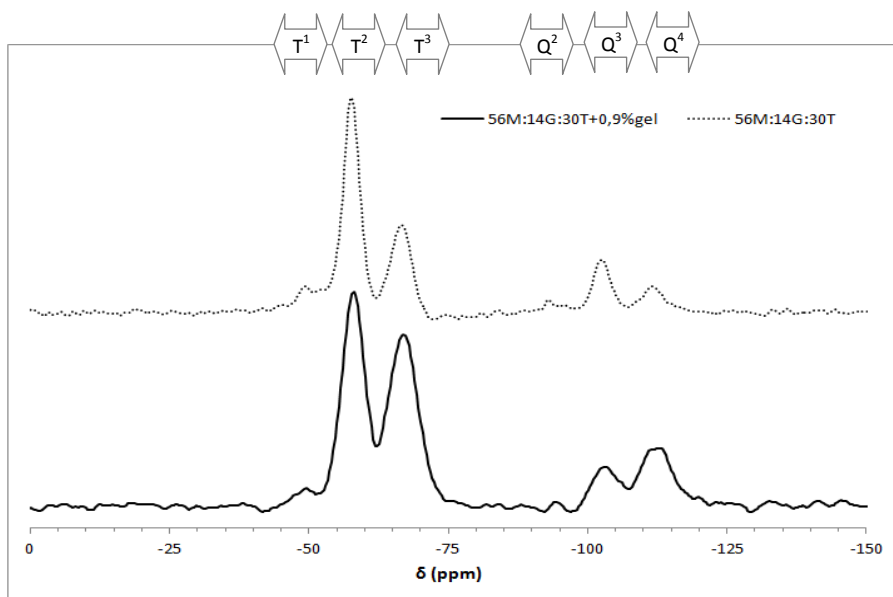


Figure 4. 51 - Solid state ^{29}Si NMR spectra of 56M:14G:30T and 56M:14G:30T + 0,9wt. % gelatin.

Figure 4.51 show the solid state ^{29}Si NMR spectra of 56M:14G:30T and 56M:14G:30T with incorporation of 0,9wt.% gelatin coatings. It can be identified on both biomaterials the presence of T^1, T^2 and T^3 units with higher intensity signal detected for T^2 structural units. On the other hand,

RESULTS

Q species show structures Q^2, Q^3 and Q^4 with higher intensity signal detected for Q^3 and Q^4 species.

Careful inspection reveals that the incorporation of 0,9wt. % gelatin to the composition 56M:14G:30T did not affect in a perceptible way the crosslinking degree of the matrix. Important to notice the increase of the intensity of T^3 and Q^4 structural units' signals (Table 4. 20), thus the number of Si-O-Si bridging bonds is expected to increase with gelatin incorporation to the composition 56M:14G:30T.

Table 4. 20 - ^{29}Si solid NMR peaks intensity proportion of compositions 76M:14G:10T and 56M:14G:30T with and without 0,9wt.% gelatin incorporation.

Composition	Gelatin content (wt.%)	Peak intensity proportion	
		$T^1/T^2/T^3$	$Q^2/Q^3/Q^4$
76M:14G:10T	0	-/89/79	-/4/8
	0,9	-/81/99	-/5/9
56M:14G:30T	0	12/99/40	6/24/12
	0,9	8/100/80	2/18/27

Although NMR study does not show any structural change of the silica based matrix with gelatin incorporation, it is noticeable a small increase of peaks intensity of species with highest condensation degree T^3 and Q^4 , more noticeable in the composition with higher TEOS content. This result suggest that gelatin improve the crosslinking degree of the polysiloxanic network, a possible cause may be the water absorbed by gelatin that is not available (as adsorbed water or co-solvent) so the thermal treatments energy to stimulate intramolecular changes is more efficient. Interestingly, a previous work²⁰ about a gelatin-GPTMS-TEOS hybrid material with GPTMS as coupling agent to covalently link with gelatin and TEOS as separate source of silica to construct an inorganic stable structure was completed. The TEOS structure with fixed silica content allows the variation of the inorganic (GPTMS) - organic (gelatin) coupling and interesting results came out. Specifically, as the hybrids molar ratio of

GPTMS:gelatin increase, a notable increase in the T species of NMR ^{29}Si spectra show up, besides, reduced amounts of non-bridging oxygens were confirmed by FTIR (Fourier transform infrared spectroscopy) leading to the conclusion that this kind of systems cause a dense silicate network. This work ^{29}Si NMR analysis is in accordance with Mahony and co-workers conclusions²⁰, as both hybrid coatings 76M:14G:10T+0,9wt. % gelatin and 56M:14G:30T+0,9wt.% gelatin show an increase on peaks intensity of species with highest condensation degree T^3 and Q^4 , corroborating the findings previously established.

FTIR (Fourier transform infrared spectroscopy) spectroscopy was used to study the chemical interactions between the organic and inorganic structural units of MTMOS:GPTMS:TEOS+GELATIN hybrid coatings.

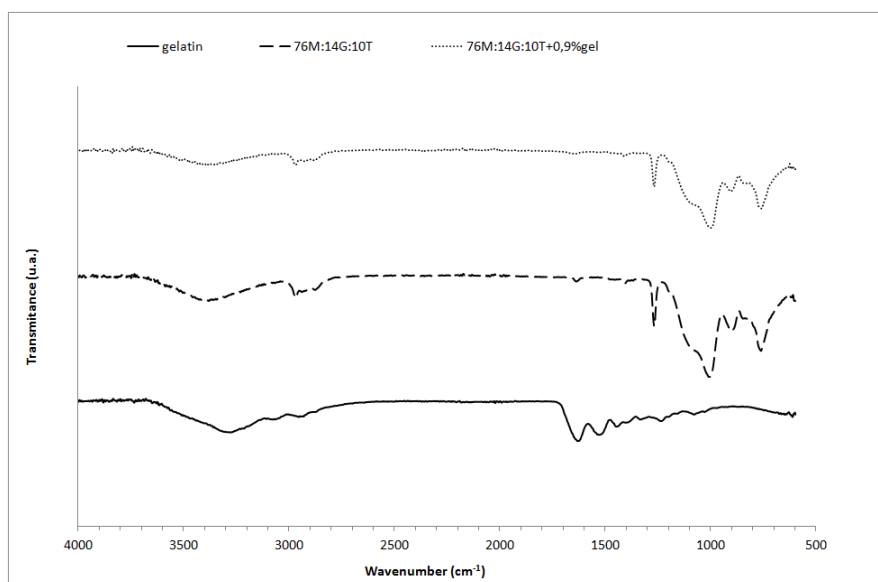


Figure 4. 52 - FTIR spectra recorded for 76M14G:10T, 76M14G:10T+ 0,9wt.% gelatin and pure gelatin.

Figure 4.52 shows the FTIR spectra of 76M:14G:10T pure and with 0,9wt.% gelatin incorporation, the spectra of pure gelatin was also recorded. The most intense band registered for both sol-gel biocoatings, at $\approx 1100\text{ cm}^{-1}$, is due to stretching vibrations of the Si-O-Si bridges and

RESULTS

at $\approx 3400\text{ cm}^{-1}$ related with water and hydroxyl group vibrations. Also a peak is observed at $\approx 1270\text{ cm}^{-1}$ related with C-H vibrations of the organic groups (epoxy opening). CH_3 asymmetric stretching vibration was identified by the peak at $\approx 2979\text{ cm}^{-1}$ and CH_3 asymmetric band can be identified at $\approx 1420\text{ cm}^{-1}$.

Gelatin spectrum characteristic absorption bands are amide I - stretching vibrations of the CO and CN groups detected at $\approx 1654\text{ cm}^{-1}$, amide II - vibration of NH and CN groups detected at $\approx 1538\text{ cm}^{-1}$ and amide III - stretching vibration of NH and CN groups identified at 1328 cm^{-1} . Also the wideband recognized in gelatin spectrum at $\approx 3400\text{ cm}^{-1}$ was related to vibration of NH groups.⁴¹

The introduction of gelatin to 76M:14G:10T biomaterial results in slight changes as the band detected at $\approx 3400\text{ cm}^{-1}$ changes due to the NH groups vibration besides the -OH groups from silanes at this same range. Besides, noticeable changes on spectra at $\approx 1654\text{ cm}^{-1}$ may also be identified as the vibrations related with adsorbed water detected at $\approx 1640\text{ cm}^{-1}$ for pure silane 76M:14G:10T biomaterial changes when gelatin is incorporated, in all probability due to the amide I - stretching vibrations of the CO and CN groups.

The results show a successful functionalisation of the polysiloxanic coatings, besides, it proves that the gelatin incorporation does not affect the macromolecular structure of the material.

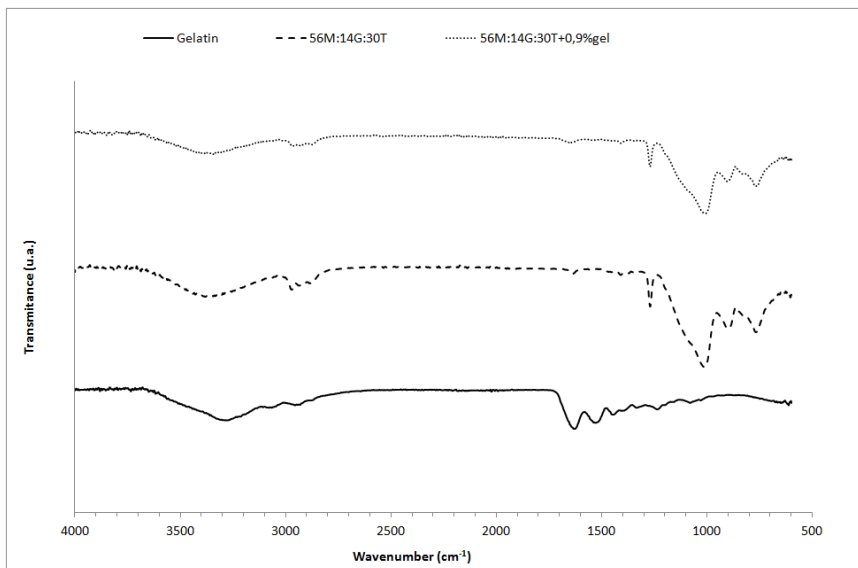


Figure 4. 53 - FTIR spectra recorded for 56M14G:30T, 56M14G:30T+ 0,9wt.% gelatin and pure gelatin.

Figure 4.53 shows the FTIR spectra of 56M:14G:30T pure and with 0,9wt.% gelatin incorporation, the spectra of pure gelatin was also recorded. The most intense band registered for both sol-gel biocoatings, at $\approx 1100 \text{ cm}^{-1}$, is due to stretching vibrations of the Si-O-Si bridges and at $\approx 3400 \text{ cm}^{-1}$ related with water and hydroxyl group vibrations. Also a peak is observed at $\approx 1270 \text{ cm}^{-1}$ related with C-H vibrations of the organic groups (epoxy opening). CH_3 asymmetric stretching vibration was identified by the peak at $\approx 2979 \text{ cm}^{-1}$ and CH_3 asymmetric band can be identified at $\approx 1420 \text{ cm}^{-1}$.

Gelatin spectrum characteristic absorption bands are amide I - stretching vibrations of the CO and CN groups detected at $\approx 1654 \text{ cm}^{-1}$, amide II - vibration of NH and CN groups detected at $\approx 1538 \text{ cm}^{-1}$ and amide III - stretching vibration of NH and CN groups identified at 1328 cm^{-1} . Also the wideband recognized in gelatin spectrum at $\approx 3400 \text{ cm}^{-1}$ was related to vibration of NH groups.⁴¹

The introduction of gelatin to 56M:14G:30T biomaterial results in slight changes as the band detected at $\approx 3400 \text{ cm}^{-1}$ changes due to the NH groups vibration besides the -OH groups from silanes at this same

RESULTS

range. Besides, noticeable changes on spectra at $\approx 1654\text{ cm}^{-1}$ may also be identified as the vibrations related with adsorbed water detected at $\approx 1640\text{ cm}^{-1}$ for pure silane 56M:14G:30T biomaterial changes when gelatin is incorporated, in all probability due to the amide I - stretching vibrations of the CO and CN groups.

The results show a successful functionalization of the polysiloxanic coatings, besides, it proves that the gelatin incorporation does not affect the macromolecular structure of the material.

Thermogravimetric analysis (TGA) was performed to ascertain the thermal decomposition of the silica based coatings with and without gelatin incorporation and prove the accomplishment of a hybrid biomaterial perfectly coupled with the natural polymer (gelatin).

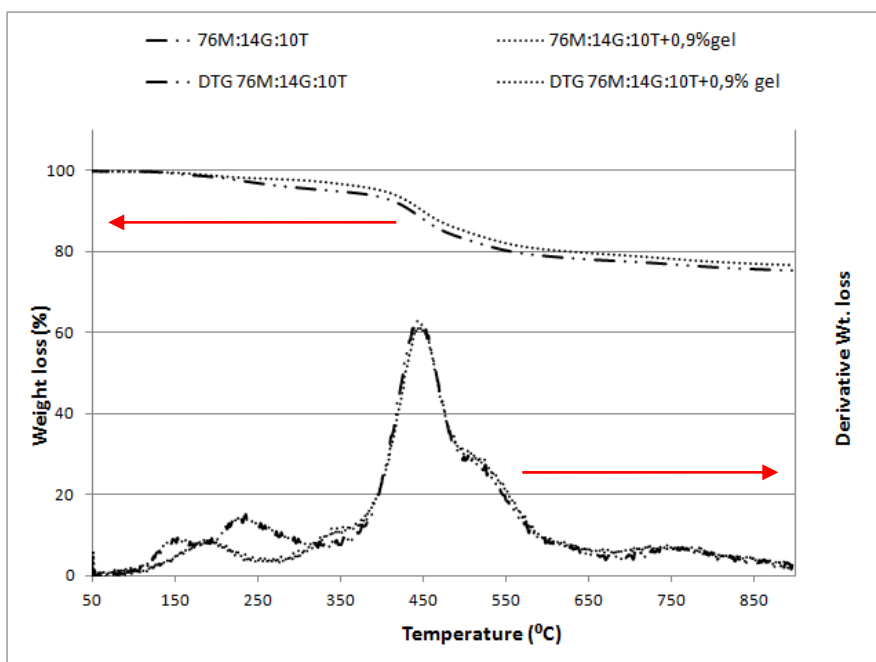


Figure 4. 54 - TG and DTG profiles of the hybrid coatings 76M:14G:10T and 76M:14G:10T+0,9wt.% gelatin.

Pure 76M:14G:10T and 76M:14G:10T with incorporation of gelatin are characterized by the same thermal degradation profile (Figure 4.54).

Briefly, the mass loss starts with derivative peaks sited below 270°C assigned to water and volatiles evaporation. The next peak, identified at 350-500°C is associated with the volatilization of small molecular oligomers or unreacted precursors. Finally, above 500°C the slight weight loss registered may be related with the decomposition of the polymeric structure and the dehydration of silanol groups.^{21,23-26}

The results show that the gelatin incorporation does not affect the thermal degradation behavior of the biomaterial. All the same, it is important to refer the slight differences on the derivative chart identified at below 270°C related with water evaporation and volatiles evaporation. The displacement of the first peak from 150°C (76M:14G:10T) to 180°C (76M:14G:10T+0,9wt.%gel) and its higher intensity suggests a difficult water removal process for the composition with gelatine incorporation due to the presence of hydroxyl and amino groups highly hydrophylic. The same trend was verified for the peak related with volatiles evaporation, for 76M:14G:10T come into view at ≈230°C and for 76M:14G:10T+0,9wt.%gel show up at ≈325°C suggestive of a difficult evaporation process maybe related with density changes of the matrix.

RESULTS

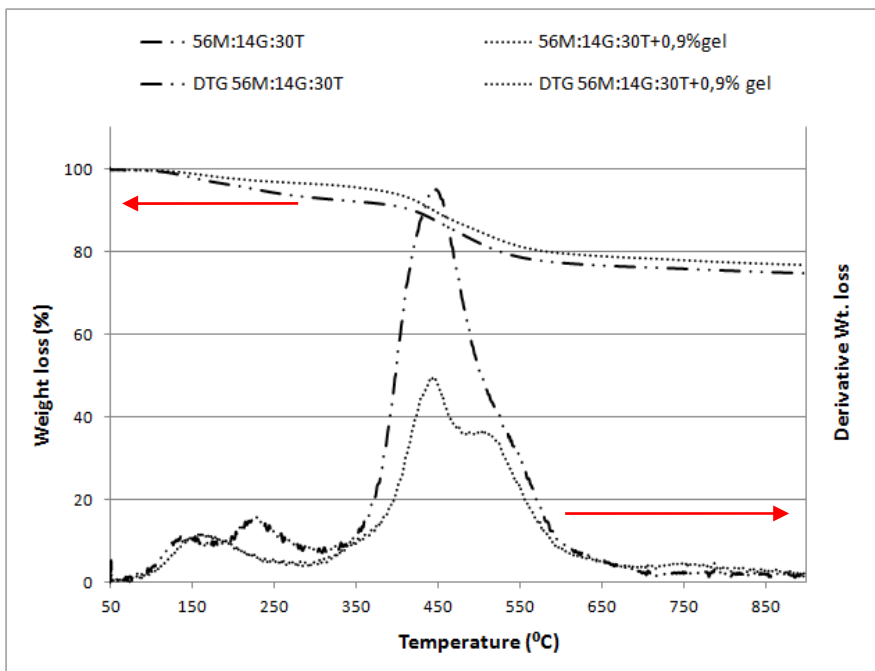


Figure 4.55 - TG and DTG profiles of the hybrid coatings 56M:14G:30T and 56M:14G:30T+0,9wt.% gelatin.

Pure 56M:14G:30T and 56M:14G:30T with incorporation of gelatin are characterized by the same thermal degradation profile (Figure 4.55).

Briefly, the mass loss starts with derivative peaks sited below 270°C assigned to water and volatiles evaporation. The next peak identified at $\approx 350\text{--}600^\circ\text{C}$ is associated with the volatilization of small molecular oligomers or unreacted precursors.^{21,23–26}

Interestingly, below 270°C the materials show different character, specifically pure 56M:14G:30T show two peaks at 140°C and 220°C related with water evaporation ($\approx 2\%$) and volatiles evaporation ($\approx 2,5\%$) respectively. On the other hand, 56M:14G:30T+0,9wt.% gelatin present a single width peak at 160°C suggesting the elimination of greater water amount ($\approx 10\%$) overlaying probably the volatiles evaporation peak.

The results show that the gelatin incorporation does not affect in a significant way the thermal degradation behavior of the biomaterial as it was not detected any important peak displacement. Nevertheless, to

refer the split of the peak identified at $\approx 350\text{-}600^\circ\text{C}$ related with 56M:14G:30T+0,9wt.% gelatin suggestive of a different volatilization process with special thermal energy necessary to volatilize the small molecular oligomers or unreacted precursors.

Table 4. 21 collect the weight loss (%) of pure materials 76M:14G:10T and 56M:14G:30T and 76M:14G:10T and 56M:14G:30T with 0,9wt.% gelatin incorporation in each identified thermal degradation stage.

Table 4. 21 - Weight loss (%) of hybrid coatings 76M:14G:10T, 76M:14G:10T+0,9%gel, 56M:14G:30T and 56M:14G:30T+0,9%gel in the most important degradation stages.

Biomaterial	Stage 1 \approx 150°C (%)	Stage 1 \approx 230°C (%)	Stage 2 \approx 450°C (%)	Stage 3 \approx 500°C (%)	Stage 4 \approx 800°C (%)
76M:14G:10T	1,2	2,5	12,0	8,0	2,0
76M:14G:10T+0,9%gel	1,6	0,9	11,0	6,0	2,0
56M:14G:30T	2,0	2,5	12,0		--
56M:14G:30T+0,9%gel	3,5		8,3	6,5	1,3

Since the hybrid materials are created for tissue regeneration and surface properties are extremely important to find a proper biological response, topographic analysis and surface energy measurements were prepared.

The evaluation of coatings pure 76M:14G:10T and pure 56M:14G:30T and the same compositions with 0,9wt.% gelatin incorporation surface roughness is in evidence in Figure 4.56 and Figure 4.57.

RESULTS

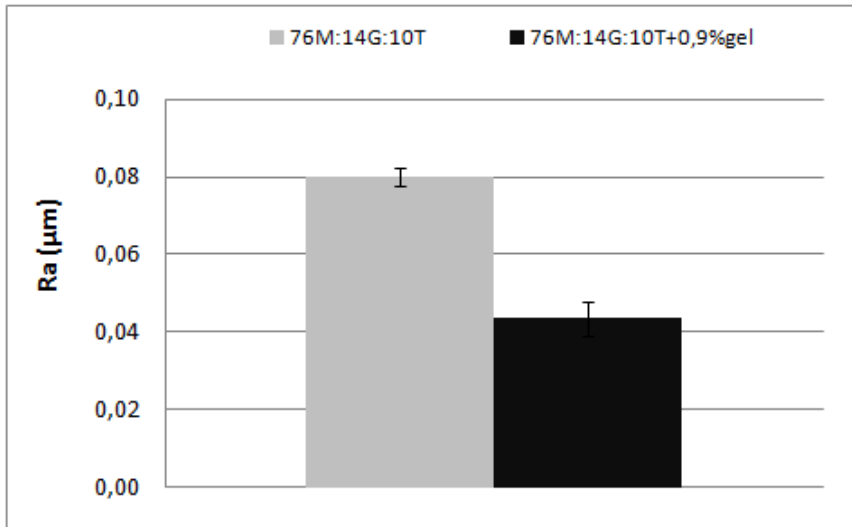


Figure 4. 56 - Average roughness (R_a) of 76M:14G:10T and 76M:14G:10T + 0,9wt.% gelatine biomaterials estimated by profilometry.

Average roughness (R_a) registered for pure 76M:14G:10T biocoating was $\approx 0,08 \mu\text{m}$ and when 0,9wt.% gelatin was incorporated to the composition R_a decrease to $\approx 0,04 \mu\text{m}$. A possible cause for R_a decline may be the tridimensional structure of gelatin molecules that may fill the open spaces and reduce the surface roughness. Consequently, R_a decrease leads to a decrease of the contact surface with surrounding medium suggesting a difficult access to the matrix interstices.

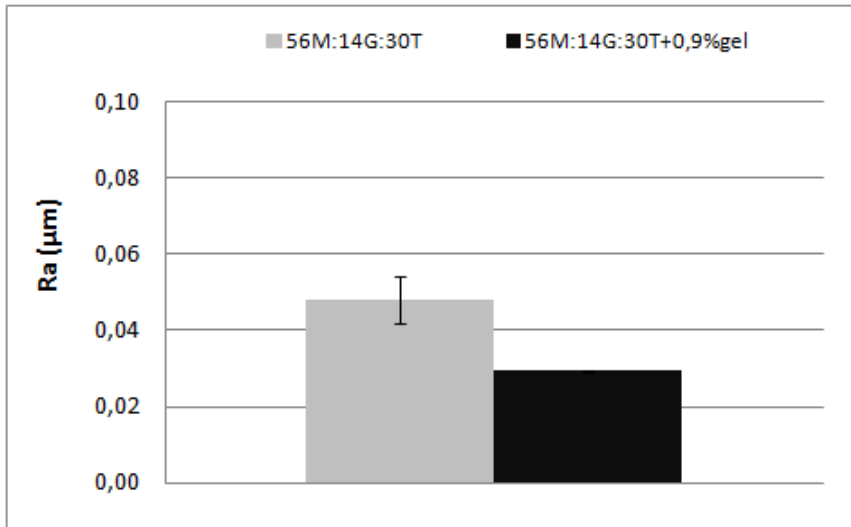


Figure 4. 57- Average roughness (R_a) of 56M:14G:30T and 56M:14G:30T + 0,9wt.% gelatine biomaterials estimated by profilometry.

Average roughness (R_a) registered for pure 56M:14G:30T coating was $\approx 0,05 \mu\text{m}$ and when 0,9wt.% gelatin was incorporated to the composition R_a decrease to $\approx 0,03 \mu\text{m}$. A possible cause for R_a decline may be the tridimensional structure of gelatin molecules that may fill the open spaces and reduce the surface roughness. Consequently, R_a decrease leads to a reduced contact surface with surrounding medium suggesting a difficult access to the matrix interstices.

Generally, gelatin incorporation reduces the surface R_a whatever it is the TEOS content on the sol-gel compositions. However, the decreasing amount is proportional to pure coatings average roughness, the higher the R_a value of pure material greater the R_a reduction when gelatin is incorporated.

Surface roughness is strongly affected by coatings thickness, for that reason a mass control was prepared to investigate the weight gain with gelatin incorporation.

RESULTS

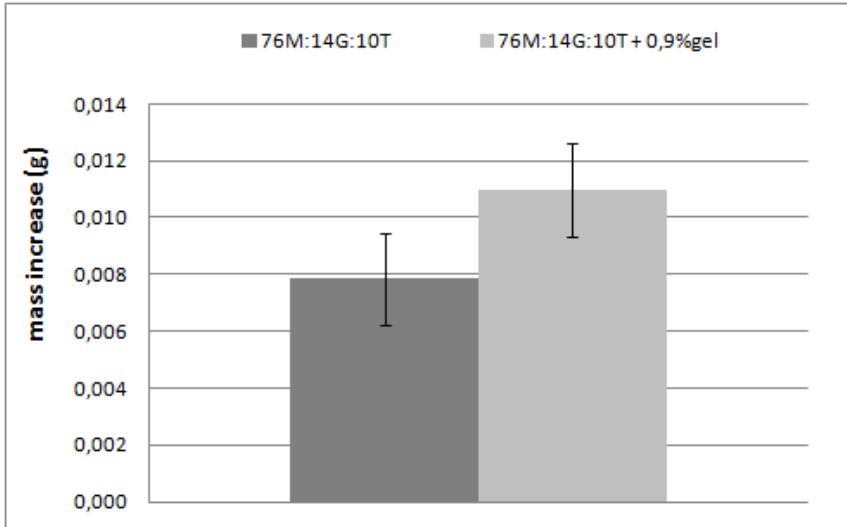


Figure 4. 58 - Weight gain of metal plates after coating with 76M:14G:10T and 76M:14G:10T+0,9wt.% gelatine.

The measured values of weight gain for metal plates coated with 76M:14G:10T pure and with 0,9wt.% gelatin incorporation were plotted in Figure 4.58. The results show a clear effect of the gelatin incorporation on the weight gain. Almost certainly, the higher molecular weight of gelatin causes this mass increase.

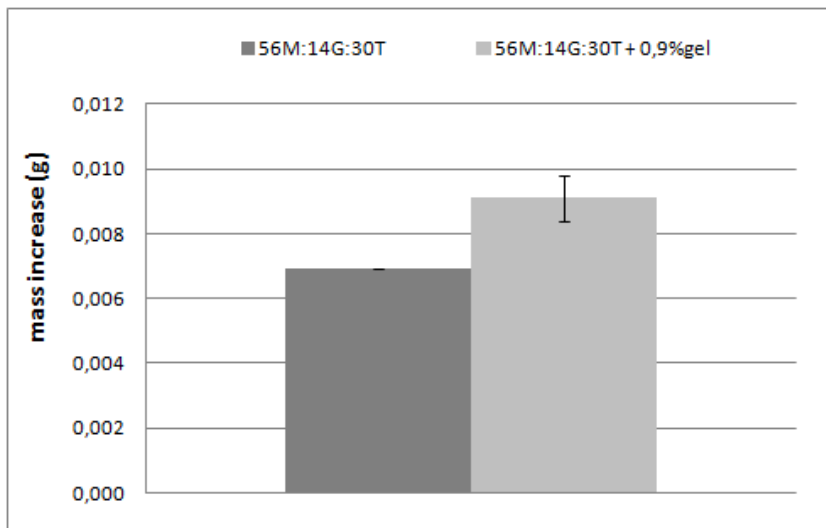


Figure 4. 59 - Weight gain of metal plates after coating with 56M:14G:30T and 56M:14G:30T+0,9wt.% gelatine.

The measured values of weight gain for metal plates coated with 56M:14G:30T pure and with 0,9wt.% gelatin incorporation were plotted in Figure 4.59. The results show a clear effect of the gelatin incorporation on the weight gain. Almost certainly, the higher molecular weight of gelatin causes this mass increase.

The tridimensional characteristics of the new hybrid coatings created with gelatin incorporation intimately related with weight gain and the changes of the matrix density may be the cause for the reduction of average roughness previously detected for both tested compositions (with 10% TEOS and 30% TEOS, Figure 4.56 and Figure 4.57). Accordingly, besides the weight gain increase with gelatin incorporation also coatings width raises (Figure 4.49).

Hybrid sol-gel materials with gelatin incorporation were coated on stainless steel plates and were subjected to water contact angle measurements intimately related to surface wettability, the results are represented in Figure 4.60 and Figure 4.61.

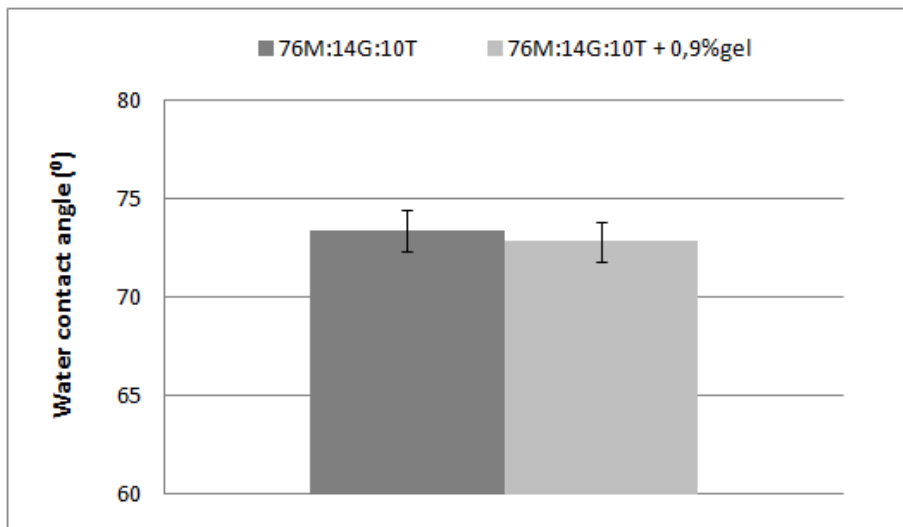


Figure 4. 60 - Contact angle (degrees) of 76M:14G:10T and 76M:14G:10T+0,9wt.% gelatine.

RESULTS

The registered values (Figure 4.60) show similar wettability of 76M:14G:10T coating when gelatin was incorporated.

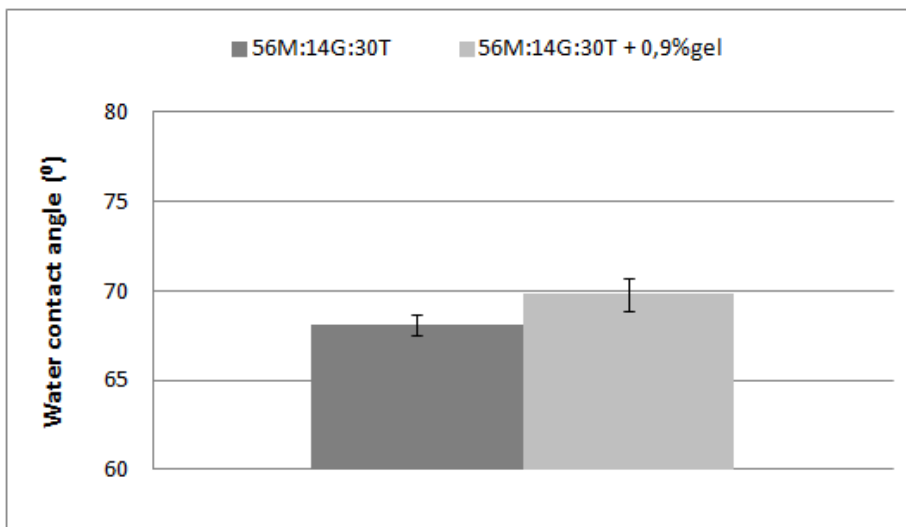


Figure 4. 61- Contact angle (degrees) of 56M:14G:30T and 56M:14G:30T+0,9wt.% gelatine.

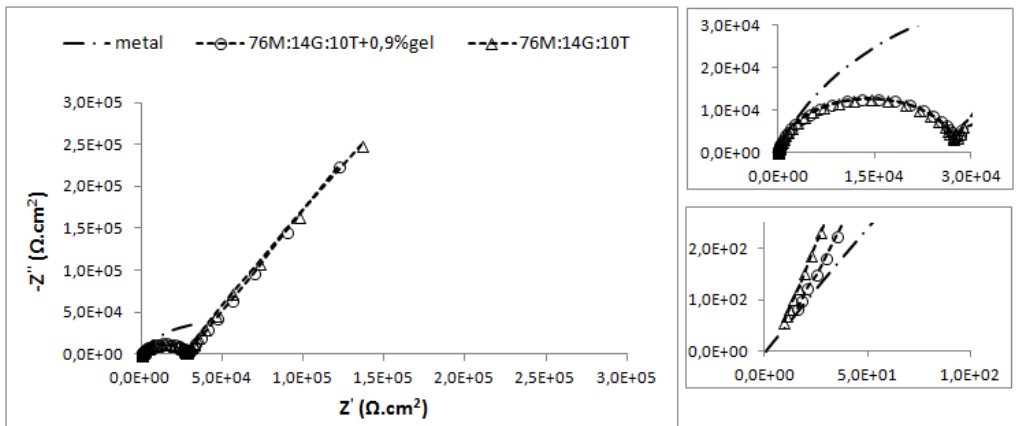
The registered values show a slight decrease on the wettability of 56M:14G:30T coating when gelatin was incorporated.

The increase in hydrophobicity can be ascribed to the higher crosslinking degree detected for 56M:14G:30T+0,9wt.% gelatin biomaterial (Figure 4.61) and reduction of available hydroxyl groups that improve hydrophilic properties of the biomaterials.

Finally, TEOS content affects in an important manner surface wettability when gelatine is incorporated to the pure trisilane coatings. That is to say, although gelatine affects sol-gel coatings measured water contact angles the effect caused by TEOS content still remain the factor that most influence the results. Taking into account that cellular adhesion is maximized in intermediate wettability surfaces (50°-70°)³⁰, 56M:14G:30T and 56M:14G:30T+0,9%gel coatings represent the most favorable surfaces to support cellular adhesion.

To determine if gelatine incorporation to the sol-gel silica based biocoatings cause any variation on the access and diffusion of a liquid environment through the matrix, electrochemical impedance spectroscopy (EIS) technique was employed with impedance measurements in NaCl 3,5wt% saline solution and Hank's solution. This analysis will also give information about the barrier effect of the hybrid biomaterials and about its degradation with time evolution.

a)



b)

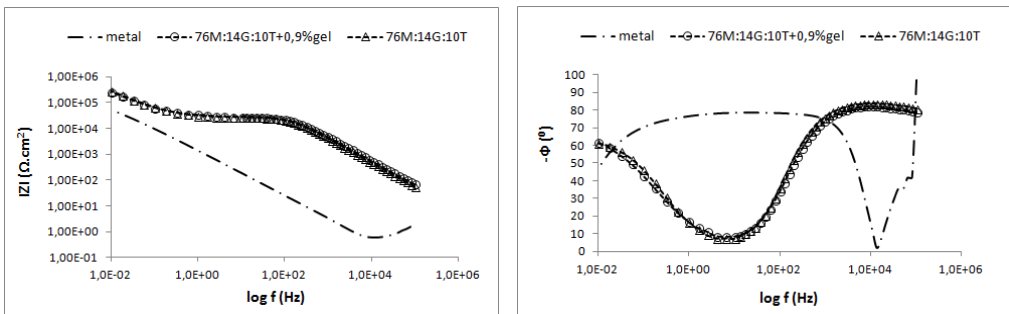


Figure 4. 62 - Nyquist diagram (a) and Bode plots (b) of the materials 76M:14G:10T, 76M:14G:10T+0,9wt.% gel and metal substrate after 0h immersion on NaCl 3,5wt.% solution.

RESULTS

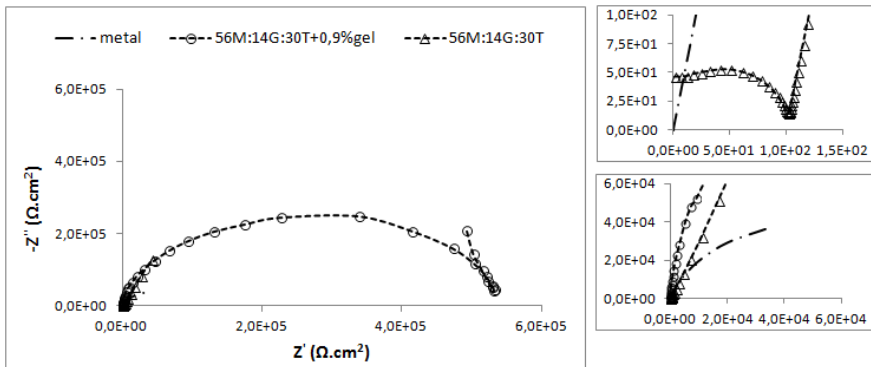
Pure 76M:14G:10T coating and 76M:14G:10T with 0,9wt.% gelatine incorporation impedance performance, at 0h contact time with NaCl saline solution electrolyte, is depicted in Figure 4.62.

At the first instant of metal substrate immersion Bode plots show one time constant at medium-high frequency range, certainly associated with the passive layer formed by oxides that cause a capacitive spectrum.

After coating with sol-gel silica based materials two time constants can be recognized in the spectra, one at low-medium frequency range related with the activation of metal substrate and another one at medium frequency range associated with the barrier coatings properties against electrolyte circulation through pores or cracks.

76M:14G:10T and 76M:14G:10T+0,9wt.% gelatin biomaterials show similar impedance profiles, with capacitive behaviour at high frequency range. In this special case, at 0h contact time with saline solution, the incorporation of gelatine to 76M:14G:10T does not affect in a considerable way the pure silane coating performance.

a)



b)

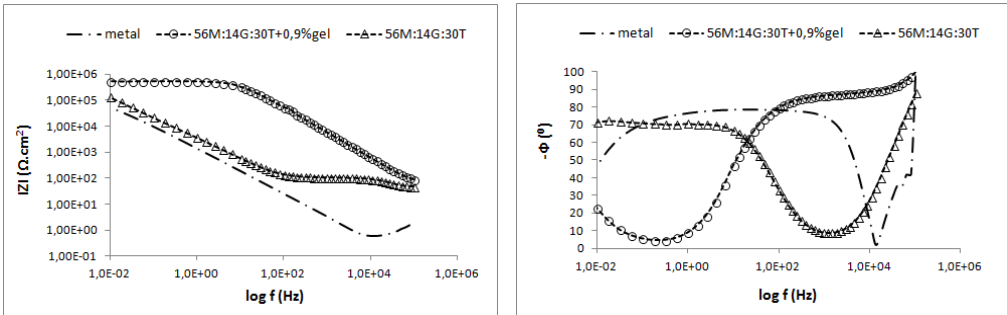
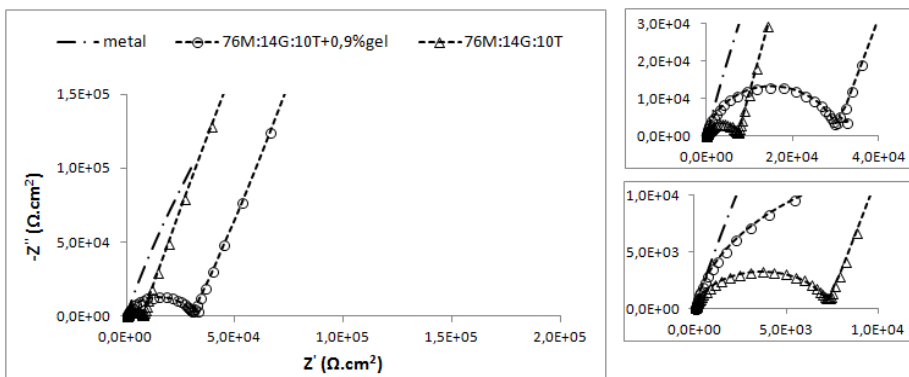


Figure 4. 63 - Nyquist diagram (a) and Bode plots (b) of the materials 56M:14G:30T, 56M:14G:30T+0,9wt.% gel and metal substrate after 0h immersion on NaCl 3,5wt.% solution.

Figure 4.63 shows the impedance variation for 56M:14G:30T pure and with 0,9wt.% gelatine incorporation coatings in the first instant contact with NaCl 3,5wt.% saline solution.

Pure 56M:14G:30T biocoating Bode plot show two time constants, one at higher frequency range associated with the barrier properties of the coating and another one at medium frequency range related to the corrosion processes that take place at metal interface. Nonetheless, when gelatine is incorporated to this composition is noticeable the displacement of the phase angle to lower frequency range predicting the improvement on the barrier effect of the coating. Besides, it can be seen by the superior impedance modulus values the improvement of the coating resistive properties.

a)



RESULTS

b)

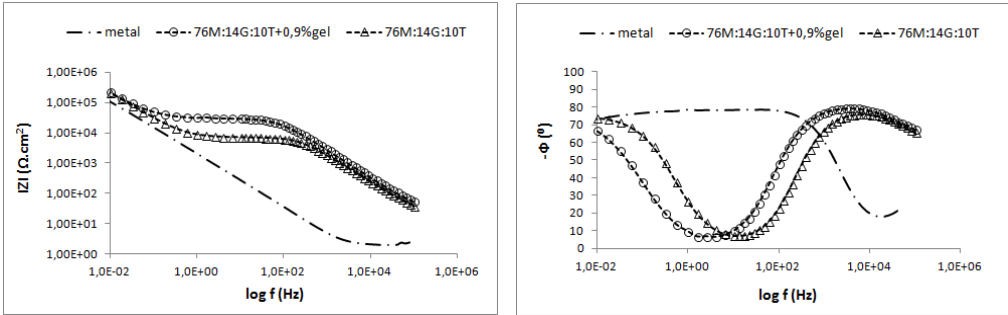


Figure 4. 64 - Nyquist diagram (a) and Bode plots (b) of the materials 76M:14G:10T, 76M:14G:10T+0,9wt.% gel and metal substrate after 48h immersion on NaCl 3,5wt.% solution.

After 48h immersion time of pure 76M:14G:10T and with incorporation of 0,9wt.% gelatine in NaCl saline solution, Bode diagram (Figure 4.64) show a similar impedance profile for both biomaterials. Two time constants may be recognized, one at low-medium frequency range related with the liquid-metal interface and another one at medium frequency range attributed to the barrier properties of the sol-gel coatings. Important to refer that 76M:14G:10T+0,9wt.% gelatin biocoating show a displacement of the phase angle to lower frequency range predicting a better performance of the barrier effect of the coating. Accordingly, the impedance of the coating with gelatine incorporation is notably higher revealing that the new structure of this biomaterial improves its impedance. A possible cause for this improvement may be the higher compactness of the layer and the lesser surface roughness (Figure 4.56) registered for the material with gelatine incorporation. To refer that both coatings 76M:14G:10T and 76M:14G:10T+0,9%gel present capacitive behaviour at high frequency range.

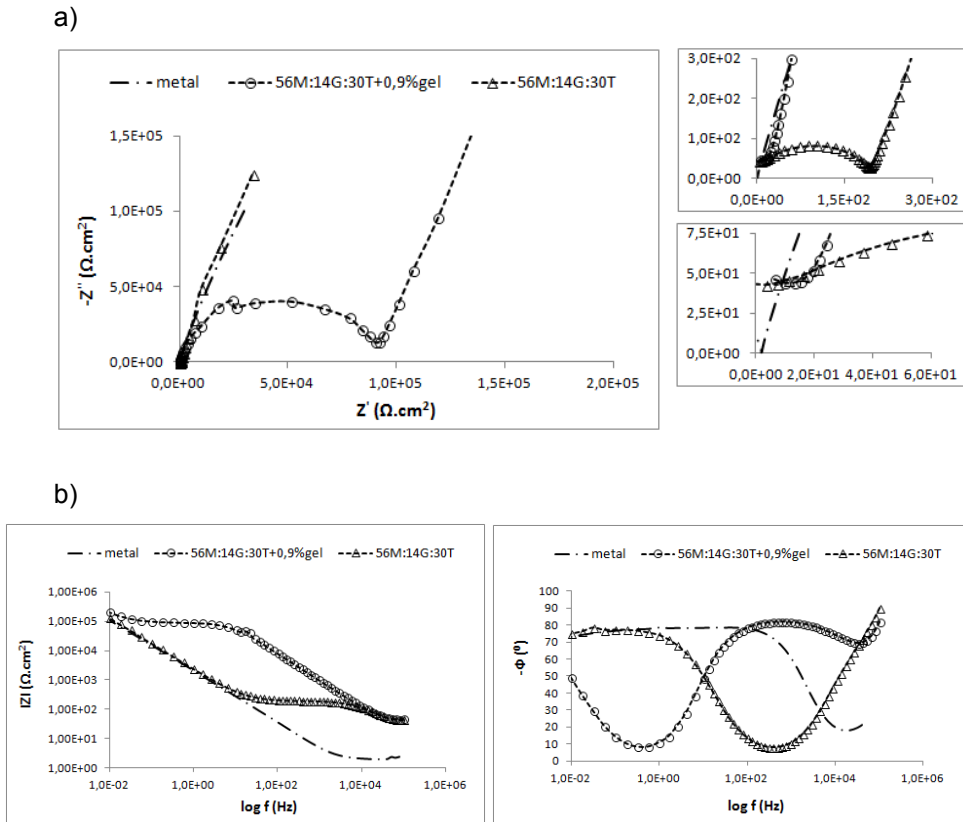


Figure 4. 65 - Nyquist diagram (a) and Bode plots (b) of the materials 56M:14G:30T, 56M:14G:30T+0,9wt.% gel and metal substrate after 48h immersion on NaCl 3,5wt.% solution.

Nyquist and Bode plots of 56M:14G:30T pure and with 0,9wt.% gelatine incorporation after 48h contact with NaCl saline solution are exposed in Figure 4.65.

Pure 56M:14G:30T show two time constants located at medium and high frequency ranges. The first one registered at medium frequency range is related with the metal substrate activation and the second one identified at high frequencies attributed the coating.

On the other hand, when gelatine is incorporated to the pure coating the impedance profile change and a third constant time arises (after 48h time contact with the electrolyte). The first constant time registered at low frequency range is related with the liquid-metal interface, at medium

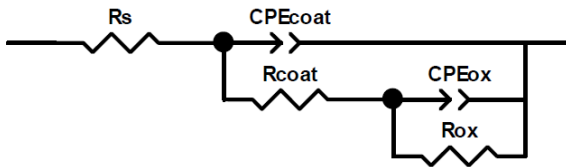
RESULTS

frequency range appear the second time constant related with the barrier properties of the coating and finally a third time constant is identified at high frequency range related with a possible external layer created on top of the hybrid coating.

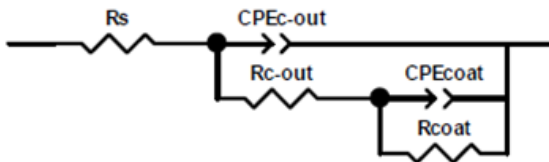
The TEOS content variation from 10% to 30% (taking into account that the GPTMS proportion is the same on the hybrid materials 76M:14G:10T+0,9wt.%gel and 56M:14G:30T+0,9wt.%gel) affects positively the barrier effect of the coating. This improvement may be caused by the higher crosslinking degree and probable higher compactness of the coating with 30% TEOS and gelatin.

In order to better understand the deterioration mechanism of the coatings, EIS results were fitted using equivalent circuits (EC). The ECs that best describe the impedance behaviour of the materials 76M:14G:10T+0,9wt.%gel and 56M:14G:30T+0,9wt.%gel immersed in NaCl 3,5wt.% saline solution are the ones exposed in Figure 4.66.

a)



b)



c)

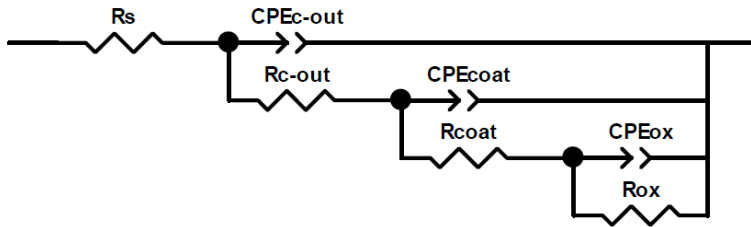


Figure 4. 66 - Equivalent circuits that best describe the impedance behaviour of the systems metal substrate coated with 76M:14G:10T+0,9wt.%gel and metal substrate coated with 56M:14G:30T+0,9wt.%gel in contact with NaCl saline solution. - a) metal substrate coated with 76M:14G:10T+0,9wt.%gel, b) metal substrate coated with 56M:14G:30T+0,9wt.%gel from 0h - 1,5h and c) metal substrate coated with 56M:14G:30T+0,9wt.%gel from 3h - 48h

For 76M:14G:10T+0,9wt.%gel coating, two time constants were used to fit the experimental EIS data. The first time constant related with the sol-gel film can be identified at medium-high frequency range correlated with the barrier properties of the silane coatings, and another one at medium-low frequency range can be attributed to the substrate activation and liquid-metal interface phenomenon. The equivalent circuit that best describes this systems is represented as a solution resistance (R_s) connected in series with capacitive-resistive elements (CPE_{coat} , R_{coat}) related with the sol-gel coating capacitance and pore resistance associated in parallel joined in series with other capacitive-resistive elements (CPE_{ox} , R_{ox}) associated in parallel related with the stainless steel oxide layer (Figure 4.66 - a)).

Exceptionally, 56M:14G:30T+0,9wt.%gel coating at initial contact times (0h and 1,5h) with the NaCl 3,5wt.% saline solution also show two time constants and the EC that best fits with impedance results is the model illustrated in Figure 4.66 - b). The equivalent circuit that best describes this system is represented as a solution resistance (R_s) connected in series with capacitive-resistive elements (CPE_{c-out} , R_{c-out}) related with the external film capacitance and resistance to the electrolyte inlet associated in parallel joined in series with capacitive-resistive elements (CPE_{coat} ,

RESULTS

R_{coat}) related with the sol-gel coating capacitance and pore resistance associated in parallel.

Finally, for longer time periods in contact with the saline electrolyte 56M:14G:30T+0,9wt.%gel coating behavior was adjusted to the equivalent circuit represented by a solution resistance (R_s) connected in series with capacitive-resistive elements ($\text{CPE}_{\text{c-out}}$, $R_{\text{c-out}}$) related with the external film capacitance and resistance to the electrolyte inlet associated in parallel joined in series with capacitive-resistive elements (CPE_{coat} , R_{coat}) related with the sol-gel coating capacitance and pore resistance associated in parallel also joined in series with other capacitive-resistive elements (CPE_{ox} , R_{ox}) associated in parallel related with the stainless steel oxide layer (Figure 4.66 - c)).

Constant phase elements (CPE) instead of capacitors were used in the equivalent circuit models to take into account the dispersive character of the time constants and inhomogeneous properties of the layers.³⁵

R_s is the electrolyte resistance usually $\approx 17 \Omega \cdot \text{cm}^2$ for NaCl 3,5wt.% saline solution, $R_{\text{c-out}}$ and $\text{CPE}_{\text{c-out}}$ represent the high frequency range phenomenon related with an external layer, R_{coat} (or R_{po}) and CPE_{c} (or CPE_{coat}) represent medium-high frequency range phenomenon associated with the coating degradation. CPE_{ox} and R_{ox} also show up at medium-low frequency range and are related with corrosion phenomenon.

Very good correlation was observed between experimental results and the equivalent circuit fitting model, as the Chi-squared (χ^2) calculated values were lower than 10^{-2} .

The different parameters acquired with impedance data fitting are collected in Table 4. 22.

Table 4. 22 - Parameters of the equivalent circuits (EC) used to describe the physical-chemical phenomenon of 76M:14G:10T+0,9wt.%gel (a) and 56M:14G:30T+0,9wt.%gel (b) coatings in contact with NaCl 3,5wt.% saline solution from 0h until 48h.

a) 76M:14G:10T+0,9wt.% gel							
t (h)	Time constants	R _{coat} (Ω.cm ²)	CPE _{coat} (F.cm ²)	n	R _{ox} (Ω.cm ²)	CPE _{ox} (F.cm ²)	n
0	2	27741	6,49E-8	0,92	1,0E20	2,98E-5	0,72
1,5	2	23204	9,35E-8	0,92	1,0E20	3,66E-5	0,74
3	2	21128	9,34E-8	0,91	1,0E20	3,89E-5	0,75
4	2	20568	9,99E-8	0,91	1,0E20	3,99E-5	0,75
6	2	20375	1,02E-7	0,91	1,0E20	4,09E-5	0,75
8	2	19682	1,03E-7	0,91	1,0E20	4,19E-5	0,76
10	2	18340	1,04E-7	0,91	1,0E20	4,35E-5	0,76
24	2	19287	1,23E-7	0,91	1,0E20	4,89E-5	0,80
48	2	30169	1,20E-7	0,91	1,0E20	4,61E-5	0,82

b) 56M:14G:30T+0,9wt.% gel										
t (h)	Time constants	R _{c-out} (Ω.cm ²)	CPE _{c-out} (F.cm ²)	n	R _{coat} (Ω.cm ²)	CPE _{coat} (F.cm ²)	n	R _{ox} (Ω.cm ²)	CPE _{ox} (F.cm ²)	n
0	3	547350	8,75E-8	0,93	1,0E20	1,26E-4	1,15	--	--	--
1,5	3	98	1,26E-7	0,96	1,0E20	7,60E-5	0,83	--	--	--
3	3	53887	2,37E-8	1,02	159350	3,10E-8	0,91	1,0E20	2,78E-5	0,63
4	3	74889	2,37E-8	1,02	139400	7,61E-8	0,85	1,0E20	4,54E-5	0,77
6	3	232	2,65E-7	0,83	185160	7,18E-8	0,99	1,0E20	5,89E-5	0,82
8	3	233	2,86E-7	0,84	176970	8,15E-8	1,00	1,0E20	5,73E-5	0,82
10	3	189	2,75E-7	0,83	166960	8,69E-8	1,01	1,0E20	5,70E-5	0,81
24	3	210	3,60E-7	0,84	39365	2,72E-8	1,05	1,0E20	6,56E-5	0,83
48	3	174	3,18E-7	0,86	92148	7,62E-8	0,98	1,0E20	6,60E-5	0,85

The electrolyte uptake in coatings can be monitored by the analysis of CPE_{coat} time evolution; on the other hand, R_{coat} evolution can provide information about the barrier properties of the coatings. In view of the before cited, diagrams of temporal evolution of CPE_{coat} and R_{coat} are exposed in Figure 4.67 and Figure 4.68.

RESULTS

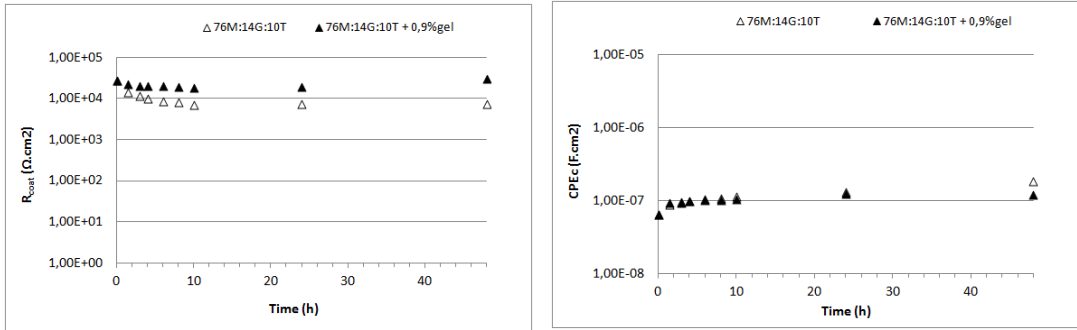


Figure 4. 67 - Evolution of dielectric properties R_{coat} (left) and CPE_{coat} (right) with immersion time evolution of 76M:14G:10T and 76M:14G:10T+0,9wt.% gelatine in NaCl 3,5wt.% solution from 0h until 48h.

Evolution of coating resistance (R_{coat}) and capacitance (CPE_{coat}) of pure 76M:14G:10T and with gelatine incorporation during immersion in NaCl saline solution is shown in Figure 4.67. Similar profiles were identified for both materials, decreasing R_{coat} and increasing CPE_{coat} with time evolution.

Gelatin incorporation to 76M:14G:10T coating results in a small increase of coating resistance and a slight decrease of coating capacitance. These results agree with the effects that gelatine molecules cause on the coating matrix structure, specifically, gelatine originate a more compact material with higher crosslinking degree (Figure 4.50). Consequently, the barrier effect is enhanced and water absorption (related with CPE_{coat}) decrease due to the reduction of the matrix interstitial spaces.

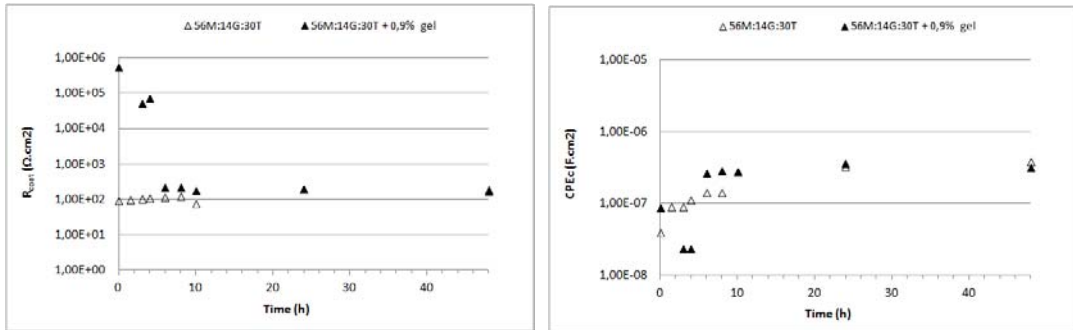


Figure 4. 68 - Evolution of dielectric properties R_{coat} (left) and CPE_{coat} (right) with immersion time evolution of 56M:14G:30T and 56M:14G:30T+0,9wt.% gelatine in NaCl 3,5wt.% solution from 0h until 48h.

Evolution of the resistance (R_{coat}) and water uptake (CPE_{coat}) of 56M:14G:30T pure and with 0,9wt.% gelatine incorporation is depicted in Figure 4.68.

Resistance values of coating with gelatine incorporation are evidently higher, particularly in the first 4h contact with the electrolyte. From 6h until 10h contact time the coating resistance is slightly higher than pure 56M:14G:30T and from 24h until the end of the experiment both materials show the same resistive abilities. Accordingly, CPE_{coat} of 56M:14G:30T + 0,9wt.% gelatin initially (0h until 4h) suggest lesser water uptake but from 6h contact with electrolyte until the end of the experiment go with pure 56M:14G:30T results.

Generally, gelatine incorporation improves or equalizes resistive pure coatings abilities improving its barrier effect. On the other hand, the water uptake was never enhanced by gelatine incorporation. The higher compactness and established improvement of crosslinking degree may be the cause for the better barrier effect against electrolyte access and diffusion.

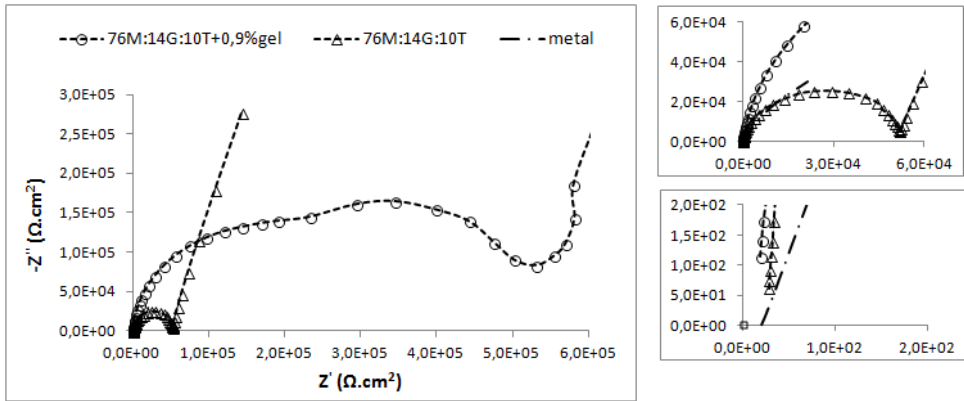
It is also important to notice that TEOS affect in a perceptible way the performance of hybrid coatings with gelatin incorporation. Although the profiles of 76M:14G:10T + 0,9wt.% gelatin and 56M:14G:30T + 0,9wt.% gelatine are similar, the higher content on TEOS (30%) still cause a drop of the coatings barrier effect and increasing of water uptake suggesting

RESULTS

an ease electrolyte access to the matrix and a consequent faster degradation process.

In order to better reproduce the physiological medium conditions on the EIS degradation study, the experiment was replicated using Hank's Balanced Salt Solution as electrolyte. This solution resembles the physiological fluids because it combines several inorganic salts (plus NaCl) and carbohydrates (see Table 4. 13) and results interesting the study of the interaction between this medium and the hybrid silica based-gelatin materials.

a)



b)

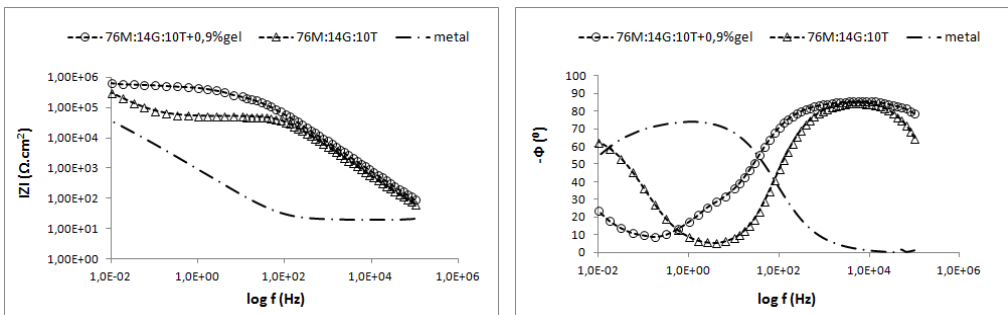


Figure 4. 69 - Nyquist diagram (a) and Bode plots (b) of 76M:14G:10T and 76M:14G:10T +0,9wt.% gelatine after 0h immersion in Hank's solution.

76M:14G:10T+0,9wt.% gelatine barrier performance, at 0h time contact with Hank's solution is depicted in Figure 4.69.

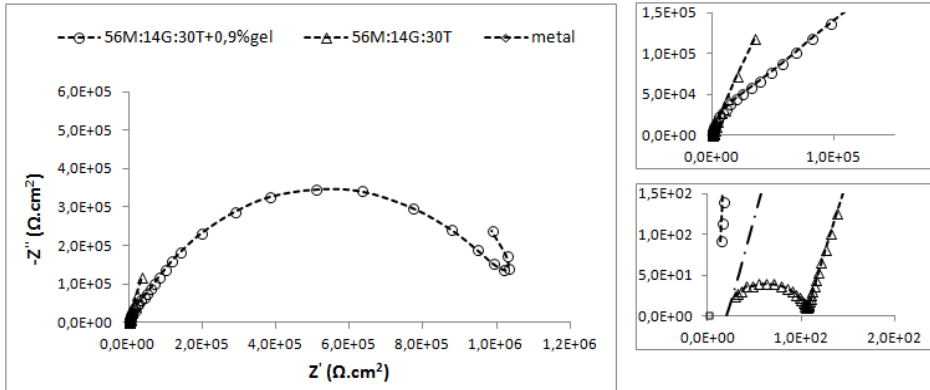
Hybrid coating immersion first instants generate a Bode plot with three time constants, two of them identified in low and medium frequency range and the third time constant registered at high frequency range. On the other hand, Nyquist diagram explicitly show, for this special case, two semi-circles corresponding to the two time constants detected at medium-high frequency range.

Pure 76M:14G:10T show a different behaviour, three time constants can also be identified at low, medium and high frequency ranges but displaced to higher frequency range. The displacement of the phase angle to lower frequency ranges when gelatine was incorporated predicts an improvement of the barrier properties, otherwise than the perceptible higher impedance modulus.

With this previous analysis of Nyquist and Bode plots, the three time constants identified at low and medium frequency range can be related with the metal corrosion process, the coating barrier performance and the resistive effect of an external layer. This external layer (high frequency range time constant) also detected in the results of series 90(M:G):10T and series 70(M:G):30T (Figure 4.37 and Figure 4.38) could be associated with external depositions from electrolyte, nevertheless, gelatin presence may possibly intensify the barrier effect of this external film.

RESULTS

a)



b)

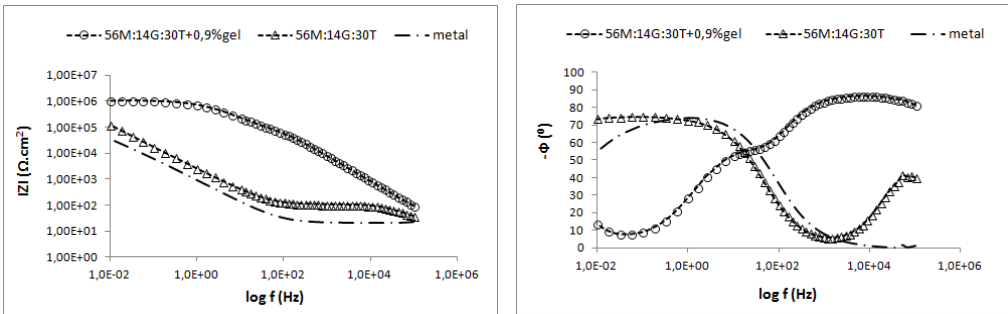


Figure 4. 70 - Nyquist diagram (a) and Bode plots (b) of 56M:14G:30T and 56M:14G:30T +0,9wt.% gelatine after 0h immersion in Hank's solution.

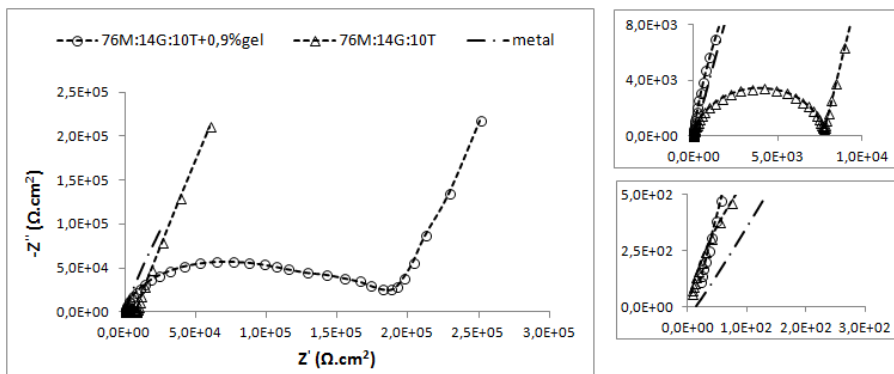
It can be seen in Figure 4.70 the Nyquist diagram (a) and Bode plots (b) of pure 56M:14G:30T and 56M:14G:30T+0,9wt.% gelatin at 0h contact time with Hank's solution.

Remarkable differences can be perceived on the Bode plots, the noticeable displacement of the two time constants (related with corrosion processes and barrier coating effect) identified for pure 56M:14G:30T from medium-high frequency ranges to lower frequency range otherwise than the third time constant that come into view only for 56M:14G:30T+0,9wt.% gelatine at medium frequency range. Therefore, there is clear evidence on the improvement of the barrier effect and anticorrosive properties of this coating when gelatine is incorporated: first the displacement of phase angle to lower frequency range predicts the

improvement on the barrier properties of the layers, in second place the impedance modulus magnification.

The results on the first instant contact with Hank's solution show that the coating imperfections caused by TEOS higher content (30%) are surpass by the structural changes induced by gelatine incorporation (generate a more compact material) and by the external layer of salts deposits from electrolyte (electrolyte uptake process becomes more complex).

a)



b)

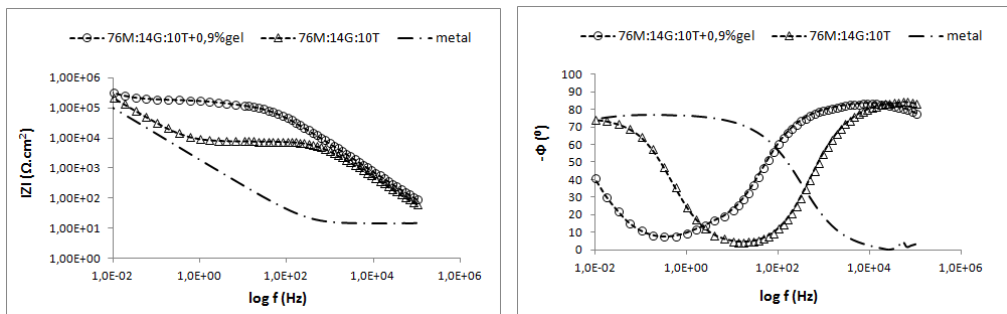


Figure 4. 71 - Nyquist diagram (a) and Bode plots (b) of 76M:14G:10T and 76M:14G:10T +0,9wt.% gelatine after 48h immersion in Hank's solution.

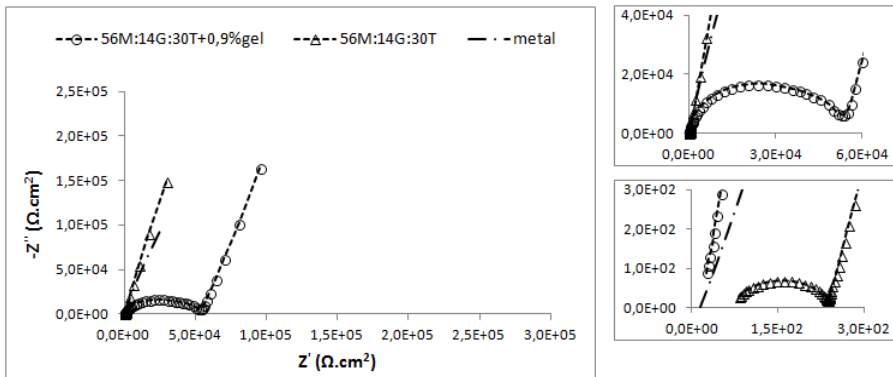
After 48h immersion time of 76M:14G:10T+0,9wt.% gelatin in Hank's solution the Bode plots show three time constants identified in low, medium and high frequency range (Figure 4.71 - b)). The first time

RESULTS

constant registered at low frequency range is related with metal corrosion processes, the second time constant placed at medium frequency range was attributed to the coating barrier properties and finally the third time constant identified at high frequency range was associated with an external layer of salts deposits from electrolyte. The displacement of phase angle to lower frequencies predicts an improvement on the resistive properties of the coating. This behaviour is also detectable on the capacitive profile registered for the coating (high frequency range) when gelatin was incorporated, besides the highest impedance modulus.

After 48h contact with Hank's solution the coating with 0,9wt.% gelatin incorporation still improves the pure biomaterial barrier performance.

a)



b)

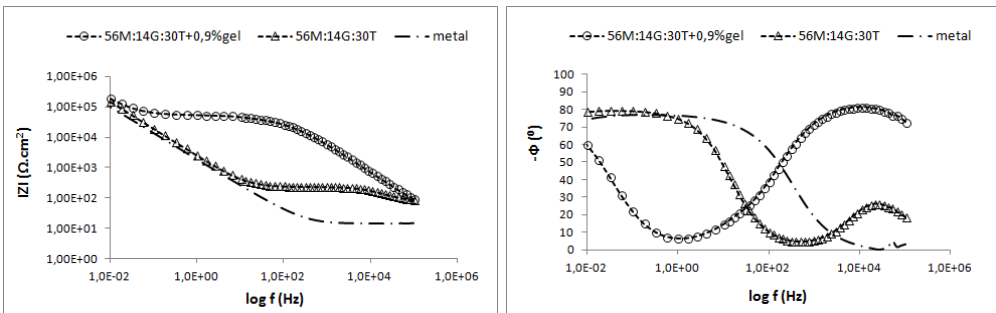


Figure 4. 72 - Nyquist diagram (a) and Bode plots (b) of 56M:14G:30T and 56M:14G:30T +0,9wt.% gelatine after 48h immersion in Hank's solution.

Figure 4.72 depicts the EIS spectra registered for 56M:14G:30T pure and with 0,9wt.% gelatin incorporation after 48h immersion in Hank's solution. Nyquist diagram of 56M:14G:30T+0,9wt.% gelatin show three semi-circles, two semi-circles correspond with the two time constants detected at low-medium frequency range in Bode plot related with corrosion processes and coating barrier properties, respectively, and a third semi-circle related with the time constant registered at medium-high frequency attributed to the external deposits film.

The displacement of the phase angle to lower frequency range, the higher impedance modulus and the change of the impedance profile from resistive behaviour to capacitive behaviour when gelatin was incorporated suggest that the natural degradation processes affect the general resistive performance of the coating but still preserve its better behaviour than pure 56M:14G:30T material.

Clearly, TEOS higher content (30%) still cause a decrease in impedance modulus, an obvious tendency in pure materials and gelatin hybrid coatings. The imperfections caused by TEOS in the first contact times with the electrolyte are surpassed by the compactness of the coating increased by gelatin addition. What is more, the external layer of deposits also helps in overcome the imperfections of the coatings (with gelatine incorporation). Nevertheless, degradation signs of the coatings with time evolution are evident as the TEOS content increase, possibly to the imperfections originated in the coatings matrices.

TEOS content represent the system element that most affect coatings performance (above other factors as GPTMS content and gelatine incorporation).

In order to better understand the deterioration mechanism of the coatings, EIS results were fitted using equivalent circuits (EC). The EC that best describe the impedance behaviour of the materials 76M:14G:10T+0,9wt.%gel and 56M:14G:30T+0,9wt.%gel immersed in Hank's solution is the one exposed in Figure 4. 70.

RESULTS

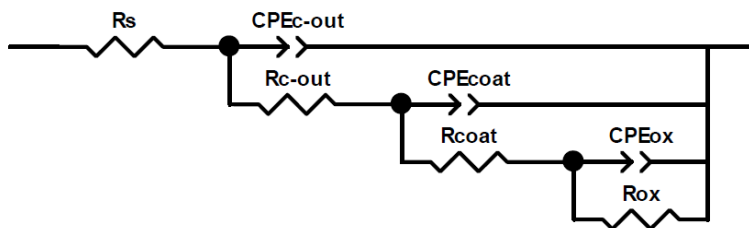


Figure 4. 73 - Equivalent circuit that best describe the impedance behavior of the hybrid systems 76M:14G:10T+0,9wt.%gelatin and 56M:14G:30T+0,9wt.%gelatin in contact with Hank's solution.

The coatings behavior was adjusted to the equivalent circuit represented by a solution resistance (R_s) connected in series with capacitive-resistive elements (CPE_{c-out} , R_{c-out}) related with the external film capacitance and resistance to the electrolyte inlet associated in parallel joined in series with capacitive-resistive elements (CPE_{coat} , R_{coat}) related with the sol-gel coating capacitance and pore resistance associated in parallel also joined in series with other capacitive-resistive elements (CPE_{ox} , R_{ox}) associated in parallel related with the stainless steel oxide layer (Figure 4.73).

Constant phase elements (CPE) instead of capacitors were used in the equivalent circuit models to take into account the dispersive character of the time constants and inhomogeneous properties of the layers.³⁵

R_s is the electrolyte resistance usually $\approx 9,5 \Omega \cdot \text{cm}^2$ for Hank's solution³⁵, R_{c-out} and CPE_{c-out} represent the high frequency range phenomenon related with the external film of depositions, R_{coat} (or R_{po}) and CPE_c (or CPE_{coat}) represent medium-high frequency range phenomenon associated with the coating degradation. CPE_{ox} and R_{ox} also show up at medium-low frequency range and are related with corrosion phenomenon.

Very good correlation was observed between experimental results and the equivalent circuit fitting model, as the Chi-squared (χ^2) calculated values were lower than 10^{-2} .

The different parameters acquired with impedance data fitting are collected in Table 4. 23.

Table 4. 23 - Parameters of the equivalent circuits (EC) used to describe the processes that take place when 76M:14G:10T+0,9wt.%gel and 56M:14G:30T+0,9wt.%gel coatings are immersed in Hank's solution from 0h until 48h.

a)

76M:14G:10T+0,9wt.% gel										
t (h)	Time constants	Rc-out ($\Omega.cm^2$)	CPEc-out ($F.cm^2$)	n	Rcoat ($\Omega.cm^2$)	CPEcoat ($F.cm^2$)	n	Rox ($\Omega.cm^2$)	CPEox ($F.cm^2$)	n
0	3	222150	3,15E-8	0,96	341730	4,18E-7	0,72	1,0E20	2,90E-5	0,82
1,5	3	142710	3,32E-8	0,95	224270	5,83E-7	0,73	1,0E20	3,23E-5	0,79
3	3	116710	3,38E-8	0,95	177960	6,80E-7	0,72	1,0E20	3,12E-5	0,76
4	3	111420	3,53E-8	0,95	174990	7,26E-7	0,70	1,0E20	3,60E-5	0,80
6	3	5089	5,44E-8	0,92	57603	2,92E-7	0,79	1,0E20	6,23E-5	0,84
8	3	5215	7,23E-8	0,90	58164	2,64E-7	0,80	1,0E20	6,21E-5	0,84
10	3	85528	3,66E-8	0,95	112880	1,01E-6	0,67	1,0E20	3,75E-5	0,79
24	3	80738	3,90E-8	0,94	74350	1,58E-6	0,65	1,0E20	4,00E-5	0,80
48	3	104140	4,33E-8	0,93	101750	1,72E-6	0,56	1,0E20	4,22E-5	0,85

b)

56M:14G:30T+0,9wt.% gel										
t (h)	Time constants	Rc-out ($\Omega.cm^2$)	CPEc-out ($F.cm^2$)	n	Rcoat ($\Omega.cm^2$)	CPEcoat ($F.cm^2$)	n	Rox ($\Omega.cm^2$)	CPEox ($F.cm^2$)	n
0	3	100610	2,59E-8	0,97	955790	1,87E-7	0,72	1,0E20	6,68E-5	1,03
1,5	3	71214	2,72E-8	0,97	342700	2,76E-7	0,74	1,0E20	4,74E-5	0,83
3	3	62533	2,83E-8	0,97	173370	3,76E-7	0,74	1,0E20	4,71E-5	0,80
4	3	55061	2,88E-8	0,97	126250	4,52E-7	0,73	1,0E20	4,99E-5	0,81
6	3	46024	3,07E-8	0,96	73629	6,84E-7	0,70	1,0E20	5,47E-5	0,81
8	3	39999	3,15E-8	0,96	49821	9,79E-7	0,66	1,0E20	5,57E-5	0,81
10	3	26906	2,88E-8	0,97	57071	1,70E-6	0,46	1,0E20	5,68E-5	0,85
24	3	27317	4,79E-11	1,05	54257	2,02E-7	0,74	1,0E20	5,72E-5	0,81
48	3	34381	5,99E-8	0,91	20094	1,18E-6	0,77	1,0E20	5,83E-5	0,84

The electrolyte uptake in coatings can be monitored by the increase in CPE_{coat} as well as R_{coat} can be correlated with the compactness of the

RESULTS

coating, for that reason diagrams of temporal evolution of the upper cited parameters are exposed in Figure 4.74 and Figure 4.75.

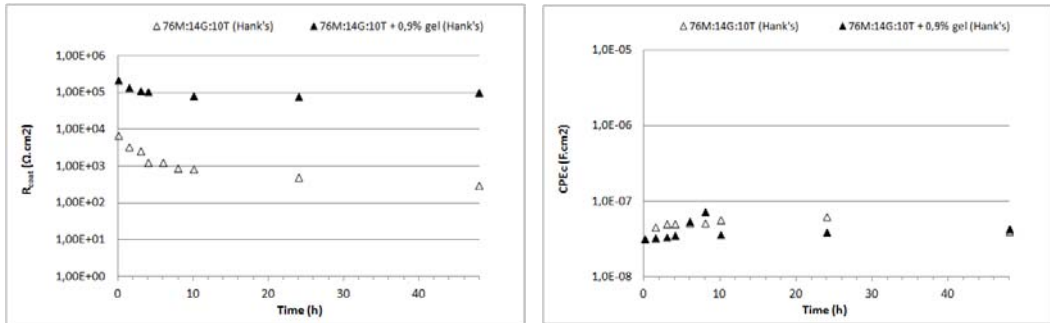


Figure 4. 74 - Time evolution of pure 76M:14G:10T and 76M:14G:10T+0,9wt.%gelatine coatings properties R_{coat} (left) and CPE_{coat} (right) immersed in Hank's solution from 0h until 48h.

The results for 76M:14G:10T with 0,9wt.% gelatin incorporation show a magnification on the R_{coat} in comparison with pure 76M:14G:10T, already detected on Nyquist and Bode plots previous analysis (Figure 4.69, Figure 4.71). The R_{coat} magnitude of pure 76M:14G:10T is $1E+3$ ($\Omega.cm^2$) and when gelatine is incorporated to the matrix rise to $1E+5$ range ($\Omega.cm^2$) (Figure 4.74).

The profile of R_{coat} shows an expectable decrease of coating resistive ability with time evolution. However, 76M:14G:10T+0,9wt.% gelatin remains fairly constant from 10h until the end of the experiment, on the other hand, pure 76M:14G:10T show a decreasing tendency from the beginning until the end of the experiment revealing major coating deterioration with time evolution.

CPE_{coat} profiles of pure 76M:14G:10T and 76M:14G:10T+0,9wt.% gelatin are similar and show a constant trend during all the experimental time.

Generally, gelatin incorporation causes a significant increasing of the barrier effect of the coating without affecting in an important manner the electrolyte uptake capacity.

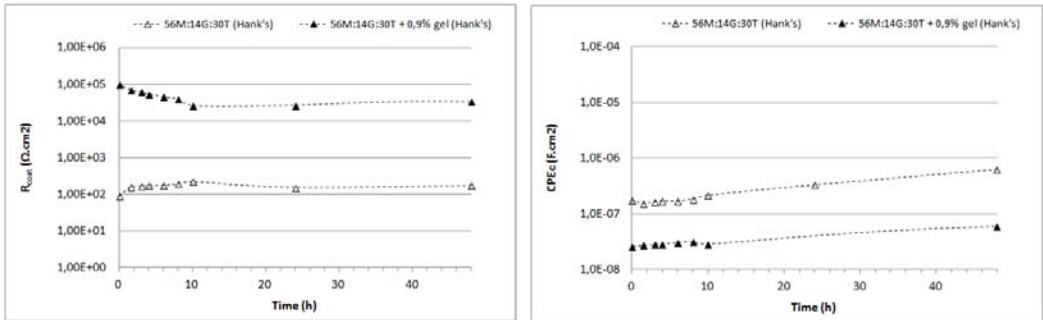


Figure 4.75 - Time evolution of pure 56M:14G:30T and 56M:14G:30T+0,9wt.% gelatine coatings properties R_{coat} (left) and CPE_{coat} (right) immersed in Hank's solution from 0h until 48h.

The results for 56M:14G:30T with 0,9wt.% gelatin incorporation show a magnification on the R_{coat} already detected on Nyquist and Bode plots previous analysis (Figure 4.70 and Figure 4.72). The R_{coat} magnitude of pure 56M:14G:30T is $1E+2$ ($\Omega \cdot cm^2$) and when gelatine is incorporated to the matrix rise to $1E+4$ range ($\Omega \cdot cm^2$) (Figure 4.75).

The profile of 56M:14G:30T+0,9wt.% gelatin R_{coat} shows an expectable decrease of coating resistive ability with time evolution. However, pure 56M:14G:30T show a constant trend during all the experiment.

56M:14G:30T+0,9wt.% gelatin reveal major coating deterioration with time evolution nonetheless the barrier effect of this coating is always higher than pure 56M:14G:30T.

CPE_{coat} profiles of pure 56M:14G:30T and 56M:14G:30T+0,9wt.% gelatin are similar and show a growing trend during all the experimental time. However, ΔCPE_{coat} is analogous for pure 56M:14G:30T and 56M:14G:30T+0,9wt.% gelatin coatings the magnitude of 56M:14G:30T+0,9wt.% gelatin biomaterial is clearly inferior revealing less electrolyte uptake. This result suggests that gelatin incorporation, in this special case, generate a matrix with less ability for water uptake.

Finally, gelatin incorporation to compositions with different TEOS content produces materials with different abilities. Though the coatings barrier

RESULTS

effect is always improved when gelatin is incorporated, independently from TEOS content, the electrolyte uptake is clearly reduced for the composition with 30% TEOS.

Important to notice that, although the performance of pure composition with 30% TEOS is without doubt inferior to the performance of pure 10% TEOS composition, the improvements caused by gelatin addition are more noticeable.

The study of the hydrolytic degradation is also interesting and complements EIS results about coatings deterioration. In addition if one of the strategies of this new materials is to improve the osseointegration process by means of Si release (osteoinductive ability) is imperative to know the degradation kinetics of the coatings 76M:14G:10T and 56M:14G:30T with gelatin incorporation.

Hydrolytic degradation of the hybrid coatings was evaluated by measuring the weight loss with time evolution (until 63 days). Figure 4.76 and Figure 4.77 show the dissolution profiles of pure 76M:14G:10T, 76M:14G:10T+0,9wt.% gelatine, pure 56M:14G:30T and 56M:14G:30T+0,9wt.% gelatin.

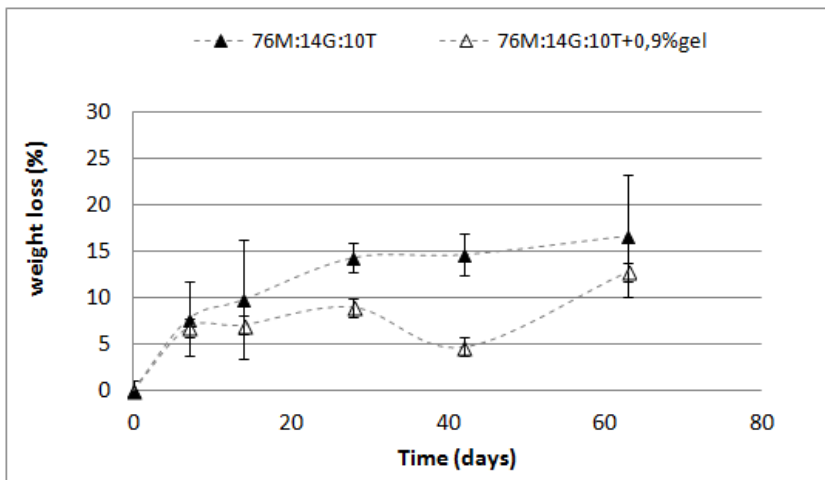


Figure 4. 76 - Dissolution profiles of pure 76M:14G:10T and 76M:14G:10T+0,9wt.% gelatin.

The weight loss of pure 76M:14G:10T was significantly affected by gelatin incorporation, decreasing it from $\approx 16,5\%$ to $\approx 12,5\%$.

Hydrolytic degradation show two different stages, a faster degradation rate characteristic of the first 14 days and a slower degradation second stage from 23 days until 63 days.

As the experiment was accomplished with plentiful water to avoid Si saturation, the dissolution process depends mainly on the ability of the aqueous medium to diffuse through the matrix. The flexibility of gelatin molecule causes an increase of the biomaterials compactness otherwise than generate flat surfaces (Figure 4.56).²⁰

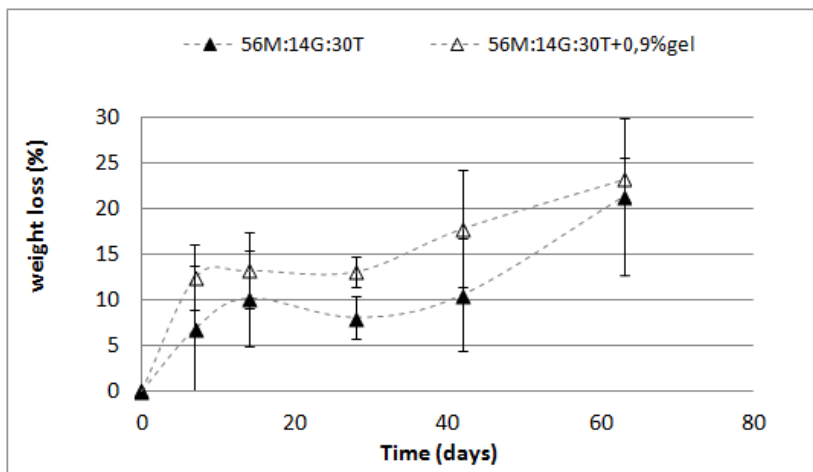


Figure 4. 77 - Dissolution profiles of pure 56M:14G:30T and 56M:14G:30T+0,9wt.% gelatin.

Surprisingly, gelatin incorporation to 56M:14G:30T biomaterial cause an increasing of weight loss as it can be appreciate in Figure 4.77.

Hydrolytic degradation profiles are similar to pure 56M:14G:30T and 56M:14G:30T+0,9wt.% gelatin, with two different degradation stages. An initial (first 7 days) and faster degradation stage is followed by a slower degradation stage from 14 days until 63 days. The second stage show an increasing weight loss trend until reach about 23% and 21% for 56M:14G:30T+0,9wt.% gelatin and pure 56M:14G:30T respectively.

RESULTS

This hydrolytic degradation results suggest that the TEOS content (30%) affects in a superior way the coatings structure than gelatin incorporation, that is to say, the imperfections caused by TEOS silane affects largely the diffusion process than the higher compactness caused by the flexible gelatin molecules.

As the aqueous medium used in the present hydrolytic degradation experiment does not have any mineral salts, the equilibrium between structural changes induced by TEOS content and gelatin incorporation are the two main factors that play a significant role in the degradation process.

BIOLOGICAL PERFORMANCE

CELL-BIOMATERIAL INTERACTION *IN VITRO*

The influence of the sol-gel biocoatings in osteoblastic cell line MC3T3 proliferation and mineralization was evaluated *in vitro*.

As reference material in *in vitro* biological experiments was used the cp Ti (commercially pure titanium) surface without any coating. In addition, 50M:50G coating is also mentioned as reference biomaterial as the main goal of the new materials developed on this work is the improvement of its biocompatibility.

Preliminary cytocompatibility evaluation of the coatings was conducted and the results are exposed in Figure 4.78 and Figure 4.79.

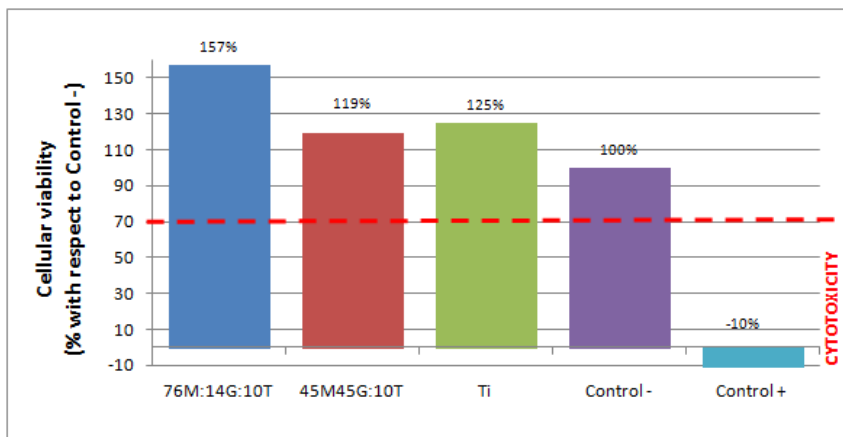


Figure 4. 78 - Cell viability results for 76M:14G:10T and 45M:45G:10T sol-gel coatings and for titanium substrate. The cell culture dish was used as control - and latex was used as control +.

The assayed materials of series 90(M:G):10T are not cytotoxic as any of the silica based coatings show cellular viability minor than 70% (cellular viability limit established in ISO 10993-5 that entails the standards for the Biological evaluation of medical devices) (Figure 4.78).

RESULTS

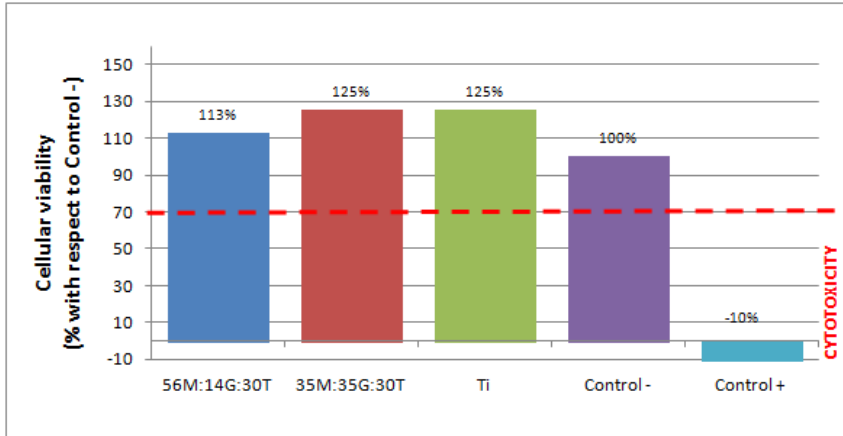


Figure 4. 79 - Cell viability results for 56M:14G:30T and 35M:35G:30T sol-gel coatings and for titanium substrate. The cell culture dish was used as control - and latex was used as control +.

The assayed materials of series 70(M:G):30T are not cytotoxic as it can be seen in Figure 4.79. 35M:35G:30T and 56M:14G:30T coatings show cellular viability superior to 70% (cellular viability limit established in ISO 10993-5 that entails the standards for the Biological evaluation of medical devices).

The addition of MTMOS and TEOS to pure GPTMS seems to reduce its toxic character as detected in previous works.^{1,5} However, 10% TEOS content materials were found to allow higher cellular viability than 30% TEOS content compositions.

The following cellular proliferation and mineralization results are presented as percentage taking as reference the titanium substrate used in each well plate. As example, the data associated with material A normalized with respect to titanium substrate will be:

$$D.O._{(respect\ to\ Ti\ reference)} = \frac{D.O._{(material\ A)}}{D.O._{(Ti)}} \times 100$$

That is to say, 100% D.O. corresponds to the titanium metal substrate reference cellular proliferation and mineralization performance.

Cellular proliferation on titanium coated with 90(M:G):10T and 70(M:G):30T series biomaterials was measured and the results are collected in Figure 4.80 and Figure 4.81.

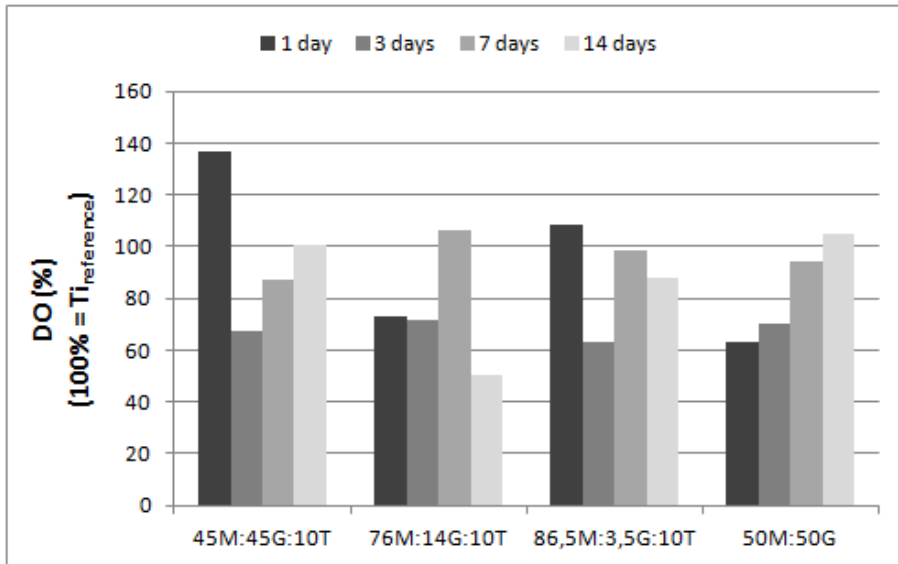


Figure 4.80 - Cellular proliferation of coated titanium with 90(M:G):10T series coatings and reference material 50M:50G. (Titanium substrate match with 100% DO) Measured absorbance at 570 nm.

The results show that reference material 50M:50G does not achieve the titanium reference performance until 14 days culturing time suggesting an increase of cellular activity with time evolution.

Triple compositions results does not show a clear relation between GPTMS content and cellular proliferation as 45M:45G:10T and 86,5M:3,5G:10T apparently show the best results and most similar to cellular behavior on titanium surfaces. Both compositions show the best proliferation results for 1 day culturing time (higher than titanium cells growth) and after that time proliferation results decrease significantly (69% and 45% respectively). 45M:45G:10T show a progressive

RESULTS

improvement until reach titanium cellular activity at 14 days culturing time and 86,5M:3,5G:10T shows a significant increase after 7 days culturing time (43%) followed by a slight decrease at 14 days culturing time below titanium proliferation results.

76M:14G:10T coating shows the lowest results on cellular proliferation with a maximum registered for 7 days culturing time (only 6% above titanium proliferation results) and a final cellular proliferation result of 50% than the cellular activity registered for titanium substrate for the same 14 days culturing time.

It is not noticeable a significant improvement on 50M:50G reference material cellular proliferation activity by any of the new developed coatings, only noticeable the apparent cellular attachment and proliferation enhancement registered for 45M:45G:10T coating at 1 day culturing time.

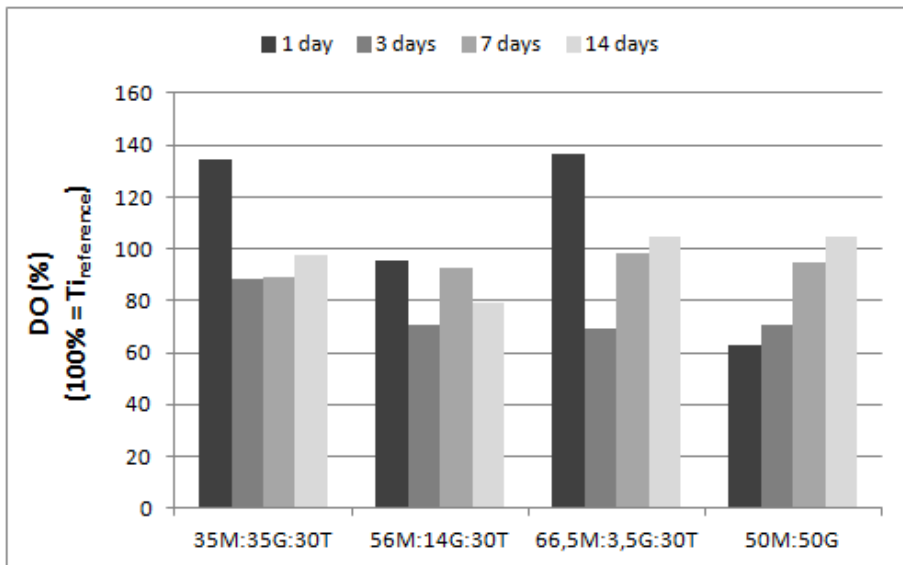


Figure 4.81 - Cellular proliferation of coated titanium with 70(M:G):30T series biocoatings and reference material 50M:50G. (Titanium substrate match with 100% DO) Measured absorbance at 570 nm.

It is interesting to notice that in this series it is not possible to find any relation between GPTMS content and proliferation results, nevertheless,

the patron followed on series 90(M:G):10T may be find on this series 70(M:G):30T proliferation results. That is to say, compositions with higher and lower GPTMS content show the best results. As verified previously, 35M:35G:30T and 66,5M:3,5G:30T show an exceptional result at 1 day culturing time clearly improve titanium substrate results in cellular proliferation. What is more, a similar patron identified on 10% TEOS series materials was detected on this 30%TEOS series where 35M:35G:30T coating after 1 day of culturing time induce a strong decrease on cellular proliferation (46%) followed by a progressive improvement until almost reach titanium substrate level. Besides, 66,5M:3,5G:30T coating after the excellent results from 1 day culturing also suffer a strong decrease on cellular proliferation (67%) followed by a progressive improvement until reach titanium proliferation results and reference material 50M:50G.

Increasing TEOS content from 10% to 30% clearly involve an improvement on cellular proliferation. In addition, TEOS incorporation to the reference material 50M:50G affects hydrophilic properties of the surface usually increasing it, possibly due to an increment on -OH available groups (see contact angle results Table 4.7 and Table 4.8).

Taking into account that hydrophilic properties affects in a special way cellular activity the better results on cellular proliferation detected for 35M:35G:30T could be due to the TEOS content on this composition and higher disposition of -OH groups consequence of a lower condensation rate verified on rubbing tests results (Table 4.3).

The bone regeneration process is a complex mechanism that follows a specific order, initiation and ceasing of proliferation, the onset of differentiation and beginning of mineralization.

For that reason, besides cellular proliferation results and proved non cytotoxic effect of the developed coatings (Figure 4.78 and Figure 4.79) it is also important to identify cellular mineralization on biomaterials surface in order to verify a proper cellular activity.

RESULTS

ALP (alkaline phosphatase) is an enzyme expressed by cells during osteogenesis and is widely used as primary marker for cellular differentiation.⁴² Accordingly, to get a proper relation between the cellular quantity and the ALP (for a certain time period) the protein concentration (related with the concentration of adhered cells) was analyzed by bicinchromic acid (BCA) assay.

Figure 4.82 and Figure 4.83 show the mineralization rate on the different coated surfaces after 7 and 14 days in culture.

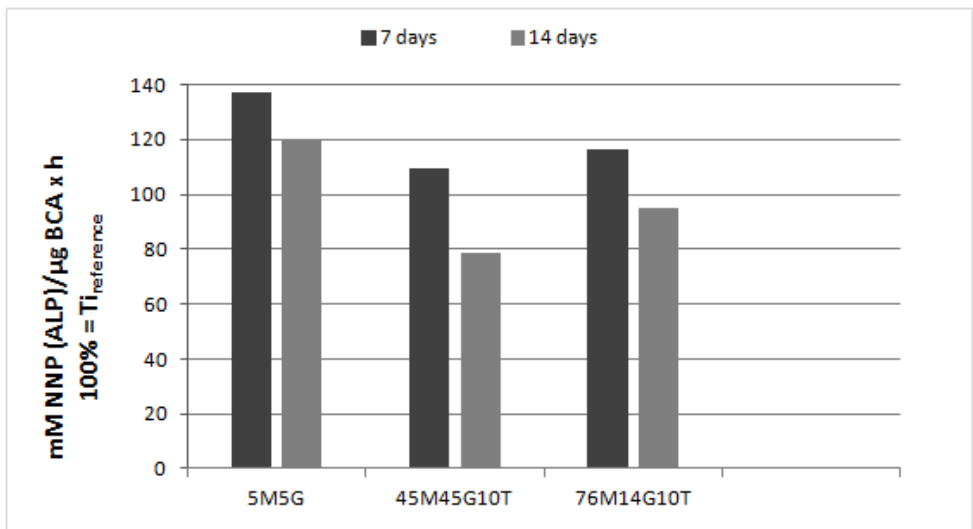


Figure 4. 82 - Mineralization rate (mM NNP(ALP)/ μ g BCA x h) of coated titanium with 90(M:G):10T series biocoatings and reference material 50M:50G. (Titanium substrate match with 100% mineralization rate)

ALP activity of the coatings 45M:45G:10T and 76M:14G:10T apparently decrease in comparison with the cellular results achieved for reference material 50M:50G. However, on the 7 days coated substrates with series 90(M:G):10T materials the cellular activity was slightly better than the titanium substrate (without any coating) mineralization rate.

On the other hand, ALP activity on 14 days coated samples were significantly lower (20-30% approximately) than that measured on 7 days for all sol-gel coatings (included reference material 50M:50G), possibly

due to the degradation process of the layers and consequential instability of surface structure.

In addition, ALP activity registered for 14 days on coated substrates with 45M:45G:10T and 76M:14G:10T was lower than uncoated titanium substrate.

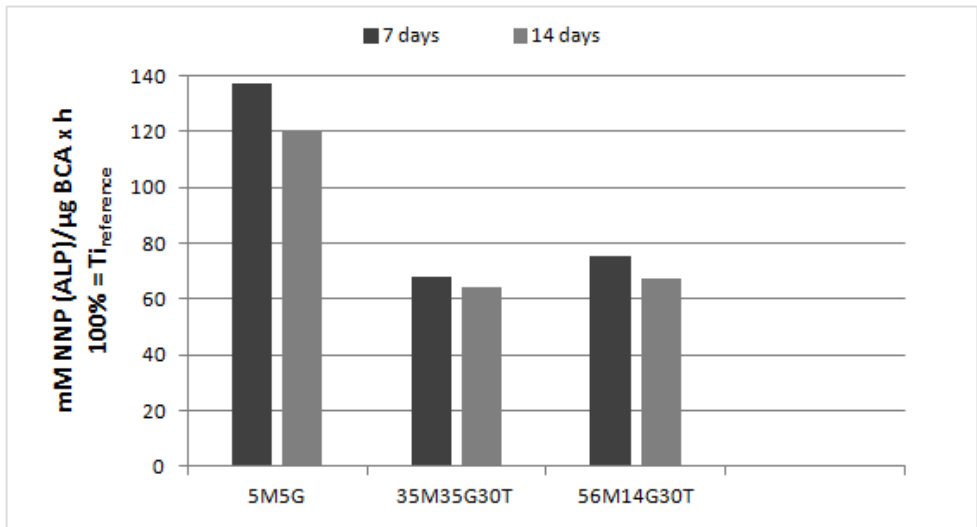


Figure 4. 83 - Mineralization rate (mM NNP(ALP)/µg BCA x h) of coated titanium with 70(M:G):30T series coatings and reference material 50M:50G. (Titanium substrate match with 100% mineralization rate)

Figure 4.83 show a remarkable decrease of ALP activity on coated substrates with series 70(M:G):30T biocoatings, with worse mineralization rate than uncoated titanium substrate and reference material 50M:50G.

Series 70(M:G):30T materials mineralization results show that the ALP activity at 14 days was considerably lower than those measured at 7 days for all sol-gel coatings (14 days: 3,5% and 7 days: 8 %), possibly due to a degradation process of the layers and consequential instability of surface structure. Furthermore, the hydrolytic degradation results (Figure 4.46) corroborates the suspicion about the instability of surface as the degradation kinetics of 35M:35G:30T and 56M:14G:30T for the first 14 days contact is slower than series 90(M:G):10T materials leading to a

RESULTS

minor difference on mineralization results between the studied cellular culture times (7 days and 14 days).

The higher dissolution level registered for series 70(M:G):30T materials (Figure 4.43) may give an explanation for the low cellular mineralization rate achieved on these coatings. Cellular activity may be affected by the instable surface activated by a degradation dynamic process.

The results show that cellular mineralization is specially affected by TEOS incorporation to the sol-gel coatings as it diminish the cellular mineralization rate registered for 50M:50G reference material. The new structural characteristics motivated by TEOS silane, as the magnification of surface imperfections and ease access of any aqueous medium, does not enhance cellular mineralization; nevertheless, in the first days of culturing time tri-silane composition new materials seems to improve cellular proliferation (with respect to reference material 50M:50G) possibly due to the Si ion release as an active ingredient that previously was referred as an element with ability to increased osteoblastic activity.^{42,2,3,4}

***IN VIVO* STUDY**

The evaluation of the *in vivo* performance of a biomaterial is crucial to come to a decision about its employment as biocompatible and bioactive external layer on metallic prosthetic devices.

From a materials science point of view, the new coatings of series 90(M:G):10T and 70(M:G):30T respect the minimum requirements of a coating with ability to protect against a possible initial corrosion products exchange between the metallic implant and the physiological surrounding medium. Besides, the improvement of the *in vitro* degradability behavior of reference material 50M:50G was reached (Figure 4.45 and Figure 4.46), this result leads to the expectation of better results on *in vivo* experiments.

Taking into account the *in vitro* measurements on wettability with results within 60-80° that prove the hydrophilic trait of sol-gel coatings (Table 4.7 and Table 4.8) and the surface roughness results (Figure 4.23 and Figure 4.24), 45M:45G:10T and 35M:35G:30T represent the most suitable biomaterials with regard to surface properties.

On the other hand, from a structural integrity point of view, EIS experiments show that 70(M:G):30T series materials have a structure with more imperfections (Figure 4.36) leading to an ease diffusion process throughout the matrix and consequently higher degradation degree possibly matching with higher silicon release.

Finally, *in vitro* cellular tests on proliferation show that 45M:45G:10T and 35M:35G:30T compositions improve in an important manner cellular proliferation at the first contact time and though it decreases after 3 days recovers until a rank similar to reference material (50M:50G) and to titanium uncoated substrate (Figure 4.80 and Figure 4.81). Otherwise, mineralization results does not show good cellular mineralization capability over the new trisilane coatings perhaps due to the instability of the matrix caused by the degradation process kinetics.

Considering all the experimental results of surface properties, structural integrity and cellular bioactivity the selected coating to be tested *in vivo* was 35M:35G:30T. It is expected that this designated trisilane composition improve on the degradation performance of the reference biomaterial (50M:50G) avoiding the formation of a fibrous capsule and increasing the biocompatibility.

In vivo study entails several measurements in order to evaluate the biocompatibility, rate of osseointegration and degradation ability of the coating. With optical microscopy was possible to make a histological study and degradation degree estimation of the biomaterial.

A full cross section of 50M:50G coated titanium implant after 8 weeks healing time is shown in Figure 4.84.

RESULTS



Figure 4.84 - Cross section of coated implants with 50M:50G reference material after 8 weeks healing time (light microscope images 1000X). (reproduced by courtesy of ¹)

Full cross sections of implanted titanium screws coated with 35M:35G:30T were observed and representative images of 1 week and 2 weeks healing time are presented in Figure 4.85 and Figure 4.86.

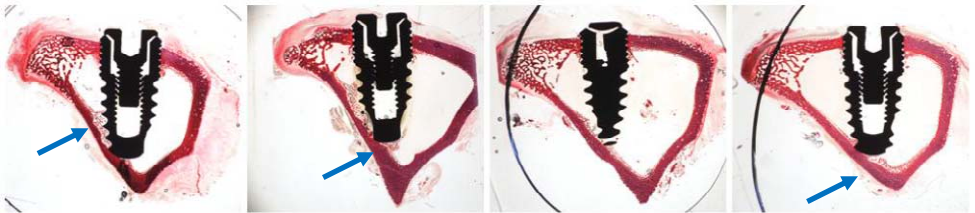


Figure 4.85 - Cross section of coated implants with 35M:35G:30T after 1 week healing time (light microscope images 1000X). (reproduced by courtesy of ¹)

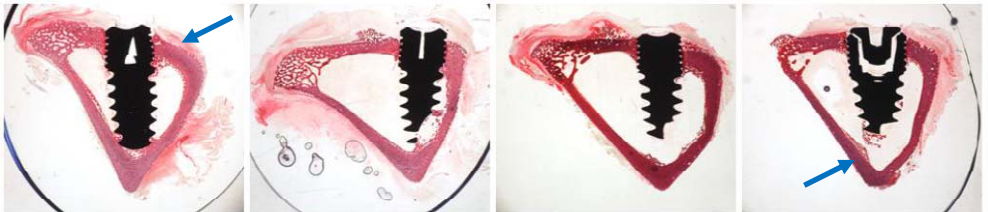


Figure 4.86 - Cross section of coated implants with 35M:35G:30T after 2 weeks healing time (light microscope images 1000X). (reproduced by courtesy of ¹)

Titanium implants without any coating were also observed and full cross sections of 1 week and 2 weeks healing times are illustrated in Figure 4.87 and Figure 4.88.

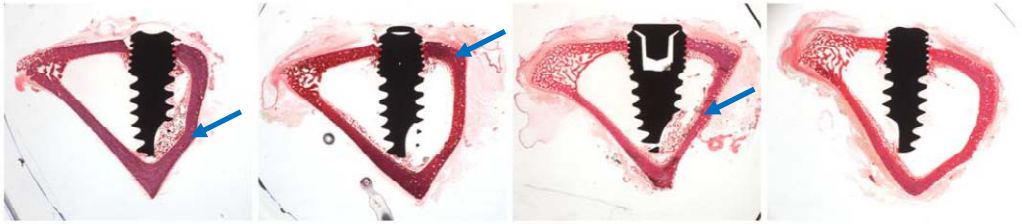


Figure 4. 87- Cross section of uncoated titanium implants after 1 week healing time (light microscope images 1000X). (reproduced by courtesy of ¹)



Figure 4. 88 - Cross section of uncoated titanium implants after 2 weeks healing time (light microscope images 1000X). (reproduced by courtesy of ¹)

Reference material (50M:50G) coated implant cross section does not show any sign of new bone formation (Figure 4.84), nevertheless, new triple composition material (35M:35G:30T) coated implant (Figure 4.85 and Figure 4.86) and uncoated titanium implant (Figure 4.87 and Figure 4.88) show in some images activity in trabecular bone area (sign with arrows).

Generally, after visualization of the cross section implants seems like the sol gel coating 35M:35G:30T do not show a clear advantage with respect to uncoated titanium implants.

Nevertheless, to make a correct evaluation of the biocompatibility of the new biomaterial 35M:35G:30T several parameters were taken into account, namely, bone marrow condition, signs of inflammation and fibrous capsule presence/condition.

Bone marrow condition:

RESULTS

At the study periods (1 and 2 weeks), bone marrow show a traumatic architecture with altered physiological balance between fat cells and blood cells. Precisely, it was detected low proportion of marrow fat cells and extensive cellular load at the bone marrow tissue especially in close proximity to the implants.

It was stated in bibliography¹¹ that bone marrow architecture was modified to traumatic and aplasic tissue when in contact with titanium implant coated with the reference material 50M:50G (Figure 4.89). However, the tissue recovers its physiological balance between fat cells and blood cells at 8 weeks healing times though it does not achieve the initial proportion before implantation.

Fibrous capsule formed around the implants in the bone marrow contact areas is in evidence in Figure 4.89 (right image).

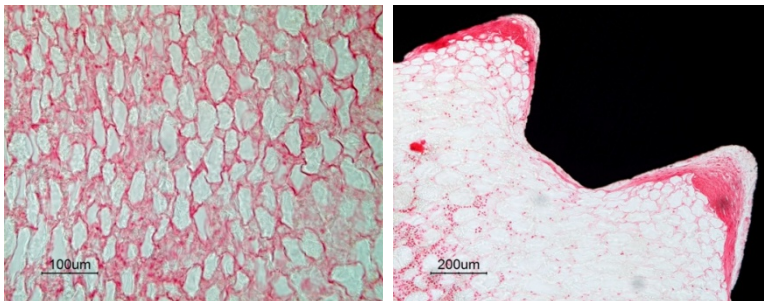


Figure 4. 89 - Light microscope image of bone marrow in contact with titanium implant coated with 50M:50G reference material after 1 week healing time (left) and after 8 weeks healing time (right).¹¹

35M:35G:30T coated implants generates a gross fibrous tissue with lax condition after 1 week healing time that changes into a dense condition and reduces considerably its thickness after 2 weeks healing time. Fibrous capsule evolution formed around the implants in the bone marrow contact areas is in evidence in Figure 4.90 and Figure 4.91. The bone marrow acquire the characteristics of a traumatic tissue, with low

content on fat cells with apparent traumatic structure and exaggerated blood cells content, for 1 week and 2 weeks healing times

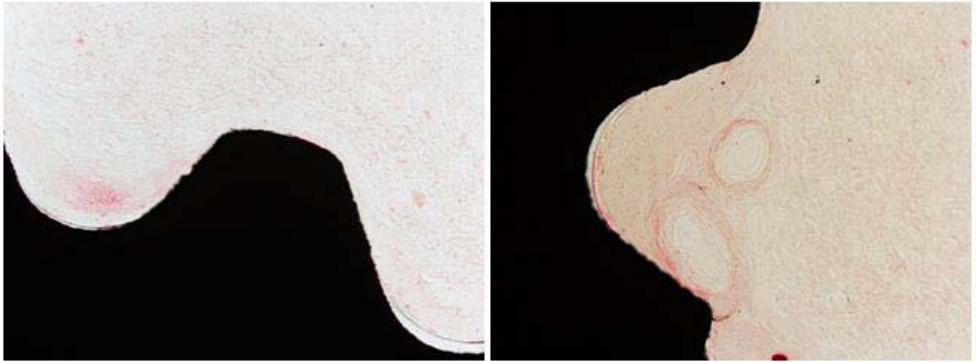


Figure 4.90 - Light microscope images (10X) of fibrous capsule of coated implants with 35M:35G:30T (marrow contact area) after 1 week healing time. (reproduced by courtesy of ¹)

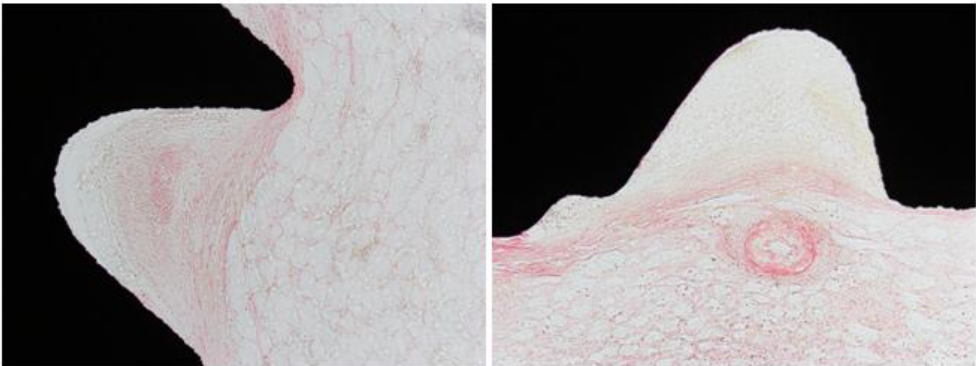


Figure 4.91 - Light microscope images (10X) of fibrous capsule of coated implants with 35M:35G:30T (marrow contact area) after 2 weeks healing time. (reproduced by courtesy of ¹)

Uncoated titanium implants, named as control, generates also a traumatic bone marrow tissue at short periods (1 week - Figure 4.92) accompanied by cellular aplasia, but the tissue starts a noticeable restore process at 2 weeks healing time (Figure 4.93).

RESULTS

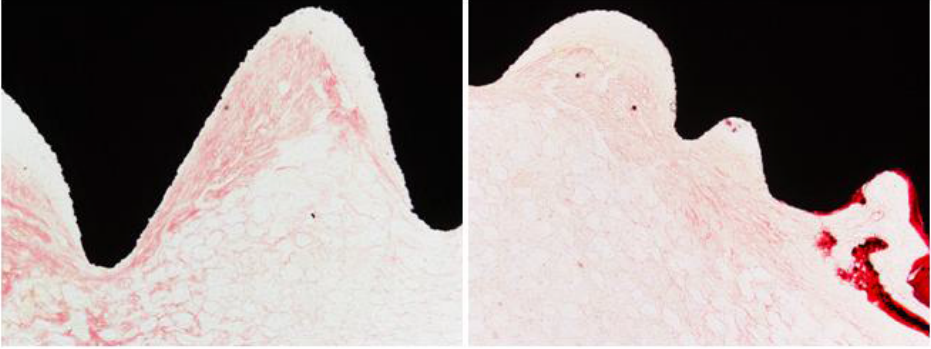


Figure 4.92 - Light microscope images (10X) of fibrous capsule of uncoated implants (control) (marrow contact area) after 1 week healing time. (reproduced by courtesy of ¹)



Figure 4.93 - Light microscope images (10X) of fibrous capsule of uncoated implants (control) (marrow contact area) after 2 weeks healing time. (reproduced by courtesy of ¹)

No signs of infection around the implants were observed for the evaluated samples. Exceptionally, foreign-body giant cells were detected at 2 weeks healing time in some uncoated titanium implants (control) samples in a small proportion not assigned to an infection process but to a normal foreign-body response (Figure 4.94). No foreign-body giant cells were detected for coated implants with 35M:35G:30T or reference material 50M:50G in the experimental study periods.

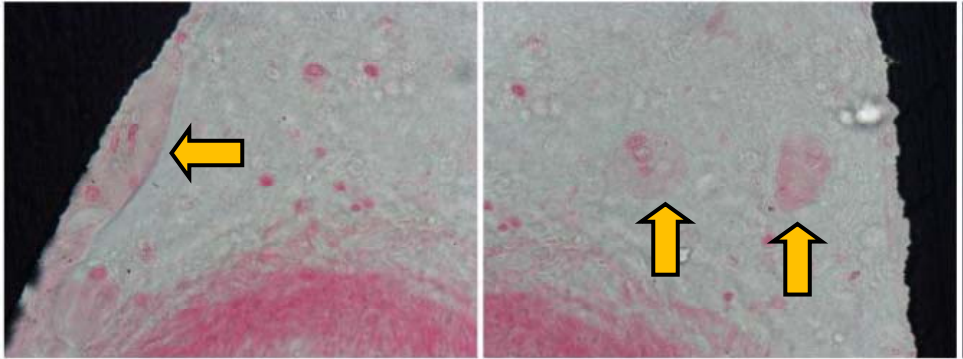


Figure 4.94 - Light microscope images (10X) of foreign-body giant cells detected at 2 weeks healing time of implantation of uncoated implants (control). (reproduced by courtesy of ¹)

All the implanted samples (35M:35G:30T, reference material and uncoated titanium implants) show a gross fibrous tissue with lax condition after 1 week healing time that changes into a dense condition that reduces considerably its thickness after 2 weeks healing time. This fibrous tissue was found in the areas without direct contact with bone tissue (marrow space).

Besides biocompatibility, a study about the osseointegration of coated implants and uncoated implants was made. With that purpose two special areas, implant in contact with cortical bone and implant in contact with trabecular bone will be considered from now on (Figure 4.95). Those areas are especially important because cortical bone is the tissue that sets with the implant the initial primary stability that will allow the neoformation of trabecular bone around the implant conducting to a biological long-term stability also identified as secondary stability. On the other hand, if the primary stability takes place, new trabecular bone formation can happen in areas in contact with implant surface (trabecular bone area) basis of the secondary stability and indicative of implantation success.

RESULTS

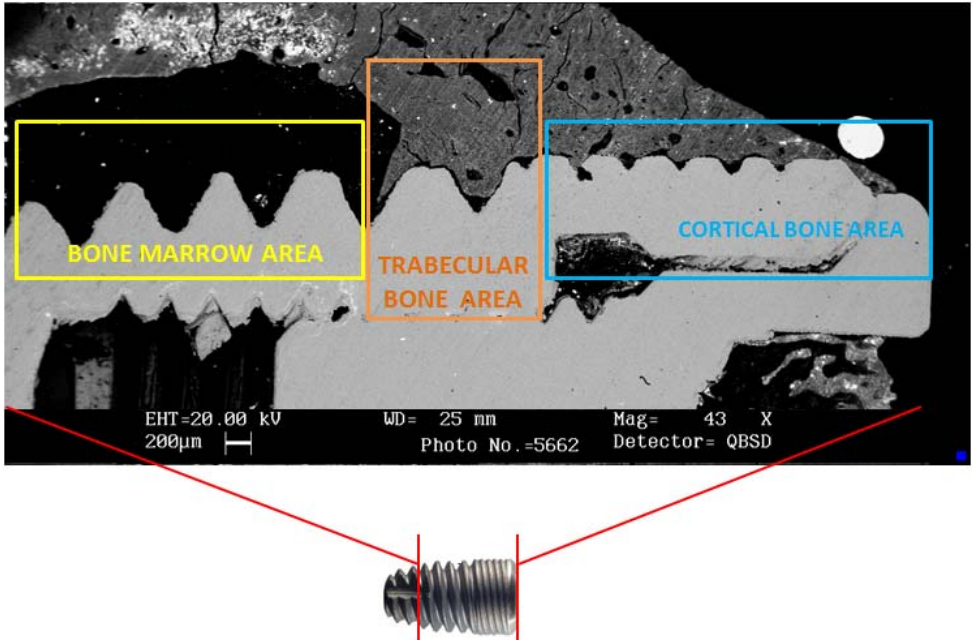


Figure 4. 95 - Schematic representation of revised areas in *in vivo* osteointegration study.

Osseointegration in cortical bone:

In a previous research work with 50M:50G (reference material)¹¹ it was stated that there was not identified a total osseointegration in the cortical bone contact area because a thin fibrous layer was formed between bone and coated implants.

Figure 4.96 and Figure 4.97 show the contact interface between coated titanium implants with 35M:35G:30T and cortical bone at 1 week and 2 weeks healing times respectively.

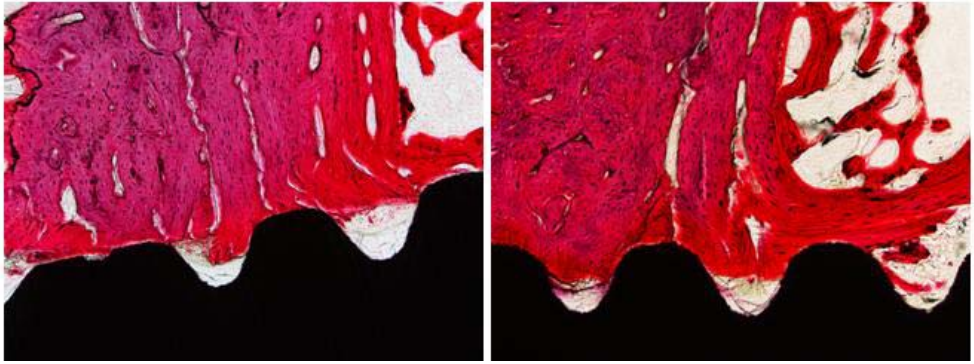


Figure 4.96 - Light microscope images (10X) of in vivo samples of coated implants with 35M:35G:30T in contact with cortical bone after 1 week healing time. (reproduced by courtesy of ¹)

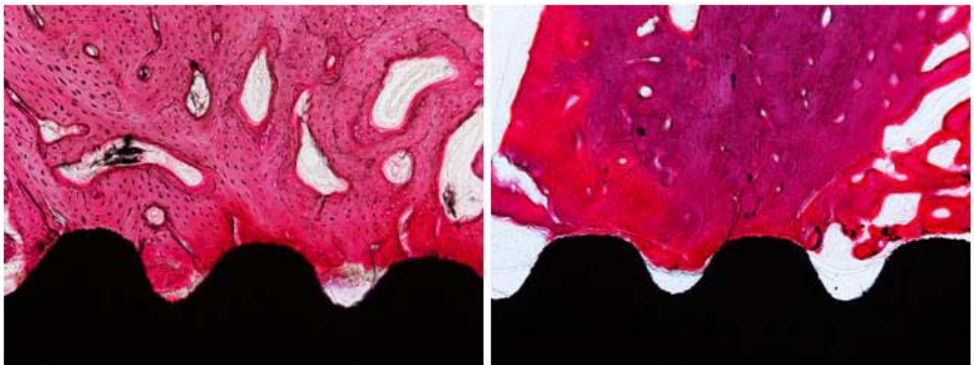


Figure 4.97 - Light microscope images (10X) of in vivo samples of coated implants with 35M:35G:30T in contact with cortical bone after 2 weeks healing time. (reproduced by courtesy of ¹)

It is perceptible a direct contact between the cortical bone and the sol-gel layer, nevertheless, the coating did not degrade totally on the 2 weeks experimental period. Besides, any sign of fibrous layer is detected hence the partial degradation of the sol-gel may be attributable to the short healing times used on the *in-vivo* study. In the main, it is acceptable to say that 35M:35G:30T coated implants show osseointegration at cortical level without any appreciable change detected between 1 week and 2 weeks healing times.

Uncoated titanium implants (control) show osseointegration at cortical level as well, nevertheless in this case was detected a positive evolution

RESULTS

between 1 week (Figure 4.98) and 2 weeks (Figure 4.99) healing periods.

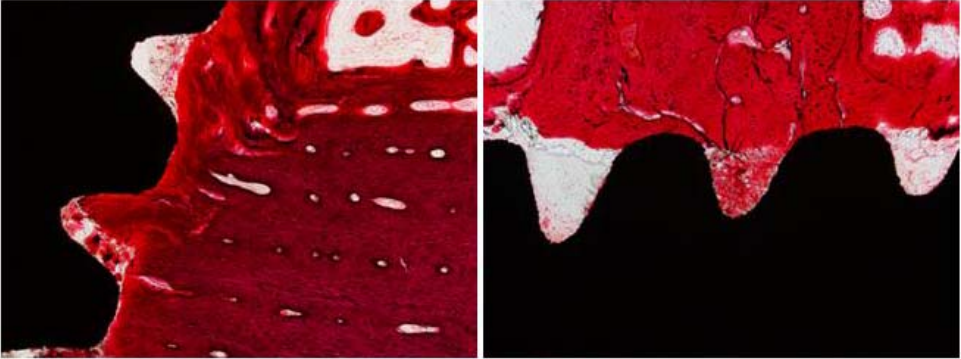


Figure 4. 98 - Light microscope images (10X) of in vivo samples of uncoated implants (control) in contact with cortical bone after 1 week healing time. (reproduced by courtesy of ¹)

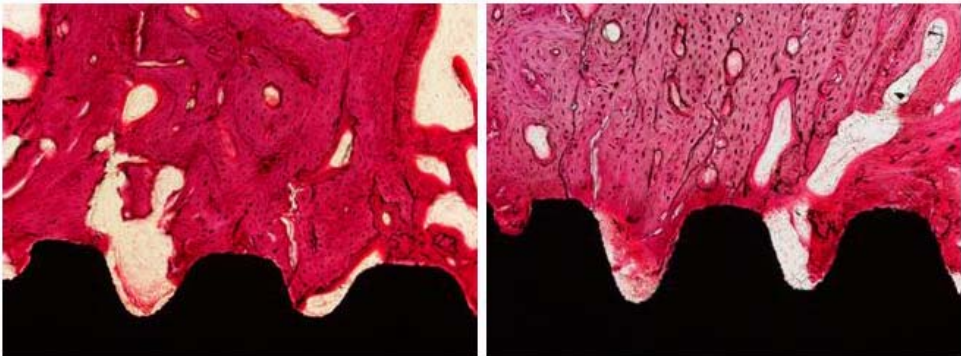


Figure 4. 99 - Light microscope images (10X) of in vivo samples of uncoated implants (control) in contact with cortical bone after 2 weeks healing time. (reproduced by courtesy of ¹)

The absence of fibrous tissue between uncoated implants or 35M:35G:30T coated implants and cortical bone able a primary mechanical stabilization of the implants in the early healing phase. The primary stabilization and direct contact with the cortical bone osseous microfractures promotes the osseointegration of the implants coated with 35M:35G:30T in cortical bone, consequently, improving the reference material 50M:50G results.

Also worth to note that the fibrous tissue detected in the bone marrow area disappear in cortical bone area for uncoated titanium implants and 35M:35G:30T coated implants, revealing that the fibrous capsule is not continuous and do not surround all the implant area. For reference material (50M:50G) coated implants this fibrous tissue remains and is detected in the cortical region revealing an unsuccessful osteointegration in this area.

Osseointegration in trabecular bone:

Due to the fibrous tissue layer that covers all the coated implant with 50M:50G reference material (Figure 4.100 - right picture) it was not detected a good osteointegration of the implant during 8 weeks healing time.¹¹

It can be seen that the osteoblastic activity is very slight and the trabecular spicules are narrow and slightly branched (Figure 4.100).

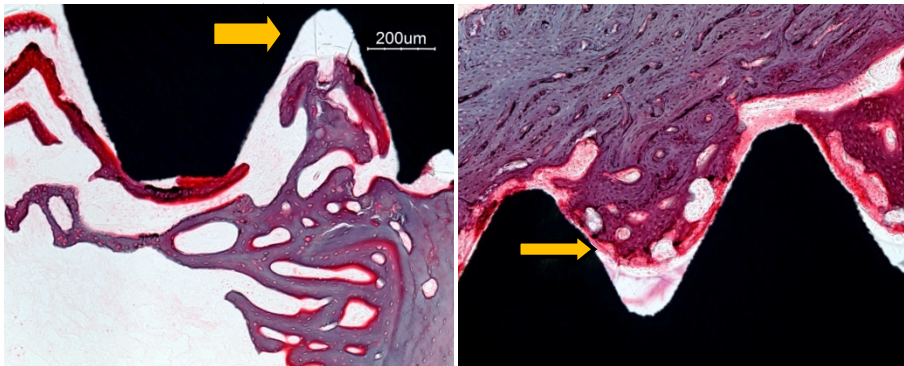


Figure 4. 100 - Light microscope images (10X) of in vivo samples of implants coated with 50M:50G in contact with trabecular bone after 8 weeks healing time.¹¹ (left image - highlight of the 50M:50G coating that remains adhered to the implant surface after 8 weeks healing time; right image - highlight of the thin fibrous tissue that covers all the 50M:50G coated implant)

RESULTS

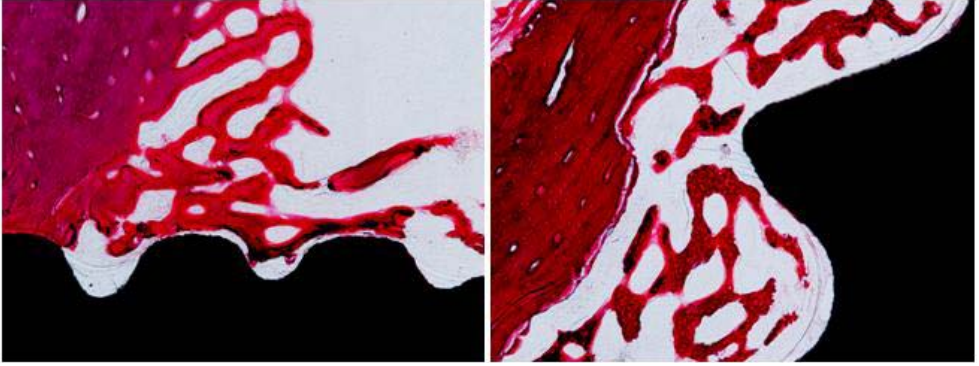


Figure 4.101 - Light microscope images (10X) of in vivo samples of implants coated with 35M:35G:30T in contact with trabecular bone after 1 week healing time. (reproduced by courtesy of ¹)

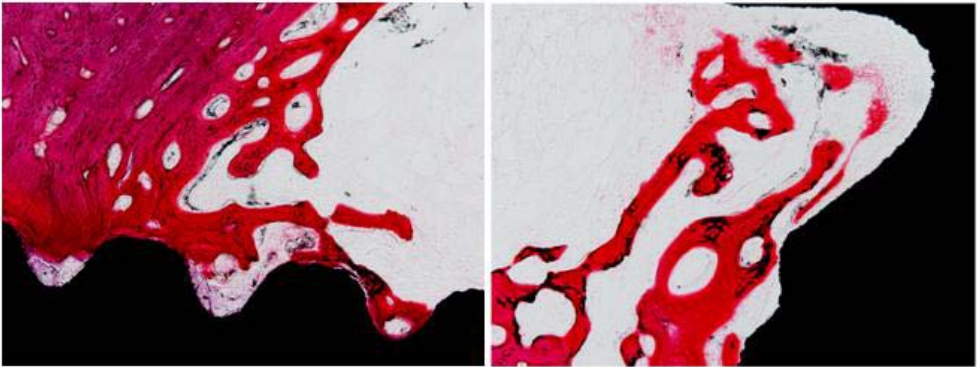


Figure 4.102 - Light microscope images (10X) of in vivo samples of implants coated with 35M:35G:30T in contact with trabecular bone after 2 weeks healing time. (reproduced by courtesy of ¹)

Trabecular bone is inherently related with the formation and growth of new bone, as a result the study of its evolution is crucial to evaluate the osteointegration level achieved by the new biomaterial 35M:35G:30T.

At the first week of healing contact (Figure 4.101) the formed spicules are straight and slightly branched. After two weeks healing time (Figure 4.102), the spicules structure changes and form a branched trabecular bone. During all the experimental period (2 weeks) it was detected a direct contact between trabecular bone tissue and 35M:35G:30T biomaterial that encourage the osteoblastic activity.

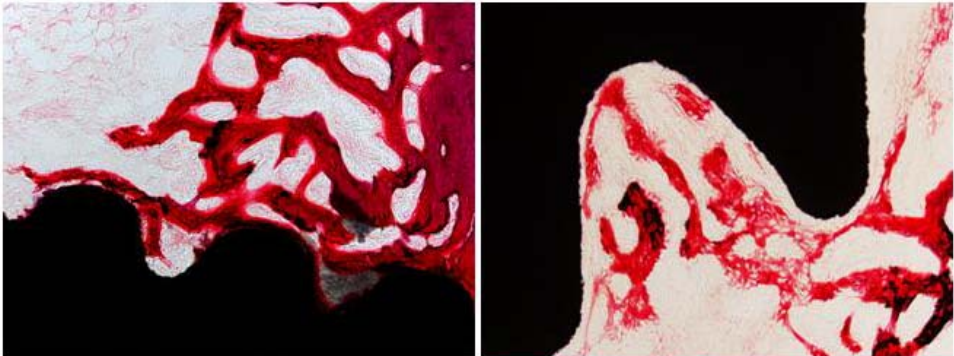


Figure 4. 103 - Light microscope images (10X) of in vivo samples of uncoated implants (control) in contact with trabecular bone after 1 week healing time. (reproduced by courtesy of ¹)



Figure 4. 104 - Light microscope images (10X) of in vivo samples of uncoated implants (control) in contact with trabecular bone after 2 week2 healing time. (reproduced by courtesy of ¹)

It is clear the osteoconductive skill of uncoated titanium implant (control) as it was verified since the beginning the formation of new bone attached to the implant surface (Figure 4.103 and#Figure 4.104) otherwise than a proper cellular activity.

It was stated on bibliography¹¹ that 50M:50G reference biomaterial does not achieve a complete osteointegration in the cortical section neither at the endostium region (related with the trabecular bone formation) due to the fibrous capsule formed that surrounds the coated implant. Besides, it

RESULTS

was identified a slight cellular activity and not appropriate trabecular spicules structure until the end of the experiment (8 weeks healing period).

The results of the new biocating 35M:35G:30T reveal a different cellular activity without a fibrous capsule that avoids the direct contact between the bone tissue (cortical or trabecular) and the biomaterial. This study, taking into consideration that the experimental period is brief, suggest an important improvement on the *in vivo* reference biomaterial (50M:50G) performance.

Although spicules architecture of the trabecular bone in contact with 35M:35G:30T coating in the first week is not satisfactory (straight spicules and slightly branched) it recovers the adequate form at 2 weeks healing time, achieving a branched architecture similar to the one registered for the control (uncoated implant) since the first week healing time.

Uncoated titanium implants show expectable osteoconductive skills since the first week healing time but is biologically inactive.

The new triple silane composition biocoating may be considered as a promising and versatile material, biocompatible, that enables biomolecules incorporation for specific treatments that finally improve bone regeneration and recovery from the clinical practice of dental implant surgeries.

REFERENCES

1. Sáez, I. L. Evaluación biológica de nuevos recubrimientos osteoinductores sintetizados vía sol-gel para aplicación en implantología dental. (Universidad Politécnica de Valencia, 2015).
2. Henstock, J. R., Canham, L. T. & Anderson, S. I. Silicon: The evolution of its use in biomaterials. *Acta Biomater.* (2014). doi:10.1016/j.actbio.2014.09.025
3. Carlisle, E. M. Silicon: A possible factor in bone calcification. *Science (80-)*. **167**, 279–280 (1970).
4. Matsko, N. B. *et al.* Silicon: The key element in early stages of biocalcification. *J. Struct. Biol.* **174**, 180–6 (2011).
5. Escolano, M. H. Desarrollo de Recubrimientos Híbridos Osteoinductores para Implantes Dentales. (Universidad Politécnica de Valencia, 2011).
6. Gabrielli, L. *et al.* Epoxide opening versus silica condensation during sol-gel hybrid biomaterial synthesis. *Chem. - A Eur. J.* **19**, 7856–7864 (2013).
7. Juan-Díaz, M. J. *et al.* Study of the degradation of hybrid sol-gel coatings in aqueous medium. *Prog. Org. Coatings* **77**, 1799–1806 (2014).
8. Lung, C. Y. K. & Matinlinna, J. P. Aspects of silane coupling agents and surface conditioning in dentistry: an overview. *Dent. Mater.* **28**, 467–77 (2012).
9. Rios, X. *et al.* Ethyl group as matrix modifier and inducer of ordered domains in hybrid xerogels synthesised in acidic media using ethyltriethoxysilane (ETEOS) and tetraethoxysilane (TEOS) as precursors. *Mater. Chem. Phys.* **141**, 166–174 (2013).
10. C. J. Brinker; G. W. Scherer. *Sol-Gel Science: The Physics and Chemistry of Sol-Gel Processing*. Elsevier (Academic Press, 1990).

RESULTS

at

<<http://scholar.google.com/scholar?hl=en&btnG=Search&q=intitle:No+Title#0>>

11. Juan-Díaz, M. J. *et al.* Development of hybrid sol–gel coatings for the improvement of metallic biomaterials performance. *Prog. Org. Coatings* (2016). doi:10.1016/j.porgcoat.2016.01.019
12. Weininger, S. J. & Stermitz, F. R. *Química Orgánica*. (1988).
13. Chan, Z. *et al.* Microstructures and properties of ORMOSIL comprising methyl, vinyl, and γ -glycidoxypropyl-substitued silica. *Opt. Mater. (Amst)*. **29**, 1543–1547 (2007).
14. Chruściel, J. J. & Leśniak, E. Modification of epoxy resins with functional silanes, polysiloxanes, silsesquioxanes, silica and silicates. *Prog. Polym. Sci.* **41**, 67–121 (2014).
15. Silverstein, R. M., Webster, F. X. & Kiemle, D. Spectrometric Identification of Organic Compounds, 7th Edition. 512 (2005). at <<https://books.google.com/books?id=mQ8cAAAAQBAJ&pgis=1>>
16. Ahola, M., Korteso, P., Kangasniemi, I., Kiesvaara, J. & Yli-Urpo, A. Silica xerogel carrier material for controlled release of toremifene citrate. *Int. J. Pharm.* **195**, 219–227 (2000).
17. Liu, Q., Ding, J., Mante, F. K., Wunder, S. L. & Baran, G. R. The role of surface functional groups in calcium phosphate nucleation on titanium foil: a self-assembled monolayer technique. *Biomaterials* **23**, 3103–3111 (2002).
18. Yasakau, K. A., Carneiro, J., Zheludkevich, M. L. & Ferreira, M. G. S. Influence of sol-gel process parameters on the protection properties of sol–gel coatings applied on AA2024. *Surf. Coatings Technol.* **246**, 6–16 (2014).
19. Vignesh, R. B. & Sethuraman, M. G. Corrosion protection behaviour of sol–gel derived N,N-dimethylthiourea doped 3-glycidoxypropyltrimethoxysilane on aluminium. *Prog. Org. Coatings* **77**, 136–141 (2014).

20. Mahony, O. *et al.* Silica-Gelatin Hybrids with Tailorable Degradation and Mechanical Properties for Tissue Regeneration. *Adv. Funct. Mater.* **20**, 3835–3845 (2010).
21. Luo, W. & Zhao, L. The influence of GPTMS on the performance of silica-ionic liquid hybrid membrane. *Solid State Ionics* **268**, 94–101 (2014).
22. Smitha, S., Shajesh, P., Mukundan, P., Nair, T. D. R. & Warriar, K. G. K. Synthesis of biocompatible hydrophobic silica–gelatin nano-hybrid by sol–gel process. *Colloids Surfaces B Biointerfaces* **55**, 38–43 (2007).
23. Bakhshandeh, E., Jannesari, A., Ranjbar, Z., Sobhani, S. & Saeb, M. R. Anti-corrosion hybrid coatings based on epoxy–silica nanocomposites: Toward relationship between the morphology and EIS data. *Prog. Org. Coatings* **77**, 1169–1183 (2014).
24. Sarmento, V. H. V. *et al.* Corrosion protection of stainless steel by polysiloxane hybrid coatings prepared using the sol–gel process. *Surf. Coatings Technol.* **204**, 2689–2701 (2010).
25. Eduok, U., Suleiman, R., Khaled, M. & Akid, R. Enhancing water repellency and anticorrosion properties of a hybrid silica coating on mild steel. *Prog. Org. Coatings* **93**, 97–108 (2016).
26. Almeida, J. C. *et al.* Structural characterization of PDMS–TEOS–CaO–TiO₂ hybrid materials obtained by sol–gel. *Mater. Chem. Phys.* **143**, 557–563 (2014).
27. Vanithakumari, S. C., George, R. P. & Kamachi Mudali, U. Influence of silanes on the wettability of anodized titanium. *Appl. Surf. Sci.* **292**, 650–657 (2014).
28. Park, J. H. *et al.* The responses to surface wettability gradients induced by chitosan nanofilms on microtextured titanium mediated by specific integrin receptors. *Biomaterials* **33**, 7386–93 (2012).
29. Rupp, F., Scheideler, L., Rehbein, D., Axmann, D. & Geis-Gerstorfer, J. Roughness induced dynamic changes of wettability

RESULTS

- of acid etched titanium implant modifications. *Biomaterials* **25**, 1429–1438 (2004).
30. Tonda-Turo, C. *et al.* Comparative analysis of gelatin scaffolds crosslinked by genipin and silane coupling agent. *Int. J. Biol. Macromol.* **49**, 700–6 (2011).
 31. Kirtay, S. Preparation of hybrid silica sol–gel coatings on mild steel surfaces and evaluation of their corrosion resistance. *Prog. Org. Coatings* **77**, 1861–1866 (2014).
 32. Hernández-Escolano, M. *et al.* The design and characterisation of sol–gel coatings for the controlled-release of active molecules. *J. Sol-Gel Sci. Technol.* **64**, 442 (2012).
 33. Sakai, R. T. *et al.* Electrochemical study of TEOS, TEOS/MPTS, MPTS/MMA and TEOS/MPTS/MMA films on tin coated steel in 3.5% NaCl solution. *Prog. Org. Coatings* **74**, 288–301 (2012).
 34. Kunst, S. R. *et al.* Corrosion resistance of siloxane–poly(methyl methacrylate) hybrid films modified with acetic acid on tin plate substrates: Influence of tetraethoxysilane addition. *Appl. Surf. Sci.* **298**, 1–11 (2014).
 35. Shi, X., Xu, L. & Wang, Q. Porous TiO₂ film prepared by micro-arc oxidation and its electrochemical behaviors in Hank's solution. *Third Spec. Issue Dedic. to Plasma Electrolysis Plasma Electrolysis Inc. Pap. from 'EUROMAT 2009' Congr. Adv. Mater. Process. 7–10 Sept. 2009, Glas. UK* **205**, 1730–1735 (2010).
 36. Radin, S., Chen, T. & Ducheyne, P. The controlled release of drugs from emulsified, sol gel processed silica microspheres. *Biomaterials* **30**, 850–858 (2009).
 37. Teoli, D. *et al.* Wet sol-gel derived silica for controlled release of proteins. *J. Control. Release* **116**, 295–303 (2006).
 38. Costache, M. C., Qu, H., Ducheyne, P. & Devore, D. I. Polymer–xerogel composites for controlled release wound dressings. *Biomaterials* **31**, 6336–6343 (2010).

39. Mladenović, Ž. *et al.* Soluble silica inhibits osteoclast formation and bone resorption in vitro. *Acta Biomater.* **10**, 406–18 (2014).
40. Ren, L., Tsuru, K., Hayakawa, S. & Osaka, A. Synthesis and characterization of gelatin-siloxane hybrids derived through sol-gel procedure. *J. Sol-Gel Sci. Technol.* **21**, 115–121 (2001).
41. Voron'ko, N. G., Derkach, S. R., Kuchina, Y. A. & Sokolan, N. I. The chitosan-gelatin (bio)polyelectrolyte complexes formation in an acidic medium. *Carbohydr. Polym.* **138**, 265–72 (2016).
42. Qiu, X., Wan, P., Tan, L., Fan, X. & Yang, K. Preliminary research on a novel bioactive silicon doped calcium phosphate coating on AZ31 magnesium alloy via electrodeposition. *Mater. Sci. Eng. C. Mater. Biol. Appl.* **36**, 65–76 (2014).

RESULTS

CHAPTER 5. CONCLUSIONS

CONCLUSIONS

This research work leads to the following conclusions:

- Several silica based sol-gel materials were synthesized and used as coatings on metal substrates. They were based on different proportions of the silane precursors MTMOS, GPTMS and TEOS and all of the coatings had homogeneous semblance and bright surface.
- The physical-chemical properties of the developed materials are different in accordance with the inorganic-organic content of the matrices. Generally, the incorporation of TEOS to the double reference material (50%MTMOS:50%GPTMS) increases surface roughness and wettability. The GPTMS content affects the surface roughness and coatings' weight: higher GPTMS contents result in higher surface roughness, weight gain and wettability.
- The barrier effect of the coatings against possible metal corrosion products released at the first instants of their contact with an aqueous medium, was proven for both 90(M:G):10T and 70(M:G):30T series. Materials with 10% TEOS improve the protection degree, as compared with the reference material (50%MTMOS:50%GPTMS) while the series with 30% TEOS show worsened protection behaviour against corrosion in saline solution.
- 90(M:G):10T materials' series in contact with Hank's solution show the formation of an external layer of deposits. The GPTMS content increase results in a decrease of the coatings resistive skills. On the other hand, 70(M:G):30T materials' series in contact with Hank's solution show the worst barrier properties in Hank's solution, as detected when a saline solution was used as aqueous medium.

CONCLUSIONS

- Coatings' *in vitro* degradation profiles show two different degradation stages when in contact with water: a fast degradation rate during the first 7 days followed by a slower degradation rate up to 63 days. Both 90(M:G):10T and 70(M:G):30T series improve *in vitro* degradation behavior as compared with the reference material 50%MTMOS:50%GPTMS.
- A successful functionalization was achieved for the silane coatings with the incorporation gelatine. The crosslinking degree of the materials was not affected by gelatine incorporation. The surface roughness and wettability of the coatings are barely affected with gelatin incorporation. In a similar way, protection against corrosion in saline solution remains fairly analogous to pure silane coatings. The results corresponding to 30% TEOS materials with gelatine incorporation suggest the formation of an external layer of mineral deposits. Hank's Balanced Salt solution promotes the formation of an external layer of deposits for both series (10% and 30% TEOS with gelatine incorporation) and the systems silanes + gelatine + Hank's electrolyte improve in an important manner the anticorrosive properties of the pure coatings. The weight loss profiles during hydrolytic degradation of functionalized coatings is very similar to pure materials behaviour. Nevertheless, 30% TEOS materials registered greater degradation rates.
- The trisilane developed materials are not cytotoxic. The incorporation of TEOS to the double reference material (50%MTMOS:50%GPTMS) slightly improved cellular proliferation but it offered no advantage with respect to mineralization rate.
- 35M:35G:30T coating improved the biocompatibility of the reference material (50%MTMOS:50%GPTMS). Furthermore, a direct contact between the sol-gel coating and the bone tissue was detected

CONCLUSIONS

without impairing the osteoconductive attributes of the metallic titanium substrate of the implants.

To sum up, new trisilane-based composition sol-gel coatings were developed with different degradation profiles (regulated by TEOS incorporation) and with regulable organic content (GPTMS) which enable the incorporation of bioactive elements to improve the osseointegration process of current metallic implants. Overall, the formulation with the best properties to improve the biocompatibility of the reference material (50%MTMOS:50%GPTMS) is the one based on a 35%MTMOS:35%GPTMS:30%TEOS molar composition.

CONCLUSIONS

CONCLUSIONES

De la investigación realizada en este trabajo se extraen las siguientes conclusiones:

- Se han sintetizado varios recubrimientos sol-gel de base silicio y se han aplicado en sustratos metálicos. La síntesis se basa en la utilización de diferentes proporciones de silanos utilizados como precursores: MTMOS, GPTMS y TEOS. Todos los recubrimientos presentan una apariencia homogénea, sin imperfecciones y superficie brillante.
- Las propiedades físico-químicas de los materiales desarrollados son distintas y varían según el contenido orgánico-inorgánico de la matriz formada. De forma general, la incorporación de TEOS al material de referencia 50%MTMOS:50%GPTMS aumenta la rugosidad superficial y mojabilidad. La variación del contenido en GPTMS afecta visiblemente la rugosidad superficial y aumento de peso de los recubrimientos, es decir, cuanto mayor el contenido en GPTMS mayor la rugosidad superficial, aumento de peso y mojabilidad detectados.
- El efecto barrera de los distintos recubrimientos contra el hipotético intercambio de iones derivados de la corrosión del sustrato metálico en los primeros instantes de contacto con medios acuosos se ha comprobado para ambas series de recubrimientos, materiales de mezcla global 90(M:G):10T y materiales de mezcla global 70(M:G):30T. Los materiales con 10% TEOS mejoran el efecto protector frente a la corrosión cuando comparado con las prestaciones registradas para el material de referencia (50%MTMOS:50%GPTMS). No obstante, los materiales con 30%

CONCLUSIONES

TEOS empeoran el efecto barrera detectado para el material de referencia (50%MTMOS:50%GPTMS) en medio salino.

- La serie de materiales de composición global 90(M:G):10T en contacto con la disolución de Hank's estimula la formación de una capa externa de depósitos. El aumento del contenido en GPTMS provoca la disminución de la resistencia del recubrimiento al paso de iones (corrosión). Por otra parte, la serie de materiales 70(M:G):30T en contacto con disolución de Hank's muestra un significativo descenso de las propiedades barrera de los recubrimientos en comparación con los materiales de la serie 90(M:G):10T).
- Los perfiles de degradación hidrolítica *in vitro* muestran dos fases distintas: en los primeros 7 días de contacto ocurre una degradación rápida seguida de una cinética de degradación más lenta hasta la finalización del ensayo (63 días). Ambas series de materiales, 90(M:G):10T y 70(M:G):30T, mejoran los resultados de degradación registrados para el material de referencia 50%MTMOS:50%GPTMS.
- Se ha logrado la funcionalización de los recubrimientos con la incorporación de gelatina. El grado de entrecruzamiento no resultó afectado por la incorporación de la biomolécula (gelatina) ni tampoco la rugosidad y mojabilidad superficial. La protección frente a la corrosión de los recubrimientos no sufrió cambios significativos con respecto a los materiales puros (sin gelatina). En los ensayos electroquímicos (medida de la resistencia al paso de electrones) en medio salino con los materiales de la serie con 30% TEOS + gelatina se ha detectado la formación de una capa externa de depósitos minerales. Por otra parte, cuando el medio acuoso utilizado fue la disolución Hank's se ha detectado la formación de una capa externa de depósitos para ambas series de materiales (con 10% y 30% TEOS). Los sistemas silanos + gelatina + disolución de Hank's han mejorado de forma significativa las

propiedades anticorrosivas de los recubrimientos puros (sin gelatina). Los perfiles de degradación hidrolítica de los recubrimientos funcionalizados con gelatina es semejante al comportamiento detectado para los materiales puros. No obstante, la serie de materiales con 30% TEOS muestra mayor grado de degradación.

- Las series de materiales desarrollados en este trabajo no presentan citotoxicidad. La incorporación de TEOS a la formulación doble de referencia, 50%MTMOS:50%GPTMS, mejora ligeramente la proliferación celular pero no ofrece cualquier ventaja en lo que respecta a la tasa de mineralización.
- La formulación constituida por 35%MTMOS:35%GPTMS:30%TEOS mejora la biocompatibilidad del material de referencia 50%MTMOS:50%GPTMS *in vivo*, puesto que se ha detectado un contacto directo entre el recubrimiento sol-gel y el tejido óseo. No se ha detectado una disminución de las prestaciones osteoconductoras de los implantes metálicos sin recubrir provocado por su recubrimiento con sol-gel de base silicio.

En resumen, se han desarrollado recubrimientos sol-gel de composición triple de silanos con diferentes perfiles de degradación y con contenido orgánico regulable (GPTMS) que permite la incorporación de elementos bioactivos que consecuentemente mejoran el proceso de osteointegración de los actuales implantes metálicos de titanio. Puesto lo anterior, la formulación con las propiedades más adecuadas para promocionar y mejorar la biocompatibilidad del material de referencia 50%MTMOS:50%GPTMS resultó ser la mezcla de silanos 35%MTMOS:35%GPTMS:30%TEOS.

ABBREVIATIONS

ALP -	alkaline phosphate activity
BCA -	bicinchoninic acid
BMP's -	bone morphogenetic proteins
cp Ti -	commercial pure titanium
CPE -	Constant phase element
EC -	equivalent circuit
ECM -	extracellular matrix
EIS -	electrical impedance spectroscopy
FTIR -	fourier transform infrared spectroscopy
GEL -	gelatine
GPTMS or G -	3-glycidoxypropyltrimethoxysilane
HA -	hydroxyapatite
MTMOS or M -	trimethoxymethylsilane
NMR -	nuclear magnetic resonance
OM -	optical microscopy
R -	resistance
SAM's -	self assembled monolayers
SEM -	scanning electron microscopy
TEOS or T -	tetraethoxysilane
Ti -	titanium
TGA -	thermogravimetric analysis
50M:50G -	reference material with molar composition 50%MTMOS:50%GPTMS

